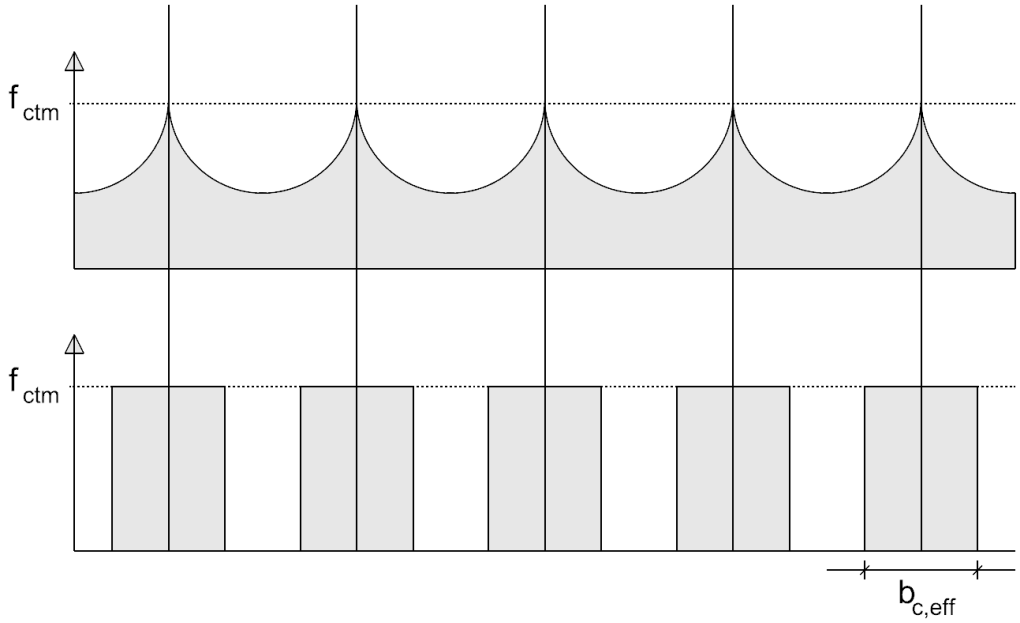

Effective area in restrained reinforced concrete

Finite Element Analysis in relation to models presented in Eurocode 2

Master's thesis in Master's Programme Structural Engineering and Building Technology

AMELIE JOSEFSSON, ALVA SVENSK

DEPARTMENT OF ARCHITECTURE AND CIVIL ENGINEERING DIVISION OF STRUCTURAL ENGINEERING AND BUILDING TECHNOLOGY

CHALMERS UNIVERSITY OF TECHNOLOGY
Gothenburg, Sweden 2026
www.chalmers.se

Master's thesis 2026

Effective area in restrained reinforced concrete

Finite Element Analysis in relation to models presented in Eurocode 2

AMELIE JOSEFSSON, ALVA SVENSK

CHALMERS
UNIVERSITY OF TECHNOLOGY

Department of Architecture and Civil Engineering
Division of Structural Engineering
Concrete Structures
Chalmers University of Technology
Gothenburg, Sweden 2026

Effective area in restrained reinforced concrete
Finite Element Analysis in relation to models presented in Eurocode 2
AMELIE JOSEFSSON, ALVA SVENSK

Supervisor at company: Thomas Appelgren, Ramboll
Supervisor at Chalmers: Carlos Gil Berrocal, Division of Structural Engineering, Concrete Structures
Examiner: Carlos Gil Berrocal, Division of Structural Engineering, Concrete Structures

Master's Thesis 2026
Department of Architecture and Civil engineering
Division of Structural Engineering
Concrete Structures
Chalmers University of Technology
SE-412 96 Gothenburg
Telephone +46 31 772 1000

Cover: Schematic illustration constructed in Rhino of concrete stress distribution illustrating the approach for calculating the effective area.

Typeset in LaTeX
Printed by Chalmers Reproservice
Gothenburg, Sweden 2026

Effective area in restrained reinforced concrete
Finite Element Analysis in relation to models presented in Eurocode 2
AMELIE JOSEFSSON, ALVA SVENSK
Department of Architecture and Civil Engineering
Chalmers University of Technology

Abstract

Cracking of concrete is a well-known phenomenon in most concrete structures, due to the low tensile strength of the material. In a reinforced concrete element, cracking initiates a redistribution of stresses from the concrete to the reinforcement. Depending on the thickness of the element, redistribution of stresses in the surroundings of a crack may create an area of concentrated stresses, an effective area, where the next crack will be created. Cracking, though, does not imply failure, as well-designed elements allow for redistribution.

Eurocode is a commonly used framework that is used as a basis for structural design, and therefore the presented models must be accurate and applicable to all elements, striving for well-designed and material-efficient structures. In the second generation of Eurocode, more specifically, SS-EN 1992-1-1, a model for the effective area in concrete structures is provided. The way of modelling this slightly changed between the old version from 2005 and the newer one published in 2023. Further on, the definition of the effective area in Eurocode is not primarily derived being applicable to restrained elements.

This thesis investigates whether these models apply to restrained elements. Theory related to cracking in restrained reinforced concrete was investigated. The models provided in the two versions were studied and compared. Evaluation of the effective area was done by non-linear Finite Element Modelling in the software DIANA, using a linear concrete material and a non-linear bond-slip interface between concrete and reinforcement. The stress distribution for a restrained reinforced concrete element with varying geometry was used for the evaluation of the effective area. Analytical calculations based on the models in the second generation of Eurocode were also performed, and the results were compared with the numerical results.

The final results obtained from Finite Element Analysis did not correlate with the models for effective area. However, the concept of effective areas, i.e stress concentrations in the concrete adjacent to reinforcement, was clearly observed, and a maximum tensile stress section was obtained, in line with the theory. The overall conclusion is that the existing models do not apply to restrained elements and that an improved model is required. Due to a lack of correlation in results, further investigation of the subject is needed.

Keywords: Bond-slip, Effective area, Eurocode, Finite Element Analysis, DIANA analysis, Restraint cracking, Reinforced concrete

Effektiv area i tvångslastade armerade betongkonstruktioner
Finita element-analyser i relation till modeller presenterade i Eurokod 2
AMELIE JOSEFSSON, ALVA SVENSK
Institutionen för arkitektur och samhällsbyggnadsteknik
Chalmers tekniska högskola

Sammanfattning

Sprickbildning i betong är ett välkänt fenomen i de flesta betongkonstruktioner, vilket beror på materialets låga draghållfasthet. I ett armerat betongelement initierar sprickbildning en omfördelning av spänningar från betongen till armeringen. Beroende på elementets tjocklek kan omfördelningen av spänningar i närheten av en spricka skapa ett område med koncentrerade spänningar, en effektiv area, där nästa spricka kommer att bildas. Sprickbildning innebär dock inte full kollaps, eftersom väl dimensionerade element tillåter omfördelning.

Eurokod är ett vanligt standardregelverk vid dimensionering av konstruktioner, och därför måste de presenterade modellerna vara korrekta och tillämpbara på alla element, i syfte att uppnå väl utformade och materialeffektiva konstruktioner. I den andra generationen av Eurokod, mer specifikt SS-EN 1992-1-1, presenteras en modell för den effektiva arean i betongkonstruktioner. Sättet att modellera detta har ändrats något mellan den äldre versionen från 2005 och den nyare som publicerades 2023. Vidare är definitionen av den effektiva arean i Eurokod inte primärt framtagen för att vara tillämpbar på tvångslastade element.

Denna tes undersöker om dessa modeller är tillämpbara på tvångslastade element. Teori relaterad till sprickbildning i inspänd armerad betong studerades. Modellerna i de två versionerna analyserades och jämfördes. Utvärderingen av den effektiva arean genomfördes genom icke-linjär finit element-analys i programvaran DIANA, med en linjär betongmodell och ett icke-linjärt vidhäftning-glidningssamband för interaktionen mellan betong och armering. Spänningsfördelningen för ett inspänt armerat betongelement med varierande geometri användes som underlag för att utvärdera den effektiva arean. Analytiska beräkningar baserade på modellerna i den andra generationen av Eurokod har också genomförts och jämförts med de numeriska resultaten.

De slutliga resultaten från finit element-analyserna korrelerade inte med modellerna för effektiv area. Däremot observerades tydligt konceptet med effektiva areor, det vill säga spänningskoncentrationer i betongen intill armeringen, och en sektion med maximal dragspänning identifierades, i linje med teorin. Den huvudsakliga slutsatsen var att de befintliga modellerna inte är tillämpbara på tvångslastade element och att en förbättrad modell krävs. På grund av bristande korrelation i resultaten behövs vidare studier inom området.

Nyckelord: Armerad betong, vidhäftning-glidningssamband , DIANA-analys, Effektiv area, Eurokod, Finita Element Analyser, Tvångssprickbildning

Preface

In this master's thesis, the effective area in restrained reinforced concrete has been studied. The project was carried out between January and June as the final work within the master's programme in Structural Engineering and Building Technology. The work was performed as a collaboration between Ramboll and Chalmers University of Technology.

We would like to thank our supervisor at Ramboll, Thomas Appelgren, for excellent guidance and expertise. We also want to thank the other employees at Ramboll, the division of bridge design, for their welcoming attitude and guidance during the project. Finally, we would like to thank our supervisor and examiner at Chalmers, Carlos Gil Berrocal, for his valuable knowledge and support.

Amelie Josefsson and Alva Svensk, Gothenburg, June 2026

List of Acronyms

Below is the list of acronyms that have been used throughout this thesis listed in alphabetical order:

AI	Artificial Intelligence
BFGS	Broyden-Fletcher-Goldfarb-Shanno
CSV	Comma-Separated Values
FE	Finite Element
FEA	Finite Element Analysis
EC	Eurocode
EC 2	Eurocode 2: Design of Concrete Structures
SLS	Servicability Limit State

Nomenclature

Below is the nomenclature of parameters and variables used throughout this thesis.

Latin upper case letter

A_c	Concrete area
$A_{c,eff}$	Effective area
A_s	Steel area
A_{truss}	Truss area
B	Element width
E_{cm}	Young's modulus for concrete, mean value
E_s	Modulus of elasticity steel
F_c	Concrete force
F_{cs}	Shrinkage force
F_s	Steel force
G_f	Fracture energy
L	Element length
L_{truss}	Truss length
N	Normal force
N_{cr}	Critical normal force
R	Restraint degree
R_{ext}	External restraint degree
R_{int}	Internal restraint degree
T	Element thickness

0.1 Latin lower case letters

a_x	Ddefinition of distance between concrete edge and reinforcement bar in x-direction in EC 2
a_y	Definition of distance between concrete edge and reinforcement bar in y-direction in EC 2
b	Definition of width in EC 2
$b_{c,eff}$	Effective width
$b_{c,eff,edge}$	Effective width for an edge bar
$b_{c,eff,2005}$	Effective width based on EC 2 version from 2005
$b_{c,eff,2023}$	Effective width based on EC 2 version from 2023
$b_{c,eff,in}$	Effective width for an mid bar
c	Cover thickness
c_x	Cover thickness in the x-direction
c_y	Cover thickness in the y-direction
d	Distance between top of concrete section to bottom reinforcement layer or vice versa in EC 2
f_{cm}	Concrete compressive strength, mean value
f_{ct}	Concrete tensile strength
$f_{ctk0.05}$	Concrete tensile strength, lower characteristic value
$f_{ctk0.95}$	Concrete tensile strength, upper characteristic value
f_{ctm}	Concrete tensile strength, mean value
f_t	Concrete tensile strength figure 2.2
f_{yd}	Steel yield strength, design value
f_{yk}	Steel yield strength, characteristic value in figure 2.4
h	Definition of height in EC 2
$h_{c,eff}$	Effective height
h_{cr}	Crack bandwidth
$h_{c,eff,2005}$	Effective height based on EC 2 version from 2005
$h_{c,eff,2023}$	Effective height based on EC 2 version from 2023
l_t	Transmission length
n_{bx}	Numbers of bars in the x-direction
n_{by}	Number of bars in the y-direction
r_x	Cover thickness in the x-direction in model Code 2020
r_y	Cover thickness in the y-direction in Model Code 2020

s	Reinforcement bar spacing or slip in bond-slip relationship
s_x	Reinforcement bar spacing in the x-direction
s_y	Reinforcement bar spacing in the y-direction
s_1	Slip parameter in bond–slip relationship
s_2	Slip parameter in bond–slip relationship
s_3	Slip parameter in bond–slip relationship
t	Time
w_1	Crack width in bilinear softening law, first change in stiffness
w_c	Crack width in bilinear softening law, ultimate crack width
w_{net}	Crack width
w_u	Ultimate crack width in figure 2.2
x	Distance to neutral axis in cross section
z_{max}	Distance where concrete capacity first is reached

0.2 Greek upper case letters

ΔL	Length difference in figure 2.2
ΔT	Temperature difference
Δr	Distance where cone failure may take place in figure 2.5

0.3 Greek lower case letters

α	Bond–slip curve shape coefficient
α_{cT}	Thermal expansion coefficient
δ_{imp}	Imposed displacement
ε	Strain
$\varepsilon_{\text{actual}}$	Actual strain
ε_c	Concrete strain
ε_{ca}	Concrete autogenous shrinkage strain
ε_{cd}	Concrete drying shrinkage strain
ε_{cs}	Concrete shrinkage strain
ε_{cT}	Thermal expansion strain
$\varepsilon_{\text{full restraint}}$	Strain in case of full restraint

ε_s	Steel strain
ε_{suk}	Characteristic strain limit in figure 2.4
ν	Poisson's ratio
σ	Stress
σ_c	Concrete stress
σ_{ct}	Concrete tensile stress in figure 2.11.
σ_{max}	Maximum stress
σ_s	Steel stress
$\sigma_{s,ext}$	External steel stress
τ_b	Bond stress
ϕ	Reinforcement bar diameter

Contents

List of Figures

List of Tables

1

Introduction

This report presents a master's thesis within the field of structural engineering. In the following chapter, an introduction to the master's thesis is given. Background, aim of the project and specification of what is to be issued are presented. In addition, the limitations of the project are discussed.

1.1 Background

Cracking in concrete members is a well-known phenomenon, since concrete as a material has a low tensile strength. When tensile stresses can no longer be carried by the plain concrete, a crack is created. To maintain load-carrying capacity after cracking, reinforcement is used to carry tensile stresses. The reinforcement itself does not prevent the concrete from cracking, it just carries the load after cracking (Engström, 2014). Adding reinforcement most often results in more cracks than for a non-reinforced concrete member.

Structural members can, apart from being subjected to stresses caused by externally applied loads, such as self-weight and live loads, also be subjected to stresses caused by the prevention of movements. This is referred to as *external restraint* (Engström, 2014). Compressive stress-independent strains, such as shrinkage or thermal expansions, result in tensile stresses for members with fixed boundaries, since movements are prevented. The distribution of restraint stresses depends on how the external restraint is applied. In figure 1.1, two typical cases of elements with external restraint are shown. In the case of an end-restrained element with fixed ends, figure 1.1a, the whole height and thickness are equally restrained. In the other case, with a wall element restrained by a bottom slab, figure 1.1b, the degree of restraint varies both along the length and height of the element.

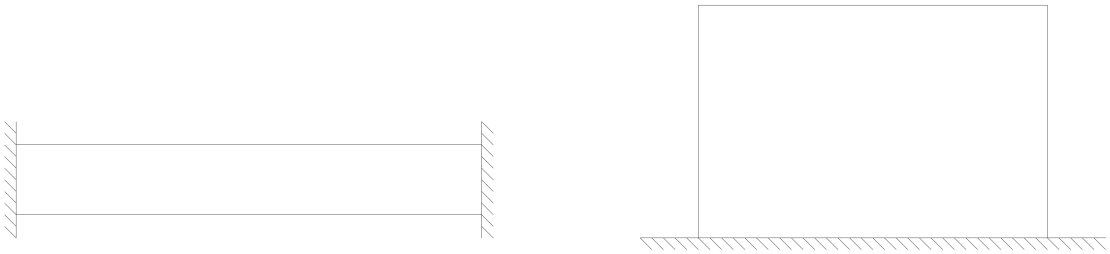

(a) End-restrained element. **(b)** Bottom-restrained wall element.

Figure 1.1: Illustration of two elements with external restraint (created by the authors).

Reinforced concrete is a composite material and because of the different material properties of steel and concrete, stresses can be induced (Engström, 2014). Stress-independent strains cause different deformations in the materials. The bond between the materials results in one material partly preventing the movements needed in the other material. In the typical case of shrinkage, the reinforcement prevents the concrete from shortening and subjects the surrounding concrete to tensile stresses. The reinforcement applies internal restraint to the surrounding concrete. The restraining effects are largest close to the reinforcement bars and therefore, tensile stresses are larger in those parts of the concrete, and the risk of cracking is increased there (Engström, 2014).

For thick members, this behaviour is modelled in the Eurocode for design of concrete structures (EC 2) using an effective concrete area, $A_{c,eff}$, around the reinforcement bars, which refers to the areas where tensile stresses appear in the concrete, and the risk of cracking is increased. For thin members, in the case when the spacing between reinforcement bars is small, the effective concrete areas around the bars cover the entire cross-section. Figure 1.2 shows an illustration of how the effective area is considered in the old EC 2 from 2005, presented by European Committee for Standardization (CEN) (2005), and the new EC 2 from 2023, presented by European Committee for Standardization (CEN) (2023). Further in the report, these versions are referred to as the old and new EC 2, respectively.

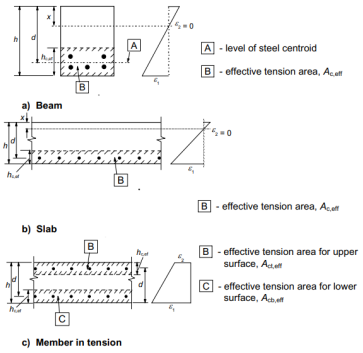

(a) Old EC 2 according to European Committee for Standardization (CEN) (2005).

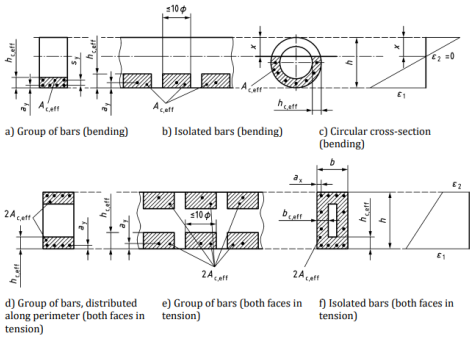

(b) New EC 2 according to European Committee for Standardization (CEN) (2023).

Figure 1.2: Example of how the effective area, $A_{c,eff}$, is considered in EC 2. More detailed figures are presented further in this thesis. Figures are retrieved from SS-EN 1992-1-1:2005 and SS-EN 1992-1-1:2023, respectively, and are reproduced with permission from SIS, Swedish Institute for Standards, who also offer the standards www.sis.se

In this master's thesis, a non-linear Finite Element Analysis (FEA) of an end-restrained reinforced concrete element is performed. The results from the analysis aim to evaluate the extent to which the models for effective area provided in EC 2 apply to reality. To study this, the stress transfer between steel and reinforcement is evaluated for an end-restrained element with varying cross-sectional geometries. Some analytical calculations are also performed for the purpose of comparison with the FEA results.

1.2 Problem formulation

To reach the proposed aim, the following specific issues aim to be answered regarding reinforced concrete members with external restraint:

- *Do the stress distributions in a restrained element based on FEA correspond well to the models for effective area, $A_{c,eff}$, provided in EC 2?*
- *What conclusions can be made regarding the effective area to provide a basis for an improved model?*
- *Can we identify a clear definition for when a cross-section can be considered thin instead of thick?*
- *How do the varying geometries affect the results from both non-linear FEA and analytical models? Can the analytical models be considered more accurate for certain parameter sets?*

1.3 Aim and objectives

This master's thesis aims to investigate concrete elements with external restraint and provide an extended understanding of how the effective area around reinforcement bars should be considered in such elements. To accomplish that, the accuracy of the new and old EC 2 is to be evaluated in relation to such elements.

The Thesis is carried out as a contribution to a research project funded by Swedish Transport Administration (Trafikverket) and carried out by Thomas Appelgren at Ramboll Sweden AB in collaboration with ELU Konsult AB and Chalmers. The research project aims to create a more uniform assessment method and give recommendations on how the restraint loading should be considered in the design performed according to the new generation of EC 2. The results and conclusions of the master's thesis aim to contribute to that research project.

1.4 Limitations

To align the project with the time frame of a master's thesis, the scope of the project is limited. Firstly, only one element type with specified boundary conditions is to be studied. A simplified model is assumed, where the local response influenced by the boundary conditions is neglected. Furthermore, only one specific case of input regarding the bond-slip interaction behaviour between concrete and reinforcement is used. Additionally, long-term effects related to creep are also disregarded.

The restrained element is analysed using variable input parameters in terms of element thickness, reinforcement diameter and reinforcement spacing. Several geometric parameters are kept constant in order to limit the number of studied cases. These constant parameters are, though, chosen in order to obtain representable results, since the selected constant factors should not have a noticeable influence on the behaviour. An example is the choice of concrete strength class, which is taken as a commonly used strength class, to obtain results applicable to similar concrete structures.

In general, issues regarding convergence in FEA are a limitation for this project. Since cracking behaviour is closely connected to effective area, it is of great interest to study the behaviour of a restrained element with non-linear concrete material. But since it turned out that convergence for such an analysis could not be reached within the time frame for the project, cracking behaviour could not be studied.

1.5 Method

The project, which is mainly a non-linear FEA of an end-restrained element subjected to pure tension, is carried out in several phases. The first phase is a review phase, which is followed by an analytical phase, a numerical phase and a result phase.

The purpose of the review phase is to obtain a deep understanding of the theory behind the subject. To obtain that, relevant investigations regarding the subject are reviewed, including experimental results. A comparison between the background of the calculation models, such as EC 2, is included in this phase as well.

The review phase is followed by the numerical phase and then an analytical phase, where a concrete element with both external and internal restraints is studied. A clamped reinforced element, as the one shown in figure 1.1a, is considered.

The clamped element is modelled as a three-dimensional element in the software DIANA, where a non-linear FEA is performed. The variable input parameters used in the hand calculations are set to the same values here to obtain comparable results. Before running the analysis, some material behaviour, such as the bond-slip relationship between concrete and reinforcement, is defined.

Further on, the element is studied analytically in terms of effective area based on the expressions presented in the Eurocode (EC). In addition, analytical calculations of transmission length are performed based on the output regarding steel stress in DIANA. The purpose of performing analytical calculations is to evaluate whether the numerical results correlate with the theory described by Engström (2014).

In the results phase, post-processing of FEA results is performed to obtain results that can be more easily evaluated. These results are discussed and compared with the analytical results. The final conclusions are then visualised and presented. Finally, a comparison of all obtained results is made.

1.6 Outline of thesis

This thesis aims to be structured in a way that gives a clear overview of the project in chronological order. Since some issues were encountered during the analysis phase, one exception from the chronological order is made where some extra material and discussions from the analysis phase regarding the Finite Element (FE) modelling in DIANA are included in the last chapter.

The first part of the report, chapter 2, covers some background theory and gives the reader a brief introduction to the topic. Secondly, chapters 3, 4 and 5 introduce the study and give detailed information about how the study is performed.

In chapter 6, the results from both the non-linear FEA and analytical study are presented and interpreted. This is followed by a discussion of the results and conclusions in chapters 7 and 9, respectively.

Finally, in chapter 8, the issues encountered in the numerical study are presented and discussed. Additionally, some results and conclusions are presented regarding how different input parameters can affect the possibilities of convergence in a non-linear FEA in DIANA.

1.7 Use of Artificial Intelligence

Artificial Intelligence (AI) is a powerful tool that, in many aspects, can be a helpful tool for performing a master's thesis. In this thesis, it has been used during the analysis phase, finding programming errors and ideas of underlying reasons for convergence issues. Furthermore, input from AI regarding spelling and grammar has been considered. All usage of AI has been reviewed by the authors of this thesis, since it is important to keep in mind that AI can not be assumed as a reliable source and should be used in addition to human skills, not as a substitute.

2

Theory

The following chapter presents background theory regarding reinforced concrete. Other topics being covered are, for example, restraint elements, cracking behaviour and modelling of effective area in EC 2.

2.1 Materials

This section focuses on the material properties of steel and concrete, as well as reinforced concrete members. For example, stress-strain relationships and how the materials can be modelled in a simplified manner are discussed.

2.1.1 Concrete

An important property of concrete is the non-linear relationship between stress, σ, and strain, ε. Especially important is the low tensile strength indicated in the stress-strain relationship in figure 2.1, which schematically illustrates the material law for concrete. The low tensile strength of concrete is a critical property that is important to consider since it may lead to cracking, which is irreversible plastic deformations that affect the stiffness and load-carrying capacity of a member. Since this Thesis focuses on the cracking behaviour of concrete members, tensile behaviour is a key material property and is therefore further described in this section.

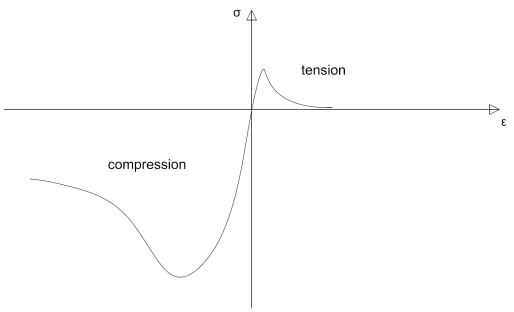

Figure 2.1: Stress-strain relationship for concrete. The graph illustrates the low tensile capacity in comparison to the capacity in compression (created by authors).

2.1.1.1 Tensile behaviour

The maximum stress that a plain concrete member can carry before cracking is referred to as the tensile strength, f_{ct}. Since variations in the composition of the material may occur within one strength class, it is beneficial to use a normal distribution function to describe the tensile strength. In figure 2.2, the distribution of the tensile strength is illustrated, where both the mean value and the 5% and 95% percentiles are indicated. The upper and lower percentiles are referred to as characteristic values. It is important to distinguish between these values and when they should be used. When designing structures to avoid cracks, the lower characteristic value, $f_{ctk0.05}$, should be used, (Engström, 2014). When evaluating restraint forces based on cracking, the upper characteristic value, $f_{ctk0.95}$, is more suitable. The mean value, f_{ctm}, is preferably used when aiming for a behaviour that corresponds best to the average.

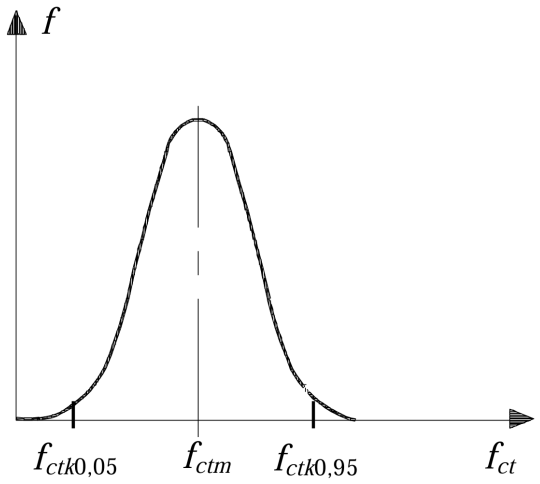

Figure 2.2: Schematic illustration of the mean and the characteristic values for concrete tensile strength according to Engström (2014).

2.1.1.2 Non-linear tensile behaviour and fracture energy

Looking more closely into the tensile part of the stress-strain relation for concrete, it can be noticed that it is mainly defined by the post-cracking behaviour. This occurs after the tensile capacity, f_{ct}, is reached and is further described in section 2.3. In figure 2.3, a typical stress-elongation relationship for a prismatic element subjected to uniaxial tensile elongation is illustrated, together with the corresponding relationship between concrete stress and crack width, referred to as the softening curve. At the maximum stress, micro-cracking starts. When the stress reaches a value of zero again, a fully opened macro-crack is created, corresponding to a specific crack width. Between these two points, the total deformation can be obtained by summing up the crack width, elastic elongation and eventually plastic elongation. After unloading, the reversible elastic strains disappear, and the remaining deformation is equal to the crack width. The area under the relation between stress and crack width represents

the fracture energy of the process, i.e. the corresponding energy required to form a fully opened crack (Plos, 2000).

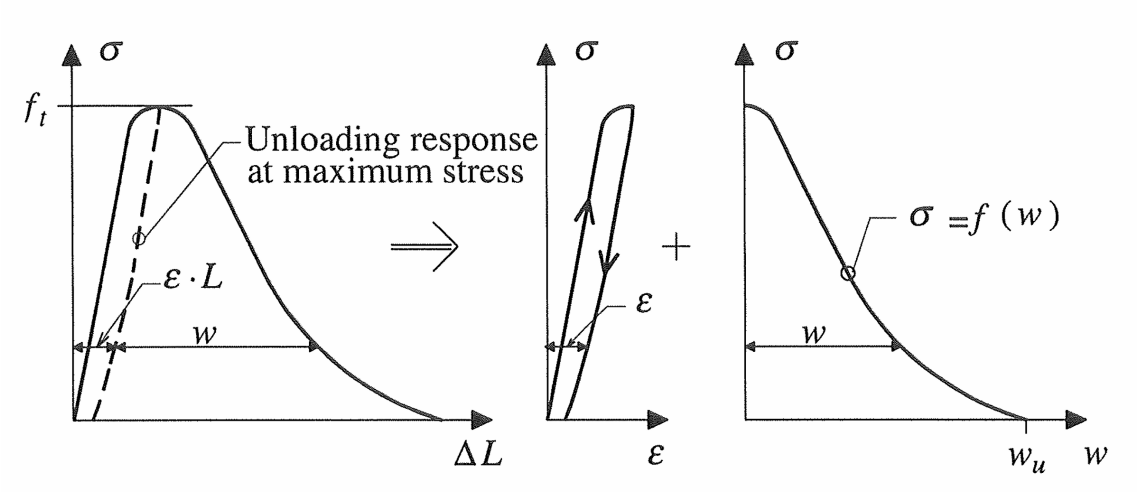

Figure 2.3: Tensile stress–strain relationship and stress–crack width relationship for concrete according to Plos (2000)[1].

[1]The tensile strength f_{ct} is here indicated with f_t only.

2.1.2 Steel

Steel is an isotropic material and can be linearly described in both compression and tension within the elastic region, if instability phenomena are disregarded. After yielding, the stress-strain relationship differs depending on the steel type, but a conservative simplification applicable to all steel types can be used. An illustration of such a stress-strain relationship is shown in figure 2.4.A common way of modelling this is with a linear stress-strain relationship until the dimensioning value of the yield stress, f_{yd}, is reached, as shown with the continuos line. Post-yielding capacity due to hardening is also modelled linearly, but with significantly decreased stiffness, until failure.

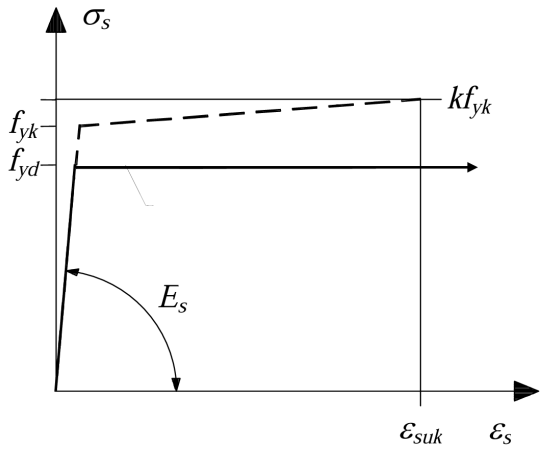

Figure 2.4: Simplified stress-strain relationship for steel according to Al-Emrani et al. (2019).

2.2 Reinforced concrete

Reinforcement increases the load-carrying capacity of concrete since it carries tensile stresses after cracking. By combining two materials with different properties, additional effects, apart from an increased capacity, are introduced. The influence of these different properties, such as tensile strength and need for movement, is further discussed in this section. Furthermore, the interaction between the two materials is described.

2.2.1 Stresses in reinforced concrete

To understand the principle of how steel and reinforcement interact, the stresses in a thin, continuous reinforced concrete member loaded at the reinforcement ends are studied. The concrete, steel, and bond stresses for such an element are shown in figure 2.5. It can be noticed that no bond takes place in the region closest to the loaded edges, due to local concrete cone failure. As the load is applied to the ends of the reinforcement, there is, on both sides of the member, a transmission length, l_t,

where the steel stresses are transferred to the concrete through bond, and strains differ between the materials accordingly (Engström, 2014). After a certain length, the strains become equal, and full interaction is reached. For a thin member, the maximum concrete stress is constant within the entire region where full interaction takes place and therefore, potential cracks appear somewhere in that region.

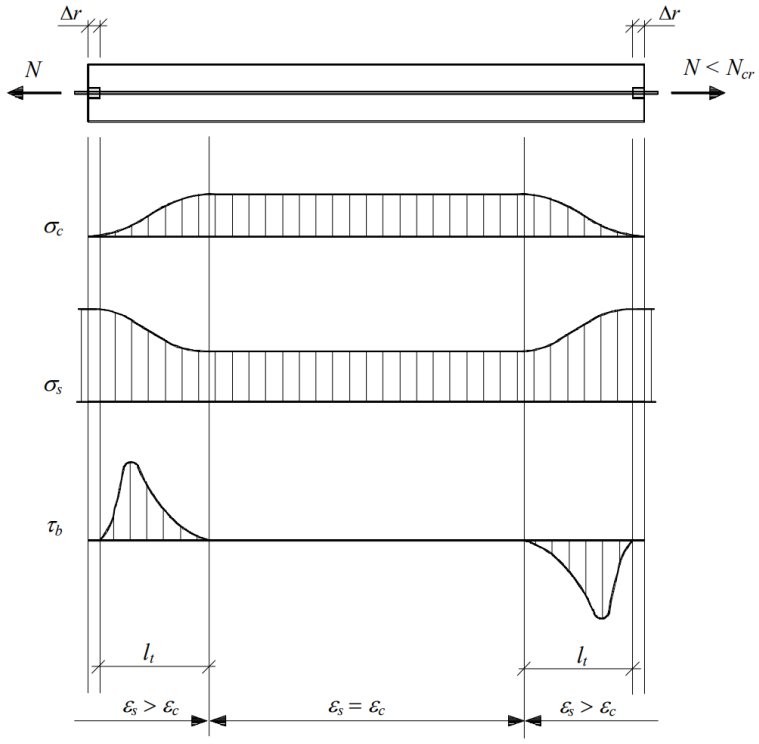

Figure 2.5: Stresses within a thin reinforced concrete member (Engström, 2014). The figure shows the concrete stress, σ_c, the steel stress, σ_s, and the bond stress, τ_b, and how they develop over the transmission length.

2.2.1.1 Bond-slip relationship

Bond stresses, τ_b, refer to shear stresses between concrete and reinforcement in regions where full interaction between the materials does not occur (Engström, 2014). This takes place within the transmission length, either close to the edges of an uncracked specimen where stresses are applied to the reinforcement only, or close to a crack in a cracked specimen, see τ_b in figure 2.5.

Because of the non-rigid behaviour of the materials, bond stresses, τ_b, are associated with a corresponding displacement, referred to as slip, s. This can be expressed as a certain bond-slip relationship, and is, for example, described in Model Code 2020 by International Federation for Structural Concrete (Fib) (2022). This is a non-linear relationship, and plastic deformations in the bond between steel and concrete may occur. Two failure modes can be observed: pull-out or splitting. The relationship between bond stress and slip differs accordingly. For well-confined concrete, pull-out is considered to be the main failure mode for the bond stresses. In figure 2.6, the

bond-slip relationships are shown.

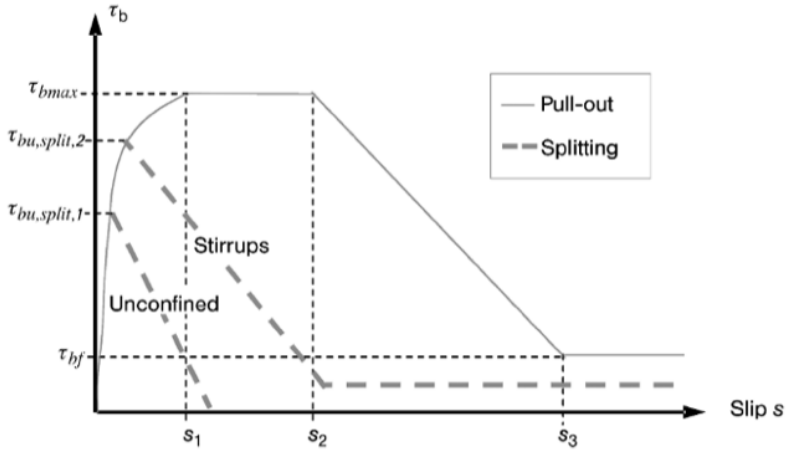

Figure 2.6: Bond-slip relationship according to Model Code 2020. Reproduced from fib Model Code for Concrete Structures (2020), page 307 - " Figure 20.5.1 Analytical bond-slip relationship (monotonic loading)" with permission from the International Federation for Structural Concrete (fib).

According to Engström (2014), the most relevant part of the bond-slip relationship in Serviceability limit state (SLS) is the one valid for $s < s_1$, since the value of s_1 is usually not exceeded in that state. Engström (2014) presents the expression in equation 2.2 for the first branch of the bond-slip relationship while the expression according to International Federation for Structural Concrete (Fib) (2022) is stated in equation 2.2.

$$\tau_b = 0.22 f_{ctm} \cdot \left(\frac{s}{s_1}\right)^{0.2} \tag{2.1}$$

$$\tau_b = \tau_{b.max} \cdot \left(\frac{s}{s_1}\right)^{\alpha} \quad \text{with} \quad \tau_{b.max} = 2.5 \cdot \sqrt{f_{cm}} \quad \text{and} \quad \alpha = 0.4 \tag{2.2}$$

where f_{ctm}, f_{cm}, s_1 and α are parameters depending on what type of reinforcement and concrete mix is being used.

2.2.1.2 Stresses in thick and thin members

For thick members, stresses are transferred between steel and concrete through bond, as well. But the situation described for thin members in figure 2.5 is not directly applicable to thick members. However, it gives a good illustration of how the exchange of stresses in a reinforced concrete element behaves over its length. For thin members, where the length is large compared to the thickness, it is assumed that the concrete stress is uniformly distributed at the end of the transmission length (Engström, 2014). On the other hand, for thick members, where the thickness has a larger impact on the behaviour, it cannot be assumed.

In addition to the transmission length, where stresses are transferred from steel to concrete, the dispersion of stresses over the concrete cross-section needs to be considered for thick members, which is often referred to as a discontinuity zone. As a combination of these two phenomena, a section of maximum concrete stress takes place within the transmission length. This behaviour is illustrated in figure 2.7 and 2.8.

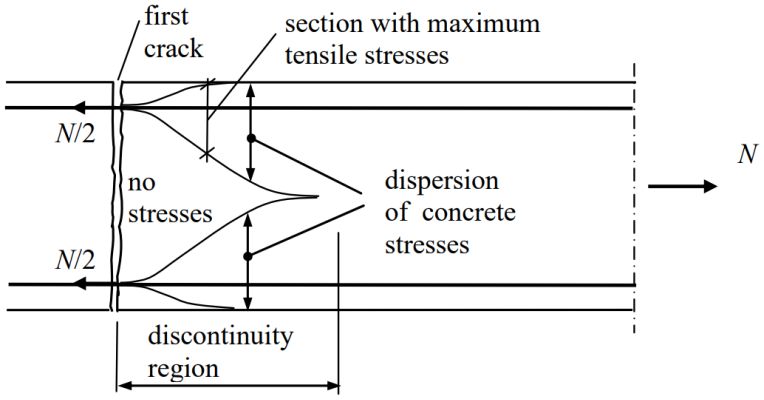

Figure 2.7: Illustration of the stress redistribution that takes place from the steel to the concrete within a through crack, where a discontinuity zone as well as a section of maximum tensile stresses can be seen (Engström, 2014).

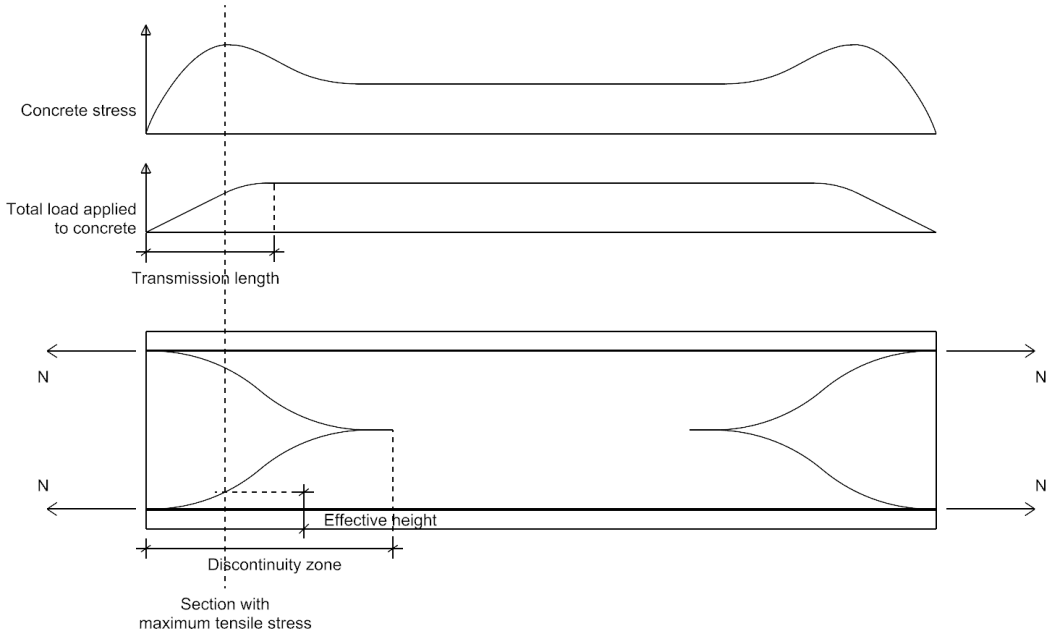

Figure 2.8: Schematic illustration of concrete stress and maximum tensile stress section in a thick member. The combination of a non-uniform stress distribution in the concrete and the transmission length generates a section with maximum tensile stresses (created by the authors).

This section of concentrated stresses within this discontinuity zone implies a higher risk for the next crack to take place there. The corresponding area of this section of concentrated stresses is therefore an important parameter for crack calculations and is referred to as the effective area (Engström, 2014). Since this section of concentrated stresses occurs only in thick members, the concept of an effective area consequently also arises in thick members only. There is no clear definition, though, of what elements geometries are expected to behave as thick members without studying the structural response.

2.2.2 Deformations in reinforced concrete

Deformation is often discussed in terms of relative displacement, commonly referred to as strain, ϵ. In reinforced concrete, the strains might differ due to different properties and behaviour between steel and concrete (Engström, 2014). Different actions cause two different types of strains, and it is important to distinguish between stress-dependent and stress-independent ones.

2.2.2.1 Stress-dependent strains

Stress-dependent strains are deformations that appear when the material is subjected to stress, for example, from an externally applied load (Engström, 2014). In the case of stress-dependent strains, compression results in shortening of the material and tension results in elongation. Two types of stress-dependent strains might occur in a specimen: elastic and viscoelastic strains. The elastic strains occur instantaneously with stress application, and viscoelastic strains mainly refer to creep deformations that develop over time.

2.2.2.2 Stress-independent strains

Stress-independent strains are the need for movement caused by other actions not related to stress. Examples of such movements are shrinkage and thermal deformation.

Shrinkage takes place in the concrete and refers to a change in size, usually shortening, of an element (Engström, 2014). Shrinkage is initiated during the hardening process and develops over a long time, but significantly faster in the beginning. Two types of shrinkage can be noticed. Drying shrinkage refers to the shortening that occurs when concrete releases water to the surrounding, less humid environment. The other type of shrinkage, autogenous shrinkage, is related to the chemical cement hydration process. In general, drying shrinkage takes place adjacent to faces exposed to the surrounding environment, while autogenous shrinkage is of higher importance in the middle of an element. The total shrinkage strain, ε_{cs}, at a certain time, t, after casting can be calculated as the sum of drying shrinkage, ε_{cd}, and autogenous shrinkage, ε_{ca}, according to equation 2.3 (Engström, 2014).

$$\varepsilon_{cs}(t) = \varepsilon_{cd}(t) + \varepsilon_{ca}(t) \tag{2.3}$$

The other common type of stress-independent strain, thermal expansion, refers to elongation caused by an increase in temperature. The thermal expansion strain, ε_{cT}, can be defined as a product of the coefficient of thermal expansion, α_{cT} and the temperature change, ΔT, see equation 2.4 (Engström, 2014). A member can be subjected to a uniform or non-uniform temperature distribution, resulting in different strains within the cross-section Engström (2015). Figure 2.9 shows examples of different thermal gradients and the associated strains. Thermal strains take place in both concrete and reinforcement, but due to different expansion coefficients, the elongation or shortening differs, which leads to internal stresses. However, these stresses can often be neglected because of their small sizes.

$$\varepsilon_{cT} = \alpha_{cT} \cdot \Delta T \tag{2.4}$$

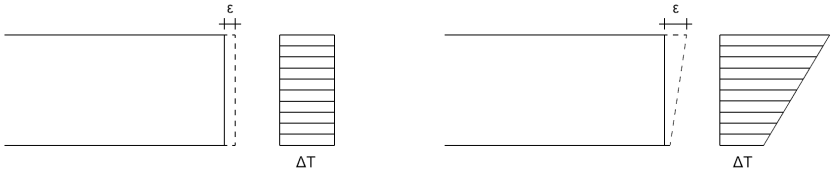

Figure 2.9: Illustration of temperature gradients and their corresponding thermal expansion strains (created by the authors).

2.3 Cracking in reinforced concrete

Due to the low tensile capacity of concrete, even small tensile stresses introduce a risk of cracking. The cracking process in a reinforced concrete member differs slightly from the plain concrete cracking process and is described in this section.

2.3.1 Cracking stages

The cracking process of a reinforced concrete member can be divided into three main stages. In figure 2.10, those stages are illustrated in a graph. Before cracking, the behaviour of the member is described with a linear model in state I, which means that the section is uncracked and that any influence of reinforcement can usually be neglected (Al-Emrani et al., 2011). When the load reaches the critical cracking load, N_{cr}, i.e. the stress in the concrete equals the tensile capacity, crack formation is initiated.

When the cracking process stops and the member is fully cracked, a state II model is used to describe the behaviour. For the model of state II, linear behaviour is still assumed, but the stiffness is significantly reduced due to cracking (Al-Emrani et al., 2011). As a conservative approximation, the cross-sectional capacity for parts subjected to tension is reduced to the capacity of reinforcement bars in the model for state II.

The graphs in figure 2.10 show the response of a section related to the state I and II model after crack initiation. To the left, the real behaviour is schematically illustrated, while the simplified model is illustrated to the right, clarifying the dramatic change between the states. In other words, the model in state II underestimates the reality, especially during the early crack formation phase. In a cracked section, there is still uncracked concrete contributing to the overall stiffness as well as the transfer of stresses. This additional capacity in the cracked section, compared to the model in state II, is referred to as tension stiffening. In reality, the total stiffness of the section is equal to the sum of the contributions from steel and the uncracked concrete between cracks. However, in the state II model, the stiffness contribution from the uncracked concrete is neglected, and the total stiffness of the section is therefore underestimated (Engström, 2015).

In the case of tensile stresses caused by an external load, the magnitude of the load remains unchanged during cracking. For that reason, the cracking process continues until stabilised cracking is reached, meaning that no more cracks are created and the section can be considered as fully cracked (Engström, 2014). Hence, an increase in load when stabilised cracking is reached leads to wider cracks only.

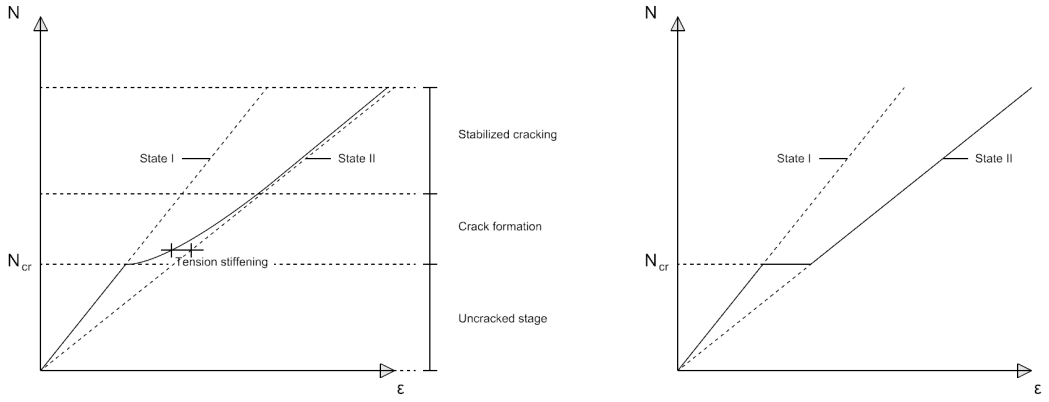

Figure 2.10: Cracking stages in reinforced concrete, based on the theory described by Engström (2014) (created by the authors).

2.3.2 Detailed post-cracking behaviour

After cracking, reinforcement plays an important role, since cracked concrete no longer carries any stress. Instead, the reinforcement bars transfer all the tensile stresses within the cracks (Engström, 2014). To reach compatibility between the materials in the surroundings of a crack, a transmission length is needed, where the transfer of bond stresses occurs. New transmission zones on each side of the crack are then formed, and each segment of uncracked concrete between through cracks can be seen as a separate element described in section 2.2.1, where a crack acts as an end section with the load applied to the reinforcement.

In figure 2.11, the evolution of stresses during the crack formation process for a thin member can be seen. The growth of cracks takes place within the region where the

stress reaches the tensile strength (Engström, 2014), meaning that each new crack is formed somewhere between two already created ones. At one point, the distance between all formed cracks is shorter than twice the transmission length, and no more cracks can be formed. Stabilised cracking is then reached, and further loading only results in widening of existing cracks.

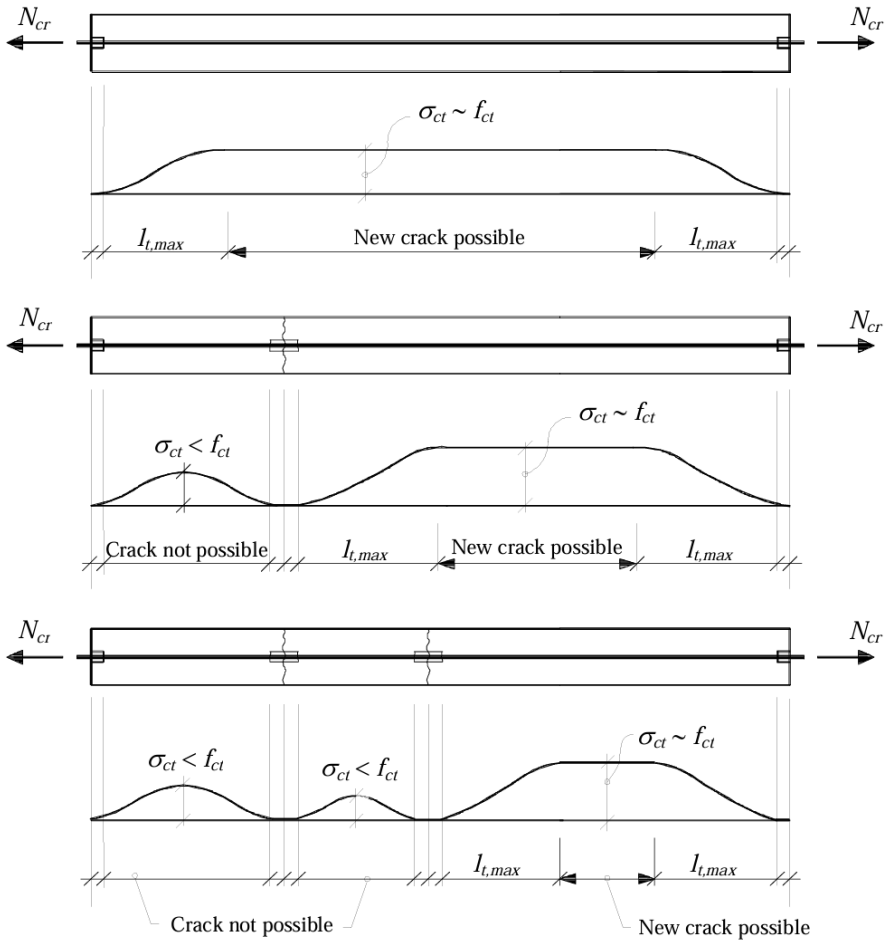

Figure 2.11: Concrete stresses development and formation of cracks during the cracking process for a thin concrete member (Engström, 2014).

On the other hand, for a thick member, the first crack is a through crack, while the following ones only take place within the effective area. The pattern of crack formation also differs, as a result of the discontinuity zone and section with maximum stresses discussed in section 2.2.1.2. As mentioned, the maximum stress appears at a certain distance from the last formed crack, and therefore, the next crack appears there. The cracking process continues stepwise outwards from the first crack, as shown in figure 2.12. The resulting crack pattern is evenly distributed, but for cases where stabilised cracking is not reached, cracking stops before the entire specimen is covered with cracks.

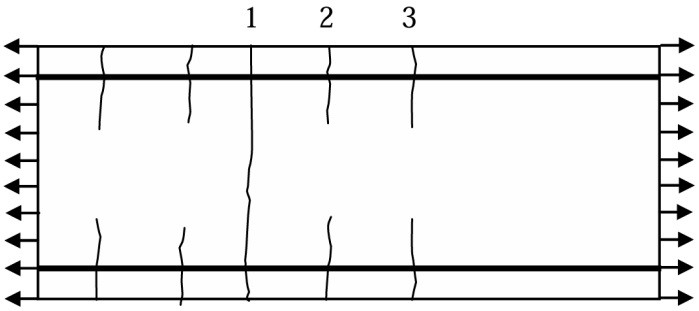

Figure 2.12: Order of crack-formation for a thick concrete member (Engström, 2014).

2.4 Cracking in restrained reinforced concrete

A concrete element can be subjected to a phenomenon called restraint. Restraint is defined as the prevention of movement. As a consequence, stress-independent strains such as shrinkage and thermal expansion lead to stresses in restrained elements (Engström, 2014). In a reinforced concrete member, two types of restraints can take place: internal and external.

2.4.1 Internal restraint

Internal restraint is restraint that takes place inside the element when the concrete and steel are subjected to different stress-independent strains (Engström, 2014). If shortening is larger for the concrete compared to the reinforcement, as in the case of shrinkage, the need for compatibility leads to tensile stresses in the concrete, applied by the reinforcement. Because of these tensile stresses, the risk of cracking arises. The need for movements in the steel and concrete in relation to the actual imposed strain of the composite member is illustrated in figure 2.13.

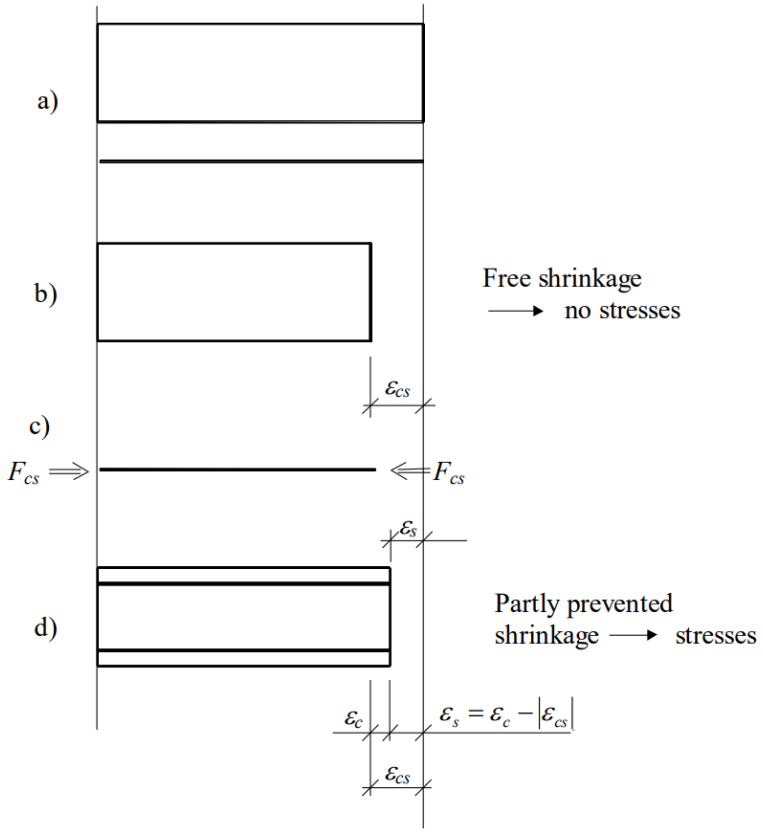

Figure 2.13: Illustration of the need for movements in a reinforced concrete member according to Engström (2014).

2.4.2 External restraint

External restraint is caused by the prevention of movements along the edges of an element (Engström, 2014). Figure 2.14 illustrates two typical cases of external restraint. In figure 2.14a, where an end-restrained element is shown, the restraint is uniformly distributed over the height. For the bottom restrained wall in figure 2.14b, the distribution varies along the height. To what extent an element is fixed is sufficiently described by an external restraint degree.

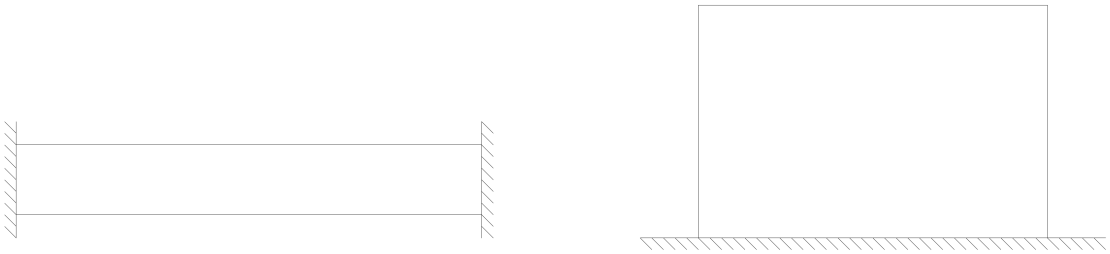

(a) End-restraint. **(b)** Wall with bottom restraint.

Figure 2.14: Illustration of two types of external restraint (created by the authors).

2.4.3 Restraint degree

A restraint degree, R, can be used to describe the amount of movement that is prevented and is, according to Engström (2014), formulated as the actual imposed strain, $\varepsilon_{\text{actual}}$, divided by the imposed elongation, in the case of full restraint, $\varepsilon_{\text{full restraint}}$. This is stated in equation 2.5 below.

$$R = \frac{\varepsilon_{\text{actual}}}{\varepsilon_{\text{full restraint}}} \tag{2.5}$$

The restraint degree depends on both internal and external restraint and can therefore be referred to as R_{tot}. To describe restraint applied by boundary conditions only, the external restraint degree, R_{ext}, is used. In case of full restraint, the external restraint degree, $R_{\text{ext}} = 1$, which applies to structures like 2.14a, where ends are completely fixed. In case of non-rigid end supports, the structure is partly restrained, and the external restraint degree is somewhere in the range $R_{\text{ext}} \in [0, 1]$. For the restrained wall in 2.14b, the external restraint degree varies according to figure 2.15.

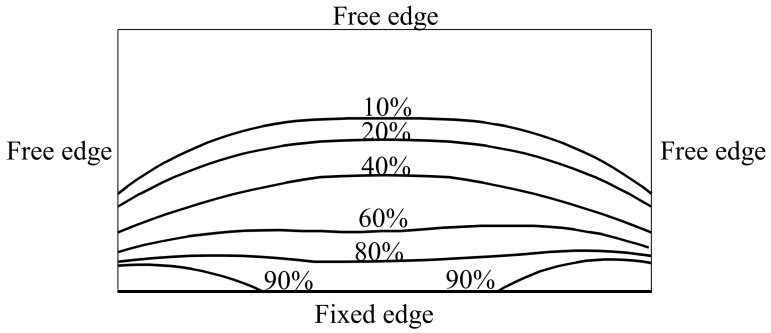

Figure 2.15: Restraint degree, here given in percentage, in a bottom-restrained wall element according to Engström (2014)

.

2.4.4 Restraint cracking

As discussed in section 2.3.1, the magnitude of an external load is not affected by cracking, and the process continues until stabilised cracking is reached. For restrained elements where the developed tensile stresses depend on the prevented stress-independent strains, and the corresponding restraint force depends on the stiffness of the section, the process often stops before this stabilised stage. For every created crack, the stiffness is reduced, implying a decrease in the restraint force. In addition, the deformation of each crack cancels out some of the needed deformation caused by the stress-independent strain (Engström, 2014). This means that for a restrained element, the cracking process stops either when the restraint force no longer reaches the critical cracking load due to reduced element stiffness, or when stabilised cracking is reached (Engström, 2014). Since the process stops by one of these conditions independently, stabilised cracking is not always reached for restrained elements. This is one of the main reasons why the provided models

for effective area in EC 2 are not fully applicable to restrained elements (Caldentey et al., 2022).

2.5 Effective area according to EC 2

The effective area, $A_{c,eff}$, describes where the next crack most probably takes place and is therefore a fundamental parameter in calculations regarding the cracking behaviour of a reinforced concrete element. As introduced in section 2.2.1.2, the effective area is a way of modelling the area around reinforcement bars subjected to concentrated tensile stresses and applies to situations where uniform stress distribution in a member cannot be assumed. This area mainly depends on reinforcement properties and layouts. In figure 2.16, a schematic illustration of tensile areas around reinforcement bars is given. The areas are two ways of illustrating the effective area that a single bar covers, and how the areas overlap with each other. The squares are more aligned with the definition in EC and can be seen as a simplification of the circular, more realistic case. Overlapping of areas determines whether the bars should be handled as a group of bars or isolated bars, according to figure 2.18. Calculation models for the effective area are presented in EC 2, where old and new versions given by European Committee for Standardization (CEN) (2005) and European Committee for Standardization (CEN) (2023) slightly differ.

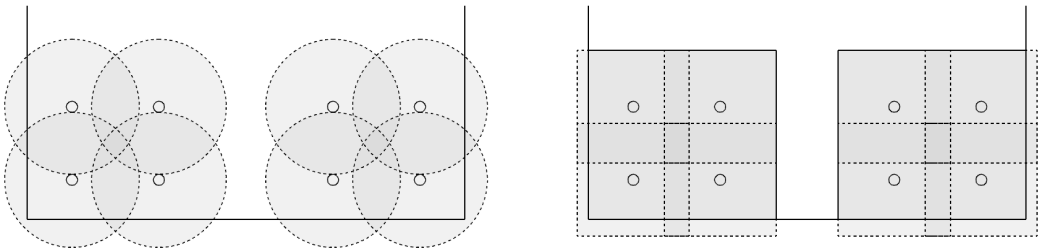

Figure 2.16: Schematic illustration of areas subjected to tension and effective areas in reinforced concrete sections (created by the authors).

2.5.1 Old version of EC 2

European Committee for Standardization (CEN) (2005) presents in the old EC 2, the expression in equation 2.6 to evaluate the effective height, $h_{c,eff}$. The corresponding effective area can be obtained by multiplying the effective height by the total width, b, of the section. The definition of included parameters and illustration of effective areas for the three defined elements are shown in figure 2.17.

The effective height, $h_{c,eff}$, is defined, independently of the member type, according to equation 2.6, where the three expressions refer to different limiting parameters and the smallest value is used as $h_{c,eff}$ to ensure a conservative choice (European Committee for Standardization (CEN), 2005). The expression $2,5(h-d)$ refers to a scaled value of the cover thickness. The second term accounts for variation of

stresses to ensure that the effective area is limited to the part of the section that is subjected to tension. Hence, this factor is relevant in flexure elements (Caldentey et al., 2022). The third term limits the effective height to half of the available section, which ensures the effective area does not exceed the cross-section area for members subjected to tension. In that case, considering an effective height as half of the cross-section is equal to considering the entire cross-section as the effective area.

For this Thesis, the relevant element is the one annotated with c), member in tension. Limiting the equation below to case c means that the value of the compression zone, x, reaches an infinitely large negative value. Therefore, the middle term in the expression is not relevant for members in tension.

$$h_{c,eff} = \min\left(\left[2,5(h-d),\ \frac{h-x}{3},\ \frac{h}{2}\right]\right) \tag{2.6}$$

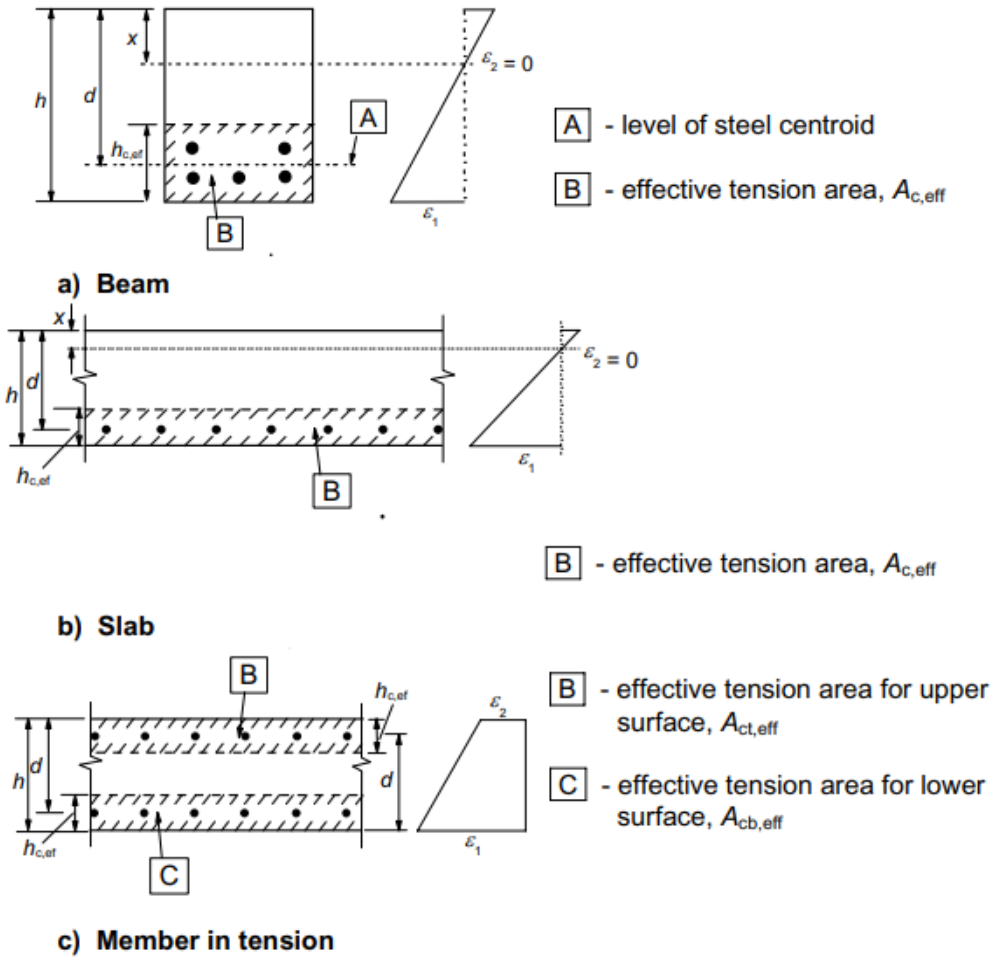

Figure 2.17: Effective area according to the old version of EC 2 (European Committee for Standardization (CEN), 2005). The figure is retrieved from SS-EN 1992-1-1:2005 and is reproduced with permission from SIS, Swedish Institute for Standards, who also offer the standard www.sis.se

2.5.2 New version of EC 2

In the new EC 2, multiple expressions that define the effective area are given according to European Committee for Standardization (CEN) (2023). In addition to the effective height, $h_{c,eff}$, the effective width, $b_{c,eff}$, is included. This version also gives two possibilities of how the effective area is distributed, either isolated areas around every single bar or overlapping areas as a group of bars. The different types of elements covered by this standard are shown in figure 2.18, where the element annotated with e) is the relevant one for this thesis. Hence, the applicable formulas are stated in equation 2.7 and 2.8 and are formulated in similar ways for both $h_{c,eff}$ and $b_{c,eff}$ (European Committee for Standardization (CEN), 2023).

$$h_{c,eff} = \min\left([a_y + 5\phi,\ 10\phi,\ 3.5a_y,\ 0.5h]\right) \tag{2.7}$$

$$b_{c,eff} = \min\left([a_x + 5\phi,\ 10\phi,\ 3.5a_x,\ 0.5b]\right) \tag{2.8}$$

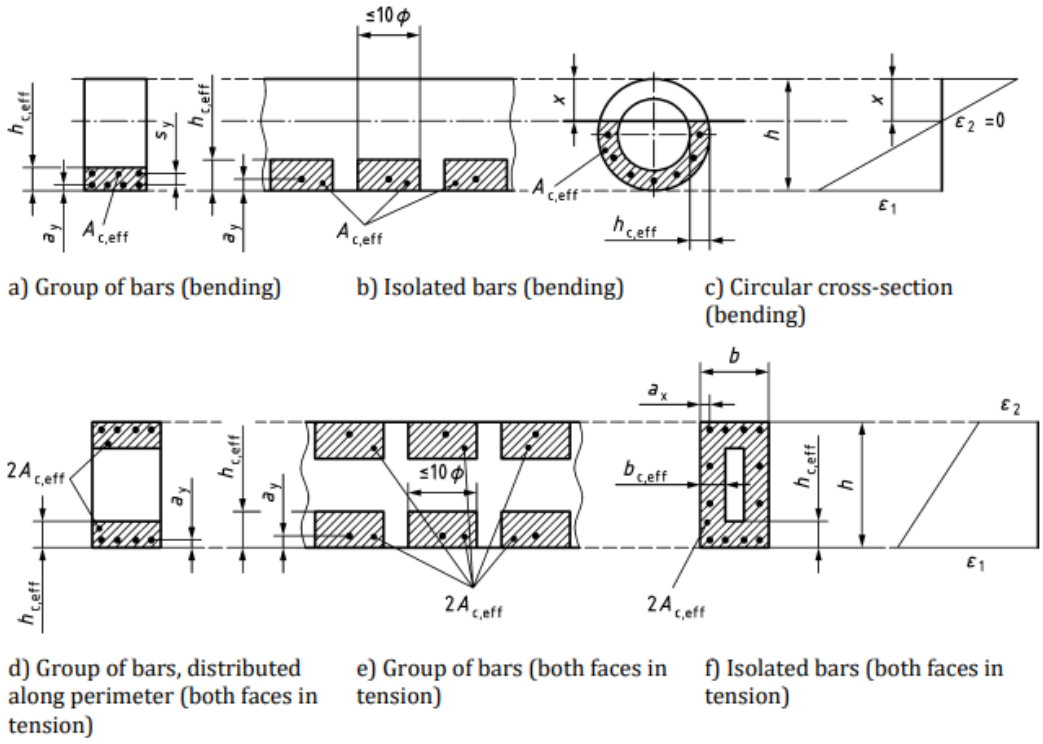

Figure 2.18: Effective area according to the new EC 2 (European Committee for Standardization (CEN), 2023). The figure is retrieved from SS-EN 1992-1-1:2023 and is reproduced with permission from SIS, Swedish Institute for Standards, which also offers the standard www.sis.se

The background to the terms in the expressions for both $h_{c,eff}$ and $b_{c,eff}$ is described by Caldentey et al. (2022). The second term represents the largest area that a single bar can transfer stresses to and is given as a multiple of the bar diameter.

The third term accounts for the cover thickness, i.e. the available space of plain concrete between the bar and the edge of the element. Furthermore, the first term is introduced as a combination of the second and third terms to account for the cases when the multiple value of the bar diameter,ϕ, exceeds the cover thickness. The multiple of ϕ then limits the area inside the reinforcement bar, and the cover thickness limits on the outside. The fourth term limits the effective height for the same reason as explained for the old EC 2. For the effective base in case e, the element width, b, is not defined in figure 2.18. This opens up for a misunderstanding where the user has to interpret the input to the formulas. For case e, the width should be equal to 2 times the bar spacing, s, to restrict the effective area to the distance between the bars. Accordingly, for a bar adjacent to an edge, the effective width may need to be restricted by half the bar spacing, $s/2$, on the inner side and the cover thickness on the outer side.

2.5.3 Comparison of old and new versions of EC 2

One difference between the two versions of EC 2 is that the new EC presents more cases where the effective area is applicable, making the model more general. Beam, slab and tension member cases are included in both versions. The new model additionally provides definitions for a group of bars and isolated bars, cases b and e in figure 2.18.

Comparing the relevant case for this thesis, one main difference is that the new model accounts for the bar diameter. By restricting the effective area to 10ϕ, the possibility of having isolated bars is introduced, depending on whether the distance of 10ϕ overlaps between bars or not. Additionally, an expression for the effective base is presented in the new standard. By limiting the effective area with a multiple value of the bar diameter, cases with unrealistic big effective areas are avoided (Caldentey et al., 2022). Since this is applied to both $h_{c,eff}$ and $b_{c,eff}$, large bar spacing may lead to several effective areas adjacent to each bar if the tension zones do not overlap, as can be seen in figure 2.18. As a consequence, the effective area might be reduced to a more accurate value.

The removed expression $2.5(h-x)$ used in the old EC 2 is originally a term accounting for the relation between curvature and cracking behaviour (Caldentey et al., 2022). According to Engström (2014), curvature is a measure of bending in an element and can be defined as the strain gradient in the cross-section. Curvature plays an important role, but it is rather the stress gradient within the effective area than the tension zone itself that matters. Therefore, the curvature is accounted for using a modified coefficient in the expression for crack spacing instead of limiting the effective area in the updated version. This eliminates the risk of obtaining an effective area where the bar is not included, in case of load cases resulting in small tension zones. However, this term is not relevant for members subjected to tension, as described in section 2.5.1.

Furthermore, the term limiting the effective height to half of the cross-section height remains unchanged, since limiting the effective area to the total cross-section area is

essential. The multiple factors accounting for cover thickness are also updated from 2.5 to 3.5 based on experimental results (Caldentey et al., 2022).

2.6 Other models defining effective area

Effective area is not only addressed in EC 2. It is also described in other documents, such as the standard code Model Code, provided by the International Federation for Structural Concrete, Fib.

2.6.1 CEB-FIP Model Code 1990

In the Model Code edition from 1990, presented by International Federation for Structural Concrete (Fib) (1998), the effective area is described according to figure 2.19. For this thesis, the element denoted with c in figure 2.19 is the relevant one. The effective height is defined as the minimum of $2.5(c + \phi/2)$ and $(h - x)/3$, which is the same as the expression given in the old EC 2, despite the fact that the effective height is not limited to $h/2$.

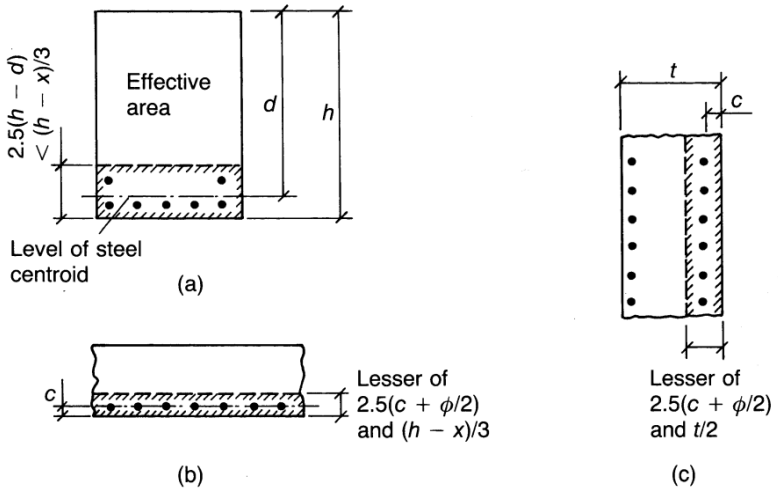

Figure 2.19: Effective area applicable for a beam, slab or a member in tension according to Model Code 1990 International Federation for Structural Concrete (Fib) (1998). Reproduced from CEB-FIP Model Code 1990: Design Code, page 250 - " Figure 7.4.2 Effective tension area: (a) beam, (b) slab, (c) member in tension" with permission from the International Federation for Structural Concrete (fib).

2.6.2 Model Code for Concrete Structures 2020

In Model Code 2020, International Federation for Structural Concrete (Fib) (2022) provides two models for calculating the effective area as well. One for a single bar and one for a group of bars applicable in the case of overlapping tension areas, as seen in

figure 2.20. The expressions for the effective height and base are given in equation 2.9 and 2.10 and are derived in the same way for the different directions (International Federation for Structural Concrete (Fib), 2022). The effective height also has an additional condition limiting $h_{c,eff}$ to the tension zone of the cross-section.

Depending on whether the bar spacing exceeds the available space between bars, the reinforcement bars are seen as single bars or as a group of bars. For a group of bars, the effective width is equal to the total width, and for single bars, the effective width of each section of effective area is defined according to equation 2.10. As the old Model Code is similar to the old EC 2, this version of Model Code is similar to the new EC 2 and accordingly, the limitation for the effective height to $h/2$ is not included.

$$h_{c,eff} = \min\left([r_y + 5\phi,\ 10\phi,\ 3.5r_y]\right) \leq h - x \tag{2.9}$$

$$b_{c,eff} = \min\left([r_x + 5\phi,\ 10\phi,\ 3.5r_x]\right) \tag{2.10}$$

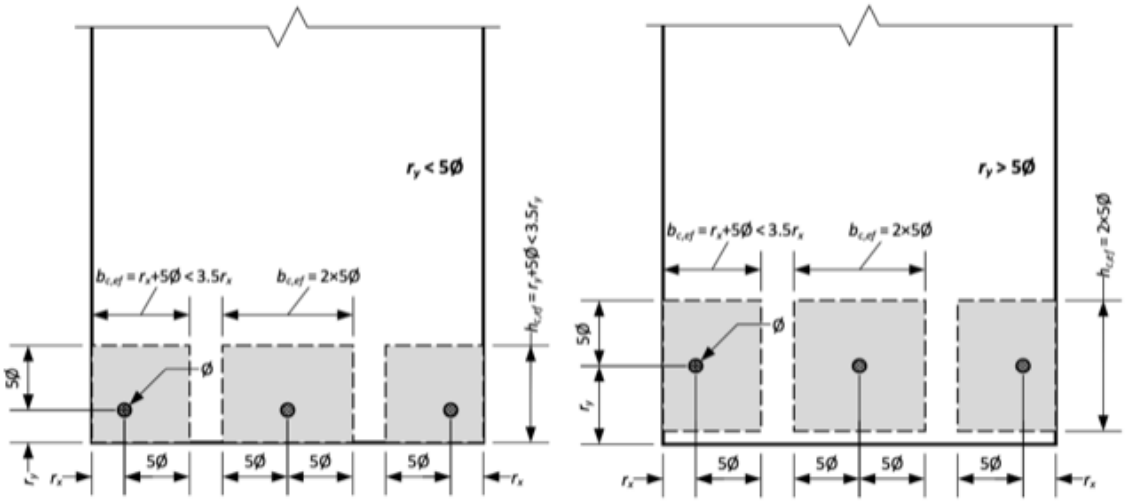

Figure 2.20: Effective area around a group of bars according to Model Code 2020 (International Federation for Structural Concrete (Fib), 2022). Reproduced from fib Model Code for Concrete Structures (2020), page 531 - " Figure 30.5.4 Effective tension area of concrete Ac,ef around a single bar (local concept)" with permission from the International Federation for Structural Concrete (fib).

3

Definition of the study

As this master's thesis aims to study how the definitions of effective area in the both versions of EC 2 are applicable to restrained elements, Finite Element Analyses for an end-restrained element with varying cross-section geometries were performed. In addition, an analytical study of the same cross-section geometries was carried out and compared with the results from FEA. The main parameters being evaluated and compared are effective area and transmission length. This chapter defines the performed study in detail regarding the geometry of the analysed structural element, as well as boundary conditions, loads and materials.

3.1 Structural element

In the following section, the studied structural element used for the analysis is presented. The same element, an end-restrained element loaded in pure tension, was used in both the FEA and the analytical study.

3.1.1 Boundary conditions and loads

In figure 3.1a, the studied structural element is illustrated, while figure 3.1b shows how the element is simplified for analysis, where L is the element length and T is the element thickness. The element is clamped, and the restraint degree is equal to 1, meaning the ends are totally fixed in the z-direction. For the study, the element is cut in its symmetry plane in the middle of its length. In that way, the analysed element illustrates an end-restrained member after the appearance of the first crack in the symmetry line. Cutting the full-length member in its symmetry line results in one edge modelled with rigid supports applied to both concrete and reinforcement, while the concrete at the opposite edge is free to move. In the symmetry line, i.e. the middle of the full-length clamped element, the reinforcement bars are loaded in tension.

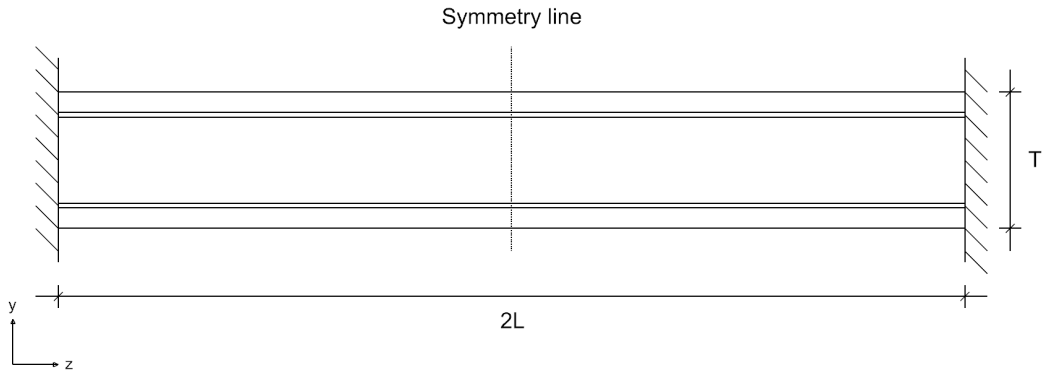

(a) The full-length element as it is modelled.

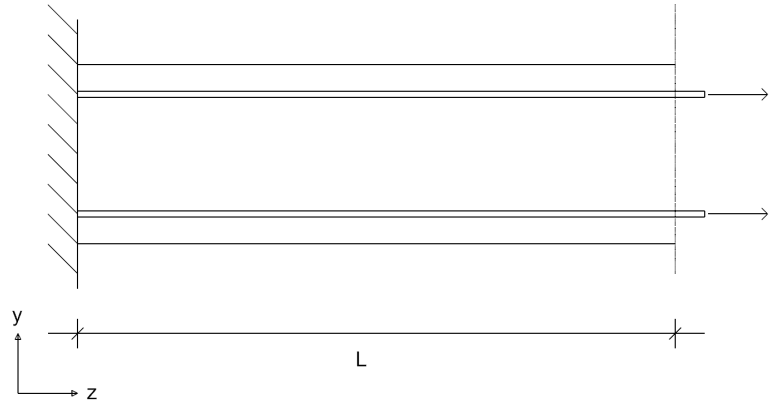

(b) The analysed section, which is a cut out of the full-length element.

Figure 3.1: The analysed section in relation to the full-length clamped element (created by the authors).

By modelling half of the element with the described boundary conditions and load, a cracked member is simulated. The load acting on the reinforcement at the free edge represents the situation within a crack, where the concrete no longer contributes to the transfer of stresses.

Loading the bars initiates the transfer of stresses via bond from the steel to the concrete. This transfer of stresses creates a discontinuity zone with a section of maximum tensile stresses, where the effective concrete area associated with each reinforcement bar contributes to carrying the stresses in the section. Therefore, the effective area can be evaluated accordingly.

Since a situation for a member in pure tension is of interest, any other load, such as self-weight, is neglected so that no bending takes place. Long-term effects were not considered in the analysis, since no certain lifetime for the element was considered. The influence of disregarding such effects is discussed in chapter 7.2.

Additionally, for the longitudinal edges in the yz-plane, symmetry boundary condi-

tions prescribing deformations in the normal direction were applied. In that way, a cut out from a wider element could be assumed.

3.2 Geometry

The cross-section of the analysed structural element can be seen in figure 3.2. The measurements of the cross section are illustrated in terms of bar spacing, s_x and s_y, cover thickness, c_x and c_y, bar diameter, ϕ, element width, B, element thickness, T, total concrete cross-section area, A_c, and total steel cross-section area, A_s. To perform a reliable study and draw accurate conclusions regarding in what manner the two calculation models for effective area apply to a restraint element, several geometries were examined and evaluated. In this section, both fixed and variable input parameters are presented.

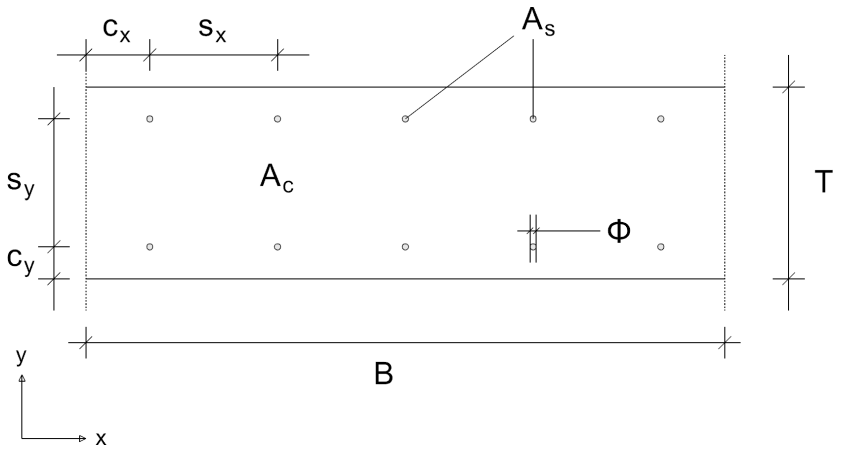

Figure 3.2: Illustration of the cross-section used in the analyses (created by the authors).

3.2.1 Fixed input parameters for geometry

During analysis, some main parameters regarding the geometry were kept constant. To the greatest possible extent, the geometry is kept constant, minimizing the cases to analyse. The length of the element was set to $L = 1$ m, since it, according to calculations of the transmission length, covers the interesting areas where transfer of stresses takes place.

The reinforcement is arranged with five bars along the width, $n_{bx} = 5$ in combination with one layer on each side of the thickness, $n_{by} = 2$. The cover thickness in the y-direction is kept constant as $c_y = 50$ mm. To reach similar results for all bars, independently of whether the bar is placed in the middle or at one edge, the cover thickness in the x-direction was set to be equal to half of the actual bar spacing in

the x-direction, $c_x = s_x/2$. In combination with the previously described boundary conditions in section 3.1, a simulation of a symmetry-cut out from a wider element is obtained.

3.2.2 Set of variable cross-sectional input parameters

The main difference between the models for the effective area in the both versions of EC 2 is the definition of isolated bars and groups of bars, depending on the ratio between bar diameter, ϕ and spacing, s, which further on is referred to as s-ϕ ratio. The defined value that distinguishes between the two cases, isolated bars and a group of bars, is when the bar spacing is equal to ten times the bar diameter, s=10ϕ, and therefore cases in the surrounding range are evaluated. These ratios are evaluated in the x-direction, i.e. along the width of the member, using the ratios expressed in equation 3.1.

$$s_x = [6, 8, 10, 12, 14]\phi \tag{3.1}$$

Obtaining different ratios was done in two ways: either by keeping the spacing constant and varying the diameter, or the other way around. These two methods are further referred to as study 1 and study 2.

Additionally, the behaviour in terms of cracking and effective area is closely dependent on the thickness of the element. For that reason, it is of interest to study the influence of the thickness on the behaviour. Two different bar spacings on the thickness, s_y, were therefore investigated in both studies. The thickness was either 0.3 or 0.5 m, depending on the ratio between bar diameter and spacing in the y-direction, as expressed in equation 3.2.

$$s_y = [10, 20]\phi \tag{3.2}$$

In the following sections, sets of variable input parameters regarding the cross-section geometry for both studies are presented. The same ratios between spacing and bar diameter, as well as the same thicknesses, are evaluated in both studies, but performed in different ways, as described above.

3.2.2.1 Study 1

In study 1, the bar spacing in the x-direction is kept constant at 200 mm. This also implies a constant width of 1 m. The bar diameter, ϕ, is defined as the spacing divided by the ratios specified in equation 3.1. The numerical values for the diameter is therefore in some of the cases equal to commonly used bar diameters in concrete structures, but to achieve consistent variation of s_x-ϕ ratio, some of them are not. Although the bar diameters used are not exactly the same as the standard sizes, it was reasoned that they still provide results representative of the range of commonly used diameters. For the thinner element, the ratio between the spacing and diameter

is satisfied both along the thickness and the width. For the thicker case, these ratios are only fulfilled along the width. In table 3.1, all the studied sets of variable inputs for study 1 are presented.

Table 3.1: Sets of variable input parameters for the cross-section geometry of the element in study 1.

ID:s	s_x **[mm]**	s_y **[mm]**	**Ratio** s_x **-** ϕ **[-]**	ϕ **[mm]**
1A	200	200	$s = 6\phi$	33
1B	200	200	$s = 8\phi$	25
1C	200	200	$s = 10\phi$	20
1D	200	200	$s = 12\phi$	17
1E	200	200	$s = 14\phi$	14
1F	200	400	$s = 6\phi$	33
1G	200	400	$s = 8\phi$	25
1H	200	400	$s = 10\phi$	20
1I	200	400	$s = 12\phi$	17
1J	200	400	$s = 14\phi$	14

3.2.2.2 Study 2

In study 2, the same ratios as previously described are evaluated, but with a constant bar diameter of $\phi = 20$ mm and a varying spacing in the x-direction. As for study 1, but for the diameter this time, the value should not influence the results. The diameter $\phi = 20$ mm is commonly found in similar structures and was deemed a reasonable choice. For this study, the width of the element varies, but the two different thicknesses are the same as for study 1. In table 3.2, all the studied sets of variable inputs for study 2 are presented.

Table 3.2: Sets of variable input parameters for the cross-section geometry of the element in study 2.

ID:s	ϕ **[mm]**	s_y **[mm]**	**Ratio** $s_x - \phi$ **[-]**	s_x **[mm]**
2A	20	200	$s = 6\phi$	120
2B	20	200	$s = 8\phi$	160
2C	20	200	$s = 10\phi$	200
2D	20	200	$s = 12\phi$	240
2E	20	200	$s = 14\phi$	280
2F	20	400	$s = 6\phi$	120
2G	20	400	$s = 8\phi$	160
2H	20	400	$s = 10\phi$	200
2I	20	400	$s = 12\phi$	240
2J	20	400	$s = 14\phi$	280

3.3 Material

The studied element is a composite member made of concrete and reinforcing steel. In the following section, each material is described, as well as the bond-slip interaction between them.

3.3.1 Concrete

The main material in the element is traditional concrete according to the classification provided in EC 2. For the study, concrete class C25 is taken. The behaviour regarding the effective area should not be noticeably influenced by concrete strength class, and therefore, a commonly used quality for similar elements seems to be a reasonable choice. Poisson's ratio, ν, for concrete is taken as 0.2. Parameters such as Young's modulus, E_{cm}, mean compressive strength, f_{cm}, and mean tensile strength, f_{ctm}, are generally evaluated according to equations presented by (Engström, 2014). The evaluation is described in more detail in appendix E. In the FEA, a linear concrete material model was considered, and for parameters evaluated by the FE software, equations presented by International Federation for Structural Concrete (Fib) (2010) were used. What parameters this regards and what consequences the use of linear material has are explained further in 4.1.2. The cracking capacity was evaluated using the mean tensile strength to obtain the most accurate representation of the average material behaviour.

3.3.2 Steel

All of the reinforcing steel class is of strength class B500B, motivated by the same argument as for the choice of concrete class. Young's modulus is considered to be $E_s = 200$ GPa, and Poisson's ratio is taken as $\nu = 0.2$.

3.3.3 Interaction modelled using a bond-slip relationship

To model the non-linear interaction between steel and concrete, a bond-slip relationship is used. For the analytical calculations, this is included in the used equations. Therefore, the bond-slip relationship used in FEA is chosen according to the same model as the equations used in the analytical calculations are based on. This was implemented with a user-defined bond-slip relationship, which is further described in section 4.1.2.

4

Definition of FE modelling in DIANA and post-processing of results

To evaluate whether the models presented for the effective area in EC 2 apply to restraint elements, a non-linear FEA using the software DIANA was performed according to the cases of interest described in chapter 3. To evaluate the behaviour of the effective area, three-dimensional stress distributions were studied for a structural member with linear concrete material and a non-linear interface between steel and reinforcement. Several analyses were performed for different cross-section geometries described in chapter 3, to investigate correlations between geometry and stress distributions, and evaluate how the cross-section geometry affects the effective area.

In this chapter, the FE modelling in DIANA, including post-processing of results, is explained. The model, in terms of geometry, boundary conditions, loads, and mesh size, is presented, along with assumptions and simplifications. Further on, the basis for FE modelling in DIANA is explained, followed by a description of the post-processing of data extracted from analyses. In general, if nothing is mentioned regarding an input parameter in DIANA, the default is used.

4.1 Input and model

To obtain an accurate behaviour for the second crack in a restrained element, half of an end-restrained reinforced concrete tension member, as the one presented in chapter 3, was modelled in DIANA. In this section, the implementation into the software, such as geometry, loads, boundary conditions, and material, is described in detail.

4.1.1 Structural element

The restrained tension member was modelled as a three-dimensional element and aimed to be as similar as possible to the structural model described in section 3.1. As mentioned, the structure was one half of an end-restrained reinforced concrete member, where the cut in the symmetry line resembles the first trough crack. It

has two main components: a concrete volume and reinforcement bars. A schematic illustration of a longitudinal section of the model used in FEA is given in figure 4.1, and the final model, for one of the studied geometries, in DIANA is shown in figure 4.2. In the DIANA-model, the yellow blocks represent concrete parts, the green arrows represent the applied load, and red symbols visualise the supports. The same coordinate system as described in chapter 3 was used, with $z = 0$ at the fixed end.

The concrete volume was modelled as a three-dimensional block geometry, while reinforcement bars were modelled using one-dimensional line geometries. To be able to attach loads in a representative manner, a truss with a length $L_{truss} = 0.1$ m was added as an extension of the reinforcement. As a consequence, the reinforcement bars needed to be slightly extended outside the concrete block with $l_{rein\ ext} = 0.01$ m to eliminate issues with the attachment of the nodes between the truss element and the reinforcement.

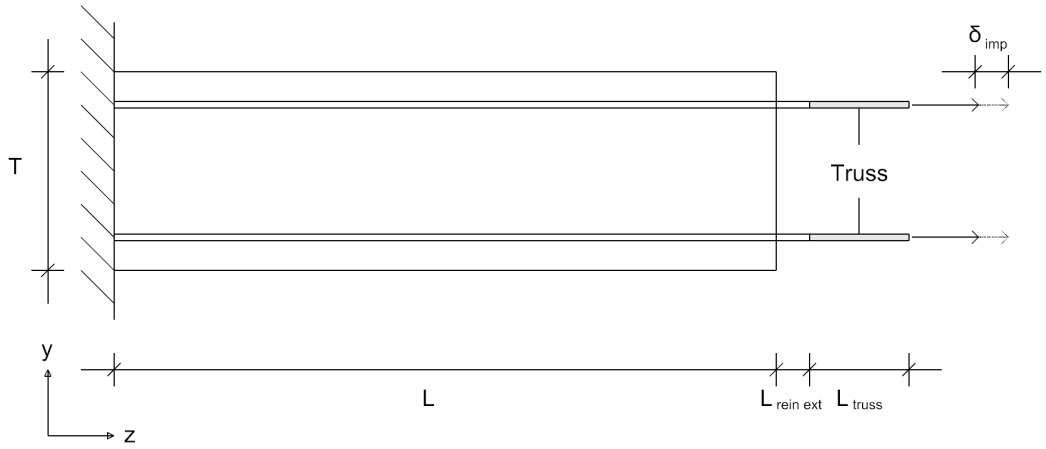

Figure 4.1: Illustration of the longitudinal section used in the final model used for analysis (created by the authors).

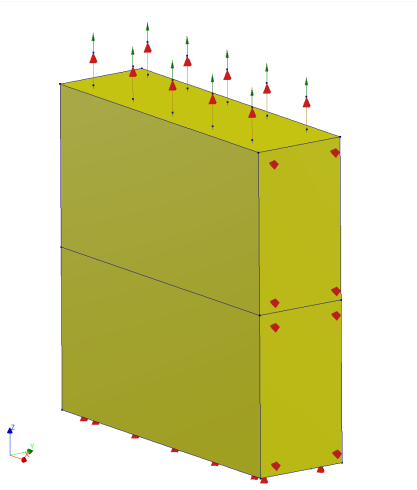

Figure 4.2: Final model for one of the studied cross-section geometries used for analysis in DIANA.

4.1.1.1 Boundary conditions and loads

At the fixed edge of the element, rigid supports in the z-direction were applied to the concrete block and reinforcement bars. For the concrete, a face support was used, fixing the whole surface, while the reinforcement bars were fixed with vertex supports at the end node. To capture a realistic behaviour within a crack, the concrete was free to move at the other edge and reinforcement bars were free to slip relative to the concrete.

To simulate a section of a continuous plate, symmetry boundary conditions were applied. To achieve that, rigid face supports in the x-direction were applied to both concrete faces in the yz-plane, at $x = 0$ and $x = B$, i.e. the left and right sides along the width of the concrete block were fully restrained in their normal directions.

To simulate the tensile stresses within a crack, the only load applied to the structure was an imposed displacement at the end node of every attached truss. Theoretically, this load could have been applied directly on the reinforcement, but since DIANA requires a support at the loaded node and the reinforcement needs to be free to move at the end to simulate a realistic behaviour within a crack, the reinforcement was extended with a short truss. The imposed displacement was therefore applied to the end node of the truss, where a rigid support was added as well. When load was applied, the rigid support moved according to the imposed displacement. The final applied load was a total displacement of $\delta_{imp} = 1.5$ mm. This was, based on evaluation of concrete stress during some test analyses, a displacement large enough to reach a stress in the concrete slightly above its capacity, which was considered sufficient to capture the behaviour of transferring of stresses, interesting for this master's thesis.

4.1.1.2 Cross-section geometries

As the analysis was performed for different cross-section geometries according to the previous chapter, dimensions for the reinforcement and concrete were set accordingly. The concrete section was set by the size of the block, since the element was modelled in three dimensions. For the reinforcement bars, the line objects were assigned a cross-sectional area calculated based on the bar diameter. The cross-sectional area for the truss was modelled as $A_{truss} = 10$ m^2 for all geometries. This is an unrealistically big area, just to ensure almost zero deformation in the truss and that all load was transferred to the reinforcement ends and the rest of the structure.

4.1.2 Material

All geometries were assigned material properties as well. A linear concrete material for the concrete block and a steel material for the reinforcement bars and for the truss.

4.1.2.1 Linear concrete material

A linear concrete material with the concrete strength class C25 was used, and specific material parameters were evaluated by the software according to Model Code 2010 (International Federation for Structural Concrete (Fib), 2010). These parameters are, for example, Young's modulus, E_{cm}, concrete tensile strength, f_{ct}, and Poisson's ratio, ν.

The reason why a linear material model was used instead of a non-linear is because of convergence issues during analysis. As a consequence of not including non-linear material in the model, non-linear phenomena like cracking could not be studied and stress distribution was evaluated according to linear material behaviour only. This means that stress distributions are accurate for loads below the capacity, but when stresses rise above the tensile strength, the results are no longer relevant. Hence, when non-linear behaviour takes place in reality, the model is not representative.

4.1.2.2 Steel material

Both the reinforcement bars and trusses were modelled using a linear isotropic steel material with parameters according to chapter 3, section 3.3.2. For the reinforcement bars, the mass density was defined as 7 853 kg/m^3 as well. Since the study only covers responses in SLS, yielding was not expected for any of the members, and no non-linearity for steel was included in the model.

4.1.2.3 Interaction modelled using a bond-slip relationship

The interface behaviour between the steel and concrete was modelled with a bond-slip relationship as described in section 2.2.1.1. An illustration of the applied bond-slip

relationship for concrete strength class C25 is presented in figure 4.3. The equation describing the first branch, $s < s_1$, was defined according to equation 4.1, which was picked according to Engström (2014). This ensures the results are more comparable with the analytical ones, since relationships used in analytical calculations are based on the same theory as the expression in equation 4.1. Since only the first branch is described by Engström (2014), the remaining parameters, such as s_1, s_2 and the proportion between the maximum shear stress and the shear stress in the third branch, $s > s_3$, are derived according to International Federation for Structural Concrete (Fib) (2022). Furthermore, the value of s_3 was assumed to be 8.5 mm, representing the clear distance between ribs. However, the definition of the first branch is the most relevant, as this thesis focuses on studying the behaviour in SLS. The implemented bond-slip relationship is attached in appendix E.

$$\tau_b = 0.22 f_{ctm} \cdot \left(\frac{s}{s_1}\right)^{0.2} \tag{4.1}$$

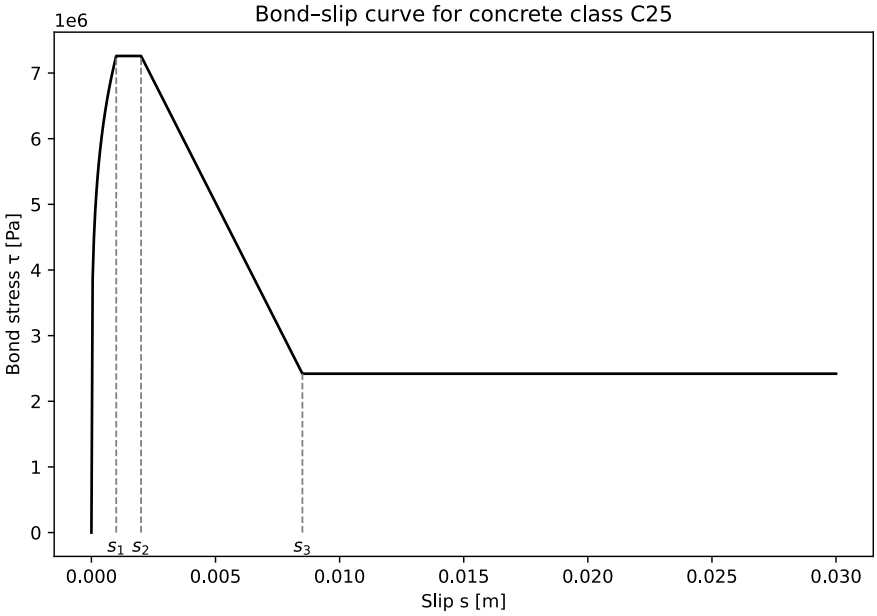

Figure 4.3: Illustration of the bond-slip relationship for concrete strength class C25 according to Model Code 2020 (created by the authors).

Additional input data given for the steel-concrete interface are the normal and shear stiffness modulus. These represent the resistance to elastic deformations in the interface in normal and tangential directions, respectively, both perpendicular to the bar direction. Those parameters were set to relatively stiff values: 100 MPa/m as normal stiffness and 1 MPa/m as shear stiffness.

4.2 Finite Element modelling in DIANA

As mentioned, the model with varying cross-sectional input sets described in the previous section was analysed with non-linear FEA in DIANA. The analysis was performed in three dimensions: x, y and z, aligned with the geometry as described in chapter 3. In this section, mesh properties and analysis setup are further described. The post-processing method is also explained.

4.2.1 Mesh

When performing a FEA for a structural geometry, a discretisation of the geometry is needed. Therefore, the structural element was divided into smaller elements as part of a discrete mesh. DIANA offers two different alternatives of shapes dominating the mesh type, tetrahedra or hexahedra. For this study, hexahedra were chosen since the shape of the studied element has a rectangular shape.

Further on, the mesh order, or order of the element shape functions, can be either linear or quadratic. Elements with quadratic shape functions contain more integration points per element. Therefore, each element is more time-consuming to evaluate Zienkiewicz et al. (2013). On the other hand, the accuracy of the results is increased for a coarser mesh. Hence, meshes with quadratic element order tend to be less expensive to evaluate for the same accuracy (Hesselmann, 2010). Consequently, the quadratic mesh order is chosen.

As a result, the final chosen element type has a hexahedral shape with 20 nodal points and is illustrated in figure 4.4 according to the theory described by DIANA FEA BV (2026).

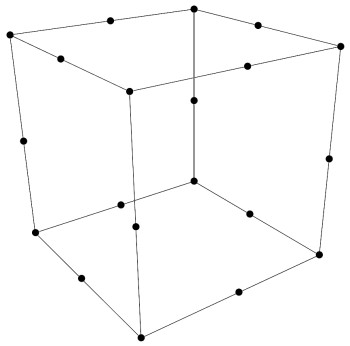

Figure 4.4: Illustration of a bric element with quadratic mesh order and its nodal points used in FE modelling (created by the authors).

4.2.1.1 Element types

The different geometries described in section 4.1.1: concrete, reinforcement bars and trusses, were assigned different types of elements. As the concrete block is a three-dimensional solid geometry, structural solids were used. Since the element shapes were defined as hexahedra, each element consisted of 6 faces, 8 corners and 20 nodes, where each node had 3 degrees of freedom, one for displacement in each direction of the coordinate system. The reinforcement bars and truss geometries were both divided into one-dimensional truss elements with one degree of freedom in each end node of the element, implying that deformations can only occur in the longitudinal direction of the reinforcement and trusses only.

4.2.1.2 Mesh convergence study

To obtain reliable results, the mesh size is of importance. A convergence study was carried out with the objective of finding an element size generating accurate results without being too computationally expensive. In the study, the mean concrete stress in an arbitrarily chosen cross-section geometry was evaluated for a certain set of element sizes. The fixed properties and analysis setup in the main study were used for all analyses in the mesh convergence study as well. Figure 4.5 shows the study results both in terms of the magnitude of the mean steel stress as well as relative change compared to previous coarseness. Both of the graphs are plotted against the number of elements across the width of the element. Based on the study, it can be concluded that convergence takes place at approximately 20 elements across the width, corresponding to an element size of 50 mm. The final mesh used in the study can be seen in figure 4.6 below.

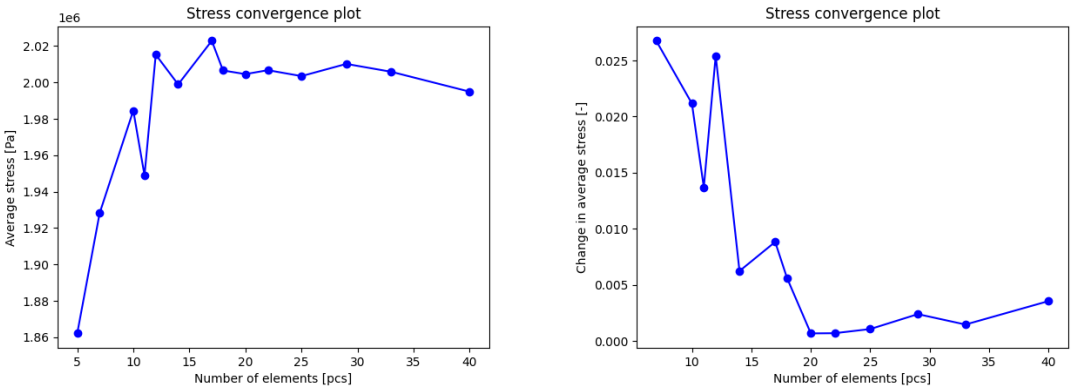

(a) Magnitude of stress value. **(b)** Relative change of stress value.

Figure 4.5: Graph illustrating how the concrete stress varies in relation to the number of elements.

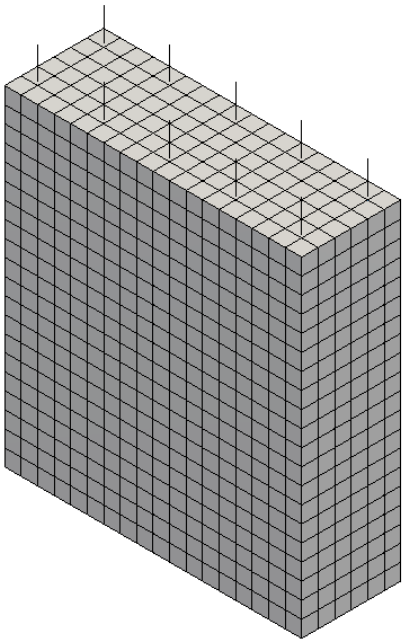

Figure 4.6: Final mesh for one of the analysed geometries in DIANA, with an element size of 50 mm.

4.2.2 Analysis

First, a linear static analysis was performed to verify the model and the transfer of stresses. However, the main goal with the FEA is to perform the earlier described non-linear analysis. Therefore, a structural non-linear analysis with respect to material non-linearity was set up in DIANA as well. This kind of analysis successively adds the applied load in steps, which in this case was the imposed displacement, and global equilibrium is solved for in each step. This is done within each load step using root-finding methods to iteratively solve the system of equations until convergence is reached.

4.2.2.1 Load stepping

To achieve accurate results, it is important to use proper load steps. The load step size in DIANA can be controlled either manually or automatically. Automatic load steps automatically reduce the step size if convergence cannot be reached within a load step and can make it easier for the analysis to continue without too many unnecessarily small steps. Therefore, automatic step size control was used for the analysis, with a maximum step size limit of 0.01 and a minimum of $1 \cdot 10^{-8}$, of the total applied load.

4.2.2.2 Equilibrium iteration

The root-finding procedure can be modified with several settings in DIANA, and for this analysis, the root-finding method was set to Modified Newton-Raphson. This method uses the stiffness relation to the last converged load step instead of computing it for every iteration, meaning that more iterations are usually needed compared to the Regular Newton-Raphson method (DIANA FEA BV, 2026). On the other hand, each iteration is less time-consuming since a new stiffness matrix does not need to be evaluated for each iteration. A schematic illustration of the regular and Modified Newton-Raphson method is shown in figure 4.7.

To evaluate convergence, several convergence criteria in terms of quantities and maximum limit values for the change of each specified quantity were used. Here, the quantities force and displacement were used with the limit value 0.01, and energy was used with a limit value of 0.0001. Based on that, convergence was considered to be reached as soon as any of these quantities changed less than the limit value between two iterations. Furthermore, the maximum number of iterations per load step was set to 500.

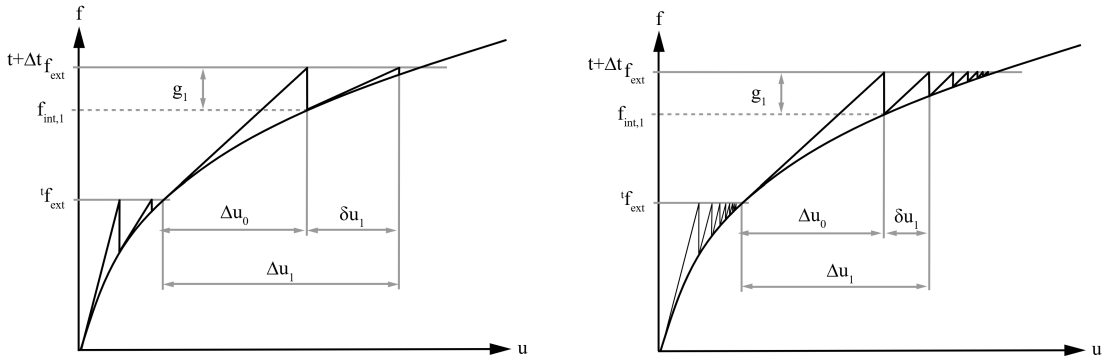

(a) Regular Newton-Rhapson. **(b)** Modified Newton-Raphson

Figure 4.7: Illustration of common root-finding methods used for non-linear FEA. (DIANA FEA BV, 2026). Reproduced with permission.

4.2.2.3 Solution method

In DIANA, the solution method used to solve the system of equations within a single iteration can be chosen as well. For this thesis, the default method, Parallel direct sparse, was used since it is a well-known efficient solution method commonly used for large systems (DIANA FEA BV, 2026).

4.2.3 Output

From the analysis, default output data was extracted as it was considered sufficient for addressing the problem formulation. In DIANA, results are extracted as nodal values or element values depending on the type of data. For example, displacements

are given as nodal values since they are evaluated in nodes directly when the system of equations is solved inside the FEA procedure. Stresses and strains, on the other hand, are evaluated based on the displacement at integration points, and therefore those values correspond to an element or an integration point of an element rather than to a specific node (DIANA FEA BV, 2026). However, from the default output, some specific result parameters, concrete stress, reinforcement stress and reaction forces in the z-direction, are extracted as Comma-Separated Values (CSV) Files. The CSV files include values for selected parameters at each load step and node, with corresponding nodal coordinates. This set of parameters for a specific nodal coordinate and stress value is further referred to as a data point.

Since the stress output, as mentioned, corresponds to element values, but the CSV files are sorted into nodal values, each nodal position contains one value corresponding to each of the adjacent elements. In section 4.3, it is further described how this was handled in cases where one value at a certain coordinate was needed.

4.3 Post-processing of results

To extract interesting data for visualisation, as well as for performance of further calculations based on the results from DIANA, post-processing of the extracted CSV files was implemented using scripting in Python. The most essential parts, such as functions for the calculation of the transmission length and the effective area, are attached in appendix G. The post-processing was done for all the analysed cross-section geometries, and the following results were obtained afterwards:

- Critical load step where f_{ctm} is first reached.
- z-coordinate for maximum tensile stress section, z_{max}.
- Transmission length, l_t, based on FEA.
- Effective area, $A_{c,eff}$, both numerical value and related to total cross-section area, A_c.
- Concrete stress values, σ_c, used for effective area calculations.
- Several plots illustrating the extracted results.

Lists for xyz-values and values of each parameter were extracted from the CSV file and sorted according to the load step. The adapted coordinate system is oriented in the same way as described in chapter 3, meaning that z varies along the length of the structural member and x and y along the cross-section.

4.3.1 Extraction of load step and section with maximum tensile stress

To evaluate the results when the structural element is subjected to a load of interest for evaluating the effective area, a critical load step, was picked based on when concrete stresses first reach f_{ctm} somewhere in the element. Hence, at least one node in the specimen was subjected to stresses at f_{ctm} or larger. As this master's thesis aims to evaluate the average behaviour, it is sufficient to use the mean value for tensile strength, according to the discussion in section 2.1.1.1.

Furthermore, since very high concentrated stresses were obtained adjacent to reinforcement bars at the free edge, probably due to local concrete cone failure explained by Engström (2014), data connected to elements facing the free edge in $z = L$ were ignored when searching for the critical load step.

Within the critical load step, a section in the xy-plane with maximum tensile stresses in the z-direction was extracted as well. This section is further referred to as the maximum tensile stress section, z_{max}, and is the section where the next crack theoretically would occur in case of a non-linear material. The critical section was obtained by extracting the z-coordinate where the maximum stress at the critical load step occurs.

4.3.2 Transmission length based on FEA

Transmission length, according to numerical results, was evaluated based on the steel stress. Since the transmission length is defined as the distance where stresses are transferred from the steel to the concrete, it was considered to be the distance between the loaded edge of the structural member and the section where the steel stress stops changing. An example of the change in stress over elements is plotted in figure 4.8. Since there are always some numerical variations in the data, a tolerance value for the change of stress was defined. According to trends in figure 4.8, the value 0.01 was chosen.

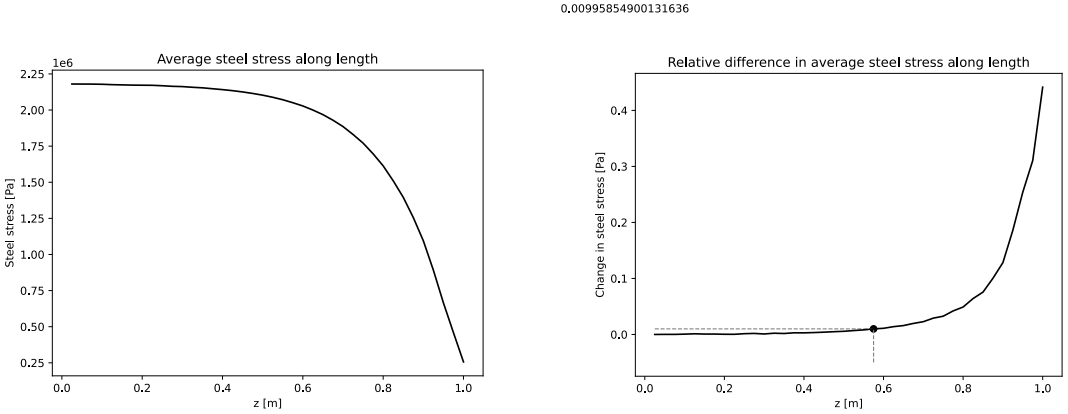

(a) Average steel stress. **(b)** Relative change.

Figure 4.8: Average steel stress along z for calculating transmission length.

4.3.3 Effective area based on FEA

The effective area was calculated based on the concrete stresses in the maximum tensile stress section at the critical load step, with inspiration from the study performed by Galkovski et al. (2021). The stresses in each data point are integrated over an equally large partition of the entire cross-section area, A_c. Here, the concrete area is simplified to $A_c = B \cdot H$, neglecting the reduction in area occupied by the reinforcement bars. It seemed as a reasonable assumption since the reinforcement area is so small in relation to the total area. The total integrated concrete force is then divided by the tensile strength, f_{ctm}, to obtain the area equivalent to what can be covered with stresses in the magnitude of f_{ctm}, by summing up all stresses in the entire cross-section. A schematic one-dimensional illustration for the principle of evaluating effective area, effective width and effective height can be seen in figure 4.9. By integrating the varying stress in the upper part of the figure, the total stress can be expressed as the boxes in the lower part of the figure.

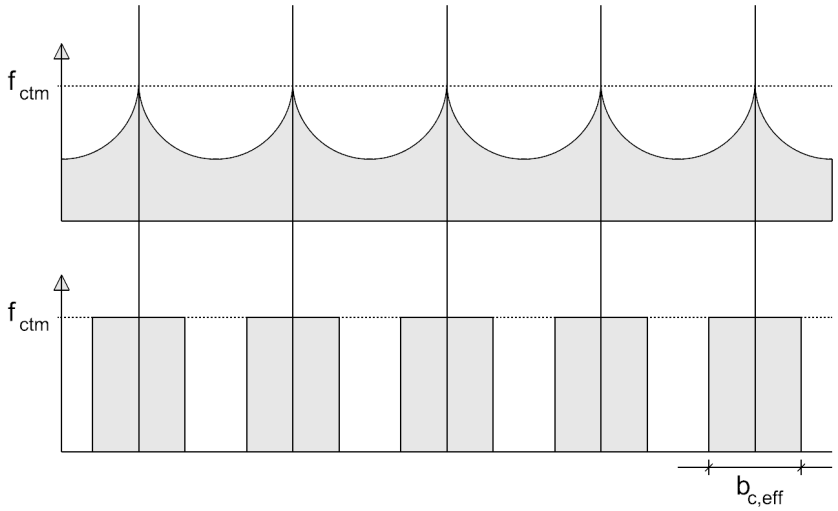

Figure 4.9: Illustration of the principle for evaluating effective area based on stress distribution from FEA results (created by the authors).

4.3.3.1 Derivation of effective area

The overall concept is based upon equilibrium between external and internal forces. As described in equation 4.2, the sum of the external load, N_{ext} applied on the reinforcement should be balanced by the internal forces in the concrete, F_c, and the reinforcement, F_s, at every z.

$$N_{ext} = F_c(z) + F_s(z) \tag{4.2}$$

This equilibrium condition can also be expressed in terms of concrete and steel stresses, σ_c and σ_s, as shown in equation 4.3. Both equation 4.2 and 4.3 applies to members with a constant cross-section, as the one studied in this thesis.

$$N_{ext} = \sigma_c(z) \cdot A_c + \sigma_s(z) \cdot A_s \tag{4.3}$$

In a certain section, at the level z, the expression in equation 4.4 applies and N_{ext} can be rewritten in terms of external steel stress $\sigma_{s.ext}$.

$$F_c(z) = N_{ext} - F_s(z) = \sigma_{s,ext} \cdot A_s - \sigma_s(z) \cdot A_s = A_s \cdot (\sigma_{s,ext} - \sigma_s(z)) \tag{4.4}$$

As a crack criterion, the concrete stress has to be equal to the tensile strength. The effective area can then be seen as the area loaded with f_{ctm} needed to carry all the load in the concrete at that section, and equation 4.5 can be considered.

$$F_c(z) = f_{ctm} \cdot A_{c,eff} \tag{4.5}$$

The effective area can therefore be expressed as in equation 4.6.

$$A_{c,eff} = \frac{F_c(z)}{f_{ctm}} = \frac{\sigma_c(z) \cdot A_c}{\sigma_{max}} \tag{4.6}$$

where σ_{max} refers to the maximum stress in the section and is approximately equal to f_{ctm} since the critical load step and maximum tensile stress section are picked according to when f_{ctm} is just recently reached. The reason why σ_{max} is used instead of f_{ctm} here, is to minimise the effect of discrete load steps making it impossible to pick values where f_{ctm} is reached exactly.

4.3.3.2 Equilibrium check

When evaluating the stresses at the maximum tensile stress section, an equilibrium check was done based on the equilibrium equation presented in the previous section. In that way, the convergence of the model could be verified if the condition in equation 4.7 was fulfilled.

$$\frac{\sigma_c \cdot A_c}{N_{ext} - F_s} \approx 0 \tag{4.7}$$

4.3.3.3 Limitation of the method for calculating the effective area

When using this method, a fully activated cross-section is very unlikely to occur, which does not correspond perfectly to reality. The entire cross-section is rarely loaded with stresses equal to f_{ctm} at the same moment when f_{ctm} is first reached somewhere in the specimen. In reality, there are usually some variations. As a consequence, this method might underestimate the effective area compared to reality and might therefore not be totally accurate. However, the method can still give a good indication of what the effective area for different cross-sectional geometries looks like.

4.3.4 Plots

Based on the extracted data at the critical load step, the following plots are created:

- Plots of effective area and concrete stresses versus s-ϕ ratio.
- Plots of transmission length versus s-ϕ ratio.
- Line plots concrete stress in the z-direction in all three planes.
- Line plots of concrete stresses in the z-direction located in the xy-plane of z_{max}.

Regarding the stress line plots, each nodal position is associated with several stress values for all adjacent elements, meaning each nodal coordinate has several data points. This gives a non-smooth set of data points that cannot be directly plotted using a line. This is solved by computing the average value at each node and plotting that value, since that method is considered to give an accurate representation of the variation in stresses in the concrete section. Furthermore, probably as a result of using quadratic mesh order with 20 nodal points, different amounts of data points were captured for different cases. Since all the z-coordinates where at least one node is present can be picked as z_{max}, the cross section where stresses are evaluated can occur between two separate elements or in the middle of the elements. The number of nodal points in the cross-section then differs accordingly, as can be seen in figure 4.4. The effects of this are further discussed in chapter 6 and 7.

5

Definition of analytical calculations

This chapter covers a description of the analytical calculations performed in this thesis. The results from these calculations are later compared with FEA results to obtain conclusions regarding cracking behaviour and the influence of the effective area. The principal concepts and equations are presented here, but calculations were performed using Python scripting, and relevant scripts are attached in appendix F.

The performed analytical calculations were the evaluation of the effective area, as well as calculations of transmission length based on the obtained effective area. The effective area was derived according to the expressions presented in the old and new EC 2. For the calculation of transmission length, DIANA output in terms of steel stress was used.

5.1 Effective area according to old EC 2

The effective height was derived based on the formulas presented in section 2.5.1, according to the old EC 2 (European Committee for Standardization (CEN), 2005). To obtain the total effective height over the cross-section, $h_{c,eff,2005}$, the effective height for one bar was multiplied by the number of bars over the height, n_{by}, which is two in all studied cases. The full expression is seen in equation 5.1.

$$h_{c,eff,2005} = n_{by} \cdot \min\left(2.5(T-d),\ \frac{T-x}{3},\ \frac{T}{2}\right) \quad \text{where} \quad d = T - c_y \tag{5.1}$$

The total effective area, $A_{c,eff,2005}$, is further given by multiplying the effective height by the width of the cross-section as in equation 5.2.

$$A_{c,eff,2005} = h_{c,eff,2005} \cdot B \tag{5.2}$$

5.2 Effective area according to new EC 2

In the new version of EC 2, expressions for both effective height and width are given according to the implementation of isolated bars, as presented in section 2.5.2 (European Committee for Standardization (CEN), 2023). For calculation of the

effective width, it has to be accounted for whether the bar is placed in between other bars or if it is on one of the edges, generating the two different expressions for the effective width, $b_{c,eff,edge}$ and $b_{c,eff,in}$, in equation 5.3.

$$b_{c,eff,edge} = \min\left(c_x + 5\phi,\ 10\phi,\ 3.5c_x,\ c_x + 0.5B,\ B\right) \quad \text{and} \quad b_{c,eff,in} = \min\left(10\phi,\ B\right) \tag{5.3}$$

These two expressions need to be further combined. Assuming equal cover thickness on both sides in the x-direction, the width for the edge bars has to be multiplied by two since there is one on each side, and accordingly, the expression for the mid bars has to be multiplied by the number of bars in between. The expression for the effective width, $b_{c,eff,2023}$, can then be expressed as in equation 5.4.

$$b_{c,eff,2023} = 2 \cdot b_{c,eff,edge} + (n_{bx} - 2)\ \cdot b_{c,eff,in} \tag{5.4}$$

The effective height, $h_{c,eff,2023}$ is then given in equation 5.5.

$$h_{c,eff,2023} = n_{by} \cdot \min\left(c_y + 5\phi,\ 10\phi,\ 3.5c_y,\ 0.5T\right) \tag{5.5}$$

The total effective area, $A_{c,eff,2023}$, in the cross-section is then given as the product of the effective width and height as in equation 5.6.

$$A_{c,eff,2023} = h_{c,eff,2023} \cdot b_{c,eff,2023} \tag{5.6}$$

5.3 Transmission length

Transmission lengths were derived based on crack calculation expressions given by Engström (2014). The theoretical crack width is needed to calculate the transmission length. What is further required is the steel stress within the crack, σ_s. This value was taken from the DIANA output as the steel stress that occurs when the critical load step is reached. Also, the effective area is needed, and the above calculated areas for the old and new versions were considered, which generated two different values of the crack width. The theoretical crack width, w_{net}, is given by the expression in equation 5.7:

$$w_{net} = 0.420 \cdot \left(\frac{\phi \cdot \sigma_s^2}{0.22 \cdot f_{cm} \cdot E_s \left(1 + \frac{E_s}{E_c} \cdot \frac{A_s}{A_{c,eff}}\right)} \right)^{0.826} \tag{5.7}$$

Based on the derived crack widths, the transmission length, l_t, based on the effective area from old and new EC 2 can be calculated as in equation 5.8.

$$l_t = 0.443 \cdot \frac{\phi\ \cdot \sigma_s}{0.22 \cdot f_{cm}\ \cdot w_{net}^{0.21} \cdot \left(1 + \frac{E_s}{E_c} \cdot \frac{A_s}{A_{c,eff}}\right)} + 2 \cdot \phi \tag{5.8}$$

6

Results

In this chapter, the results from both the analysis performed in DIANA and the analytical calculations are presented. Results are given both in terms of numerical values and illustrated in plots and graphs, visualising the observed behaviour in detail. All results are found here, but some additional results are also provided in the appendix A and B, where some of the stress plots are also shown in more detail.

6.1 Results from FEA

This section presents numerical results obtained from the FEA performed in DIANA. Results are provided as numerical values, as well as illustrated in graphs and plots. The results are described, and conclusions based on the observations are stated.

6.1.1 General clarification

Some general clarifications for the results of study 1 and study 2 need to be explained. All FEA results are defined for the critical load step. This is the load step when the tensile capacity of the concrete, f_{ctm}, is first reached somewhere in the element. All graphs illustrating the distribution of stresses in the x and y-directions are for the section where the capacity is first reached, the z_{max}-section, and at the level of the reinforcement bars.

The z-coordinate, referred to as z_{max}, is annotated with a white line in contour plots. In addition, the transmission length is also marked, but with a black line. These two distances are derived according to chapter 4.

Numerical values for $b_{c,eff}$, $h_{c,eff}$, and $A_{c,eff}$ are given according to the whole cross-section, and not for one single bar. For example, the effective height is expressed as the height covered by both layers of reinforcement bars.

As mentioned in section 4.3.3.3, this method does not correspond perfectly to reality. For that reason, numerical values are not entirely exact, implying that results for a single case, for example, for the effective area, are not totally accurate and therefore do not tell so much about behaviour. However, comparing the trend and differences between different evaluated cases gives a good description of behaviour.

Another thing that may be observed in some of the graphs is that the number of

data points differs, as explained in section 4.3.4.

6.1.2 Study 1

In the following section, the results from study 1 are presented. The results are visualised in different ways, and conclusions regarding the behaviour are stated.

6.1.2.1 Transmission length and max stress section

In table 6.1, the derived transmission length, l_t, and the maximum tensile stress section, z_{max}, are presented. Both these distances are measured from the loaded edge, $z = L$. These distances are also represented with a black and a white line, respectively, in the yz-plane stress plots in figure 6.1.

In all of the cases, the section of maximum stress is within the transmission length. According to the theory, all geometries are therefore classified as thick members. What can also be noticed is that the smaller the bar diameter is, the further from the loaded edge the max stress section appears. That pattern is reasonable, since a smaller bar implies that a smaller area is contributing to the transfer of stresses, and consequently, a longer distance is needed to transfer the same amount of stress. Additionally, it can be observed that the magnitude of the constant stress at the left edge, $z = 0$, slightly increases with an increased ratio.

Table 6.1: Maximum stress section and transmission length at critical load step, based on FEA for study 1.

Ratio	s_y=200 mm		s_y=400 mm	
	z_{max} [m]	l_t [m]	z_{max} [m]	l_t [m]
$s_x = 6\phi$	0.075	0.425	0.075	0.450
$s_x = 8\phi$	0.075	0.400	0.100	0.425
$s_x = 10\phi$	0.150	0.400	0.200	0.425
$s_x = 12\phi$	0.200	0.400	0.250	0.425
$s_x = 14\phi$	0.250	0.400	0.300	0.450

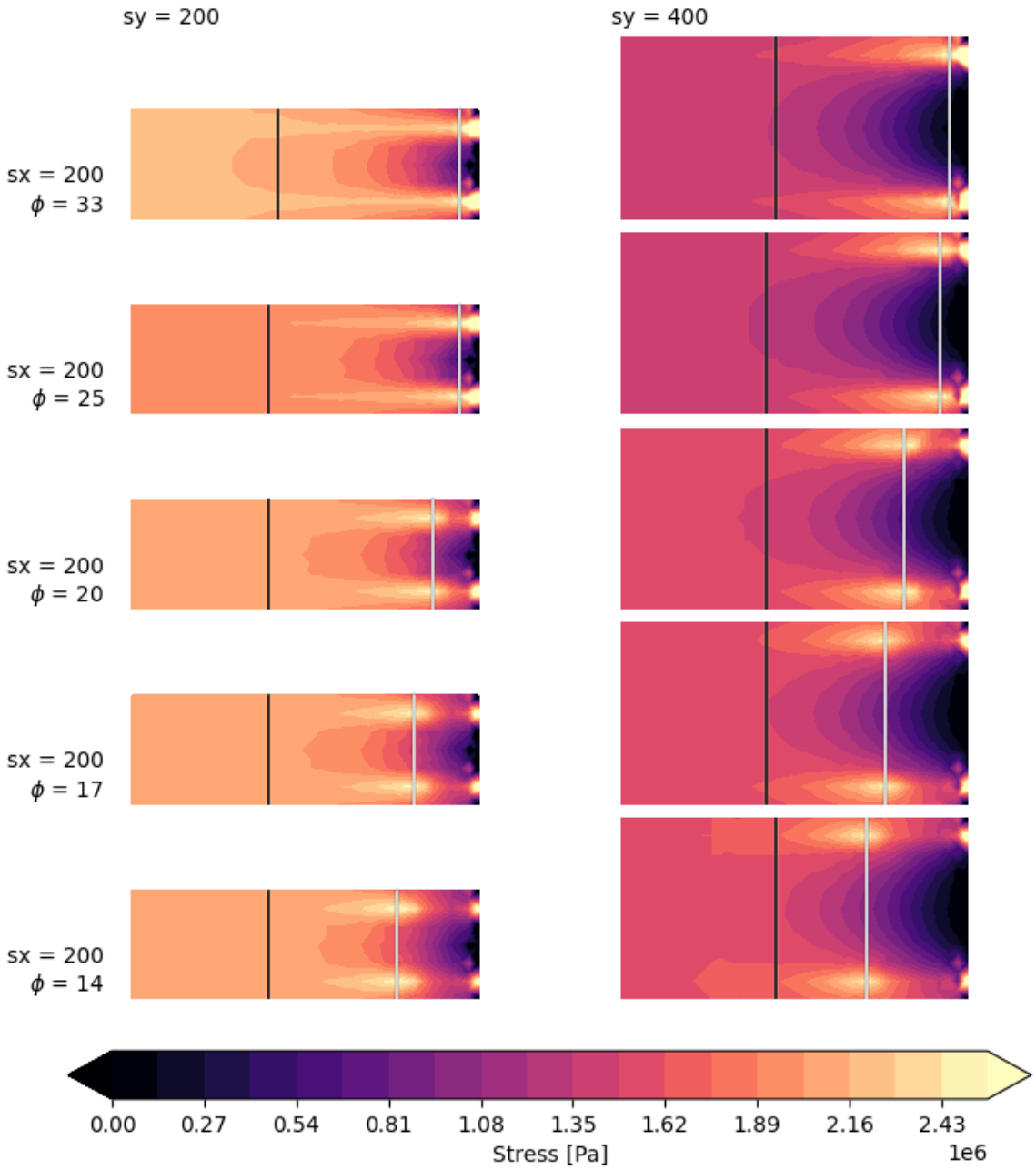

Figure 6.1: Cross-section stress plots in the yz-plane at critical load steps for varying s_x and s_y for study 1. s_x, s_y, and ϕ are provided in millimetres.

6.1.2.2 Stress distribution in xy-direction

The stress distribution in the xy-direction in figure 6.2 shows how the stresses are distributed over the cross-section. What can be observed is that a smaller diameter results in less variation of stresses throughout the cross-section. Clear differences between the thinner and the thicker geometries can also be observed. For the thinner one, where the s-ϕ ratio is the same in both directions, a similar distribution in both directions is noticed. For the thicker member, the middle part of the element

has a significantly lower stress than the parts of the concrete adjacent to the bars. This behaviour shows that the middle parts do not contribute as much to carrying stresses, indicating that the effective areas do not overlap in the y-direction. This can not be stated with total certainty due to limitation in the method for deriving the effective area as discussed in section 4.3.3.3.

To further illustrate the distribution of stresses in both the x and y-direction over the cross-section, graphs relating the different s-ϕ ratios to each other are presented in figure 6.3 and 6.4. These plots visualise the behaviour from the cross-section stress plots in greater detail. What is clearer here is that the distribution of stresses is almost the same for s_x-ϕ ratios 6 and 8, especially for the thinner element. This forms two groups of ratios with stress distributions at different levels. One group with 6 and 8 as mentioned, while 10, 12 and 14 can be seen as one group. Furthermore, in figure 6.4, it can be clearly seen that lower stress values between the layers of reinforcement bars in the y-direction are obtained for the thicker member.

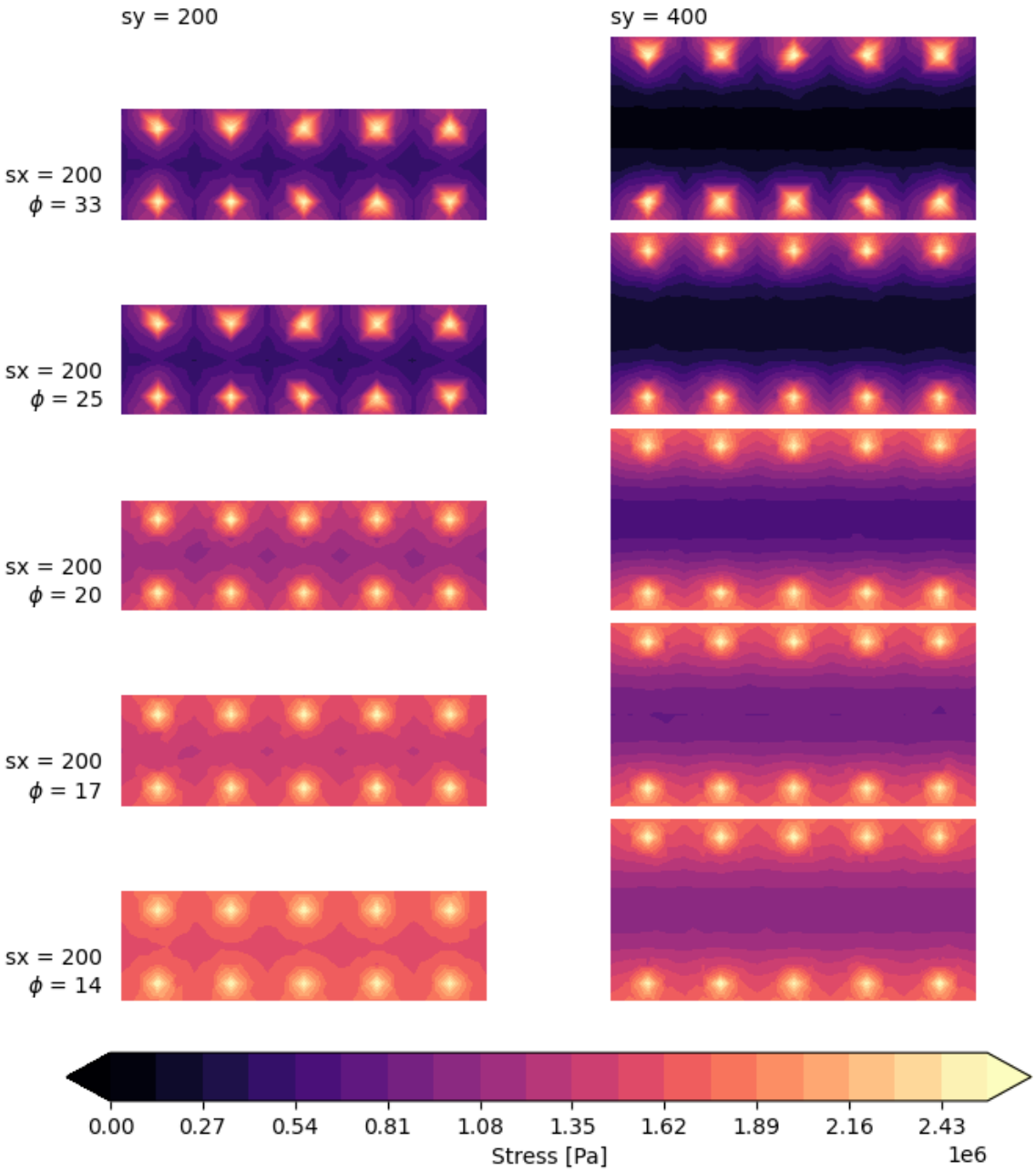

Figure 6.2: Cross-section stress plots in the xy-plane at critical load steps for varying s_x and s_y for study 1. s_x, s_y, and ϕ are provided in millimetres.

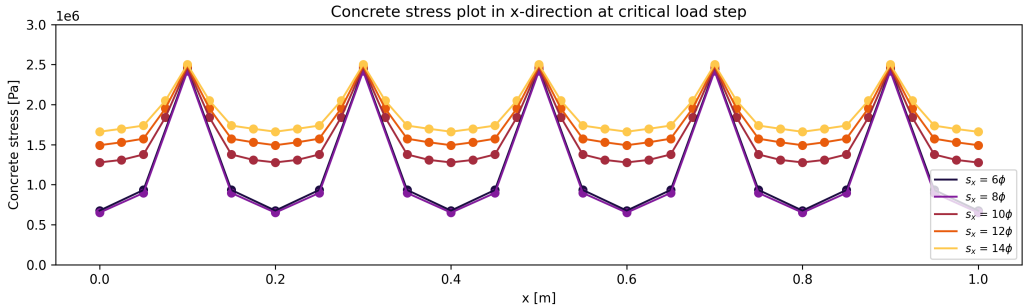

(a) s_y=200 mm

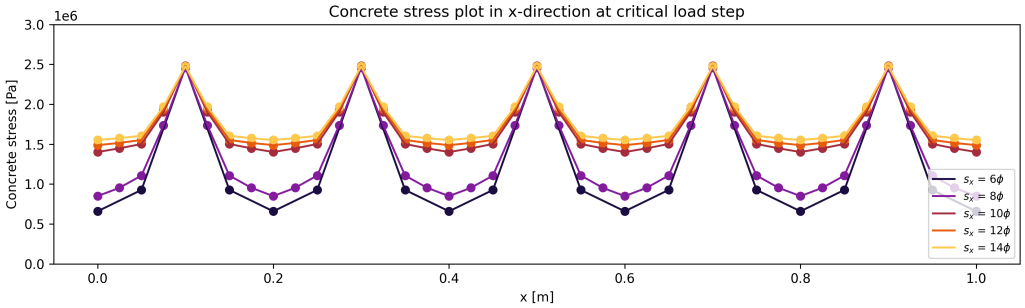

(b) s_y=400 mm

Figure 6.3: Concrete stress in the x-direction depending on the s_x-ϕ ratio for varying s_y for study 1.

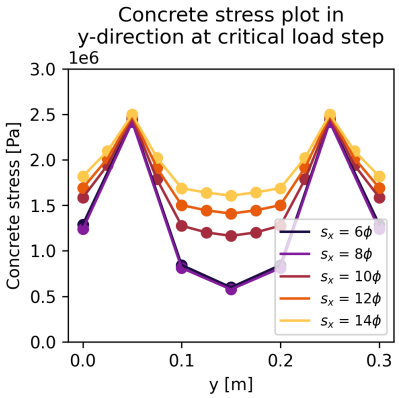

(a) s_y=200 mm

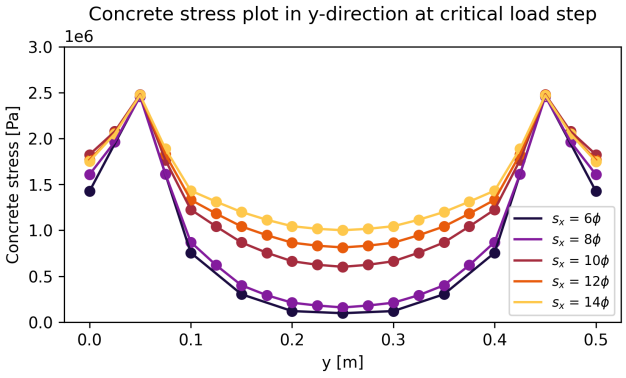

(b) s_y=400 mm

Figure 6.4: Concrete stress in the y-direction depending on the s_x-ϕ ratio for varying s_y for study 1.

6.1.2.3 Effective area

The obtained effective area from FEA are provided in table 6.2. The relative effective area in relation to the s_x-ϕ ratio is also visualised in a graph in figure 6.5 below, but then in relation to the total cross-section area. Important to consider when studying these values, especially when comparing the effective area between the two cases

of s_y, is that the thicker member has a bigger total cross-sectional area than the thinner one due to increased s_y.

The trend that can be noticed is that a smaller bar diameter implies a bigger effective area, which is not expected according to the formulas for effective area in the new EC 2. Comparing the thicker and thinner members, the thinner member has a bigger part of the cross-section effective, in line with theory. For the thinner member, the effective area is almost constant for smaller ratios. Regarding the numerical values, this trend could indicate that a group of bars is created covering all the cross-sections.

Table 6.2: Results in terms of effective area, $A_{c,eff}$ [m^2], for study 1 at the critical load step, based on FEA.

Ratio	$s_y = 200$ mm	$s_y = 400$ mm
$s_x = 6\phi$	0.103	0.106
$s_x = 8\phi$	0.101	0.132
$s_x = 10\phi$	0.160	0.216
$s_x = 12\phi$	0.183	0.240
$s_x = 14\phi$	0.203	0.262

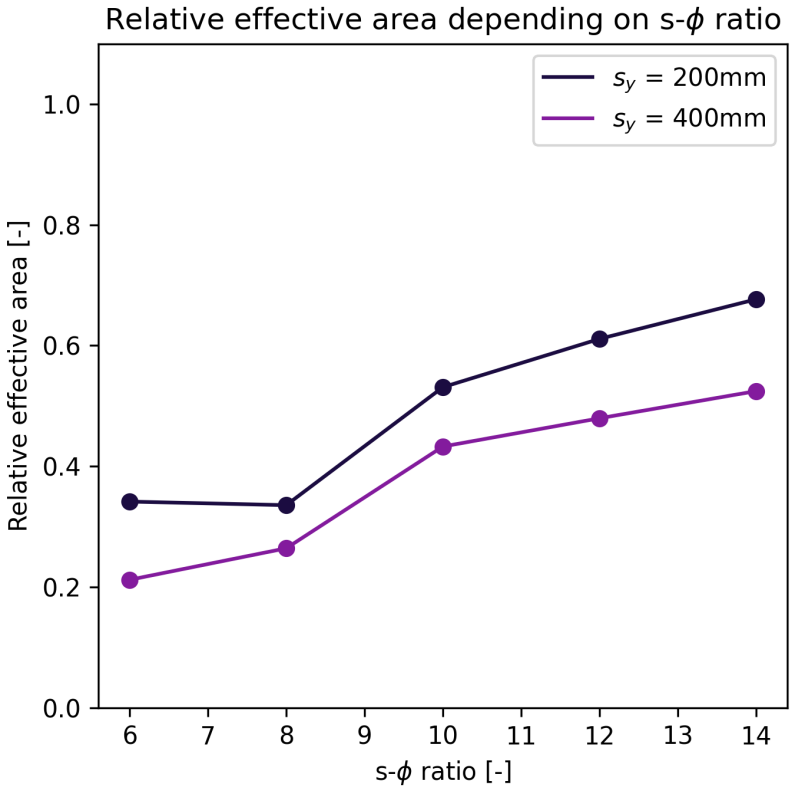

Figure 6.5: Relative effective area depending on the s_x-ϕ ratio for varying s_y for study 1.

6.1.3 Study 2

In the following section, the results from study 2 are presented. The results are visualised in different ways, and interpretations of the behaviour are stated.

6.1.3.1 Transmission length and max stress section

In table 6.3, the derived transmission length, l_t, and maximum tensile stress section, z_{max}, measured from the loaded edge in $z = L$, are presented. As for study 1, these distances are also represented with a black or a white line in the yz-plane stress plots in figure 6.6.

The same behaviour as in study 1 can be observed. The same trend regarding an increasing distance from the edge to the section of maximum tensile stresses for larger s_x-ϕ ratios. Also, the section of the maximum stress takes place within the transmission length for all cases except for one case, which is the case with the smallest spacing, both in the x and y-directions. Another observation is that the magnitude of the constant stress at the left edge, $z = 0$, increases with an increased ratio, i.e, the opposite trend compared to study 2.

Table 6.3: Maximum stress section and transmission length at critical load step, based on FEA for study 2.

Ratio	s_y=200 mm		s_y=400 mm	
	z_{max} [m]	l_t [m]	z_{max} [m]	l_t [m]
$s_x = 6\phi$	0.450	0.350	0.100	0.400
$s_x = 8\phi$	0.100	0.375	0.150	0.400
$s_x = 10\phi$	0.150	0.400	0.200	0.425
$s_x = 12\phi$	0.150	0.400	0.200	0.425
$s_x = 14\phi$	0.200	0.400	0.200	0.425

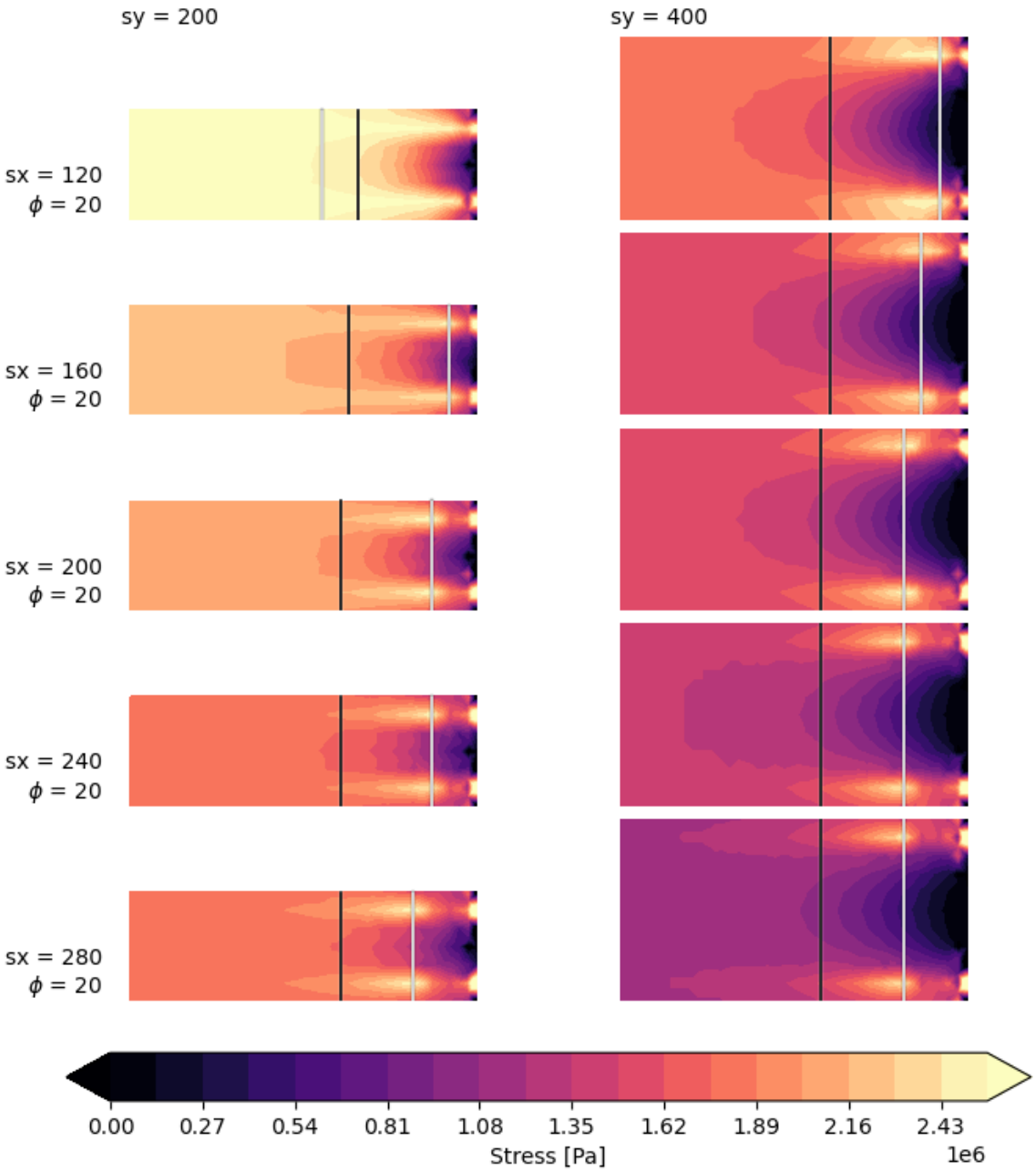

Figure 6.6: Cross-section stress plots in the yz-plane at critical load steps for varying s_x and s_y for study 2. s_x, s_y, and ϕ are provided in millimetres.

6.1.3.2 Stress distribution in xy-direction

The stress distribution in the xy-direction in figure 6.7 shows the distribution of stresses over the cross-section.

The distribution of stresses over the cross-section follows the same pattern as for study 1. Although it can be noticed that the case with the smallest spacing in both directions, i.e, case 2A with $s_x = 120$ mm and $s_y = 200$ mm, stands out, having an almost constant stress distribution. In contrast to study 1, stresses between the

reinforcement bars are not strictly increasing for a larger s-ϕ ratio.

To further illustrate the distribution of stresses in the x-direction, graphs comparing the behaviour of the two thicknesses are seen in figure 6.8. Also, the distribution in the y-direction over the cross-section is presented, comparing the different s_x-ϕ ratios in figure 6.9.

Here, case 2A clearly stands out as well, as a straight line in figure 6.9a. What can be noticed, comparing all of the other cases, is that the stress is lower between the bars for the thinner case, s_y=10ϕ, in all cases except for the case with the biggest spacing in the x-direction. The overall noticed trend is that bigger spacing in both directions shows lower values between the bars. For cases where the bars are placed closer to each other, the difference between the minimum and maximum stress is smaller.

The distribution of stresses over the thickness shows an irregular trend, where there is no clear correlation between the s_x-ϕ ratio and how much the stress decreases between the bars. The irregularity is present not only within each thickness, but also when comparing the thinner and thicker elements, where the ordering of the plotted curves differs between the two thicknesses. Comparing the thinner and thicker cases, the curves for s_x=14ϕ and s_x=6ϕ change position between the two graphs.

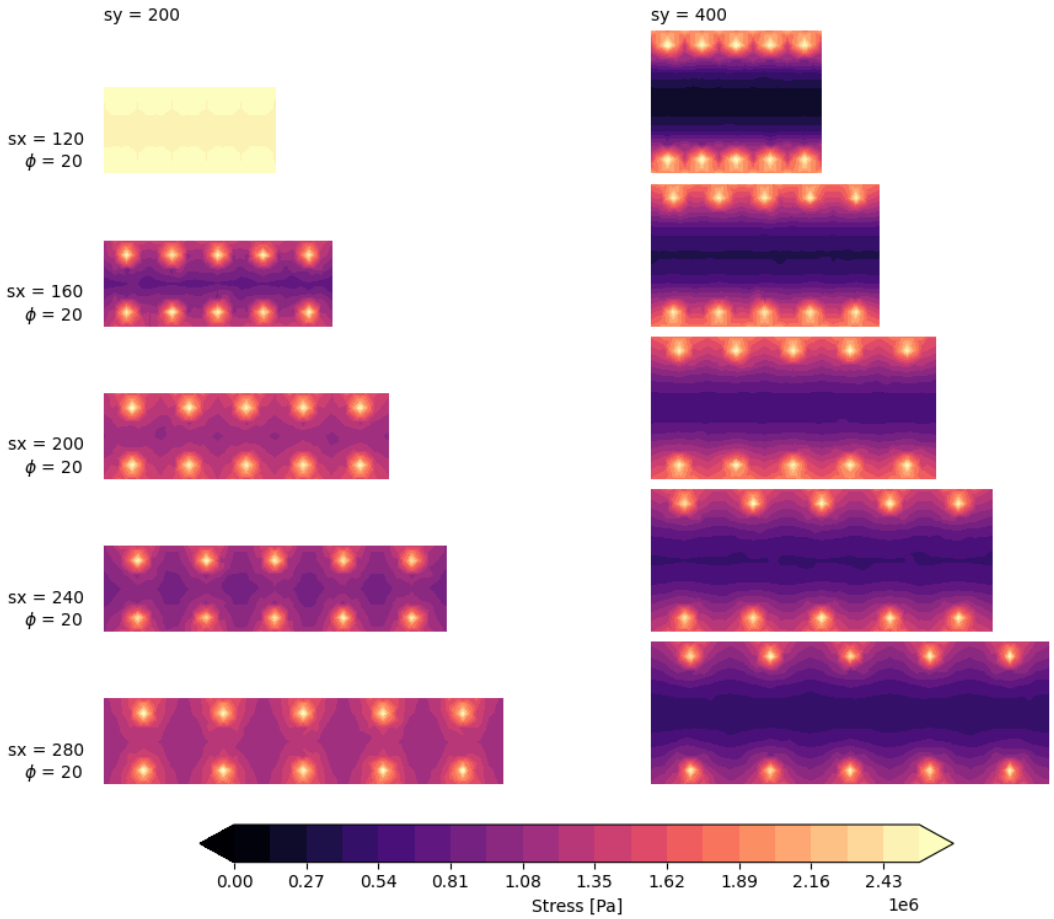

Figure 6.7: Cross-section stress plots in the xy-plane at critical load steps for varying s_x and s_y for study 2. s_x, s_y and ϕ are provided in millimetres.

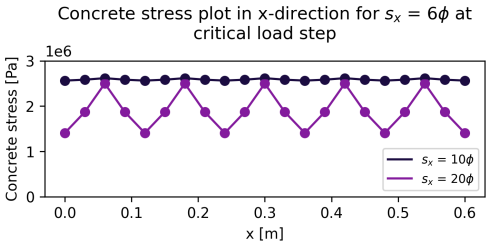

(a) s_x=120 mm

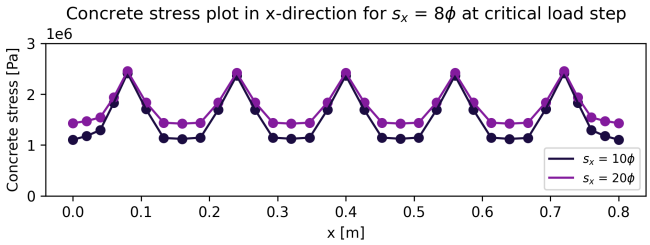

(b) s_x=160 mm

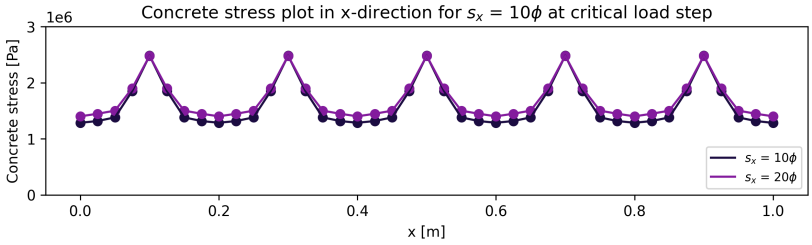

(c) s_x=200 mm

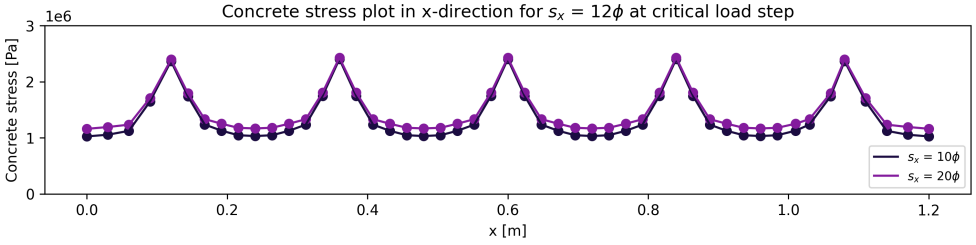

(d) s_x=240 mm

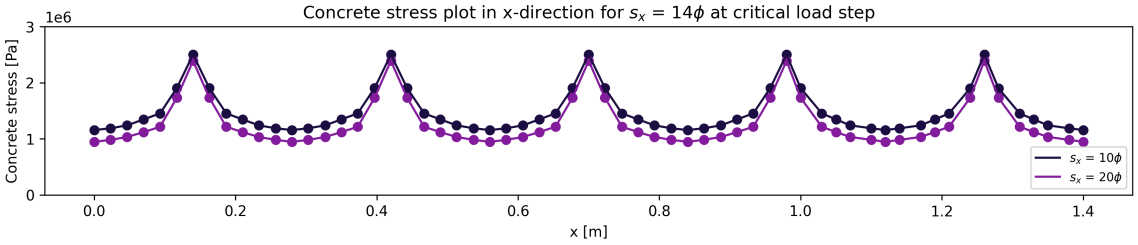

(e) s_x=280 mm

Figure 6.8: Concrete stress in the x-direction for s_y=200 mm and s_y=400 mm for varying s_x for study 2.

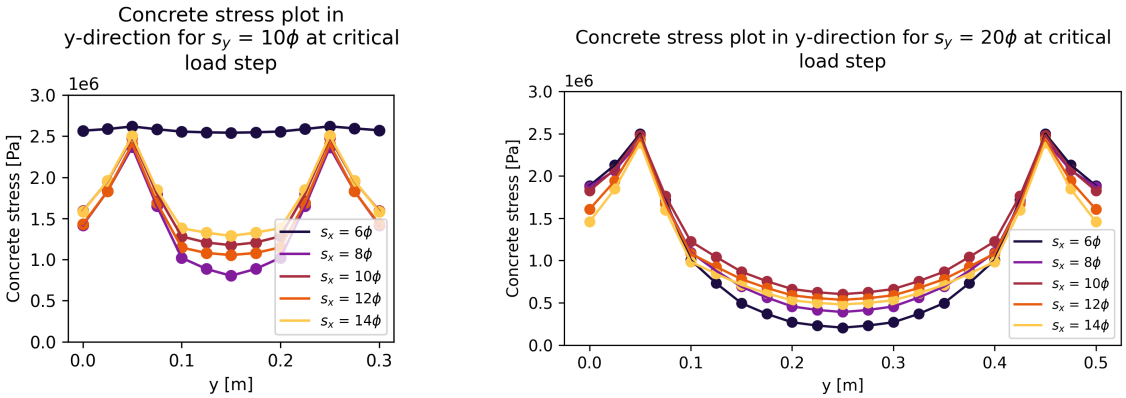

(a) s_y=200 mm **(b)** s_y=400 mm

Figure 6.9: Concrete stress in the y-direction depending on the s_x-ϕ ratio for varying s_y for study 2.

6.1.3.3 Effective area

In table 6.4, the effective area are presented. Studying the numerical values in the table shows an increasing effective area, but it is important to consider that the cross-sectional area of the structural element increases both with the increasing s_x-ϕ and s_y-ϕ ratio, in this study.

The relative effective area in relation to the s_x-ϕ ratio is also visualised in a graph in figure 6.10 below. This graph makes the trend for the effective area clearer than studying the numerical values in the table, due to the change in total cross-sectional area.

Ignoring case 2A, the shape of the graphs follows similar trends for both the thinner and the thicker elements. A discrete peak at s_x=10ϕ can be noticed for both thicknesses.

Table 6.4: Results in terms of effective area, $A_{c,eff}$ [m^2], at the critical load step for study 2, based on FEA.

Ratio	$s_y = 200$ mm	$s_y = 400$ mm
$s_x = 6\phi$	0.177	0.108
$s_x = 8\phi$	0.110	0.158
$s_x = 10\phi$	0.159	0.216
$s_x = 12\phi$	0.165	0.225
$s_x = 14\phi$	0.216	0.230

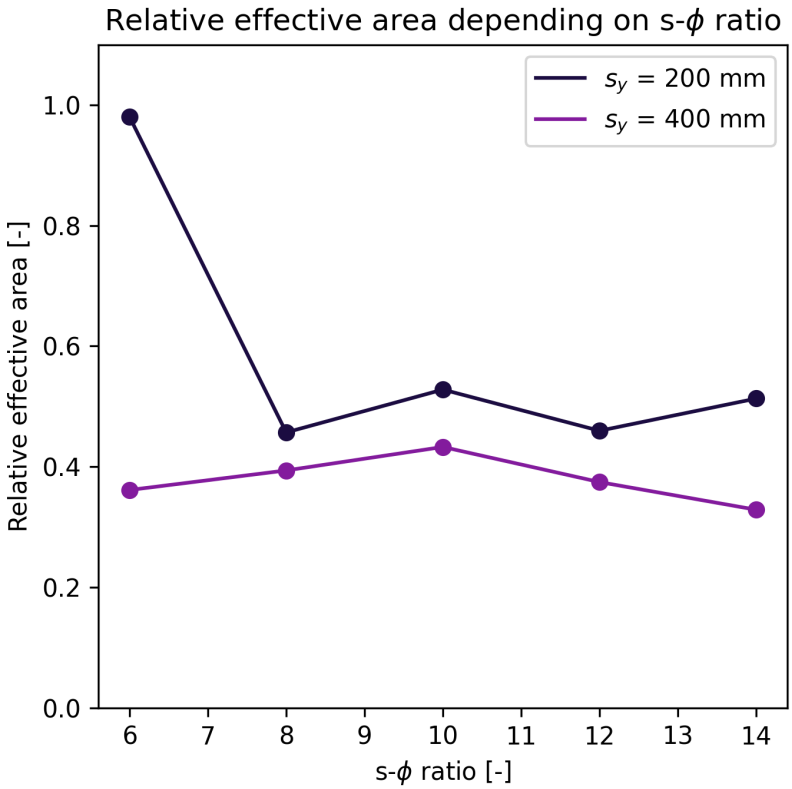

Figure 6.10: Relative effective area depending on the s_x-ϕ ratio for varying s_y for study 2.

6.2 Analytical results

In this section, results from the analytical study are presented. Both the effective area and the transmission length are derived according to the models for effective area in both versions of EC 2, as described in chapter 5. Since the steel stress is taken from the FEA results, the analytical results are representative of the critical load step as well.

6.2.1 Study 1

In the following section, analytical results for study 1 are presented. Results are given in terms of transmission length and effective area.

6.2.1.1 Transmission length

The derived transmission lengths for study 1 are presented in table 6.5, expressed based on the definitions for $A_{c,eff}$ in both versions of EC 2. For both the thicker and the thinner elements, smaller differences in the derived transmission length can be noticed. Also, some smaller differences between the old and new models can be

seen, but which model provides values bigger than the other differs depending on the s_x-ϕ ratio.

Table 6.5: Transmission length, l_t [m], based on analytical calculations for study 1, based on the definitions for $A_{c,eff}$ in both versions of EC 2.

Ratio	**Old EC 2**		**New EC 2**	
	l_t [m]		l_t [m]	
	$s_y = 200$ mm	$s_y = 400$ mm	$s_y = 200$ mm	$s_y = 400$ mm
$s_x = 6\phi$	0.308	0.312	0.315	0.324
$s_x = 8\phi$	0.318	0.337	0.322	0.345
$s_x = 10\phi$	0.348	0.385	0.351	0.389
$s_x = 12\phi$	0.372	0.422	0.370	0.420
$s_x = 14\phi$	0.397	0.460	0.391	0.454

6.2.1.2 Effective area

The effective area calculated for study 1 is presented in the tables below. It is important to consider that the two thicknesses have different total areas, due to different total thicknesses, 0.3 and 0.5 m.

What can be noticed is that the effective width for the case based on the old version remains constant and equals the total width of the element, since no definition of effective width is provided. Also, the effective height remains constant for all of the cases and is equal for both of the thicknesses. Calculations performed in line with the new version differ from the results based on the old version, since expressions for both effective width and height are presented. With an increasing z_x-ϕ ratio, i.e. a decreasing bar diameter, smaller effective areas are obtained. Another difference is that, for smaller ratios, the effective height is not equal for the different thicknesses.

Table 6.6: Effective width, height and area based on analytical calculations in line with old EC 2 for study 1.

Ratio	$s_y = 200$ mm			$s_y = 400$ mm		
	$b_{c,eff}$ [m]	$h_{c,eff}$ [m]	$A_{c,eff}$ [m^2]	$b_{c,eff}$ [m]	$h_{c,eff}$ [m]	$A_{c,eff}$ [m^2]
$s_x = 6\phi$	1.00	0.250	0.250	1.00	0.250	0.250
$s_x = 8\phi$	1.00	0.250	0.250	1.00	0.250	0.250
$s_x = 10\phi$	1.00	0.250	0.250	1.00	0.250	0.250
$s_x = 12\phi$	1.00	0.250	0.250	1.00	0.250	0.250
$s_x = 14\phi$	1.00	0.250	0.250	1.00	0.250	0.250

Table 6.7: Effective width, height and area based on analytical calculations in line with new EC 2 for study 1.

Ratio	$s_y = 200$ **mm**			$s_y = 400$ **mm**		
	$b_{c,eff}$ [m]	$h_{c,eff}$ [m]	$A_{c,eff}$ [m^2]	$b_{c,eff}$ [m]	$h_{c,eff}$ [m]	$A_{c,eff}$ [m^2]
$s_x = 6\phi$	1.00	0.300	0.300	1.00	0.350	0.350
$s_x = 8\phi$	1.00	0.300	0.300	1.00	0.350	0.350
$s_x = 10\phi$	1.00	0.300	0.300	1.00	0.300	0.300
$s_x = 12\phi$	0.833	0.267	0.222	0.833	0.267	0.222
$s_x = 14\phi$	0.714	0.243	0.174	0.714	0.243	0.176

6.2.2 Study 2

In the following section, analytical results for study 2 are presented. Results are given in terms of transmission length and effective area.

6.2.2.1 Transmission length

The derived transmission lengths for study 2 are presented in table 6.8 and are based on the definitions of $A_{c,eff}$ in both versions of EC 2, as described in chapter 5. Smaller differences can be noticed both between the thicknesses and between the two versions. Overall, an increasing ratio implies an increasing transmission length.

Table 6.8: Transmission length, l_t [m], based on analytical calculations for study 2, based on the definitions for $A_{c,eff}$ in both versions of EC 2.

Ratio	**Old EC 2**		**New EC 2**	
	l_t [m]		l_t [m]	
	$s_y = 200$ mm	$s_y = 400$ mm	$s_y = 200$ mm	$s_y = 400$ mm
$s_x = 6\phi$	0.293	0.307	0.297	0.312
$s_x = 8\phi$	0.313	0.336	0.317	0.340
$s_x = 10\phi$	0.350	0.385	0.353	0.389
$s_x = 12\phi$	0.359	0.404	0.359	0.404
$s_x = 14\phi$	0.398	0.415	0.395	0.412

6.2.2.2 Effective area

The effective area calculated for study 2 is presented in the tables below. Due to variations in spacing both along the width and the height, the total area is different for all of the studied cases, which is important to consider when studying the numerical values of effective area.

As mentioned above, the effective width for the old EC 2 is equal to the total width of the element. It can be noticed that the effective height is also constant for all of the cases, generating an effective area that behave linear in relation to the total area

of the cross-section. The new version shows a behaviour where smaller ratios have the total width as effective. For bigger ratios, the effective width does not change with increasing spacing, even though the element width is increasing. The effective height is the same for all of the cases, regardless of s_y and its corresponding element thickness, which is larger than the values obtained from the old EC 2.

Table 6.9: Effective width, height and area based on analytical calculations in line with old EC 2 for study 2.

Ratio	$s_y = 200$ **mm**			$s_y = 400$ **mm**		
	$b_{c,eff}$ [m]	$h_{c,eff}$ [m]	$A_{c,eff}$ [m^2]	$b_{c,eff}$ [m]	$h_{c,eff}$ [m]	$A_{c,eff}$ [m^2]
$s_x = 6\phi$	0.600	0.250	0.150	0.600	0.250	0.150
$s_x = 8\phi$	0.800	0.250	0.200	0.800	0.250	0.200
$s_x = 10\phi$	1.00	0.250	0.250	1.00	0.250	0.250
$s_x = 12\phi$	1.20	0.250	0.300	1.20	0.250	0.300
$s_x = 14\phi$	1.40	0.250	0.350	1.40	0250	0.350

Table 6.10: Effective width, height and area based on analytical calculations in line with new EC 2 for study 2.

Ratio	$s_y = 200$ **mm**			$s_y = 400$ **mm**		
	$b_{c,eff}$ [m]	$h_{c,eff}$ [m]	$A_{c,eff}$ [m^2]	$b_{c,eff}$ [m]	$h_{c,eff}$ [m]	$A_{c,eff}$ [m^2]
$s_x = 6\phi$	0.600	0.300	0.180	0.600	0.300	0.150
$s_x = 8\phi$	0.800	0.300	0.240	0.800	0.300	0.240
$s_x = 10\phi$	1.00	0.300	0.300	1.00	0.300	0.300
$s_x = 12\phi$	1.00	0.300	0.300	1.00	0.300	0.300
$s_x = 14\phi$	1.00	0.300	0.300	1.00	0.300	0.300

6.3 Comparison of analytical results and results from FEA

In this section, the analytical results and results from FEA in terms of effective area and transmission length are presented in comparison to each other. The results are presented for each study 1 and 2 separately.

6.3.1 Study 1

In the following section, FEA and analytical results from study 1 are compared. This is presented in both tables and graphs.

6.3.1.1 Transmission length

A comparison of the results from FEA and the analytical analysis, in terms of the transmission length, is presented in table 6.11 below. As mentioned, analytical results are evaluated based on the definitions of $A_{c,eff}$ from both versions of EC 2. These values are further visualised in two graphs in figure 6.11 for the two thicknesses, where the trend of how the transmission length changes in relation to the ratio can be seen based on FEA, the old EC 2 and the new EC 2.

Comparing the two graphs, the trends are similar for both thicknesses. Also, there are almost no differences between transmission lengths based on the old and the new model of effective area in EC 2. Comparing the results based on EC 2 with the results from FEA, it can be noticed that FEA gives a larger value for lower ratios, while it for s_x-ϕ ratio 14, give the same value. The analytical results based on EC 2 show a trend where the distance is increasing with increasing ratio, while FEA shows an almost constant value. This is also true for s_x-ϕ ratio 12 for the thicker element.

Table 6.11: Comparison of transmission length, l_t [m], from FEA and analytical analysis for study 1.

Ratio	FEA		Analytical old EC 2		Analytical new EC 2	
	$s_y = 200$ mm	$s_y = 400$ mm	$s_y = 200$ mm	$s_y = 400$ mm	$s_y = 200$ mm	$s_y = 400$ mm
$s_x = 6\phi$	0.425	0.450	0.308	0.312	0.315	0.324
$s_x = 8\phi$	0.400	0.425	0.318	0.337	0.322	0.345
$s_x = 10\phi$	0.400	0.425	0.348	0.385	0.351	0.389
$s_x = 12\phi$	0.400	0.425	0.372	0.422	0.370	0.420
$s_x = 14\phi$	0.400	0.450	0.400	0.460	0.391	0.454

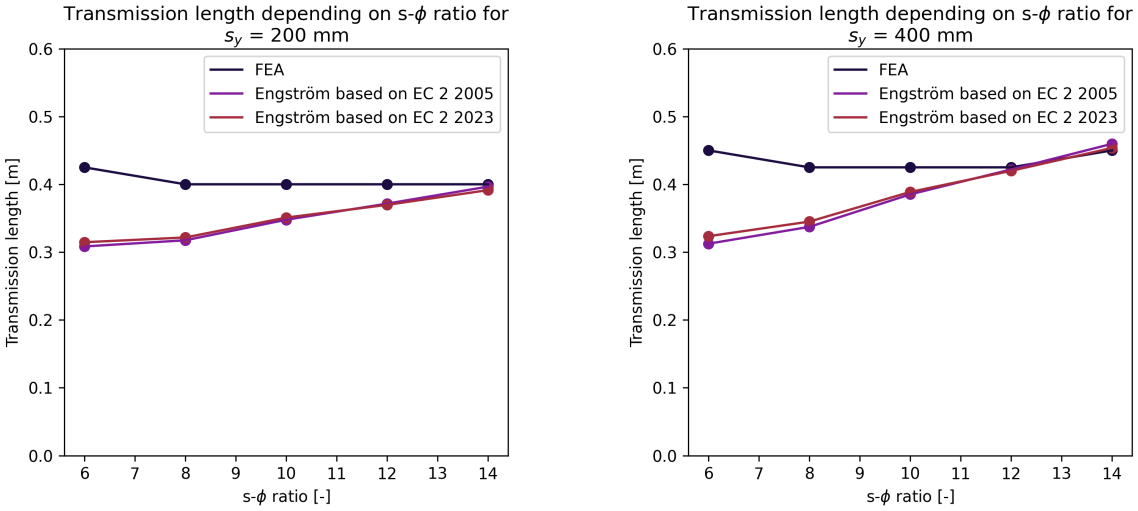

(a) s_y=200 mm. **(b)** s_y=400 mm.

Figure 6.11: Comparison of transmission length, l_t [m], from FEA and analytical analysis for study 1.

6.3.1.2 Effective area

In the following table, a comparison of the results for the effective area for study 1 is presented. The development of the effective area based on FEA, old EC 2 and new EC 2, in relation to the s_x-ϕ ratio, can also be seen in the graphs below. In figure 6.12, a comparison of the thinner and the thicker members is shown.

As can be clearly noticed in the graph, neither the thinner nor the thicker element behaves in line with the EC 2 models. According to the new version, the whole element is effective, i.e. $A_{eff,rel} = 1$, for some s_x-ϕ ratios in the thinner member. For the thicker element, this is never reached. The same is for the old model, where $A_{eff,rel}$ is constant for all cross-sectional geometries, with values around 0.8 and 0.5 respectively.

Table 6.12: Comparison of effective area, $A_{c,eff}$ [m^2], from FEA and analytical analysis for study 1.

Ratio	**FEA**		**Old EC 2**		**New EC 2**	
	$s_y = 200$ mm	$s_y = 400$ mm	$s_y = 200$ mm	$s_y = 400$ mm	$s_y = 200$ mm	$s_y = 400$ mm
$s_x = 6\phi$	0.102	0.106	0.250	0.250	0.300	0.350
$s_x = 8\phi$	0.101	0.132	0.250	0.250	0.300	0.350
$s_x = 10\phi$	0.159	0.216	0.250	0.250	0.300	0.300
$s_x = 12\phi$	0.183	0.240	0.250	0.250	0.222	0.222
$s_x = 14\phi$	0.203	0.262	0.250	0.250	0.174	0.174

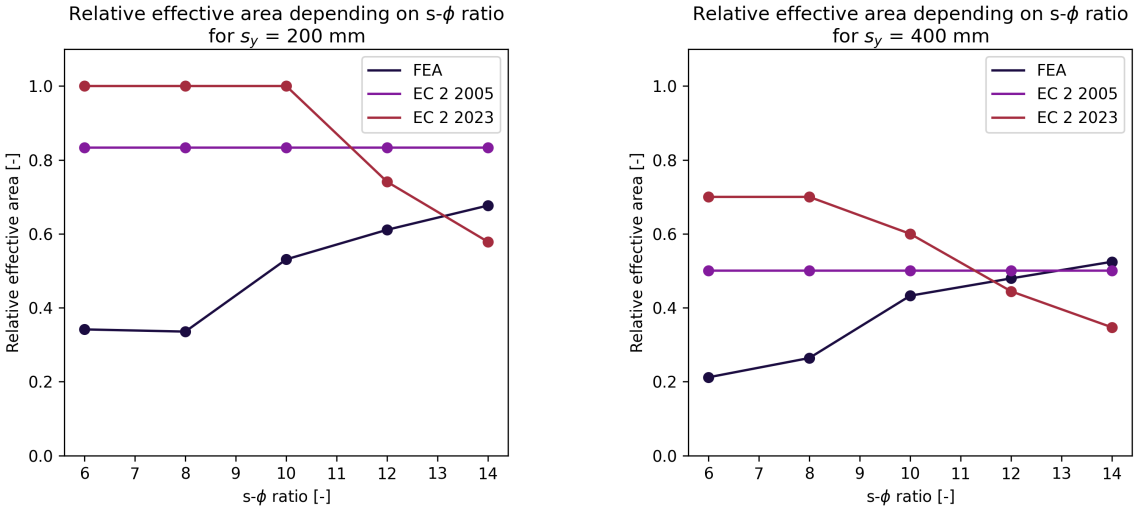

(a) s_y=200 mm. **(b)** s_y=400 mm.

Figure 6.12: Comparison of effective area, $A_{c,eff}$ [m^2], from FEA and analytical analysis for study 1.

6.3.2 Study 2

In the following section, FEA and analytical results from study 1 are compared. This is presented in both tables and graphs.

6.3.2.1 Transmission length

A comparison of the results from FEA and the analytical analysis of the transmission length from study 2 is presented in table 6.13 below. Analytical results are presented based on the definitions of $A_{c,eff}$ from both versions of EC 2. These values are further visualised in two graphs for the two thicknesses, see figure 6.13, where the trend of how the transmission length changes in relation to the ratio can be seen based on FEA, old EC 2 and new EC 2.

As for study 1, the analytical results of transmission length based on the two models for effective area are almost equal to each other. Also, the difference between the two thicknesses are neglectable. An observation here, though, is that both analytical and FEA results show an increasing transmission length with an increasing s_x-ϕ ratio.

Table 6.13: Comparison of transmission length, l_t [m], from FEA and analytical analysis for study 2.

Ratio	**FEA**		**Analytical old EC 2**		**Analytical new EC 2**	
	$s_y = 200$ mm	$s_y = 400$ mm	$s_y = 200$ mm	$s_y = 400$ mm	$s_y = 200$ mm	$s_y = 400$ mm
$s_x = 6\phi$	0.350	0.400	0.293	0.307	0.297	0.312
$s_x = 8\phi$	0.375	0.400	0.313	0.336	0.317	0.340
$s_x = 10\phi$	0.400	0.425	0.350	0.385	0.353	0.389
$s_x = 12\phi$	0.400	0.425	0.359	0.404	0.359	0.404
$s_x = 14\phi$	0.400	0.425	0.398	0.415	0.395	0.412

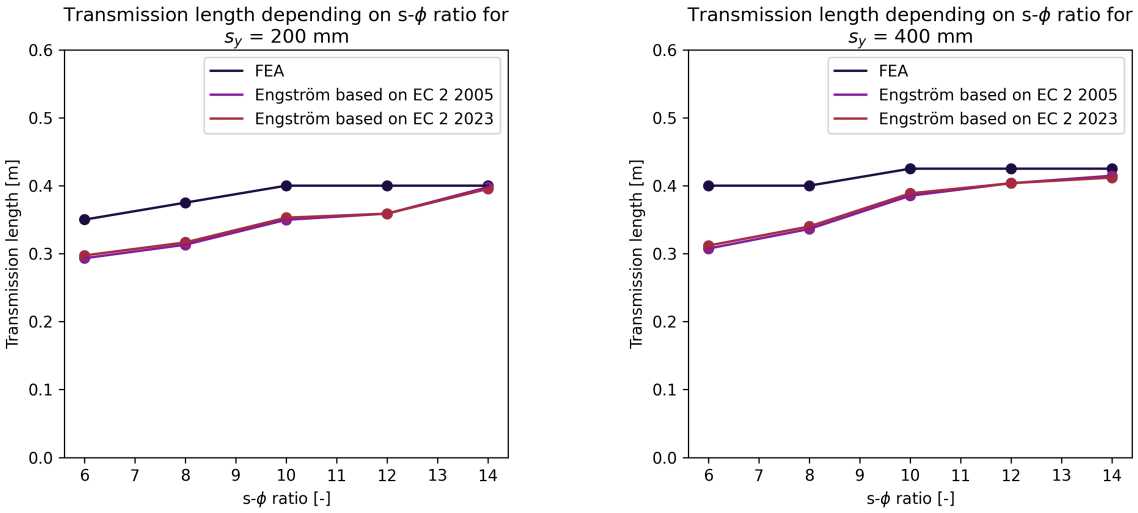

(a) s_y=200 mm. **(b)** s_y=400 mm.

Figure 6.13: Comparison of transmission length, l_t [m], from FEA and analytical analysis for study 2.

6.3.2.2 Effective area

In table 6.14, a comparison of the results for the effective area for study 2 is presented. The development of the effective area based on FEA, old EC 2 and new EC 2, in relation to the s_x-ϕ ratio, can also be seen in the graphs below. In figure 6.14, a comparison of the thinner and the thicker members is shown.

For the thinner element, FEA shows a significantly lower effective area than the EC 2 models. Comparing results from FEA with the old version, similarities of an almost constant area can be noticed. For the thicker element, better correlation can be observed. As for the thinner element, the numerical values are lower according to the FEA, but the trend corresponds quite well to the new version of EC 2. For values above s_x-ϕ=10, the new version and the analysed model behave similarly.

Table 6.14: Comparison of effective area, $A_{c,eff}$ [m^2], from FEA and analytical analysis for study 2.

Ratio	FEA		Old EC 2		New EC 2	
	$s_y = 200$ mm	$s_y = 400$ mm	$s_y = 200$ mm	$s_y = 400$ mm	$s_y = 200$ mm	$s_y = 400$ mm
$s_x = 6\phi$	0.177	0.108	0.150	0.150	0.180	0.180
$s_x = 8\phi$	0.110	0.158	0.200	0.200	0.240	0.240
$s_x = 10\phi$	0.158	0.216	0.250	0.250	0.300	0.300
$s_x = 12\phi$	0.165	0.225	0.300	0.300	0.300	0.300
$s_x = 14\phi$	0.216	0.230	0.350	0.350	0.300	0.300

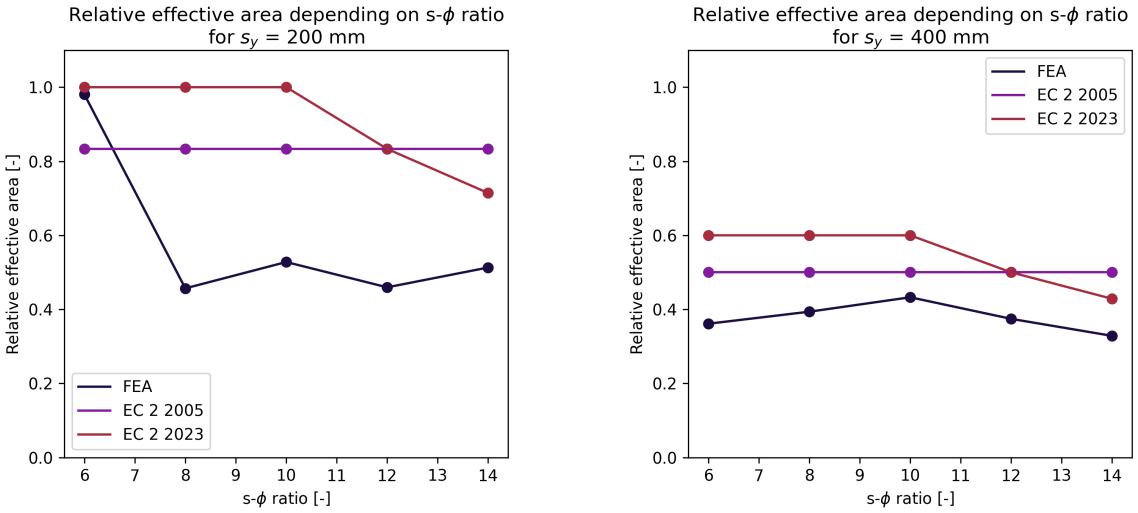

(a) s_y=200 mm. **(b)** s_y=400 mm.

Figure 6.14: Comparison of effective area, $A_{c,eff}$ [m^2], from FEA and analytical analysis for study 2.

7

Discussion

7.1 Discussions of results

In the following section, the results from the FEA and the analytical analysis are further discussed. The discussions addresses whether the result are reasonable and are aligned with theory, and if not, possible reasons for that are discussed.

7.1.1 Study 1

Comparing the trend for the effective areas obtained from the FEA with the values based on the effective area models provided in both the old and new versions of EC 2, there is a clear lack of correlation, as seen in figure 6.12. This discrepancy is especially clear when comparing the FEA results with the new EC 2 model, where the trend of the effective area in relation to the ratio is almost reversed. The old version consistently overestimates the effective area for the thinner member, while for the thicker member, it overestimates the area at small ratios and provides a reasonable estimate for larger ratios.

Overall, the numerical values from FEA correspond better to the models provided in EC 2 at higher ratios, where each bar, according to the new EC 2 model, should have an isolated effective area not overlapping the others. Since the new EC 2 states an effective width equal to 10 times the bar diameter, smaller bars should imply a smaller effective area, which is not the case in the FEA results, as the trend shows the opposite.

Comparing the thin and thick members, the thinner one shows a relative effective area larger than the one for the thicker member. A correlation between the two thicknesses, in terms of development of the relative effective area in relation to the ratio, as can be seen in figure 6.5, was expected. The observed constant difference in effective area for all s_x-ϕ ratios seems reasonable since the thicker member has a larger area between the two reinforcement layers, which does not contribute to carrying stresses. On the other hand, in figure 6.12, both of the EC 2 models shows a larger change in relative effective area compared to the FEA results. The fact that they do not change similarly indicates that the EC 2 models do not apply to all structures, either to restrained elements or to certain member thicknesses.

The trend based on FEA in figure 6.12 shows a constant relative effective area for

ratios 6 and 8, especially for the thinner member, where the thicker member shows a slightly increasing value. This part being constant indicates that these cases are considered as a group of bars, even though the effective area is significantly smaller according to FEA than according to the EC 2 models.

The distribution of stresses can further visualise the behaviour. As seen in figure 6.3 and 6.4, ratios 6 and 8 have noticeably lower values of concrete stress between the bars than the others. Based on theory, members with the entire cross-sectional area considered as effective should have an almost even stress distribution around f_{ctm} at the moment of crack formation. The obtained even stress distribution for larger ratios, which, according to theory, should not be entirely activated, is therefore unexpected. A larger bar diameter, with a larger anchor area between steel and concrete, transfers the same amount of stress over a shorter distance than a smaller bar. This may be the reason for these results, where all transfer of stresses from the steel to the concrete takes place in a smaller distance than half of the bar spacing. For a case with a smaller bar diameter, a longer distance of this transfer is subsequently needed. This theory can also be validated with the behaviour that can be studied in 6.1, where the distance to the maximum tensile stress section is longer for the cases with a smaller diameter, i.e. a longer distance is needed for the steel to transfer stresses to the concrete, so that the critical stress is reached.

On the other hand, the dispersion of stresses within the concrete seems to appear similarly, and independent of the bar diameter, since the stress distribution along the z-axis between the two layers of reinforcement, at $y = H/2$, is very similar in all cases. This can be seen in figure 6.1, where a very subtle trend of increasing stresses at the left restrained end can be seen, at least for the thick member. As stresses are distributed according to stiffness, this behaviour might be connected to the amount of total stiffness that is constituted by the concrete, which increases with larger s-ϕ ratios.

Analysing the stress distribution over the cross-section, as seen in figure 6.2, smaller bars result in a higher total stress over the cross-section. Based on the EC 2 models, a smaller diameter should imply a smaller effective area. For a constant load, higher stresses should be observed in cases where the effective area is smaller, since stress is given as the relation between the applied force and the loaded area. Therefore, a higher stress for a small bar diameter is reasonable, in case of a constant load applied. But, for the method used for analysis, as presented in chapter 4, the applied load at the critical load step varies between the studied cases, and therefore, the explained theory is not the reason for this. Another possible reason for these results could be that stresses are evaluated in different z_{max}, which capture different stress distributions between the reinforcement layers, as can be seen in figure 6.1.

Comparing the results in terms of transmission length, some differences between the results from FEA and the analytical ones based on the EC 2 models can be observed. Especially in terms of development with respect to the ratio. The numerical differences can partly be a consequence of the method used for the evaluation, which is dependent on the mesh size. However, the trend with respect to the ratio was expected to be similar for results based on FEA and EC 2 models, and it cannot be totally explained by the mesh dependency. It may be the case that the FEA results

are inaccurate, but another possible explanation could be that the models used for analytical analysis of the transmission length are not applicable for either thick or restrained members, and that both of the analysed thicknesses behave as thick members. Whether the elements behave as thin or thick members is, as mentioned, uncertain, but for all cases, the maximum stress section takes place within the transmission length, indicating that the elements are considered as thick.

7.1.2 Study 2

The two thicknesses differ in terms of how the relative effective area varies in relation to the ratio, according to figure 6.14. For cases when the s_x-ϕ ratio is 10 or above, the relative effective area for the thick member aligns with the expected behaviour based on the new EC 2 model. In those cases, bars are treated as isolated bars, according to the new EC 2. In comparison to the old version, the values of the effective area do not differ so much either, indicating that the old EC 2 model may be applicable to this type of element. But, as earlier mentioned, the numerical values from the FEA may be inaccurate, and therefore no reliable conclusions can be drawn based on that only. On the other hand, for the thinner member, the only ratio that behaves as expected according to the models in EC 2, is the s_x-ϕ ratio 6 for case 2A. In that case, when the spacing between the bars is small, the relative effective area is close to or equal to one.

The fact that the FEA results show a relative effective area equal to one for the thinner element in case 2A is, though, something that can not be trusted for sure, since that single case of the study displayed a noticeably different behaviour from the other cases. The result may be reliable, but there could also be some error in the analysis. If the results for s_x-ϕ=6 are disregarded for the thinner element, the trend of the effective area with respect to the ratio becomes more similar to that of the thicker element.

When comparing the results from FEA for the two thicknesses further, several observations similar to those in study 1 can be made. The thinner member exhibits a larger relative effective area in all cases, and the trends for the thinner and thicker elements are similar for the three mid cases, $s_x = 8, 10,$ and 12, which is reasonable, as discussed in section 7.1.1. Also for this study, the results from Eurocode show a larger change in relative effective area than the results from FEA. However, the relative effective area for the thinner member shows a different behaviour than the thicker member for the smallest and largest s_x-ϕ ratio, which is interesting, especially for case 2A where $s_x = 6\phi$. Since the relative effective area in that case is close to 1, this opens up for other discussions regarding thin and thick members and overlapping of effective areas.

Another observation is that there is no relationship between the magnitude of the concrete stress between two bars and the s_x-ϕ ratio, as seen in figure 6.9. It was expected that a larger spacing would result in lower stress at those areas. Neither this or the opposite can be noticed, which indicates that there are uncertainties in the obtained results. The results in terms of the effective area depend on the post-

processing and may therefore be inaccurate due to the evaluation in that procedure. However, since the concrete stress is a direct output from the FEA, this indicates that there are issues related to analysis itself, as further discussed in section 7.2. Alternatively, the stress distributions are influenced by several parameters that vary with the bar spacing, implying that no clear trend can be observed.

Studying the stress plots in the z-direction in figure 6.6, the transfer of stresses shows a slightly subtler but similar trend as for study 1; the maximum tensile stress section, z_{max}, is reached further away from the edge for larger s-ϕ ratios. This indicates that there are parameters besides the anchor area between the steel and the concrete creating this trend, as the bar diameter in this study is kept constant. However, in contrast to study 1, the concrete stresses at the left edge decrease for larger ratios. This may be explained by the fact that larger areas contribute to carry stresses for cases with larger s_x-ϕ ratios, and that the change in total concrete area influences the behaviour more than the overall stiffness relation between the steel and the concrete.

Regarding the transmission length, both FEA and EC 2 models show an increasing trend with increasing s_x-ϕ ratio. The differences in numerical values can, as in study 1, be explained by the mesh dependency. Regarding z_{max}, the same observations can be made as for study 1; it moves further away from the loaded edge with an increased s_x-ϕ ratio. It appears within the transmission length for all cases, except one. For case 2A, z_{max} appears at the opposite side of the transmission length, indicating thin member behaviour, which could be expected as it is the case with the largest bar diameter and the greatest amount of reinforcement relative to concrete in this study. This indicates that behaviour where the stress reaches f_{ctm} in the entire cross-section simultaneously exists, behaving as a thin member. But, as mentioned, this is the only case with this kind of result and might be caused by some error. Hence, even if it is showing a behaviour in line with the theory, a single case can not state this behaviour alone.

7.1.3 General observations from study 1 and 2

Based on the FEA results for both of the studies, a clear observation is that cross-section concrete stress concentrations in the surroundings of the reinforcement bars take place. Consequently, it can be confirmed that the concept of effective areas exists in restrained elements. It is also clearly shown that a section in the z-direction with significantly larger stress concentrations takes place. Hence, the theory of the maximum tensile stress section, where the next crack is likely to occur, is verified.

Another observation for all studied cross-sectional geometries is that the effective areas are significantly influenced by the concrete stresses between the bars, generating inaccurate effective areas. This is also a possible explanation of why the effective areas obtained from the models in EC 2 and the numerical results show opposite trends. As the stress distribution between the reinforcement bars is a direct consequence of where the maximum tensile stress section occurs, the resulting effective areas from FEA correspond well to the obtained stress plots. This indicates that the method is a subject for improvement, which is further discussed in section 7.2.

Due to previous reasoning, the total stress distribution over the element influences the obtained effective area. Consequently, the effective area is affected by the geometry of the element. For example, the thickness influences the results, since the stressed area changes accordingly. No clear trends indicating that some geometries generate better results than others can be seen, and therefore, no certain conclusion regarding applicable geometries can be stated.

According to the results, all studied members, except for case 2A, can be considered as thick members, since the maximum tensile stress section appears within the transmission length. However, no clear definition for thin and thick members based on geometry can be stated without further investigations. If the results from the case acting as a thin member can be considered valid, interesting correlations for the point of transition between the thin and thick members may be observed. As the maximum tensile stress section moves closer to the edge for a smaller s-ϕ ratio in both the x and y-direction, it is indicated that the maximum tensile section disappears immediately when the member can be considered as thin.

Due to the lack of any significant correlations of the results, no improvement for a new model can be proposed. However, due to these inconsistent results, clear evidence that the effective area in restrained elements requires further investigation. Either further evaluation of whether the existing models apply to such elements, or what improvements are needed when developing a new model.

7.2 Discussion of method and sources of error

The lack of correlation in the results might be a consequence of uncertainties in the performed study. The subsequent section reviews the adopted analysis method and proposes possible refinements, as well as it addresses possible sources of errors.

As the concrete in the FEA is modelled with a linear material, no cracking can take place. Hence, cracking behaviour cannot be studied at all, and no conclusions regarding correlations between effective area and cracking behaviour can be drawn. Furthermore, all stresses exceeding f_{ctm} are inaccurate. Since a crack forms in a process, starting with micro-cracks, the stress distributions slightly below f_{ctm} are influenced by this as well. This is, though, not captured in the linear material. As a consequence, the maximum tensile stress section, which gives the z-plane where the effective area is evaluated, might not appear at the exact same position for a linear and non-linear material. The influence of microcracks on the stress distribution may also increase the area subjected to f_{ctm} before a fully developed crack is formed, meaning that the effective area according to the evaluation method used in this thesis might be underestimated using a linear material.

Another consequence of using a linear material is that cone failure at the edge of reinforcement is not captured. In reality, bond stresses do not occur at the concrete surface due to local concrete cone failure. In the adopted model, transfer of stress is still allowed in this area, and large stress concentrations at the concrete surface adjacent to reinforcement bars are present in the model. This behaviour can be

noticed in stress plots in the yz-plane and the xz-plane. Some consideration of this has been taken, since the two elements closest to the edge were ignored during post-processing when searching for the maximum stress section. This may still result in slightly inaccurate values for the transmission length and maximum tensile stress section.

The comparison between the effective areas obtained from FEA and those predicted by both EC 2 formulations shows a clear lack of agreement. Although the FEA results cannot be dismissed as inaccurate, the extensive empirical basis and validation underlying EC 2 indicate that the deviations may stem from shortcomings in the current modelling strategy. As the evaluation of the effective area based on the FEA results uses the stress distribution over the entire cross-section equally, all stress data contribute. Since the results show increasing stress between reinforcement bars with increased s_x-ϕ ratio, at least for study 1, this makes the effective area increase with an increased s_x-ϕ ratio as well. Nevertheless, the stresses between the reinforcement bars are significantly lower than the stresses in the surroundings of each bar as well as the tensile strength, according to the obtained stress plots. Therefore, it can be discussed to what extent these stresses should influence the effective area, as they probably do not contribute to cracking. Because of this, the accuracy of the method should be carefully considered.

Regarding the method for obtaining the load step and cross-section plane where the effective area is evaluated, there are some uncertainties to consider. As previously discussed, using a linear material disregards all effects regarding cracking. Therefore, the effective area is evaluated according to the maximum tensile stress section, estimating the position of the next crack, instead of using the position for an actual crack. In reality, the crack position may occur at a slightly different location because of stress redistribution during the crack formation phase. Furthermore, since the stress distributions may be inaccurate, this can affect which load step and how much of the total loading is applied when the effective area is evaluated. These two effects, in combination with a varying stress distribution in all directions, indirectly influence the evaluation of the effective area and may cause inaccurate results.

The mesh can also be a source of inaccurate results. Since the mesh affects the positions where all data is evaluated, it is of great importance. Even if a mesh convergence study is performed and the chosen mesh is considered accurate, the mesh still influences the obtained results. For example, coarseness in the mesh influences the evaluation of transmission length based on the FEA results. Since the transmission length is evaluated based on reinforcement stresses in each node and is set based on the z-coordinate in a certain node where stresses stop changing, the accuracy of the obtained transmission length is limited to the element size.

The geometry of the specimen clearly influences the results, as all sets of variable input resulted in different behaviours. Also, the fixed input parameters connected to the geometry of the analysed element, such as cover thickness, do influence the behaviour. Even though these parameters are chosen according to realistic cases, the obtained results can not be considered accurate for members with other input values for these parameters. Another thing that may influence the behaviour is the applied boundary conditions, especially in the symmetry lines along the element's

length. Because of the symmetry boundary conditions, the element can theoretically be considered as a continuous member in the x-direction. But in the FE model, the rigid supports may result in some unrealistic local behaviour, since no entirely rigid connections exist in reality.

Another possible source of error that might be connected to the method is the variation in the number of data points, which can be observed in figure 6.4a, for example. As discussed in section 4.3.4, this behaviour is expected since the mesh order is quadratic and different numbers of nodes are present at different z_{max}. However, this might influence the results, since the non-present data points can not be assumed to correlate with the average values for the captured data points. But since the missing positions, in all cases, are equally distributed over the entire specimen, the influence can be assumed to be small.

Furthermore, long-term creep effects are disregarded throughout the study, which may have affected the results. Since creep affects the stiffness of the structure, stress distributions could have been different if effects from creep were included. On the other hand, these influences can be expected to be small, as the applied load to the structure is arbitrary, and the results are extracted based on response according to the same stress range, independent of the external load.

7.3 Further studies

As the original idea for this thesis was to study cracking behaviour related to the effective area, which was never solved, it is still of great interest to develop the original approach. That could be done by performing a similar set of FEA as in this thesis, but using a non-linear concrete material instead. It would then be possible to evaluate how the effective area influences the cracking behaviour and whether the models for the effective area presented in EC 2 are overestimating the cracking behaviour or not.

To better verify the observed behaviours, it would be of interest to evaluate more geometries. Especially to investigate whether the results for the case 2A are accurate, it would be interesting to investigate the behaviour of members with s_y-ϕ ratios below 10. Since this is the cross-section geometry with the largest amount of reinforcement and the largest bar diameter, it is hard to state if the different results in this specific case can be connected to an error or if the behaviour for members with a higher amount of reinforcement would be similar. If a similar behaviour can be observed, several interesting conclusions regarding the transformation between thin and thick members could be drawn. Additionally, results for thinner members may give a clearer overview of how the effective area forms in relation to the proportions between s_x and s_y and whether isolated bars are relevant to consider.

As discussed in section 2.3.2, thick and thin members differ in terms of the correlation between transmission length and concrete stress distribution over the cross-section. For thin members, it is assumed that the concrete stress is uniformly distributed at the end of the transmission length. On the other hand, for thick members, a longer

distance from the crack than the transmission length is needed for the dispersion of the concrete stresses, which is the reason why effective areas are created. This difference in behaviour could be of interest to evaluate in further studies, especially since there is no clear limit or definition to distinguish between thick and thin members. By varying the thickness of the element, the behaviour in terms of stress distribution over the section at different distances from a crack could be investigated, in order to come up with some conclusions about what the definitions of a thick and thin element are.

To investigate the importance of the scale of the analysed element, it could be of interest to study the behaviour in a case where both the spacing and diameter changed in a way so that the s_x-ϕ ratio is kept constant. Conclusions regarding how a change in bar diameter corresponds to a change in bar spacing could then be drawn, and the obtained results from this study may then, based on that, be easier to evaluate. Furthermore, it could be interesting to see if there are any clear differences between the change in bar spacing and the change in bar diameter, since the new version of EC 2 handles these parameters equally in the model for effective area.

8

Discussion of encountered issues in FEA

The original aim of this thesis was to evaluate the cracking behaviour in restrained elements according to the effective area, not only the stress distributions related to the cracking process. Since convergence issues occurred when modelling non-linear concrete material, the original aim was changed, and linear concrete material was used instead. As a consequence, the cracking behaviour could not be investigated. This chapter covers the original main ideas and further explains the original FEA setup. Observed effects on convergence connected to several input parameters are also addressed.

Limiting the study to linear behaviour slightly changes what results could be obtained. For example, the possibilities of what parameters could be compared between the analytical and the FEA results were limited, such as the number of cracks and crack widths. As a consequence, the research questions were slightly changed to address what could be evaluated with the new approach. The original research questions are presented below.

- *How do the results based on the effective areas $A_{c,eff}$ given in the old and new EC 2 differ in terms of cracking behaviour?*
- *Are the models provided in EC 2 accurate compared to non-linear FEA regarding the results of cracking behaviour?*
- *How do the above specified variable input parameters affect the results from both non-linear FEA and analytical models? Are the analytical models more accurate for certain parameter sets?*
- *What conclusions can be made regarding the effective area to provide a basis for an improved model?*

8.1 Original approach

The original idea was to model a three-dimensional end-restrained element subjected to tension caused by a uniform compressive deformation applied to the concrete, using a non-linear concrete material model. This original concept for the study is

hereinafter referred to as the original approach. The original element is illustrated in figure 8.1. By subjecting the element to an imposed strain, in combination with a bond-slip reinforcement material, studies of cracking behaviour were intended to be performed based on a non-linear analysis.

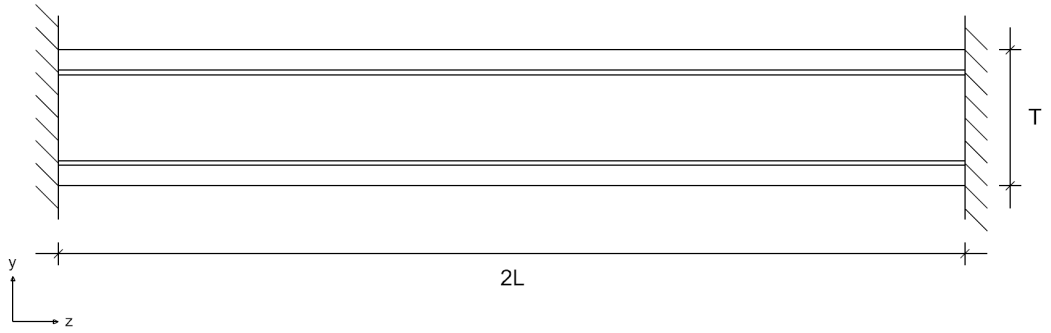

Figure 8.1: Illustration of longitudinal section used in analysis. The element is three-dimensional and therefore has a certain width out of the plane (created by the authors).

The following sections describe the DIANA setup in the original approach. Since much of the original approach was equally defined as for the performed study described in chapter 4, only the major differences are stated here.

8.1.1 Geometry and load

The initial geometry is illustrated with the longitudinal section in figure 8.1, but different models aiming to study the same problem were investigated as well. Which models that are implemented are further described in section 8.2.1. Furthermore, the cross-section geometry was varied arbitrarily during testing, which also might affect the comparability between the obtained effects when changing different parameters.

The imposed strain was initially applied as a volumetric load in the z-direction, acting equally on all concrete elements. Still, some adjustments were made for that as well, which are further described in section 8.2.1 as well. The strain was applied as the load for all models, except for the later described pull-out model, which was subjected to a load similar to the one in the performed study, an imposed displacement at one reinforcement edge.

8.1.2 Materials

The main difference between the original approach and the performed study is the non-linear concrete material and the possibility of studying cracking behaviour. The

non-linear concrete material was modelled with a softening law, i.e. a stress-strain relationship that can be evaluated in different manners according to different theories. To understand how the stress-strain curve is evaluated, some background about the total strain crack model and the adopted smeared crack approach is needed.

8.1.2.1 Total strain crack model

A total strain crack model, based on the smeared crack approach, was used. This model describes cracking behaviour in several directions, with the main concept that stresses are evaluated in the crack directions (DIANA FEA BV, 2026). The total strain model can be set as fixed or rotating, where the rotating model evaluates stress-strain relations in the actual principal direction of the stress tensor, while the fixed model uses a fixed coordinate system. Initially, the fixed model was applied, but both of these were further evaluated.

8.1.2.2 Smeared crack approach

The main idea behind the smeared crack approach is to smear out the crack over a certain distance (DIANA FEA BV, 2026). This distance is referred to as the crack bandwidth, h_{cr}, which is represented by one or several elements in the model (Broo et al., 2008). In that way, no concentrated cracks are added to the model. Instead, a plastic strain that resembles the total crack width in each affected element is obtained. This model makes it possible for cracks to appear in any element at arbitrary positions, which is preferable when the aim is to study the crack pattern, for example. On the other hand, the smeared crack approach can be mesh dependent. For most of the models that use the smeared crack approach in DIANA, a crack bandwidth is needed (DIANA FEA BV, 2026). To evaluate this crack bandwidth, there are different methods available: Roots, Govindjee and user-specified. The first two methods use the element size, meaning the smeared crack model and the softening law become mesh dependent.

8.1.2.3 Softening law

In combination with the total strain crack model used in this FEA, different softening laws describing the tensile behaviour can be used according to DIANA FEA BV (2026). For the softening law, DIANA provides pre-defined relationships based on some user-specified parameters, as well as the possibility to insert a user-defined multilinear relationship. Several different softening laws were implemented during testing, but initially, the non-linear concrete material was modelled using a bilinear softening law described by International Federation for Structural Concrete (Fib) (2022). The model is constructed by a multilinear stress-strain curve based on fracture energy, meaning that unknowns in the relationships for crack width and tensile stress are evaluated according to a known fracture energy.

The stress-strain relationship can, based on the fracture energy and the smeared

crack approach, be evaluated according to the expressions in equation 8.1-8.4, given by International Federation for Structural Concrete (Fib) (2022). Additionally, in appendix E, the Python script used for the definition of the non-linear concrete material is attached. The area under the graph in figure 8.2b is equal to the fracture energy, G_f, evaluated in equation 8.1.

$$G_f = 85 \cdot f_{ck}^{0.15} \quad \text{with } f_{ck} \text{ in mm} \tag{8.1}$$

From that, the crack widths along the x-axis in the figure can be evaluated according to equation 8.2.

$$w_1 = \frac{G_f}{f_{ctm}} \quad \text{and} \quad w_c = 5 \cdot \frac{G_f}{f_{ctm}} \tag{8.2}$$

To rewrite the $\sigma_c - w$ relationship to a $\sigma_c - \varepsilon$ relationship that can be implemented in DIANA, the element size can be used to convert the crack width deformation into a relative strain, as in equation 8.4.

Furthermore, to account for the elastic region, a critical strain, ε_{cr} is defined according to equation 8.3 and added to both strains, ε_1 and ε_c.

$$\varepsilon_{cr} = \frac{f_{ctm}}{E_{cm}} \tag{8.3}$$

$$\varepsilon = \frac{w}{l_{elm}} + \varepsilon_{cr} \tag{8.4}$$

The final $\sigma_c - \varepsilon$ relationship is then defined as in figure 8.2a for concrete strength class C25.

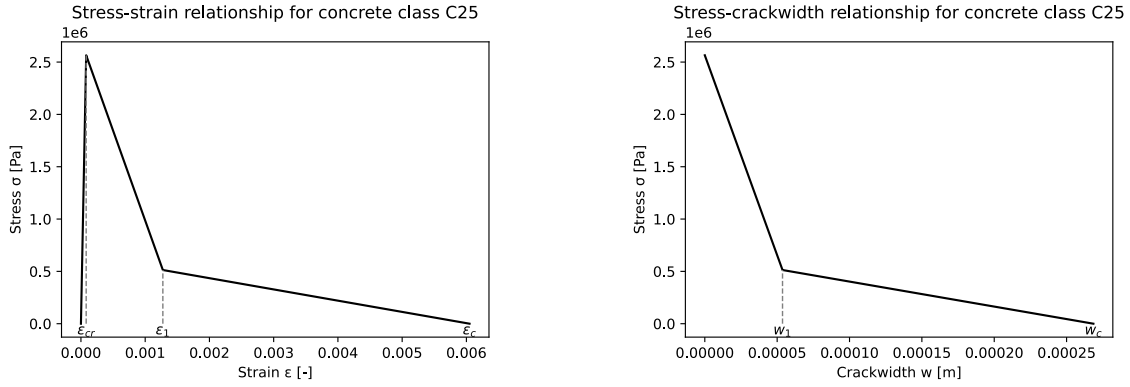

(a) Stress-strain relationship. **(b)** Stress-crack width relationship.

Figure 8.2: Fracture energy-based softening law used as initial input in DIANA (created by the authors).

Regarding the pre-defined softening laws, the Hordijk law is interesting, since it has a smoother shape in the descending branch and takes the crack bandwidth as input.

The ways of defining the crack bandwidth described in section 8.1.2.2 are applicable for the Hordijk softening law as well. The influence on convergence for the different settings associated with Hordijk softening laws is described in section 8.2.2.

8.1.2.4 Non-linear bond-slip relationship

For the non-linear bond-slip relationship, initially, the formula for the first branch was taken as equation 8.5 according to Engström (2014), as in the performed study described in section 4.1.2. But different relationships were evaluated as well. For example, the relationship presented in equation 8.6 according to International Federation for Structural Concrete (Fib) (2022) was investigated. The main difference between the two models is the expression for the first branch and its dependency on the strength class, as can be seen in the expressions below and figure 8.3.

$$\tau_b = 0.22 f_{ctm} \cdot \left(\frac{s}{s_1}\right)^{0.2} \tag{8.5}$$

$$\tau_b = \tau_{b.max} \cdot \left(\frac{s}{s_1}\right)^{\alpha} \quad \text{with} \quad \tau_{b.max} = 2.5 \cdot \sqrt{f_{cm}} \quad \text{and} \quad \alpha = 0.4 \tag{8.6}$$

where f_{ctm}, f_{cm}, s_1 and α are parameters depending on what type of reinforcement and concrete mix is being used.

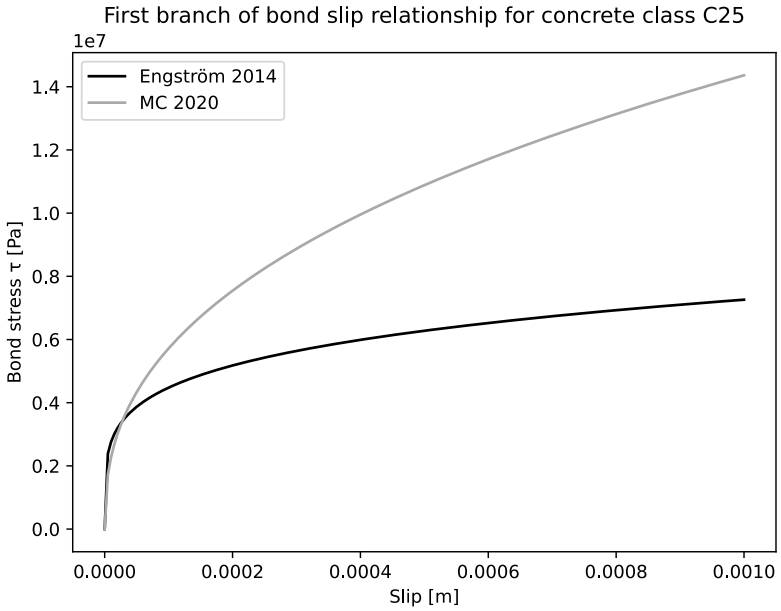

Figure 8.3: Bond slip curves for the first branch based on Engström (2014) and International Federation for Structural Concrete (Fib) (2022) for concrete class c25 (created by the authors).

8.1.3 Mesh

The initial mesh order was, because of simplicity, set to linear, but quadratic elements were tried as well. As the mesh element shape, hexahedra were mainly used, but some analyses were performed using tetrahedra. Regarding the mesh size, initially a coarser mesh, with $l_{elm} = 0.05$ m, was used to minimise time consumption during calculation, but some analyses were also performed with a finer mesh, $l_{elm} = 0.01 - 0.02$ m.

8.1.4 Analysis setup

The settings for the analysis in DIANA can be changed in terms of several parameters that influence the possibilities for convergence. The following sections describe the setup in terms of the load stepping and the equilibrium iteration procedure.

8.1.4.1 Load stepping

In the load stepping procedure, manual load steps were used to begin with, initially larger load steps that were further revised to smaller ones. Automatic load stepping procedure, with different step size limits, was evaluated as well. The load incremental procedure can also be controlled in different ways: force control, displacement control or arch length control (DIANA FEA BV, 2026). For models with large changes in stiffness, such as non-linear concrete models, it can be beneficial to use arch length control. Therefore, analyses for all cases of load stepping procedures were performed both when arch length control was applied and not.

8.1.4.2 Equilibrium iteration

The possible options for the incremental root-finding methods in DIANA are Regular or Modified Newton-Raphson, Quasi-Newton and linear stiffness method. These methods differ slightly in terms of the required number of iterations per increment and time consumption per iteration (DIANA FEA BV, 2026). Generally, the more accurate solution methods require fewer iterations per load increment. For example, as discussed in section 4.2.2.2, the Regular Newton-Raphson method is more time-consuming per iteration compared to the Modified Newton-Raphson method but less accurate and requires many iterations per load increment. In the original approach, the root-finding method was initially set to the Secant method, or Quasi-Newton method, since it has relatively high accuracy compared to Modified Newton-Raphson and is still less time-consuming than the Regular Newton-Raphson method. The Quasi-Newton method in DIANA comes with three different solution methods for evaluating the secant stiffness matrix used in the iteration procedure. These methods are called the Broyden, the Broyden-Fletcher-Goldfarb-Shanno (BFGS) and the Crisfield methods. Initially, the default setting, which is BFGS, was used, but all the others were also tried.

Furthermore, the convergence tolerance criteria can, as indicated, affect the possibility

of convergence. It is of great importance to ensure convergence criteria are properly adjusted, since too loose criteria give inaccurate results while too strict criteria result in unnecessarily many iterations before convergence is considered to be reached. If that occurs in combination with a too low limit for the maximum number of iterations within a load step, convergence is not captured even though it should be. DIANA offers force, displacement and energy as convergence criteria, and the tolerance can be varied in terms of for example how small the change between two iterations must be to be for the solution being considered as converged. Initially, they were specified in the same way as in the preformed study, described in section 4.2.2.2, but to observe their influence on convergence, several combinations of criteria were tried as well. Additionally, the maximum number of iteration within a load step were set to 500, aiming for a relatively large value to ensure the possibility of convergence not being limited by this parameter, without allowing the iteration procedure to continue too long.

8.1.5 Convergence problems

Analysing this type of case turned out more challenging than predicted, and as mentioned, large issues regarding convergence were encountered. By introducing two non-linearities: the non-linear bond-slip relationship and the non-linear concrete material, the problem gets complex. Two non-linear equations have to be satisfied in the equilibrium iteration procedure for each load increment during analysis, which might be hard to achieve. Therefore, convergence becomes very sensitive and largely dependent on the model and analysis setup. The following section, 8.2, discusses the convergence issues related to the DIANA setup and how different input parameters influenced these issues.

8.2 Varying input parameters and effect on convergence

A lot of different input parameter setups have been evaluated in order to obtain a model that converges. This section describes how these parameters have been varied and the conclusions that can be drawn regarding the convergence issues based on the outcome.

As a consequence of the encountered convergence issues, parameters were changed, and different setups were tested to successively approach a model setup that converges. Hence, testing and evaluation of effects caused by different parameter setups were made as a part of a troubleshooting process rather than an organised study, which influences the comparability of the resulting effects. However, each parameter was, as long as possible, evaluated using the same remaining setup. But there is no original constant parameter setup that each parameter was tested in combination with. Instead, the most promising setup, according to previous testing, was used when evaluating the effect of convergence for each parameter. This decreases the

comparability between the different evaluations of how different parameters influence the possibilities for convergence. Numerical values stated in the following chapter, such as the load factor, are therefore only given to state a difference within each specific evaluation and cannot be compared with values that are stated based on the evaluation of other parameters. Aware of these limitations, this method in evaluating was considered a quicker way of approaching a usable model setup.

8.2.1 Varying geometry and load

As described in section 8.1.1, the objective was to analyse the effective area of an element subjected to pure tension. For that reason, the self-weight was neglected, avoiding any influence on the behaviour due to bending. As a consequence, the distribution of stresses becomes equal all over the model, causing struggles for the software to define a location for crack initiation. Probably because of that, not one single solution could be found during the iteration process, and divergence problems took place. In reality, there are often smaller imperfections or strength variations in the material introducing possible locations for a crack to be initiated, but these aren't present in the ideal DIANA model, making this an unrealistic and hard case to study.

Therefore, as an attempt to reach convergence, the geometry of the original model was modified. Different approaches were considered: different modelling concepts, applying a weaker material in a smaller part of the element, varying the magnitude of the applied strain, as well as subjecting only some parts of the element to the applied strain. In the following section, these changes are further described in terms of what was modified and the observed outcome.

8.2.1.1 Modelling concepts

The different models can be referred to as: the original end-restrained, the asymmetric end-restrained, and the asymmetric pull-out models, and are all illustrated in figure 8.4. These models were all used when evaluating the effect on convergence for other parameters, and the effects on convergence caused by geometry parameters are further discussed.

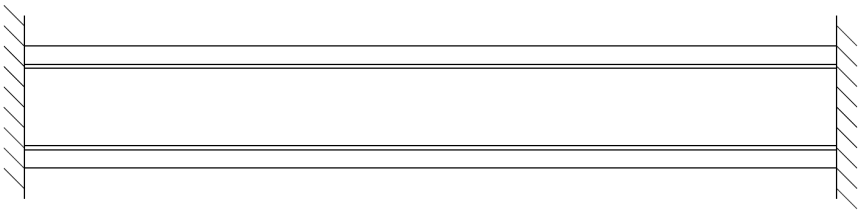

(a) Original end-restrained.

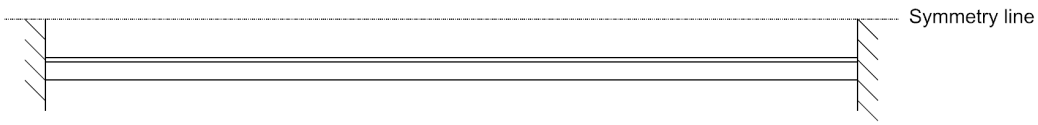

(b) Asymmetric end-restrained

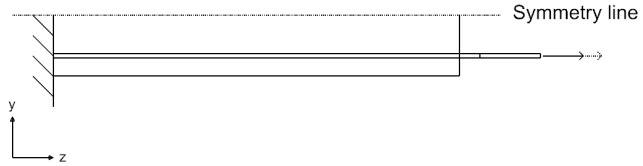

(c) Asymmetric pull-out.

Figure 8.4: Illustration of models used in FEA (created by the authors).

The original element contains several reinforcement bars. A simplification was made by cutting the element along its symmetry lines, reducing the cross-section to a single bar and its corresponding surrounding concrete, as illustrated in figure 8.4b. In such a model, the bar is not located centrally, and asymmetric loading is created, intending to make it easier to decide the location of a crack. Furthermore, considering a smaller geometry also implies a less computationally time-consuming model. This case is still considered as an end-restrained element with the concrete loaded by an imposed strain.

The expected outcome was that it should be easier to decide in which part of the element a crack would be created, due to asymmetry in geometry and consequently the distribution of stresses. This was, though, not the outcome. What could be studied were smaller asymmetries in the behaviour, such as the distribution of stresses and crack width for the first crack. But still, the model diverged after the first crack was created.

To eliminate the issues with the first crack, a pull-out model was defined and analysed. The pull-outmodel was similar to the one used in the performed study, with non-linear concrete material as the main difference. To minimise computational cost, the model

was cut into the symmetry lines in the same way as the asymmetric end-restrained model, as illustrated in figure 8.4c.

The main idea was to simulate a cracked section by loading the reinforcement at one edge in tension and to analyse only half of the length, and in that way make it easier for the model to find one single section for another crack. This was not the outcome, though, as convergence issues were encountered anyhow.

8.2.1.2 Weak material

To promote a location for crack initiation and to activate the transfer of stresses between the reinforcement within the crack and the surrounding uncracked concrete, a row of slightly weaker concrete material was implemented in the middle of the element. This approach was intended to, by introducing the first crack, force the bond-slip interaction to initiate, leading to a continuation of the cracking process. Evaluation of this tuned out with a similar behaviour as the original model: one crack was created, and after that, divergence occurred. The only difference that could be noticed was that the first crack was created at a lower load step than the original case did, which is not unexpected due to the lower strength.

As a further evaluation of this, the row of weak material was placed decentralised in the element. The background theory for this was that asymmetry would make the convergence easier, but the analysis was still aborted after the first crack was created.

8.2.1.3 Strain variation

To imitate material imperfections, which in reality cause smaller strength variations in all directions over the element, the strain was applied with a spatial variation. First, the strain was varied according to a sine curve with a certain amplitude. However, localisation problems remained. The reason why no improvement could be observed due to this implementation may be because a sine function has a certain fixed period, causing the same stress in several parts of the element simultaneously. Therefore, a case where the strain was varied over the length with a linear function, in combination with the sine function, was tried. This resulted in strain variations in both the height and along the length. No improvement could be noticed.

8.2.1.4 Application of strain

During some analysis, a crack was created adjacent to the edges, in addition to the single crack created in the middle. This behaviour seemed unrealistic and can perhaps be connected to very high stress due to totally fixed edges. Therefore, it can not be entirely considered as a realistic crack. To prevent this, the load was not applied to all elements except the ones adjacent to the edges. These changes were mainly done to disregard unrealistic behaviour rather than as a way of reaching for

convergence. As expected, no cracks were created at the edges, but no other effects on convergence behaviour could be noticed.

8.2.2 Varying material definitions

Since non-linearities are included in both materials, the material definitions likely affect the possibility of convergence. In the following section, the variations in implementation of material definitions are described, and conclusions regarding effects on convergence are discussed.

8.2.2.1 Tension softening law

Initially, the softening law was modelled using a bilinear curve based on fracture energy, as described in section 8.1.2.3. As a multilinear relationship, the curve contains sharp corners that might cause difficulties in terms of convergence. Therefore, analyses using a modified bilinear softening law, based on the same parameters as the initial one but with smoothed corners, were performed.

Furthermore, for the initial softening law, the element size is used to convert the stress-crackwidth relationship into a stress-strain curve, making the softening law mesh dependent. Therefore, several applications of Hordijk softening laws were evaluated, where the crack bandwidth was specified according to all possible options mentioned in section 8.1.2. However, the case where Hordijk softening law is used with a user-specified crack bandwidth is the only case where the softening law is mesh-independent, since the other methods use the mesh size for the evaluation of crack bandwidth. For this case, some different values for the crack bandwidth, between $8 < h_{cr} < 50$ mm, were tried as well. Illustrations of all three implemented softening laws are displayed in figure 8.5.

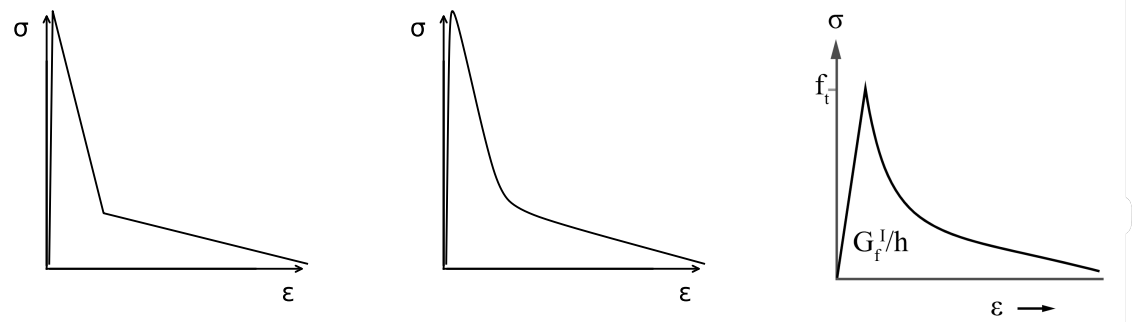

(a) Bilinear. **(b)** Smoothened bilinear. **(c)** Hordijk (DIANA FEA BV, 2026).

Figure 8.5: Illustration of softening laws tested in numerical analysis in DIANA.

When running analyses for all possible combinations of the above mentioned parameters, and the same overall setup, the case when the crack bandwidth was user-specified

as 0.01 m reached the highest load factor. In that case, approximately half the load could be applied before the analysis was aborted, while the other cases reached a maximum load factor around 0.1-0.2. In the resulting stress plot, the case with the user-specified crack bandwidth also stands out with a significantly larger area of stresses close to the tensile strength. This is illustrated in figure 8.6.

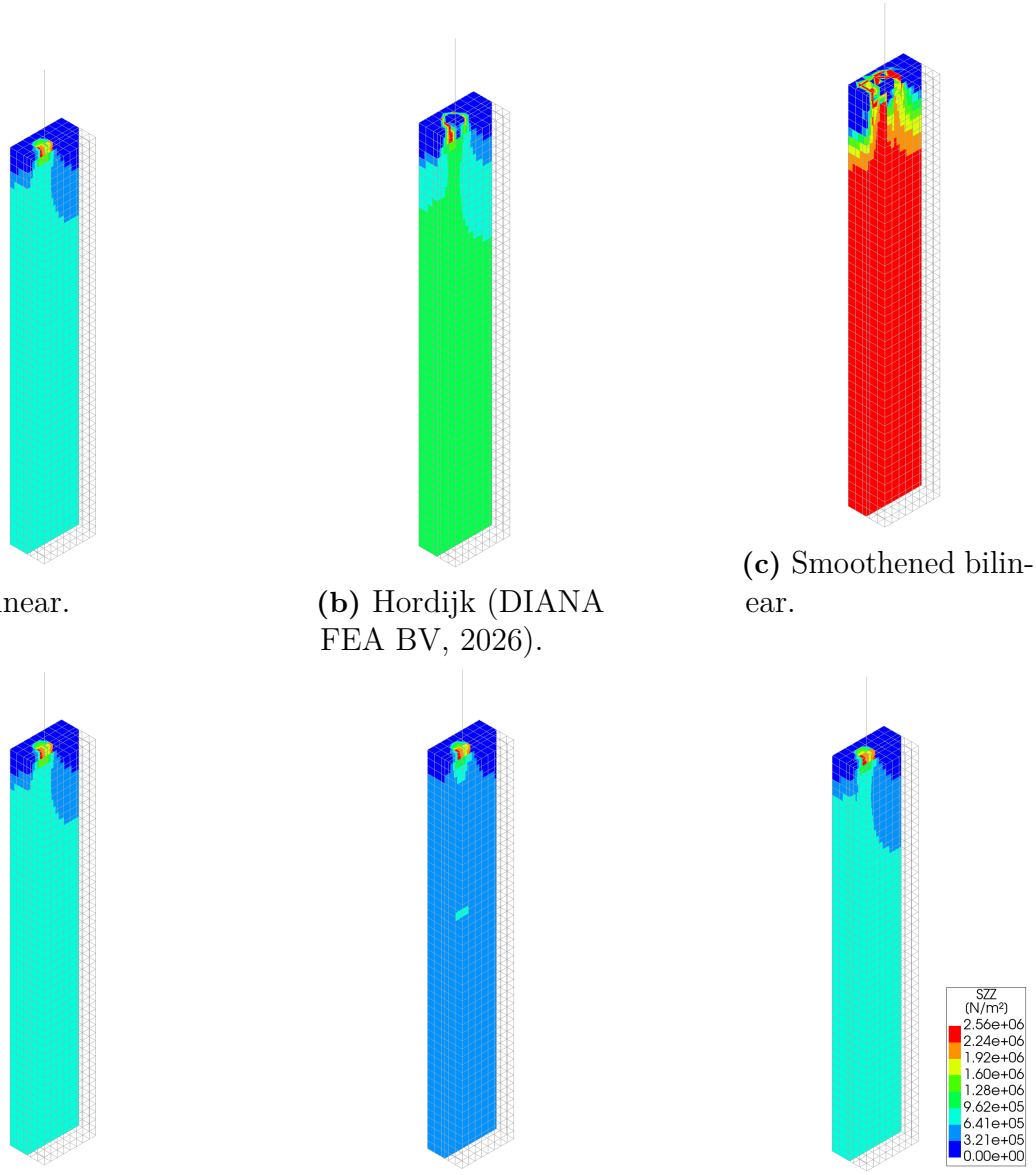

(a) Bi-linear.

(b) Hordijk (DIANA FEA BV, 2026).

(c) Smoothened bilinear.

(d) Rots, no reduction.

(e) Govindjee, no reduction.

(f) User defined 0.01 m, no reduction.

Figure 8.6: Stress plot at the last converged load step for different definitions of crack bandwidth in Hordjik material softening laws tested in numerical analysis in DIANA.

When running the analysis using the smoothed bilinear softening law, the maximum reached load factor was 0.11 compared to 0.15 as it was for the non-smoothed bilinear curve, indicating that smoothing of the curve does not increase the possibility of

reaching convergence in this case.

The overall conclusion regarding different softening laws is that a mesh-independent softening law affects the possibility of reaching convergence in a positive way, while a smooth curve does not seem to bring any benefits.

8.2.2.2 Bond-slip relationship

Different models for bond-slip behaviour were examined as well. For most analyses, the formula for the first branch was taken according to Engström (2014), but the model presented by International Federation for Structural Concrete (Fib) (2022) was investigated as well.

When running analyses, it could be noticed that the reached load factor for the same overall setup was significantly lower for the second expression, which could be an effect of the larger change in bond stiffness for the second expression, shown in figure 8.3

Another variable parameter according to the bond-slip relationship is the parameter s_3, which represents the clear distance between ribbons on the reinforcement bars and can be assumed to be a value within a reasonable range. Therefore, some different values for this parameter were evaluated. A reasonable assumption could be that the value of s_3 varies in line with the bar diameter. Therefore, a case where s_3 was set to $0.8 \cdot \phi$ was tried. The resulting load factor was exactly the same for the modified s_3 as for the original value of $s_3 = 8.4$ mm when evaluating a model with $\phi = 16$ mm. But in some cases, a larger s_3 value resulted in a slightly increased load factor.

What can be concluded regarding the bond-slip relationship is that convergence might be more easily reached if the stiffness has a steeper inclination initially, but reaches a lower maximum value in total. Another thing that might matter is the inclination of the third branch of the bond-slip curve, which is achieved both when s_3 is increased and τ_{max} is decreased, but this is clearly not influencing for all parameter setups.

8.2.3 Varying mesh

Since the mesh properties set the final geometry being analysed and generate the positions of nodes where results are evaluated, mesh properties are likely to affect the possibility of convergence.

8.2.3.1 Element types

Both tetrahedra and hexahedra were used as element shapes, where tetrahedra indicated easier convergence but generated irregular, unrealistic stress plots. For that reason, hexahedra were preferred for further analysis. One reason behind the easier convergence for tetrahedra can be that tetrahedra create a slightly more irregular

pattern of nodes, and deformations during the cracking process can therefore be solved for more easily.

8.2.3.2 Mesh order and element size

The mesh order was also varied between linear and quadratic for different element setups, and the general observation was that analyses with quadratic mesh order fail to converge at the very first load step. In contrast, analyses where linear elements were used continued for a while before convergence issues took place. The effect of changing the element size was observed to have a similar effect as changing the mesh order. When smaller elements were used, 0.01 m, the analysis was aborted already at the first load step, while it could continue in the cases where a larger mesh, 0.02 m, was used. These two scenarios can be connected since increasing the mesh order and the number of elements both generate more integration points. It can therefore be concluded that many integration points decrease the possibility of convergence at the beginning of an analysis in this case.

8.2.4 Varying analysis setup

Another thing that influences the possibilities for convergence is the settings for the analysis. In this section, different alternatives and observed outcomes are presented.

8.2.4.1 Load stepping

Manual and automatic load steps were both tried in combination with several models and analysis setups. In general, an automatic step size was observed to reach a higher load factor compared to a manual step size, but the most notable difference was the time consumption, which was significantly lower for automatic step sizes. That is probably because automatic load stepping uses as big steps as possible, and many unnecessary small load steps can then be avoided.

8.2.4.2 Equilibrium iteration

Regarding the effects on convergence connected to root-finding methods used in equilibrium iteration, analyses were performed for all different stiffness matrix evaluation methods connected to the Quasi-Newton method. The results could then be compared with results where the Modified Newton-Raphson method is used. It was observed that convergence took place more easily using the Secant method, and consequently, for the current overall setup, the analysis could be completed. In such analyses, an area of higher stress values could be seen, but no crack was created, even for an unrealistically large load. On the other hand, analysis performed with the modified Newton-Raphson method and the same overall setup resulted in the creation of one crack, but shortly afterwards, convergence problems were encountered, and failure took place.

In terms of convergence criteria, several different combinations were tried, but the effects of two combinations were studied in more detail. First, the initial combination as described in section 4.2.2.2, where any of the criteria force, displacement or energy could be satisfied to state convergence and the other one using force as a criterion only. In general, the convergence issues did not seem to be caused by the convergence criteria, but the analysis continued slightly longer when the first combination was used. Since the first combination includes several criteria that can be satisfied, easier convergence in that case makes sense.

8.2.5 General observations

The convergence issues are probably a complex problem with many interacting sources of error, making it harder to find a model setup that converges and produces reasonable results. In this thesis, the time frame was too short to fully investigate the influence of all parameters, and further studies on the topic can be made to find the perfect setup to analyse a three-dimensional end-restrained reinforced element with both non-linear concrete and bond-slip interface in FEA.

One theory behind the cause of the convergence issues could be the appearance of mesh dependency in material models. In the case when both material models require different mesh sizes to reach convergence, the same mesh can never satisfy both simultaneously, and convergence can never be reached.

Another theory could be that this geometry, loaded with uniform tension, may be too simplified, making it behave unrealistically. This has probably made it harder to reach convergence, but since modifications of the geometry to make it less symmetric have been made without any great success, the geometry being an unrealistic case is probably not the only reason for the convergence issues.

Further on, the idealisation that take place when the realistic behaviour is captured in a FE software, do also influence the possibilities for convergence. It is almost impossible to reproduce the exact realistic behaviour where, for example, natural variations are ignored and material responses are described with idealised models.

9

Conclusions

In this master's thesis, the effective area in a restrained reinforced concrete member has been evaluated, based on FEA performed in the software DIANA. The concept of effective areas existing in restrained elements could be confirmed, but the results did not show a consistent agreement with either the old or new EC 2 model for effective area. The disagreement was mainly related to the trend with an increasing ratio between the bar spacing and the bar diameter. Some better agreement was observed for larger ratios, where the bars may behave more as isolated bars. Due to the non-consistent results, a proposal for an improved model can not be stated.

Whether effective areas occur in such elements or not, i.e. where the transition from behaving as a thick to a thin member takes place, cannot be stated. All studied cases, except one, turned out to behave as thick members. Therefore, further investigations are needed to come up with a definition for when a cross-section can be considered as thin or thick.

Geometry parameters of the studied element, such as thickness and the relationship between bar diameter and bar spacing, affect the stress distribution and subsequently the effective area. However, no clear correlation could be established between specific geometries and a better agreement with the analytical models. Due to the inconsistent correlations between FEA and EC 2 results, large variations in the model's accuracy in EC 2 with respect to geometry are to be expected. Therefore, an improved model may be needed for evaluating the effective area more accurately. However, the results are not strong enough to conclude that the model in EC 2 is inaccurate.

Since these results are based on an FEA where linear concrete was used, the results should be interpreted with caution, since non-linear behaviour such as cracking is neglected. Further studies on the subject are necessary with a focus on non-linear concrete modelling, more geometries, and separating the effects of bar diameter and spacing.

Bibliography

Mohammad Al-Emrani, Björn Engström, Marie Johansson, and Peter Johansson. *Bärande konstruktioner - del 2*. Institutionen för arkitektur och samhällsbyggnadsteknik, Avdelningen för konstruktionsteknik, chalmers tekniska högskola, 2011.

Mohammad Al-Emrani, Björn Engström, Marie Johansson, and Peter Johansson. *Bärande konstruktioner – del 1*. Institutionen för arkitektur och samhällsbyggnadsteknik, Avdelningen för konstruktionsteknik, chalmers tekniska högskola, 2019.

Helén Broo, Karin Lundgren, and Mario Plos. *A guide to non-linear finite element modelling of shear and torsion in concrete bridges*. Department of Civil and Environmental Engineering Division of Structural Engineering, Concrete Structures, Chalmers University of Technology, 2008.

Alejandro Pérez Caldentey, Roberto García, Viktor Gribniak, and Arvydas Rimkus. Background document to fpren-1992-1-1:2023-04 (formal-vote-draft). In *Background document to clause 9.2.3 Refined control of cracking, CEN/TC 250/SC 2 N2087*, pages 371–383. European Committee for Standardization (CEN), 2022.

DIANA FEA BV. Diana user's manuals - theory manual (version 11), 2026.

Björn Engström. *Restraint Cracking of reinforced concrete structures*. Department of Civil and Environmental Engineering, Division of Structural Engineering, Concrete Structures, Chalmers University of Technology, 2014.

Björn Engström. *Design and analysis of continuous beams and columns*. Department of Civil and Environmental Engineering, Division of Structural Engineering, Concrete Structures, Chalmers University of Technology, 2015.

European Committee for Standardization (CEN). Eurocode 2: Design of concrete structures part 1-1: General rules and rules for buildings, 2005. Available from SIS, www.sis.se.

European Committee for Standardization (CEN). Eurocode 2 — design of concrete structures — part 1-1: General rules and rules for buildings, bridges and civil engineering structures, 2023. Available from SIS, www.sis.se.

Tena Galkovski, Jaime Mata Falcón, and Walter Kaufmann. Determination of the effective concrete area in tension relevant for modelling tension stiffening in sls and uls design. In *fib Symposium Proceedings*, 2021.

Brian Hesselmann. Accuracy of linear and quadratic finite elements when solving the boltzmann transport equation. Technical report, Delft University of Technology Physics of Nuclear Reactors, 2010.

International Federation for Structural Concrete (Fib). Ceb-fip model code 1990, 1998.

International Federation for Structural Concrete (Fib). fib model code for concrete structures 2010, 2010.

International Federation for Structural Concrete (Fib). fib model code for concrete structures 2020, 2022.

Mario Plos. *Finite element analyses of reinforced concrete structures*. Department of Civil and Environmental Engineering Division of Structural Engineering, Concrete Structures, Chalmers University of Technology, 2000.

O.C. Zienkiewicz, R.L. Taylor, and J.Z. Zhu. *The Finite Element Method: Its Basis and Fundamentals*. Butterworth-Heinemann, 2013.

A

FEA results - Study 1

The following appendix includes a complete presentation of results based on FEA for study 1. Tables of numerical results, stress plots and other plots visualising the results are presented.

A.1 Summary tables

In the following section, results from study 1 regarding the effective area, maximum tensile section and transmission length based on FEA are presented.

A.1.1 Effective area

Ratio	$s_y = 200$ **mm**	$s_y = 400$ **mm**
$s_x = 6\phi$	0.103	0.106
$s_x = 8\phi$	0.101	0.132
$s_x = 10\phi$	0.160	0.216
$s_x = 12\phi$	0.183	0.240
$s_x = 14\phi$	0.203	0.262

A.1.2 Transmission length

Ratio	s_y**=200 mm**		s_y**=400 mm**	
	z_{max} [m]	l_t [m]	z_{max} [m]	l_t [m]
$s_x = 6\phi$	0.075	0.425	0.075	0.450
$s_x = 8\phi$	0.075	0.400	0.100	0.425
$s_x = 10\phi$	0.150	0.400	0.200	0.425
$s_x = 12\phi$	0.200	0.400	0.250	0.425
$s_x = 14\phi$	0.250	0.400	0.300	0.450

A.2 Effective area plots

In the following section, plots describing the effective area calculation for study 1 are included. The first effective area for different $s-\phi$ ratios is presented for both studied s_y, and further, the stresses used for calculating the effective area are presented for both s_y as well.

A.2.1 Effective area

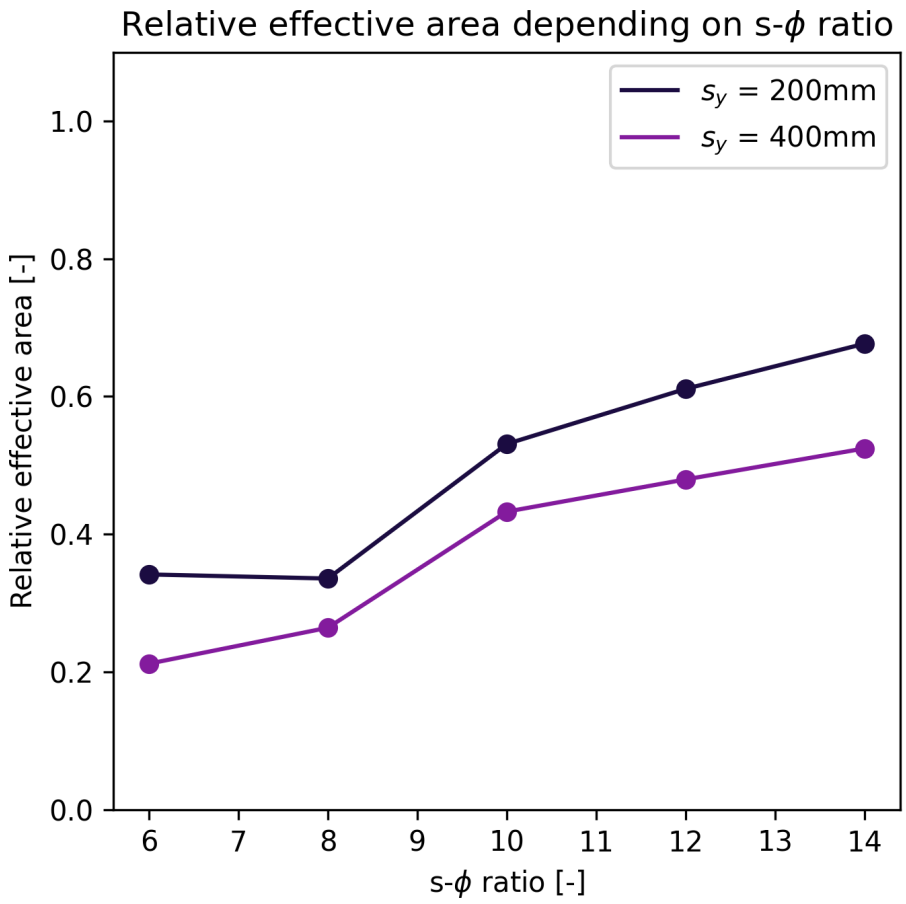

A.2.2 Concrete stresses for calculating effective area

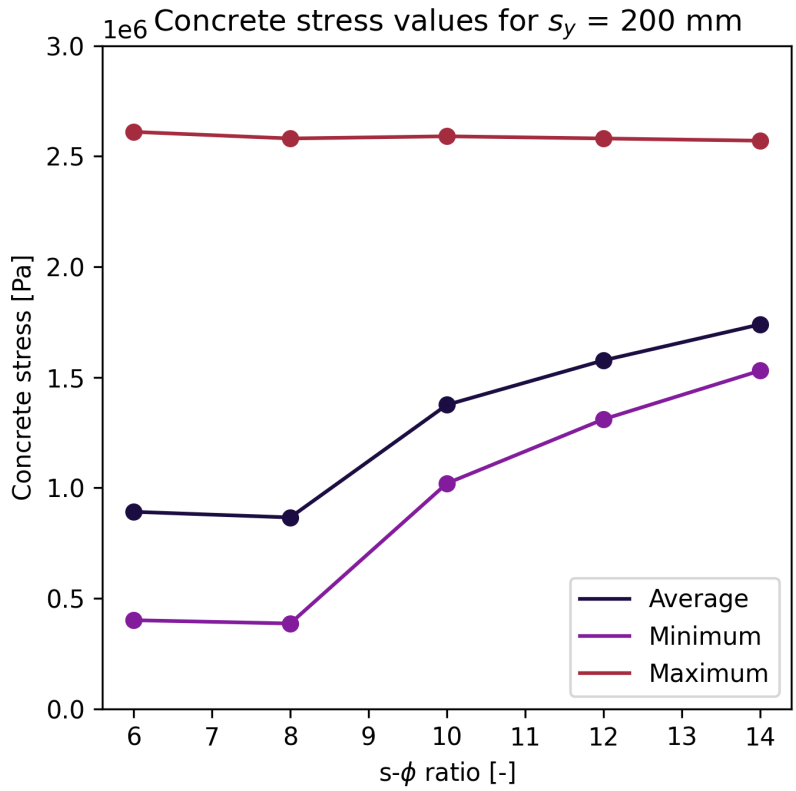

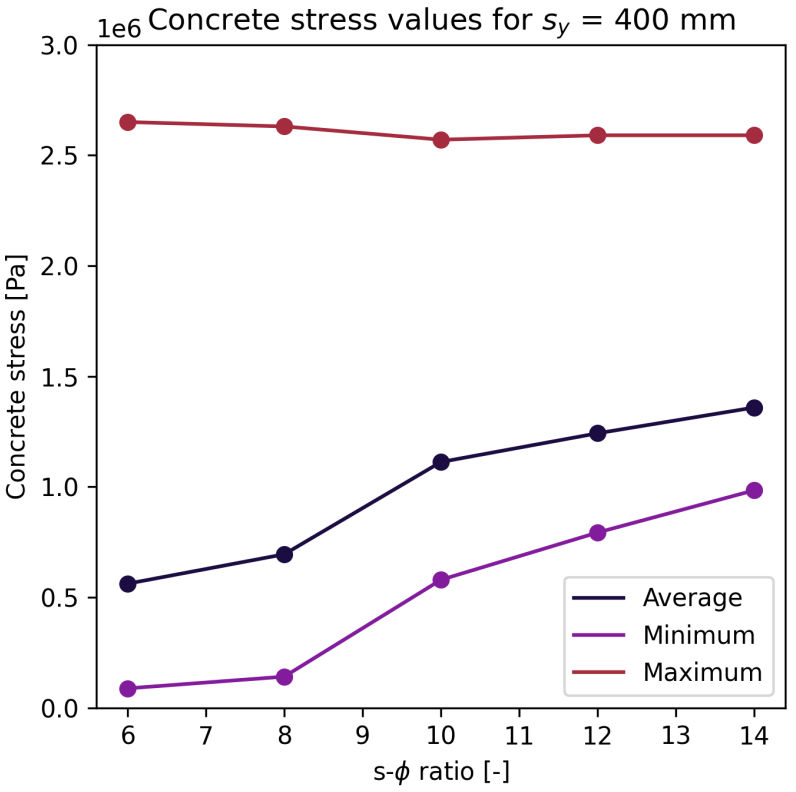

A.3 Overview of concrete stress plots

The following section includes plots illustrating stresses for cases in study 1. Stress plots are given for different directions and planes, and for varying geometries.

A.3.1 Concrete stress in xy-plane

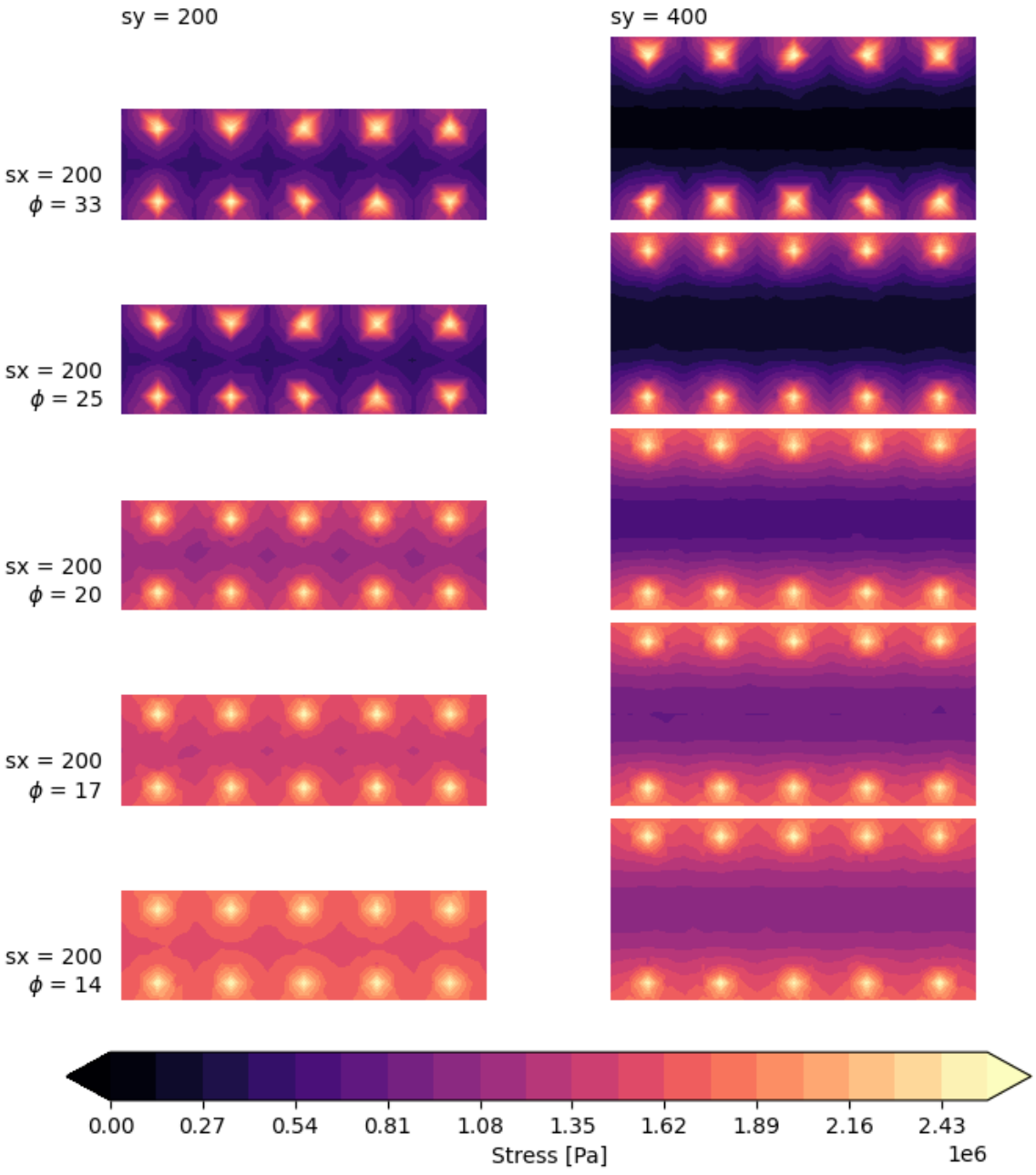

A.3.2 Concrete stress in xz-plane

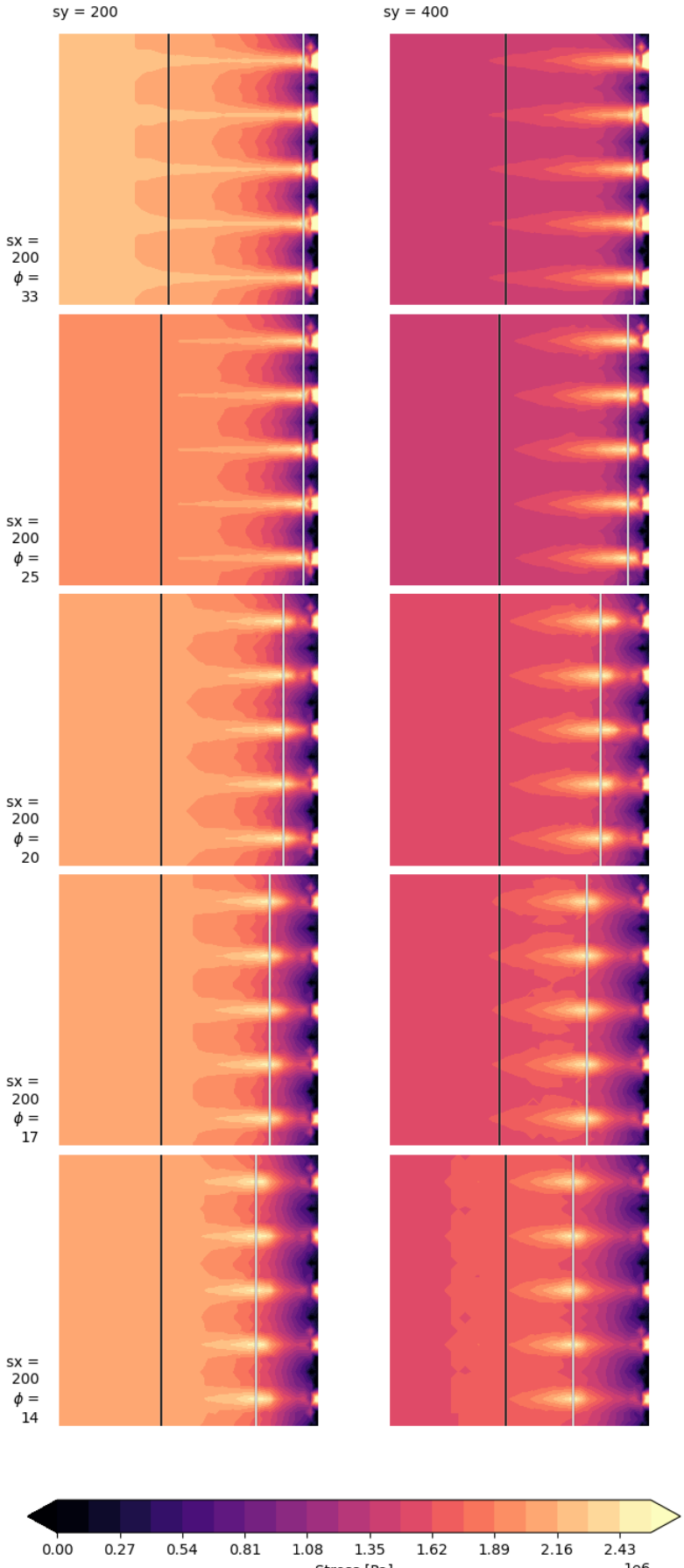

A.3.3 Concrete stress in yz-plane

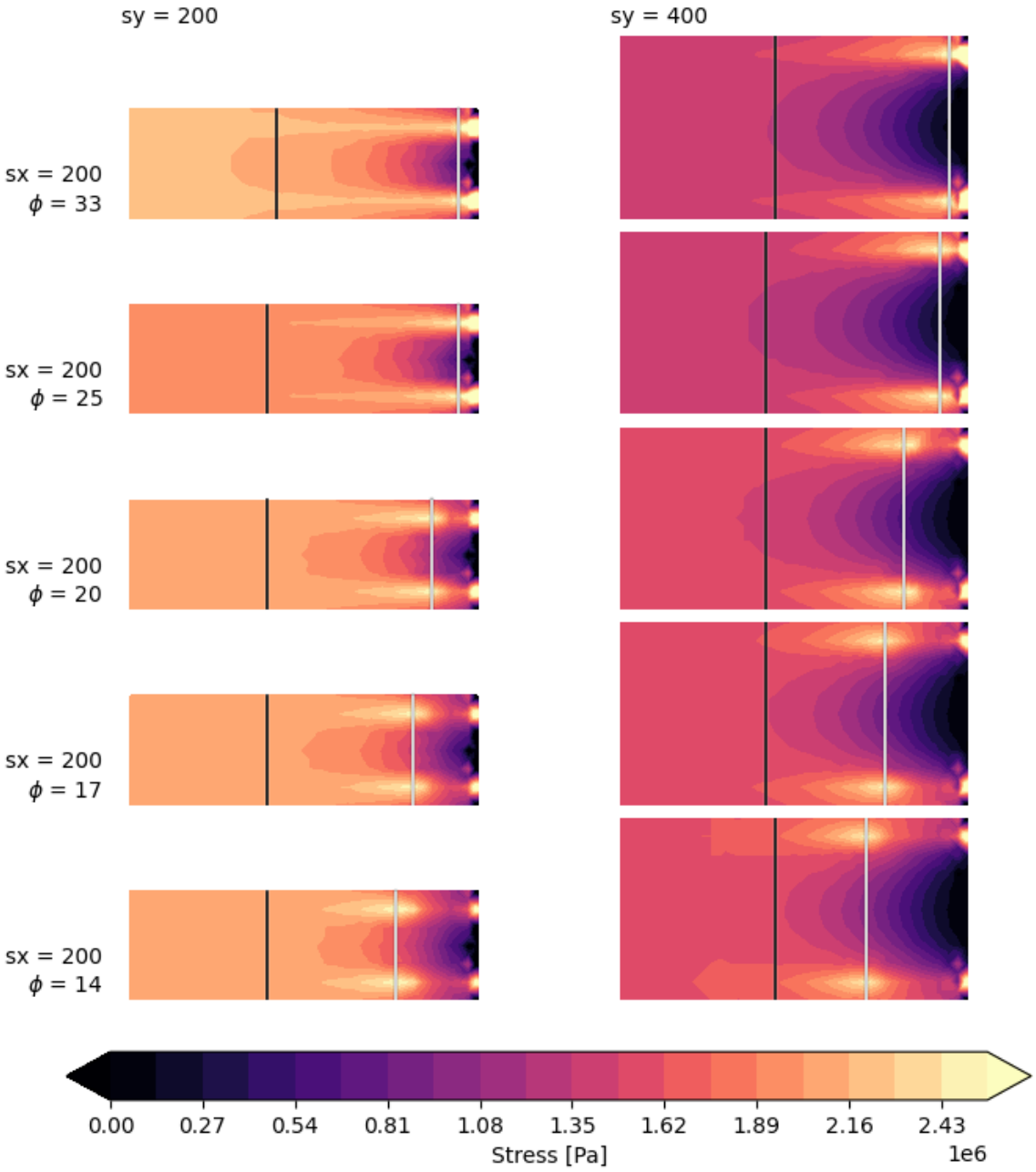

A.3.4 Concrete stress along x-direction

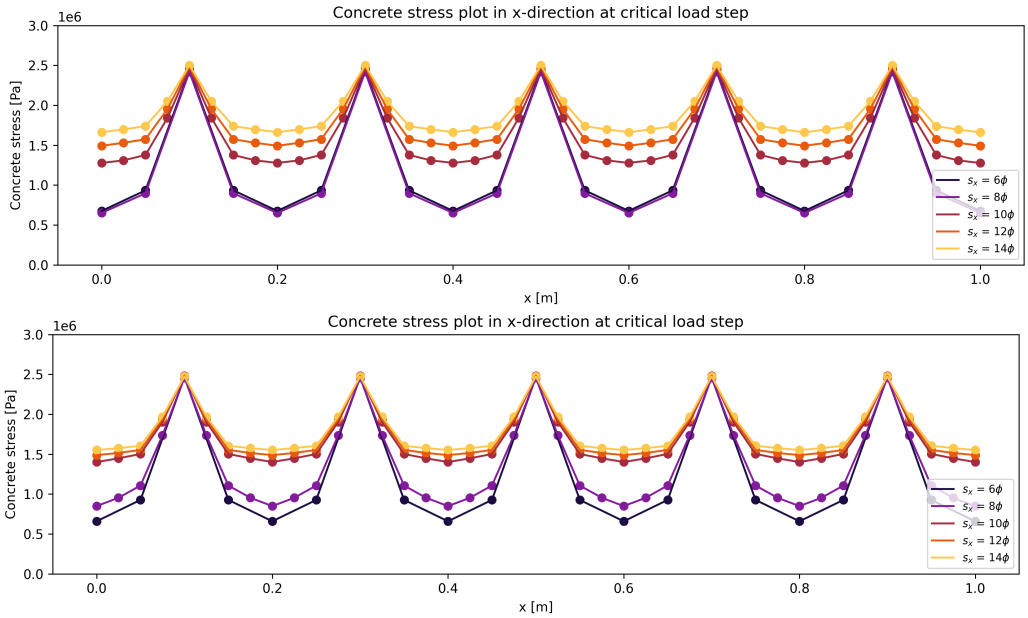

A.3.5 Concrete stress along y-direction

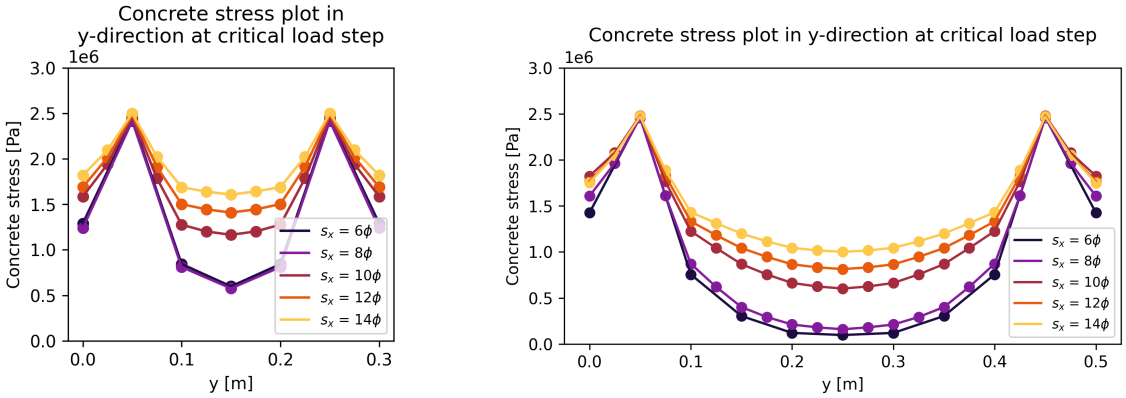

A.4 Detailed figures

In this section, the previously presented stress plots are shown in a more detailed view.

A.4.1 Cross section stress plots in xy-plane

Thinner member

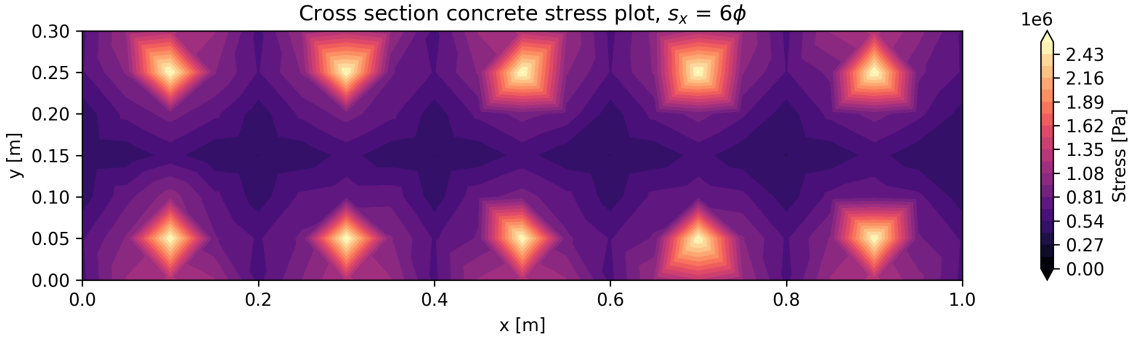

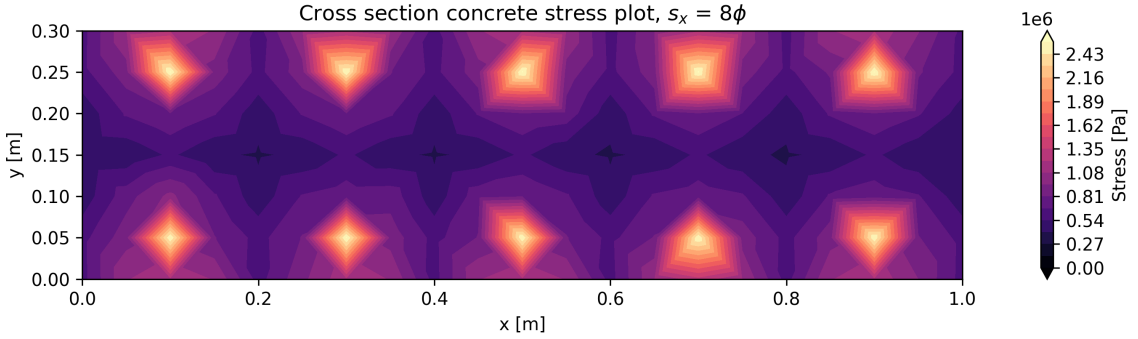

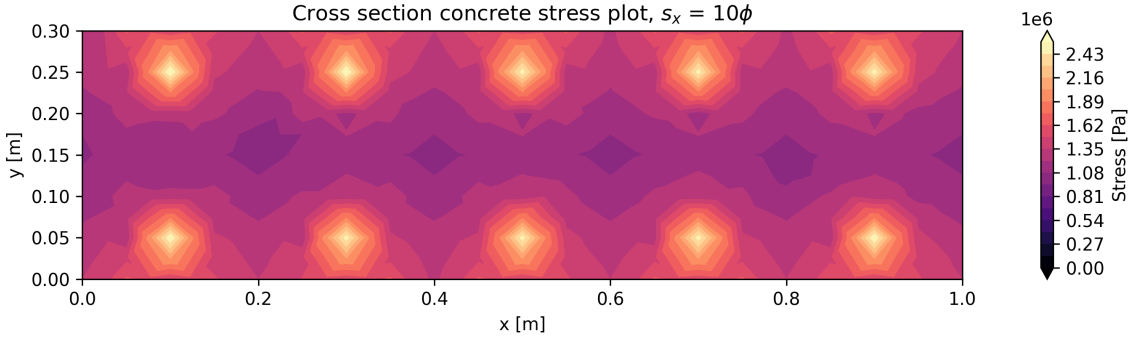

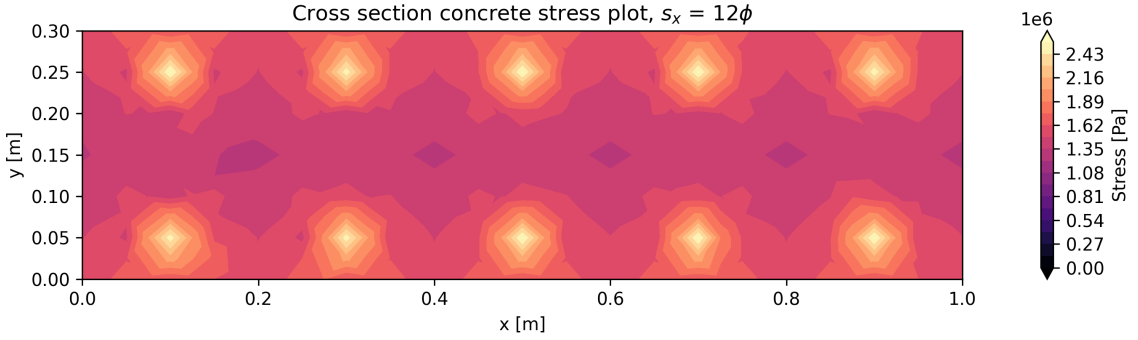

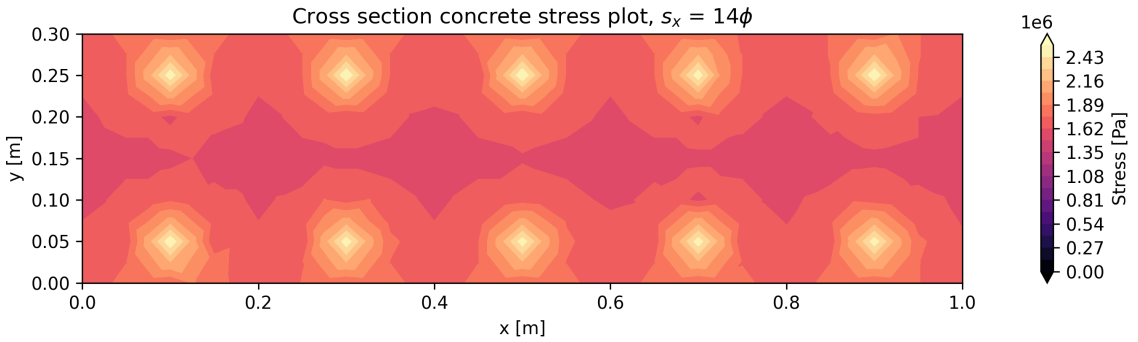

Thicker member

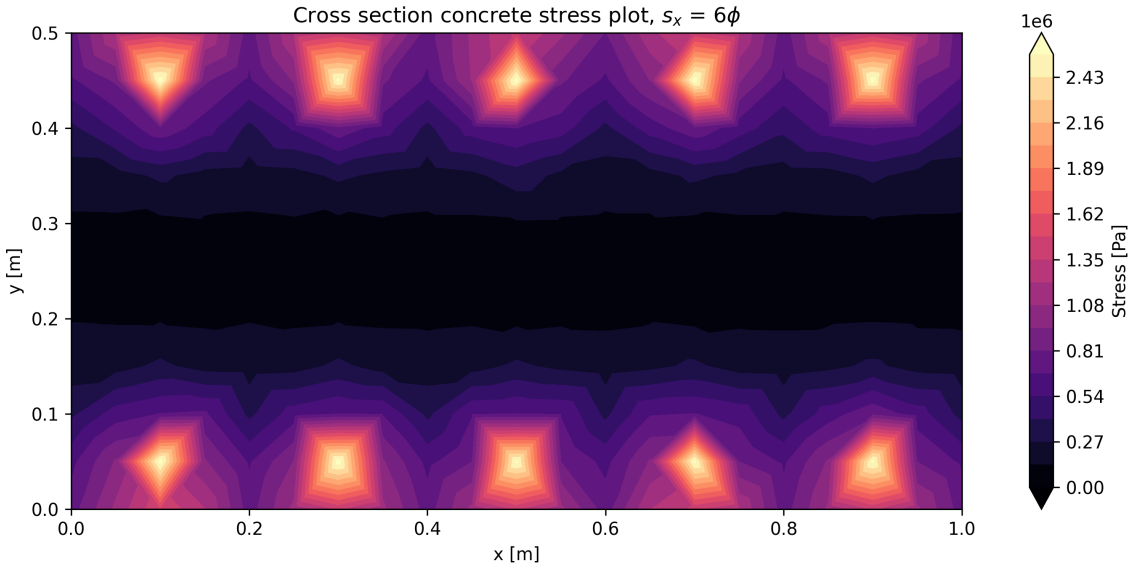

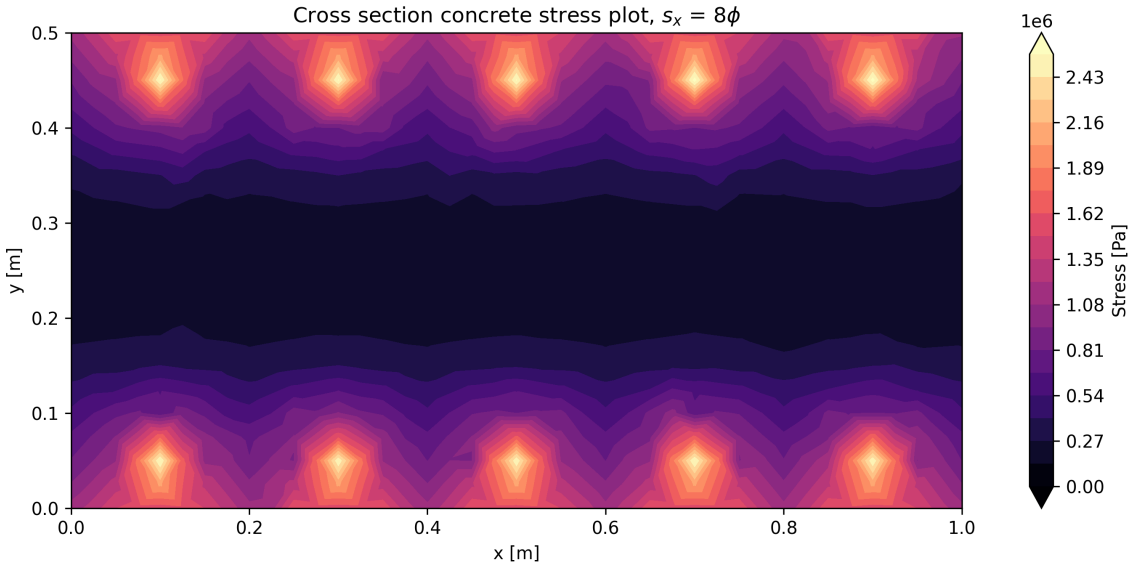

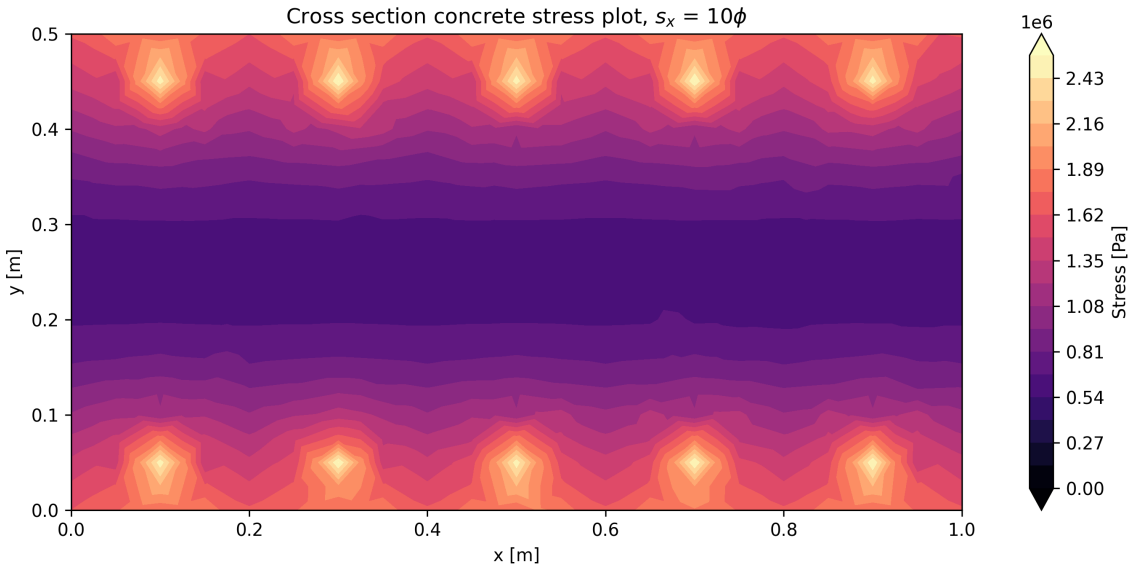
Cross section concrete stress plot, $s_x = 10\phi$
y [m]
x [m]
1e6
Stress [Pa]
0.0
0.1
0.2
0.3
0.4
0.5
0.6
0.8
1.0
0.27
0.54
0.81
1.08
1.35
1.62
1.89
2.16
2.43

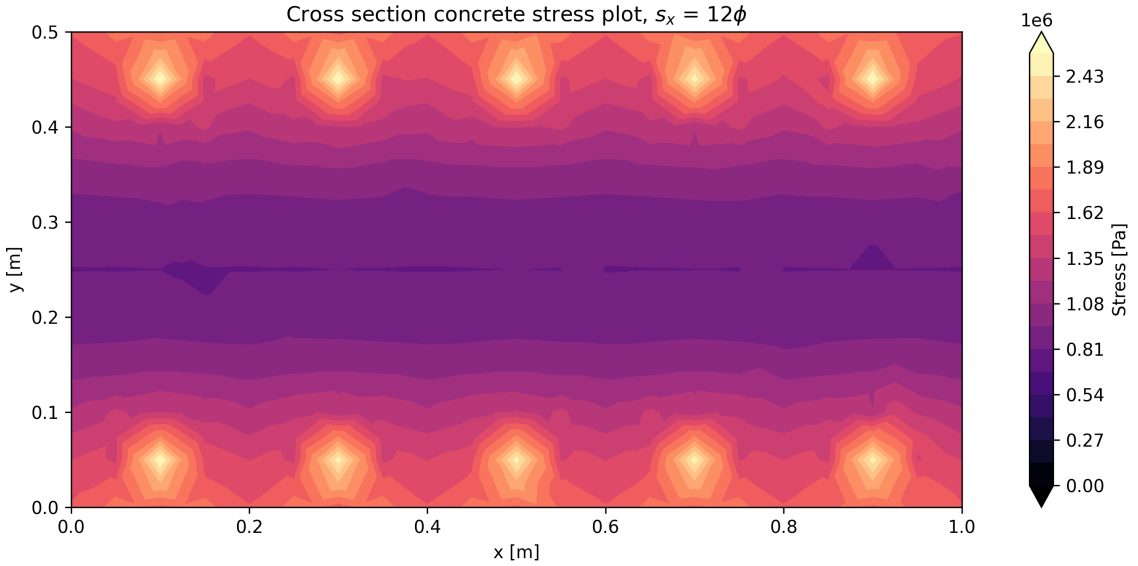
Cross section concrete stress plot, $s_x = 12\phi$
y [m]
x [m]
1e6
Stress [Pa]
0.0
0.1
0.2
0.3
0.4
0.5
0.6
0.8
1.0
0.27
0.54
0.81
1.08
1.35
1.62
1.89
2.16
2.43

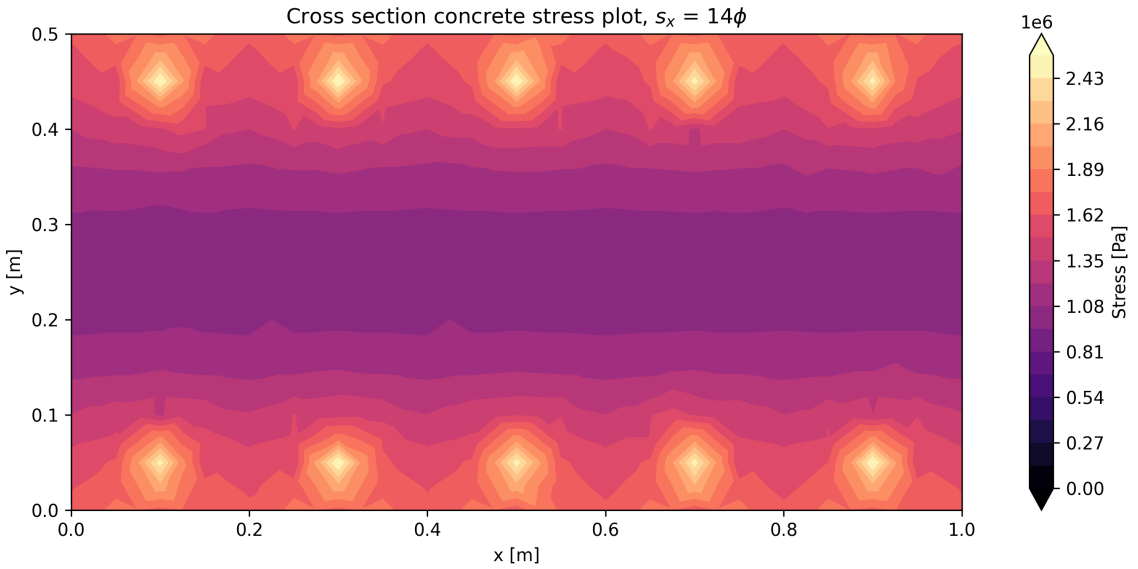
Cross section concrete stress plot, s_x = 14ϕ
y [m]
x [m]
0.0
0.1
0.2
0.3
0.4
0.5
0.0
0.2
0.4
0.6
0.8
1.0
1e6
2.43
2.16
1.89
1.62
1.35
1.08
0.81
0.54
0.27
0.00
Stress [Pa]

A.4.2 Longitudinal stress plots in xz-plane

Thinner member

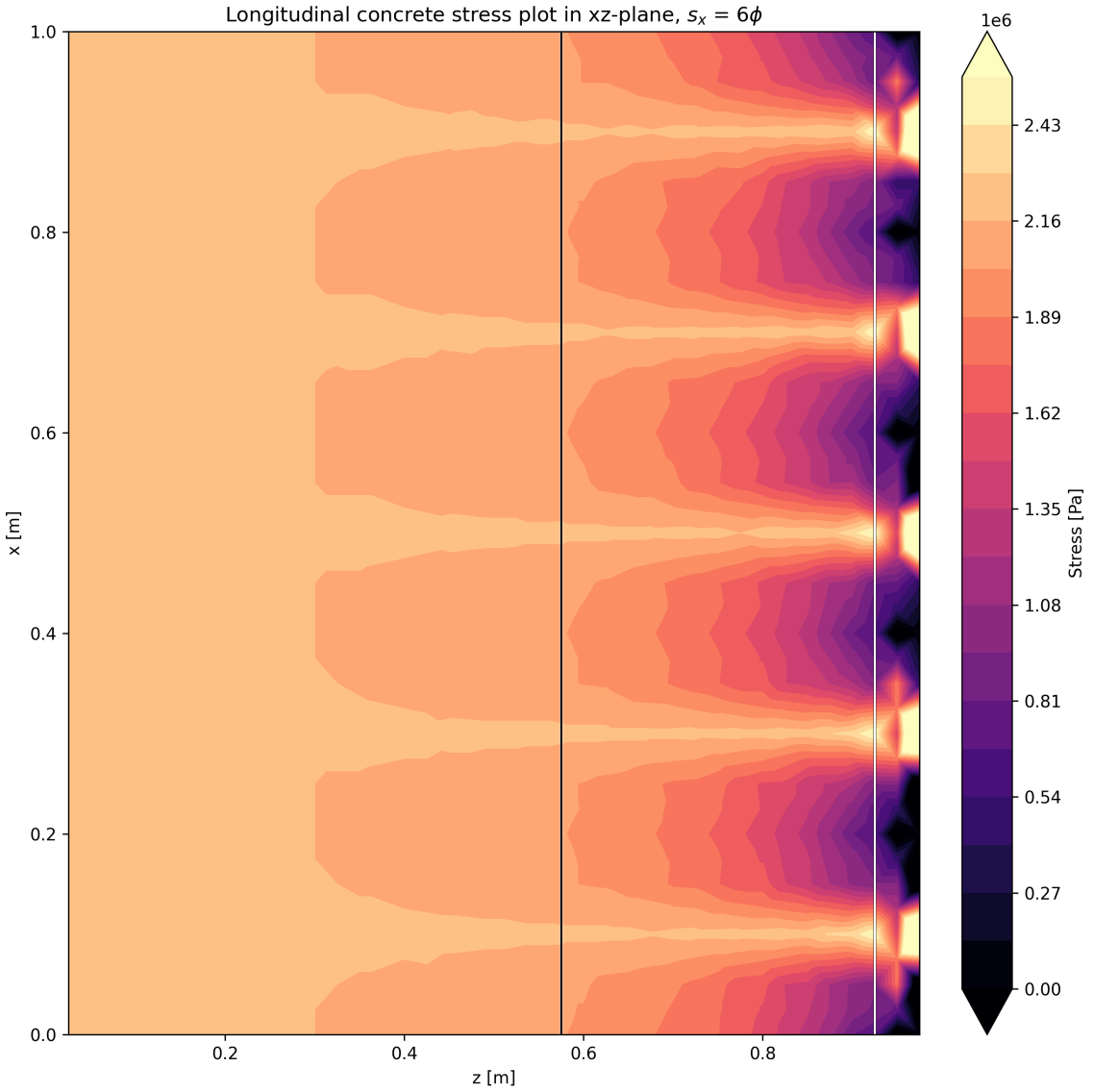

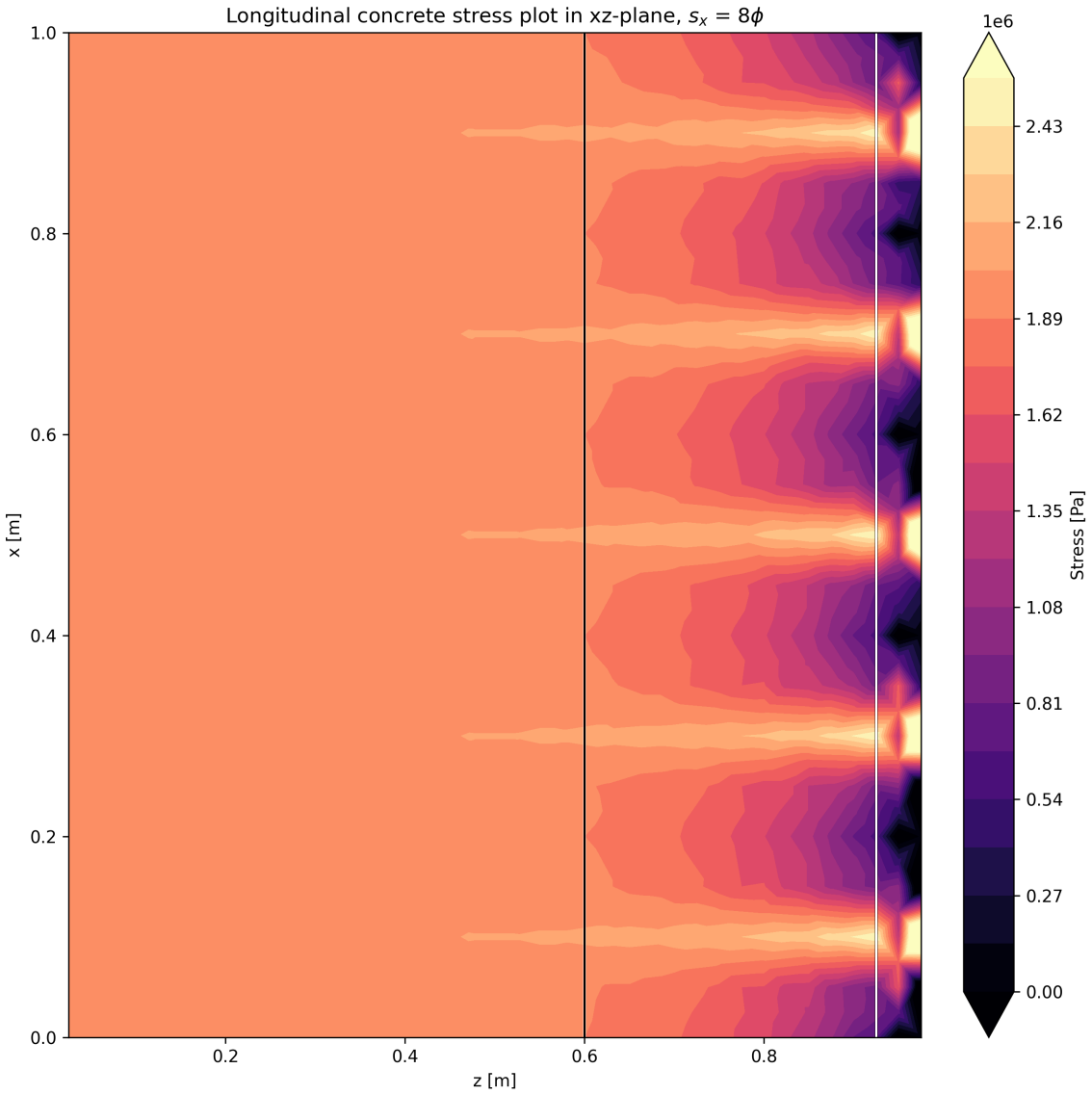
Longitudinal concrete stress plot in xz-plane, $s_x = 8\phi$
1e6
2.43
2.16
1.89
1.62
1.35
1.08
0.81
0.54
0.27
0.00
Stress [Pa]
1.0
0.8
0.6
0.4
0.2
0.0
x [m]
0.2
0.4
0.6
0.8
z [m]

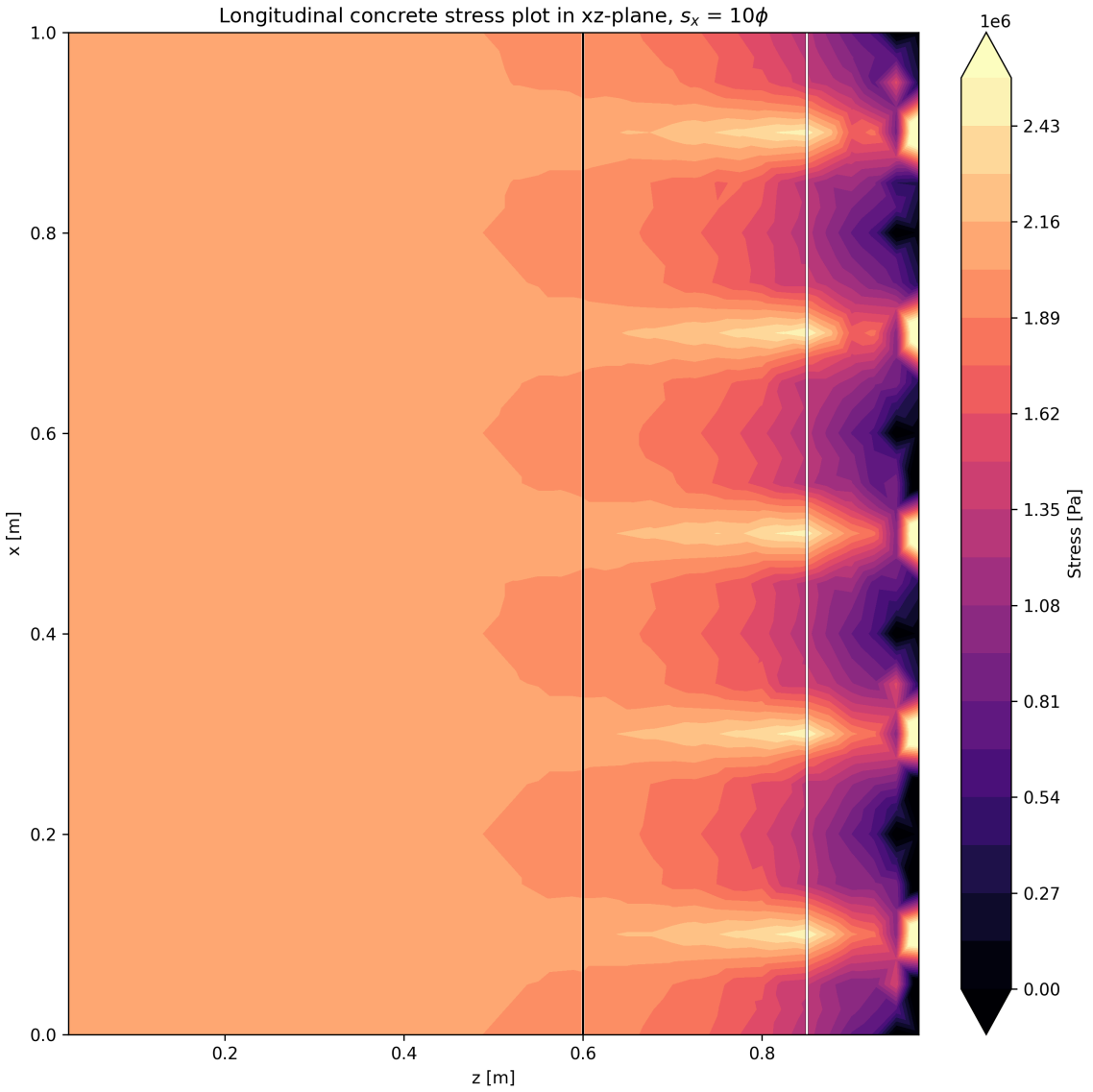
Longitudinal concrete stress plot in xz-plane, $s_x = 10\phi$
1e6
2.43
2.16
1.89
1.62
1.35
1.08
0.81
0.54
0.27
0.00
Stress [Pa]
1.0
0.8
0.6
0.4
0.2
0.0
x [m]
0.2
0.4
0.6
0.8
z [m]

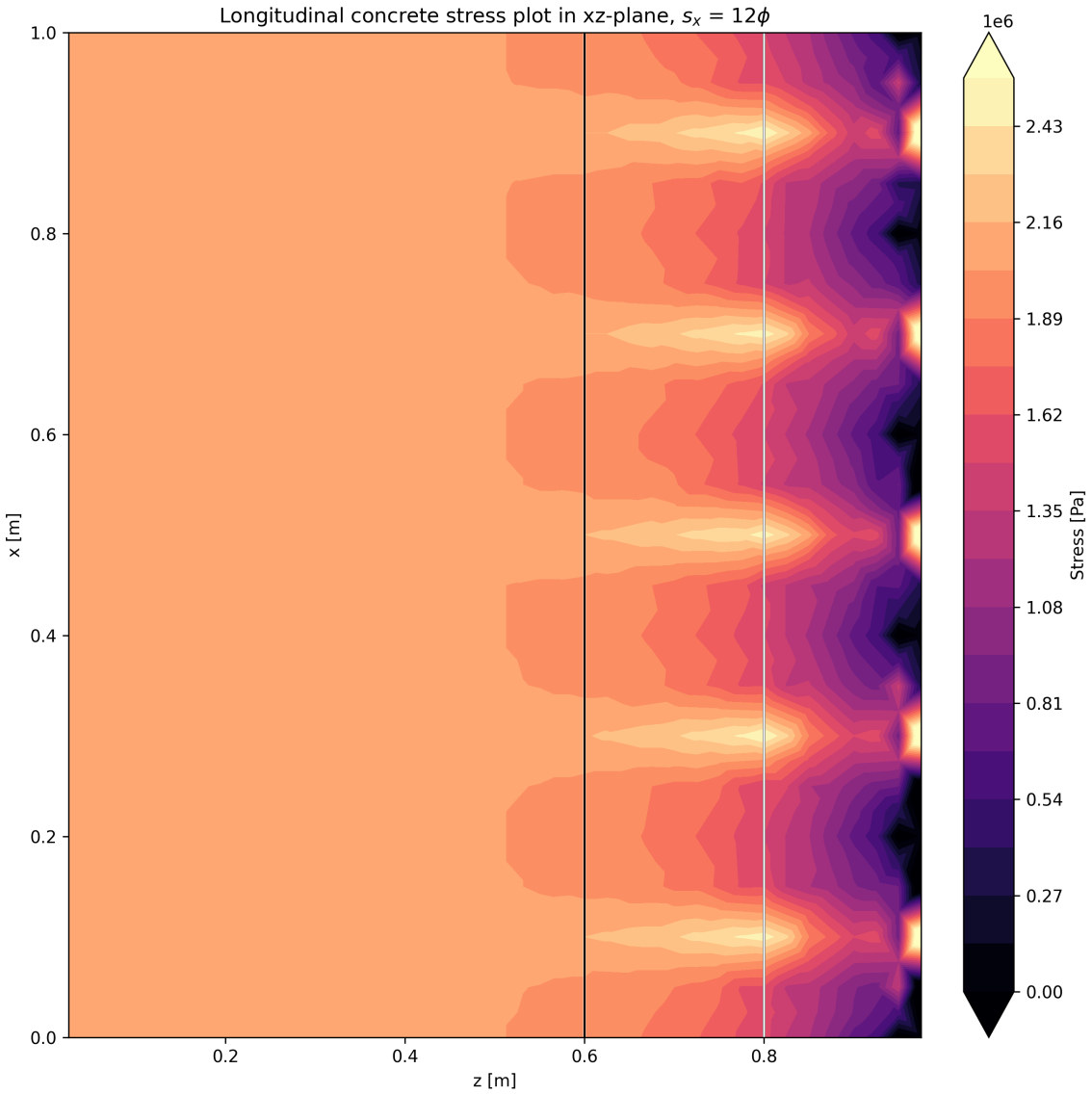
Longitudinal concrete stress plot in xz-plane, $s_x = 12\phi$
1e6
2.43
2.16
1.89
1.62
1.35
1.08
0.81
0.54
0.27
0.00
Stress [Pa]
1.0
0.8
0.6
0.4
0.2
0.0
x [m]
0.2
0.4
0.6
0.8
z [m]

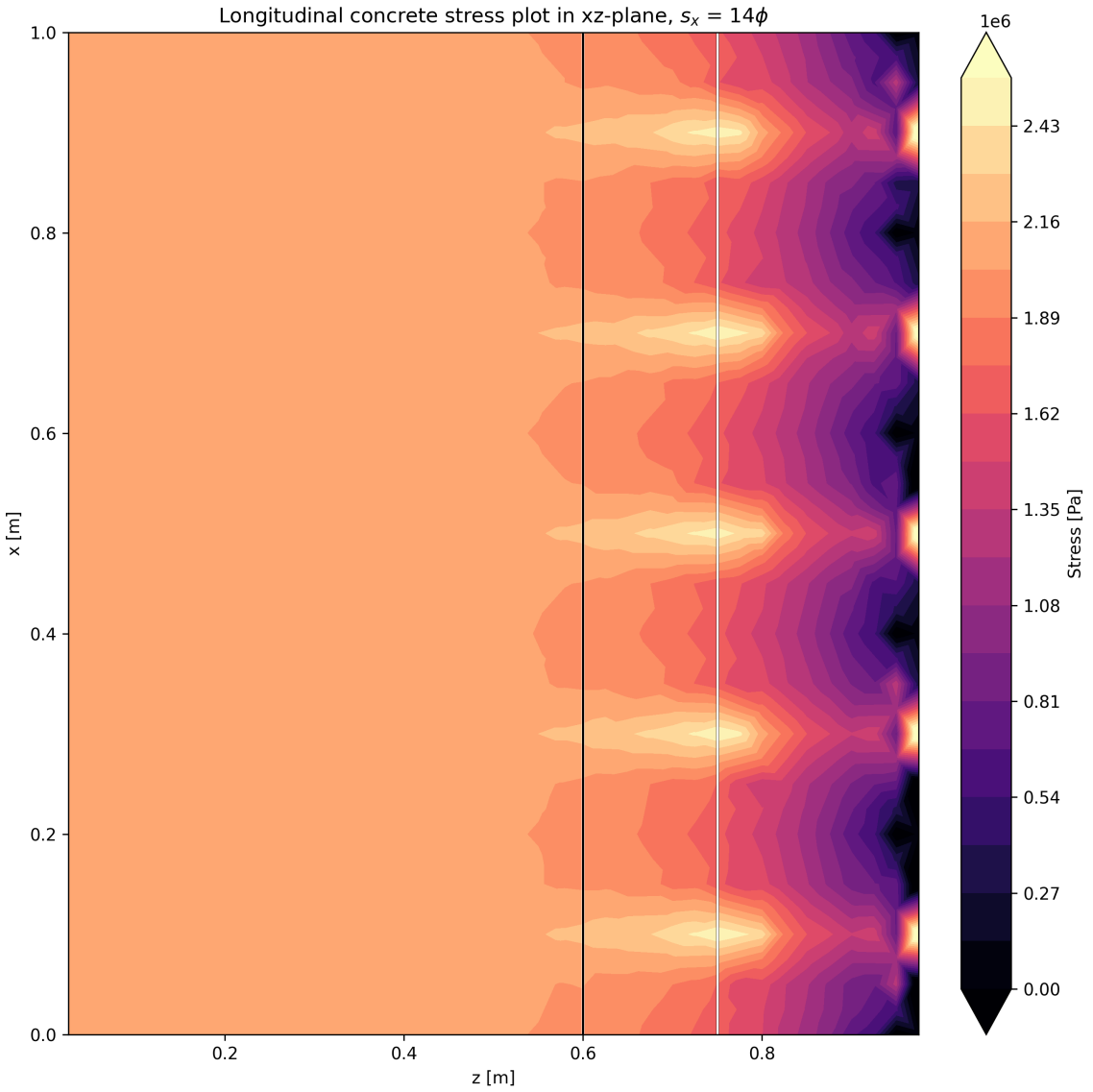
Longitudinal concrete stress plot in xz-plane, $s_x = 14\phi$
1e6
2.43
2.16
1.89
1.62
1.35
1.08
0.81
0.54
0.27
0.00
Stress [Pa]
x [m]
z [m]
0.0
0.2
0.4
0.6
0.8
1.0
0.2
0.4
0.6
0.8

Thicker member

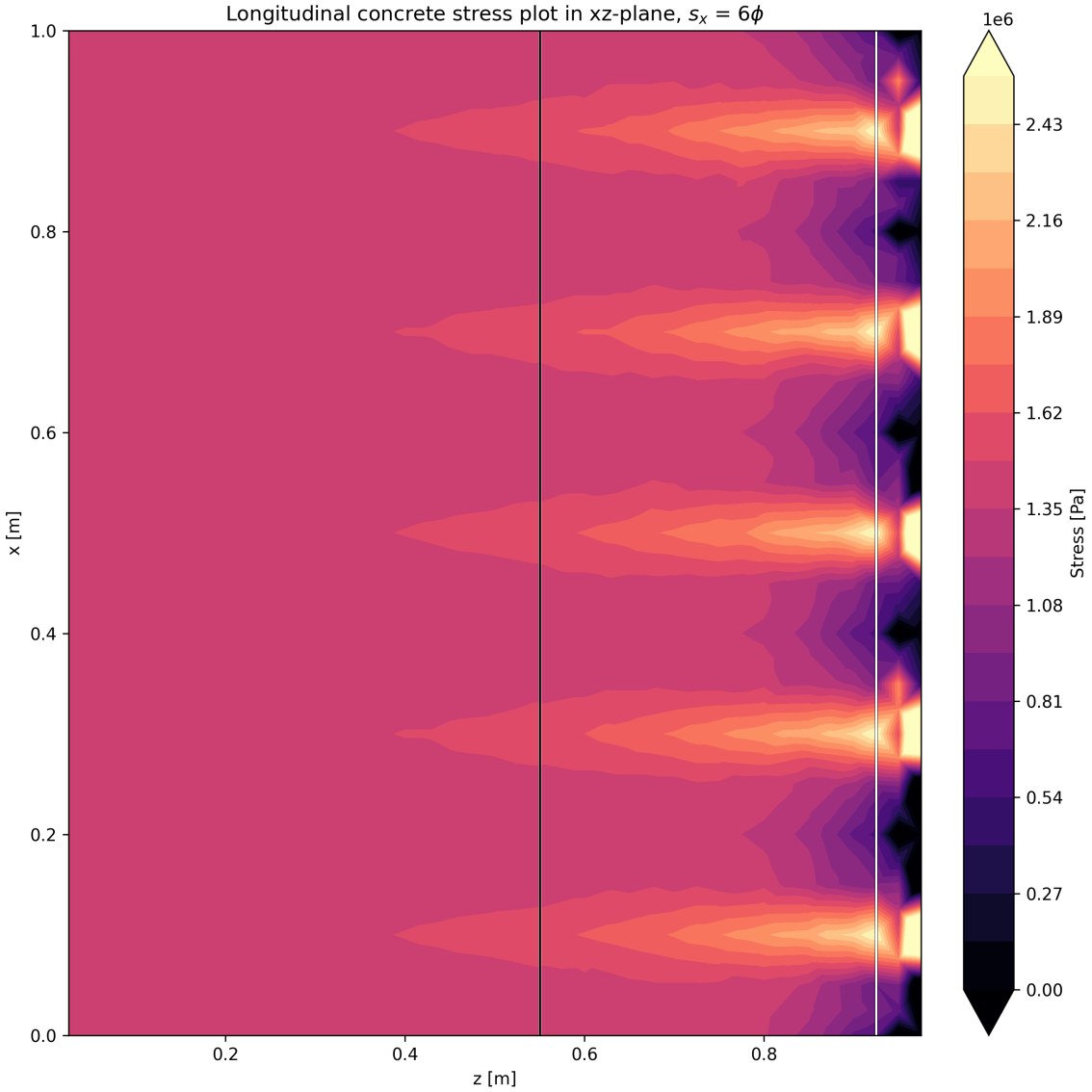

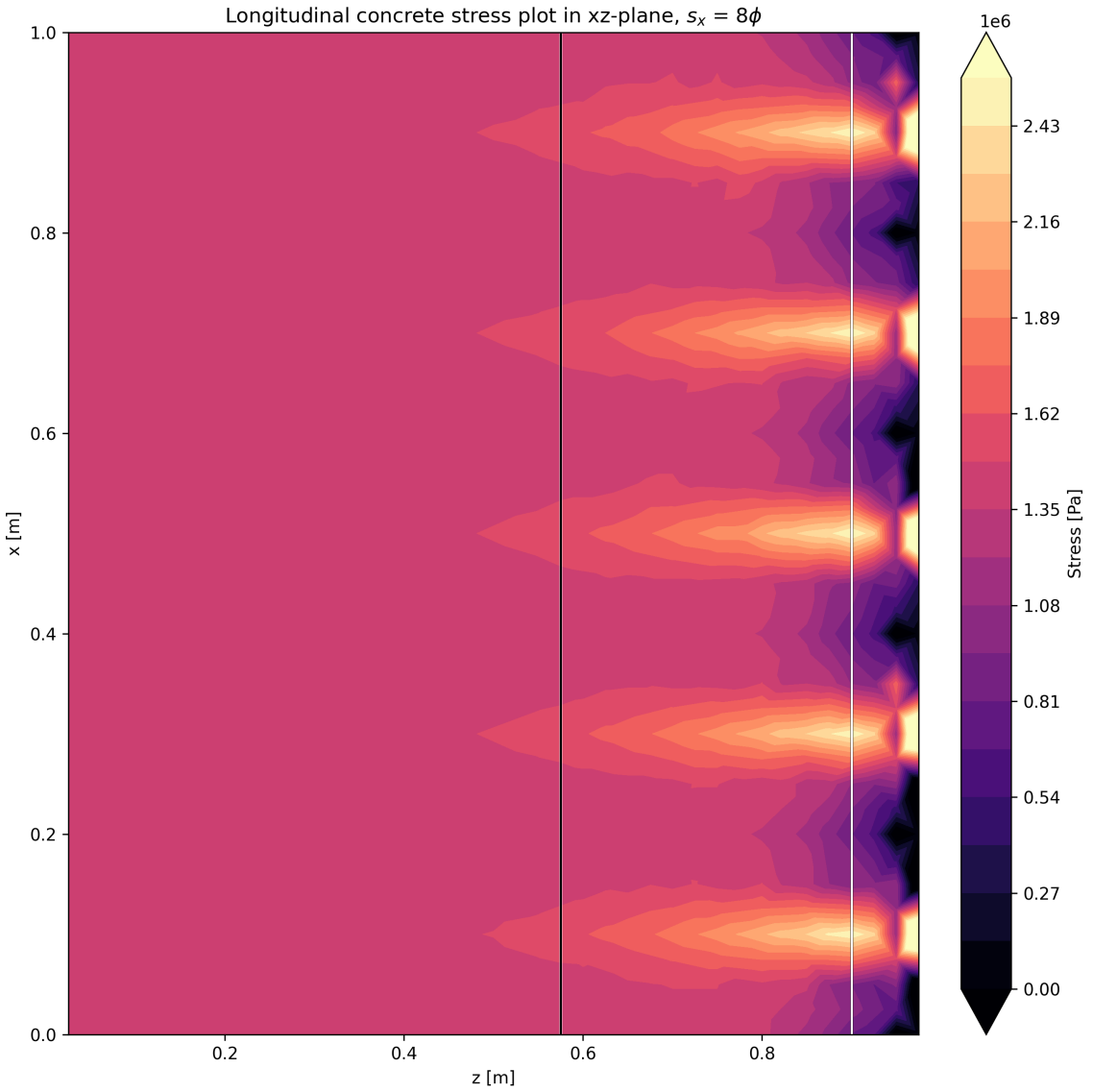
Longitudinal concrete stress plot in xz-plane, $s_x = 8\phi$
1e6
2.43
2.16
1.89
1.62
1.35
1.08
0.81
0.54
0.27
0.00
Stress [Pa]
1.0
0.8
0.6
0.4
0.2
0.0
x [m]
0.2
0.4
0.6
0.8
z [m]

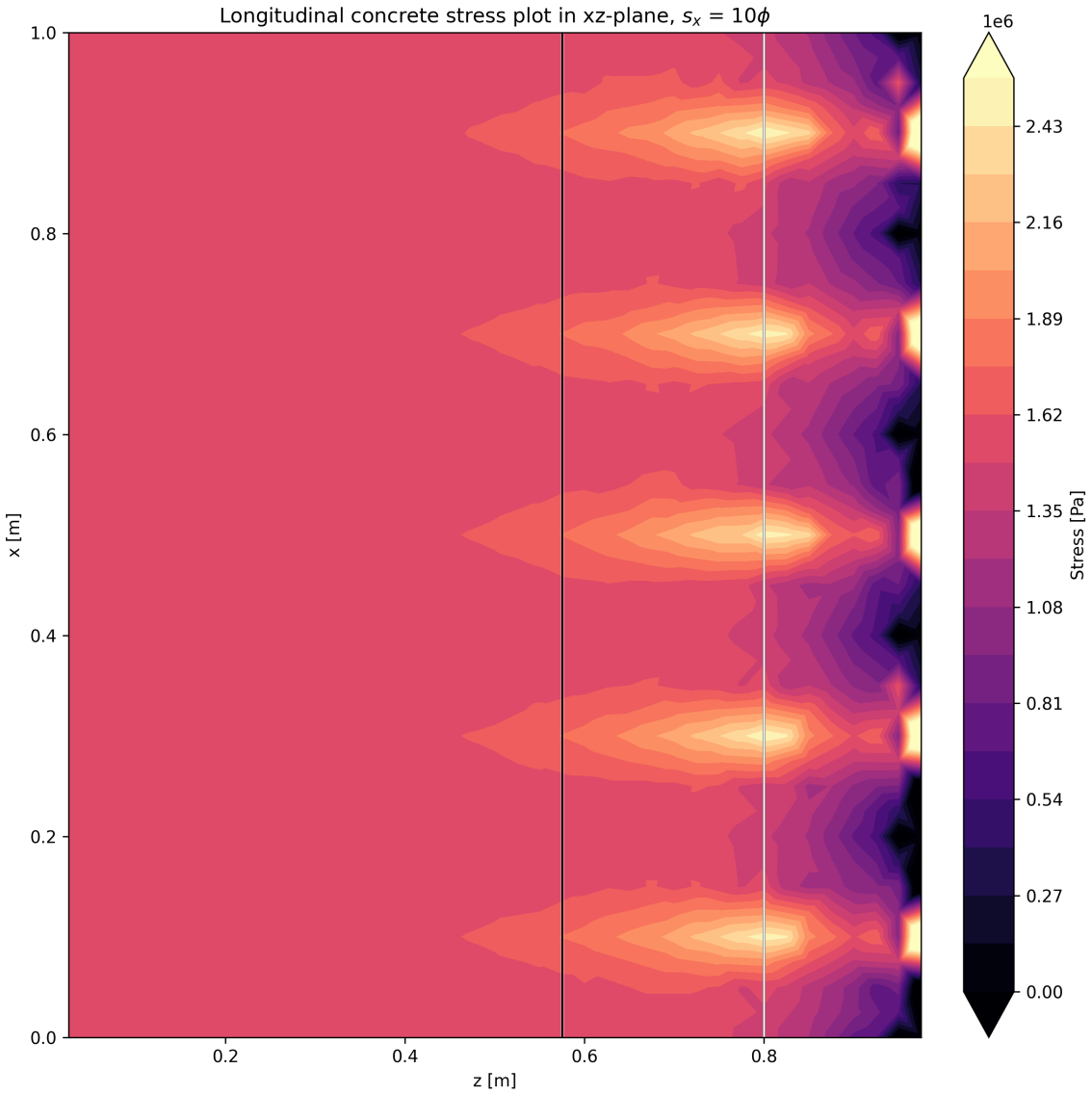
Longitudinal concrete stress plot in xz-plane, $s_x = 10\phi$
1e6
2.43
2.16
1.89
1.62
1.35
1.08
0.81
0.54
0.27
0.00
Stress [Pa]
1.0
0.8
0.6
0.4
0.2
0.0
x [m]
0.2
0.4
0.6
0.8
z [m]

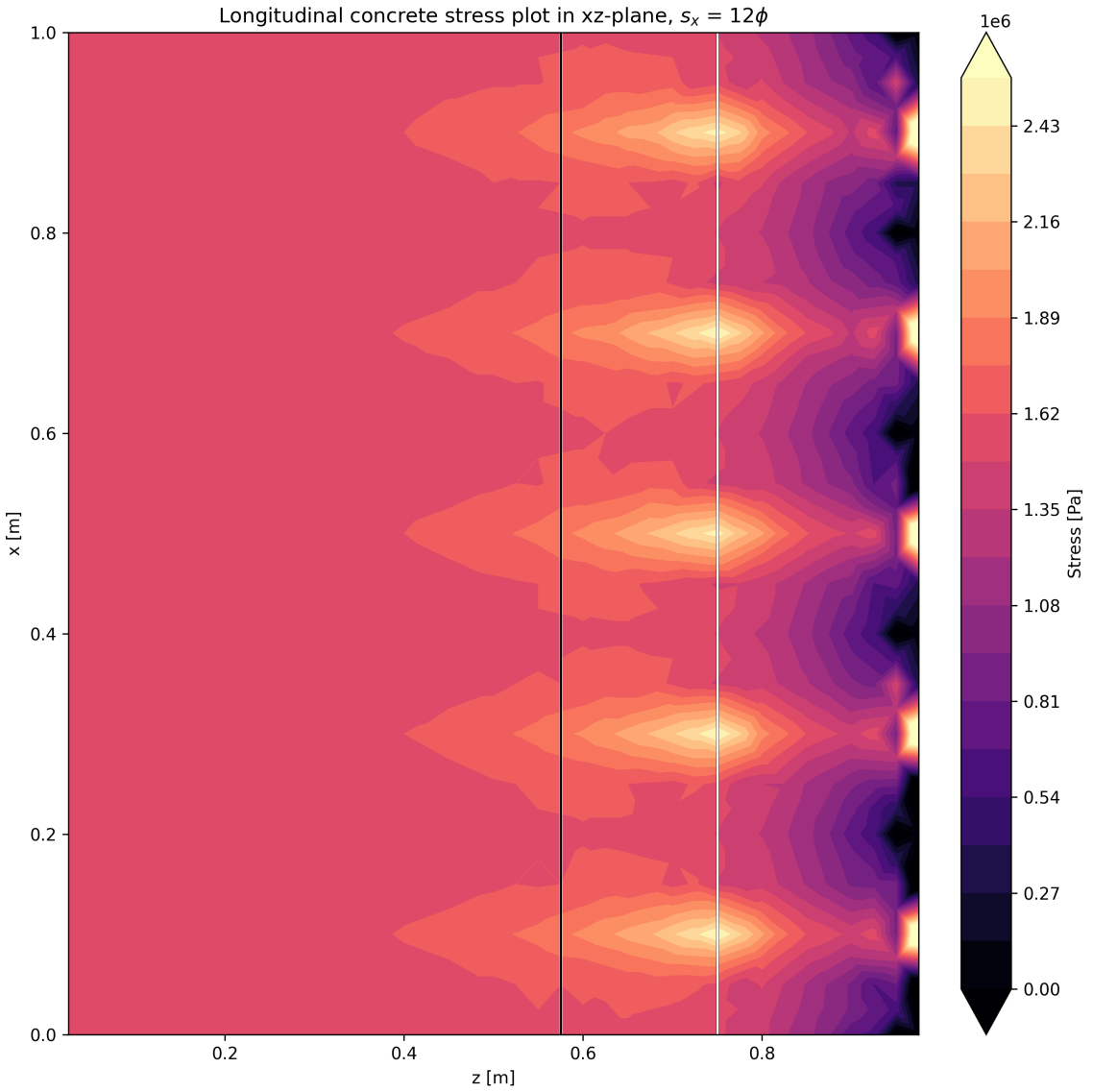
Longitudinal concrete stress plot in xz-plane, $s_x = 12\phi$
1e6
2.43
2.16
1.89
1.62
1.35
1.08
0.81
0.54
0.27
0.00
Stress [Pa]
1.0
0.8
0.6
0.4
0.2
0.0
x [m]
0.2
0.4
0.6
0.8
z [m]

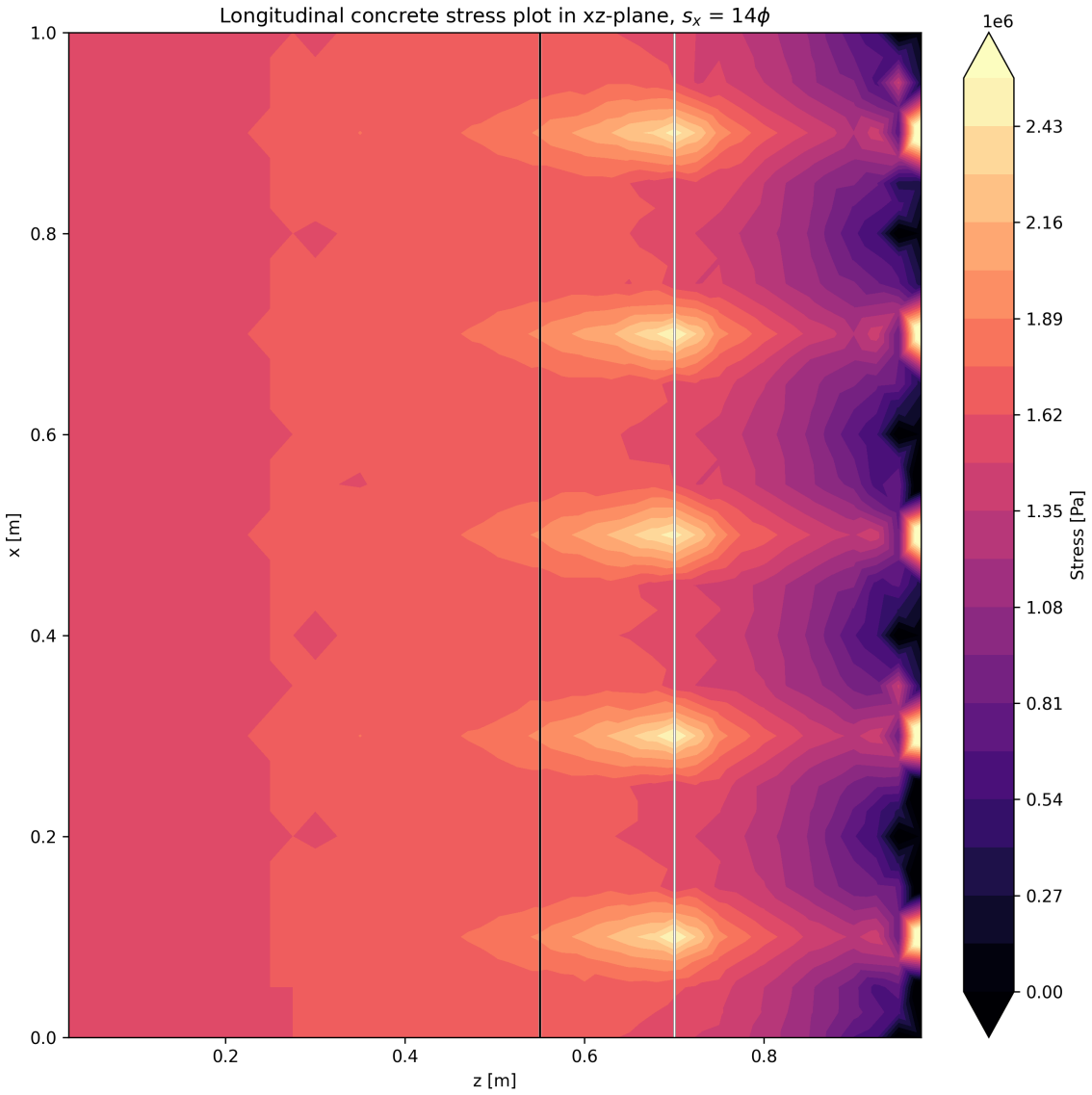

A.4.3 Longitudinal stress plots in yz-plane

Thinner member

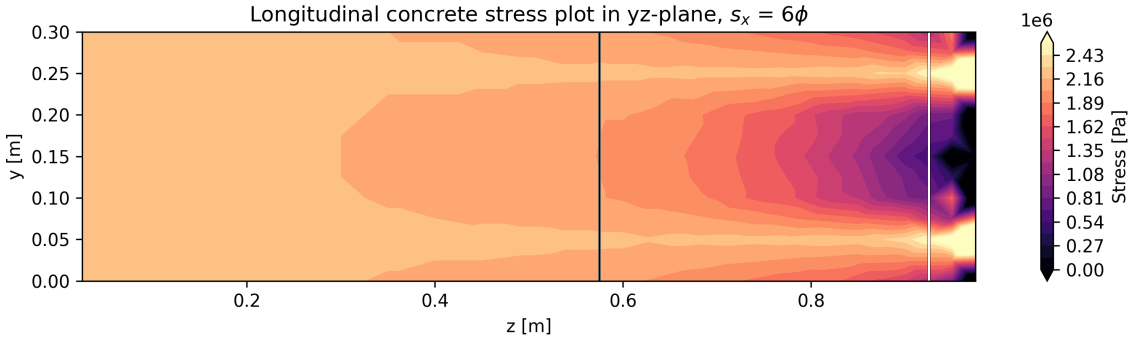

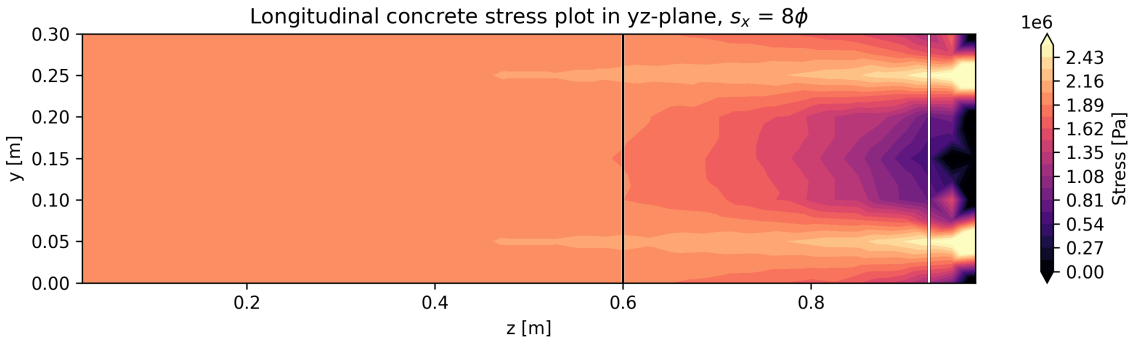
Longitudinal concrete stress plot in yz-plane, $s_x = 8\phi$
y [m]
z [m]
1e6
Stress [Pa]
0.00
0.05
0.10
0.15
0.20
0.25
0.30
0.2
0.4
0.6
0.8
2.43
2.16
1.89
1.62
1.35
1.08
0.81
0.54
0.27
0.00

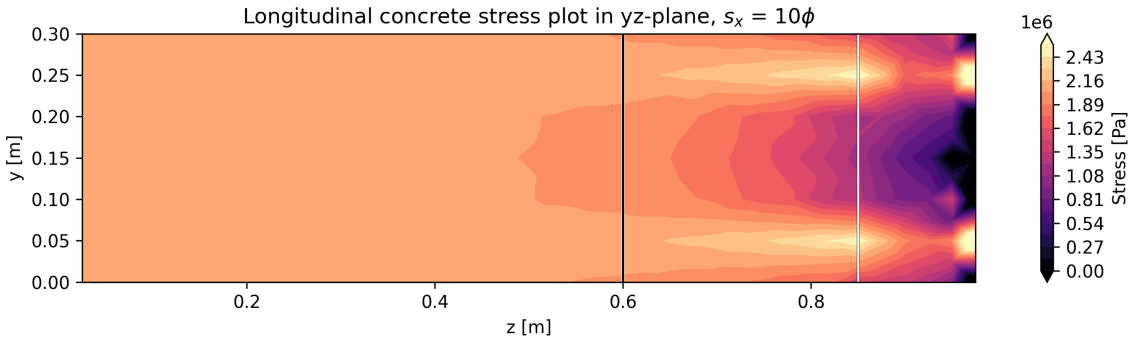
Longitudinal concrete stress plot in yz-plane, $s_x = 10\phi$
y [m]
z [m]
1e6
Stress [Pa]
0.00
0.05
0.10
0.15
0.20
0.25
0.30
0.2
0.4
0.6
0.8
2.43
2.16
1.89
1.62
1.35
1.08
0.81
0.54
0.27
0.00

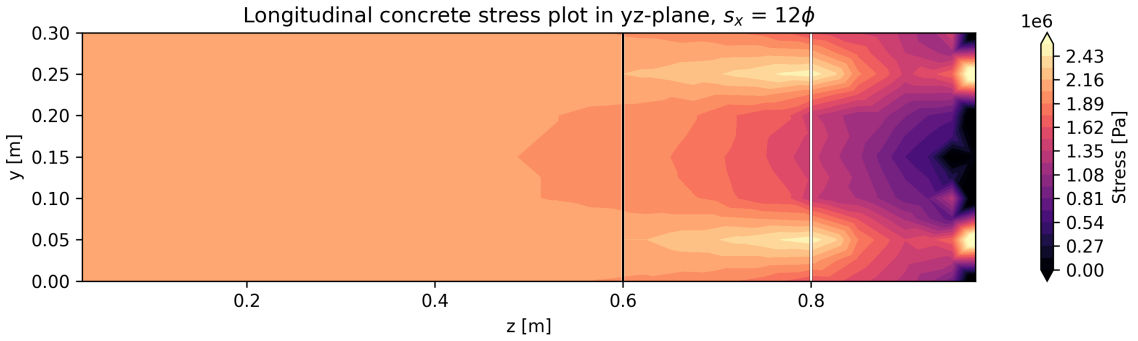
Longitudinal concrete stress plot in yz-plane, $s_x = 12\phi$
y [m]
z [m]
1e6
Stress [Pa]
0.00
0.05
0.10
0.15
0.20
0.25
0.30
0.2
0.4
0.6
0.8
2.43
2.16
1.89
1.62
1.35
1.08
0.81
0.54
0.27
0.00

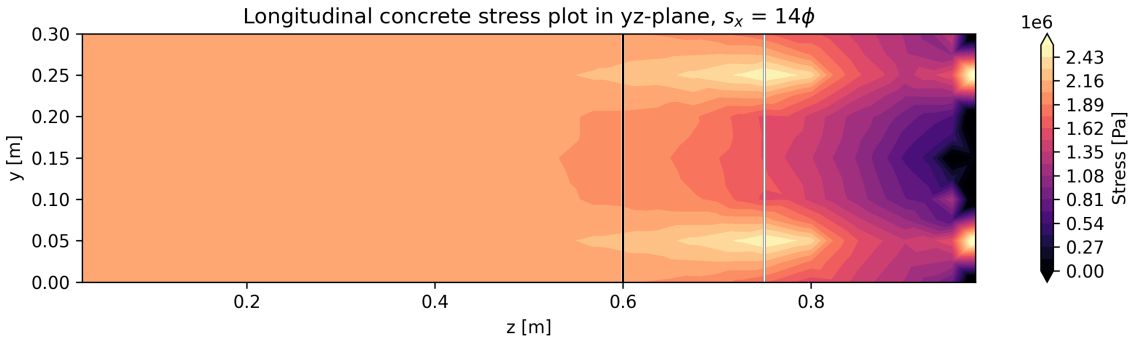
Longitudinal concrete stress plot in yz-plane, $s_x = 14\phi$
y [m]
z [m]
1e6
Stress [Pa]
0.00
0.05
0.10
0.15
0.20
0.25
0.30
0.2
0.4
0.6
0.8
2.43
2.16
1.89
1.62
1.35
1.08
0.81
0.54
0.27
0.00

Thicker member

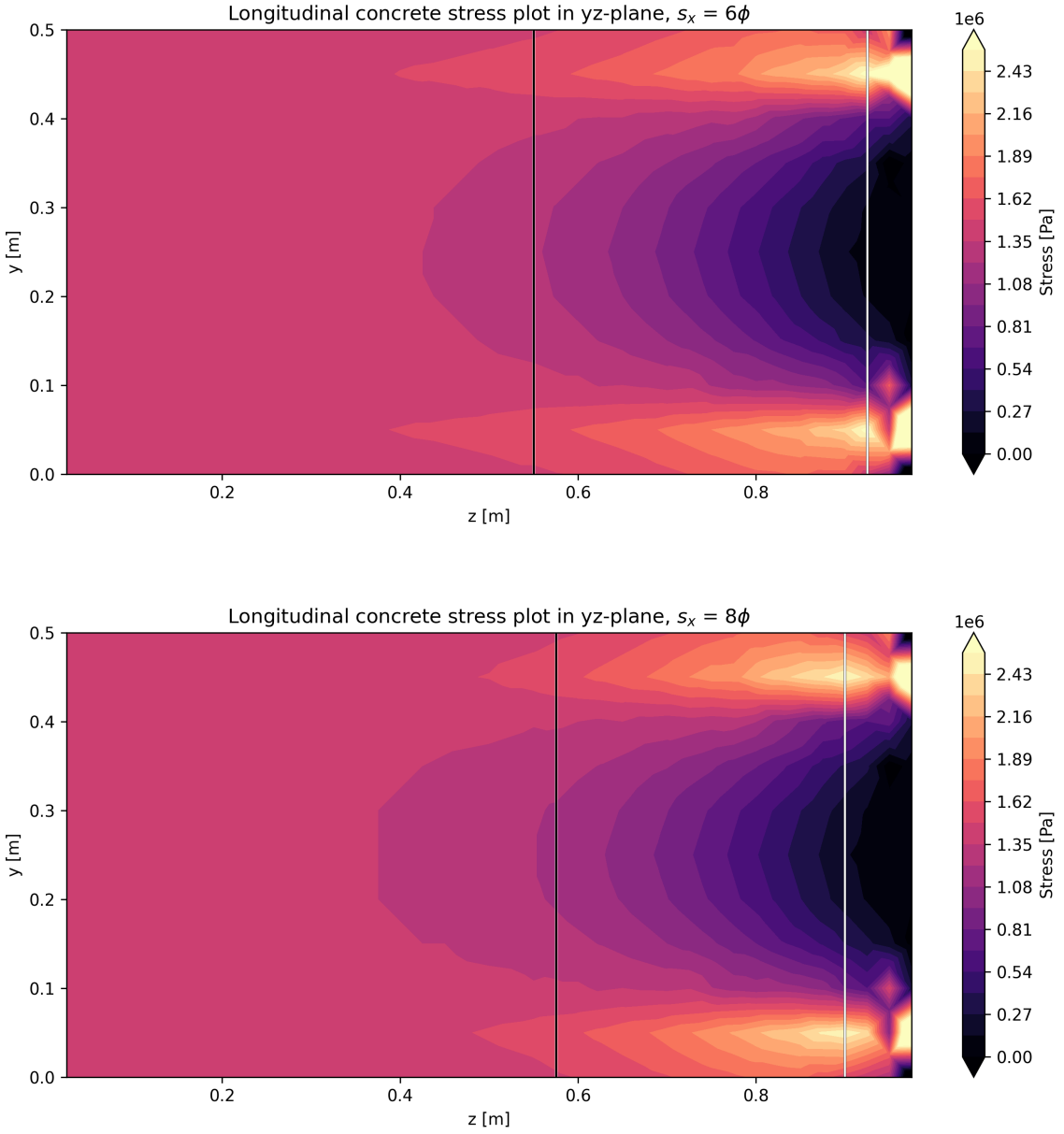

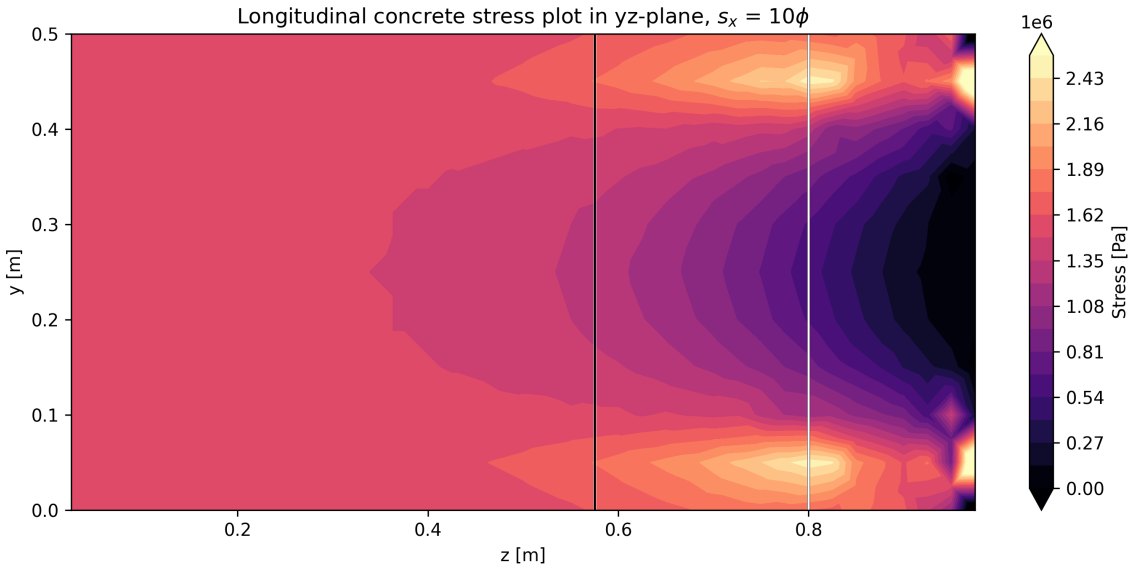
Longitudinal concrete stress plot in yz-plane, $s_x = 10\phi$
y [m]
z [m]
0.0
0.1
0.2
0.3
0.4
0.5
0.2
0.4
0.6
0.8
1e6
2.43
2.16
1.89
1.62
1.35
1.08
0.81
0.54
0.27
0.00
Stress [Pa]

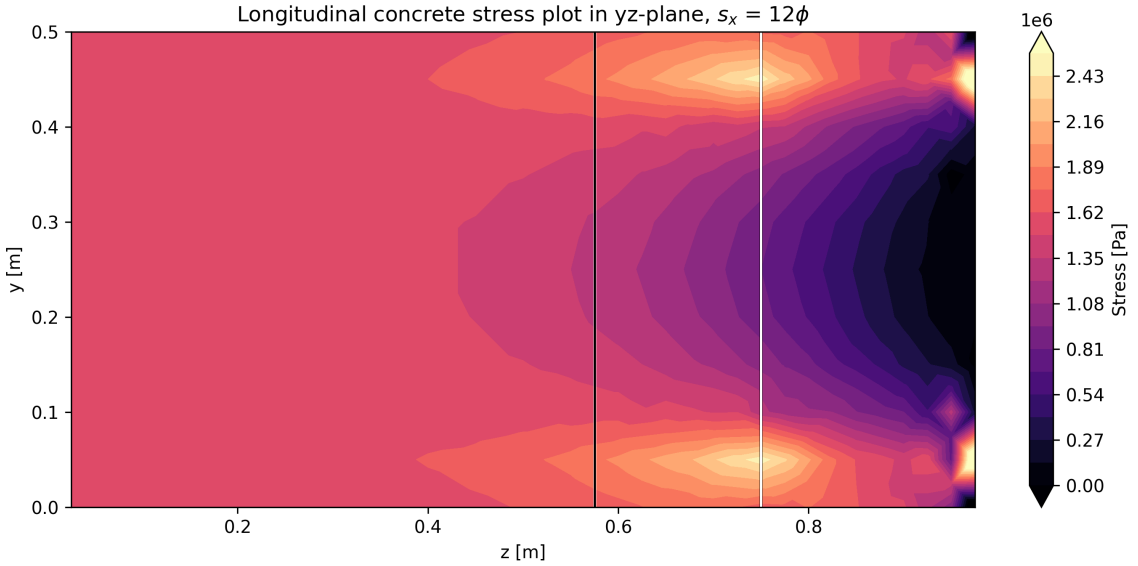
Longitudinal concrete stress plot in yz-plane, $s_x = 12\phi$
y [m]
z [m]
0.0
0.1
0.2
0.3
0.4
0.5
0.2
0.4
0.6
0.8
1e6
2.43
2.16
1.89
1.62
1.35
1.08
0.81
0.54
0.27
0.00
Stress [Pa]

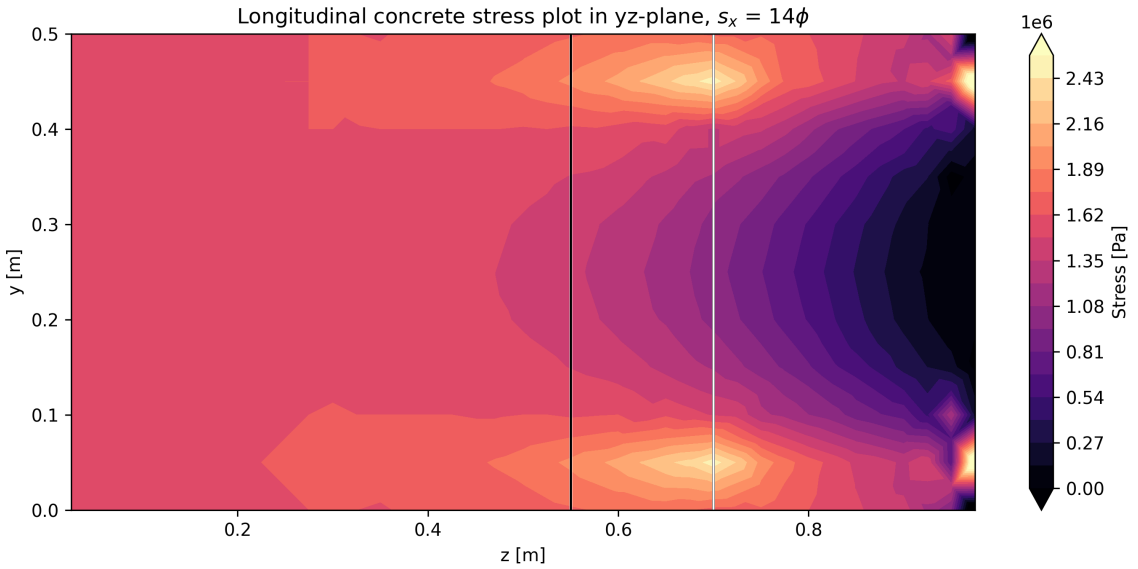
Longitudinal concrete stress plot in yz-plane, $s_x = 14\phi$
y [m]
z [m]
0.0
0.1
0.2
0.3
0.4
0.5
0.2
0.4
0.6
0.8
1e6
2.43
2.16
1.89
1.62
1.35
1.08
0.81
0.54
0.27
0.00
Stress [Pa]

B

FEA results - Study 2

The following appendix includes a complete presentation of results based on FEA for study 2. Tables of numerical results, stress plots and other plots visualising the results are presented.

B.1 Summary tables

In the following section, results from study 2 regarding the effective area, maximum tensile section and transmission length based on FEA are presented.

Ratio	$s_y = 200$ **mm**	$s_y = 400$ **mm**
$s_x = 6\phi$	0.177	0.108
$s_x = 8\phi$	0.110	0.158
$s_x = 10\phi$	0.159	0.216
$s_x = 12\phi$	0.165	0.225
$s_x = 14\phi$	0.216	0.230

B.1.1 Transmission length

Ratio	s_y**=200 mm**		s_y**=400 mm**	
	z_{max} [m]	l_t [m]	z_{max} [m]	l_t [m]
$s_x = 6\phi$	0.450	0.350	0.100	0.400
$s_x = 8\phi$	0.100	0.375	0.150	0.400
$s_x = 10\phi$	0.150	0.400	0.200	0.425
$s_x = 12\phi$	0.150	0.400	0.200	0.425
$s_x = 14\phi$	0.200	0.400	0.200	0.425

B.2 Effective area plots

In the following section, plots describing the effective area calculation for study 2 are included. The first effective area for different $s-\phi$ ratios is presented for both studied

s_y, and further, the stresses used for calculating the effective area are presented for both s_y as well.

B.2.1 Effective area

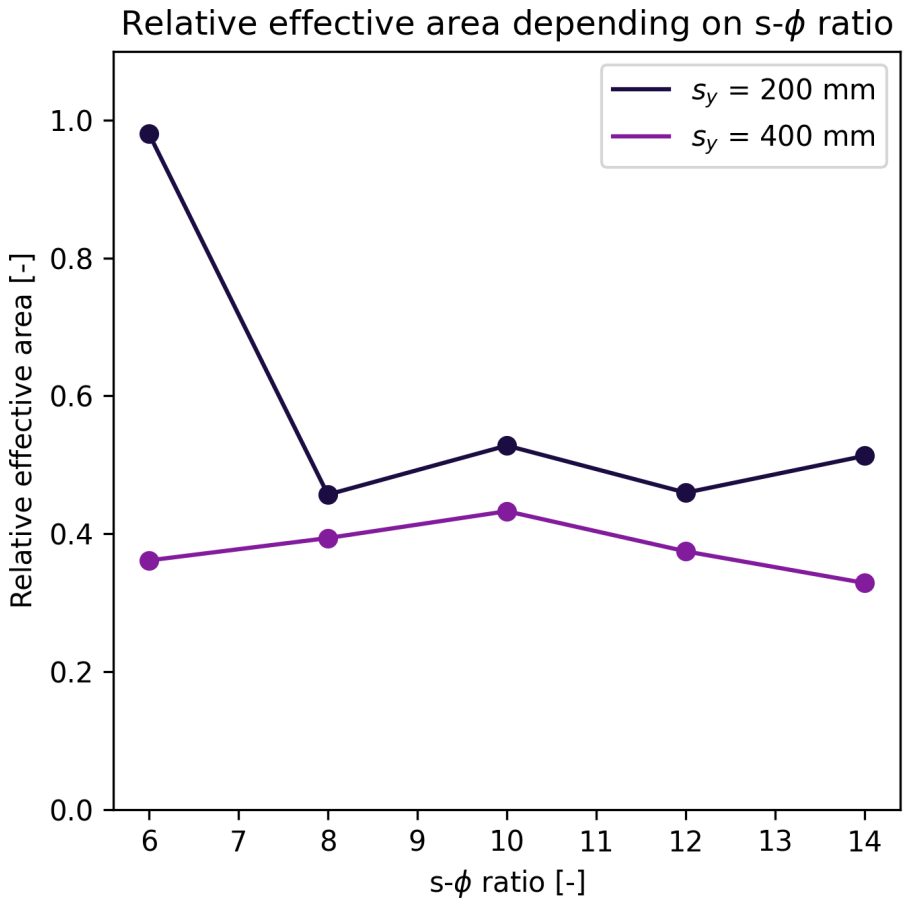

B.2.2 Concrete stress for calculating effective area

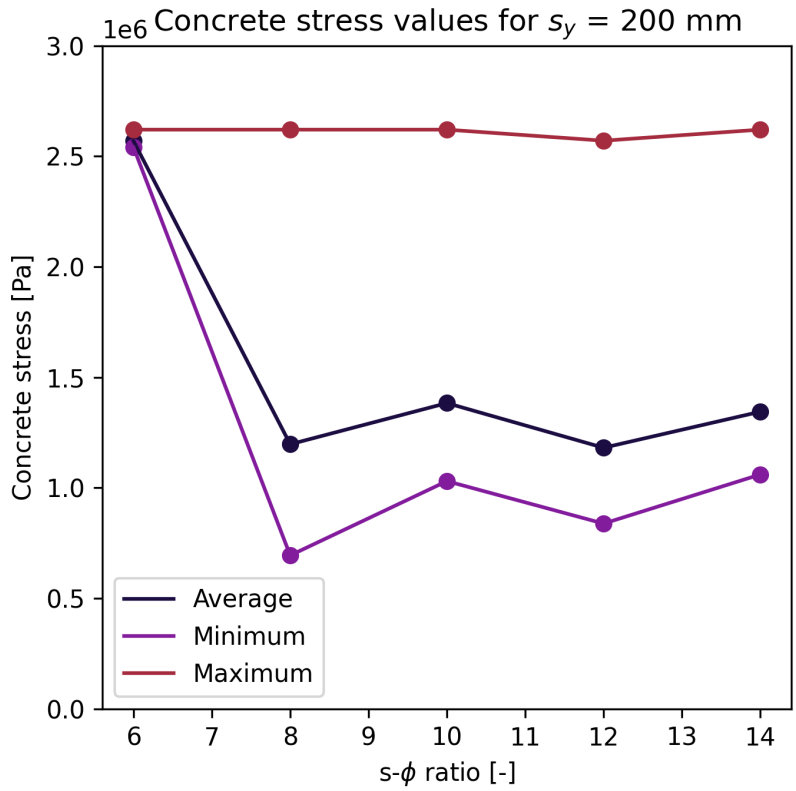

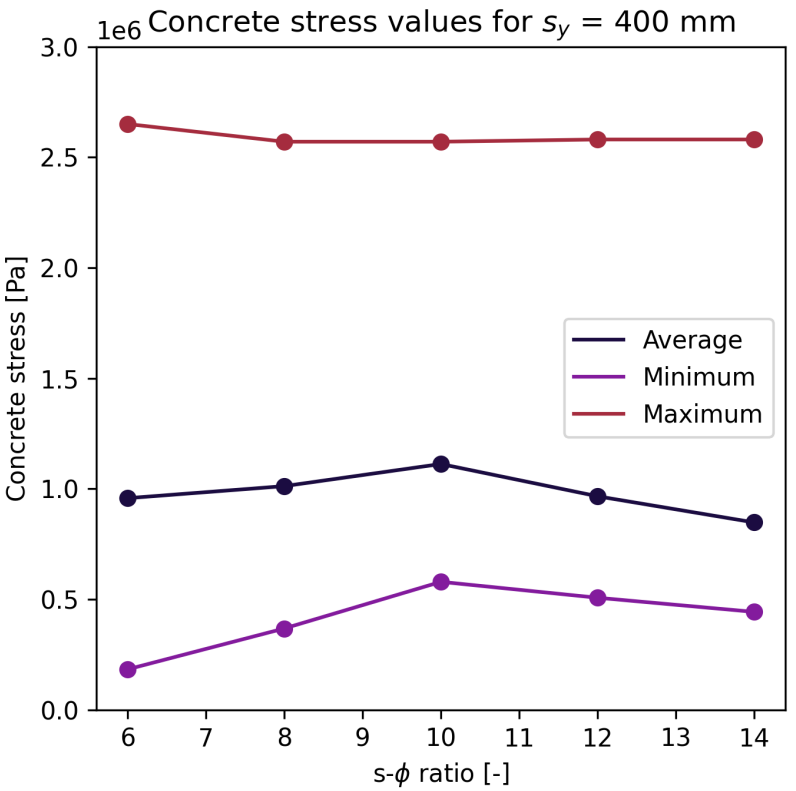

B.3 Overview of concrete stress plots

The following section includes plots illustrating stresses for cases in study 2. Stress plots are given for different directions and planes, and for varying geometries.

In the following section, the results from study 2 are presented. The results are visualised in different ways, and interpretations of the behaviour are stated.

B.3.1 Concrete stress in xy-plane

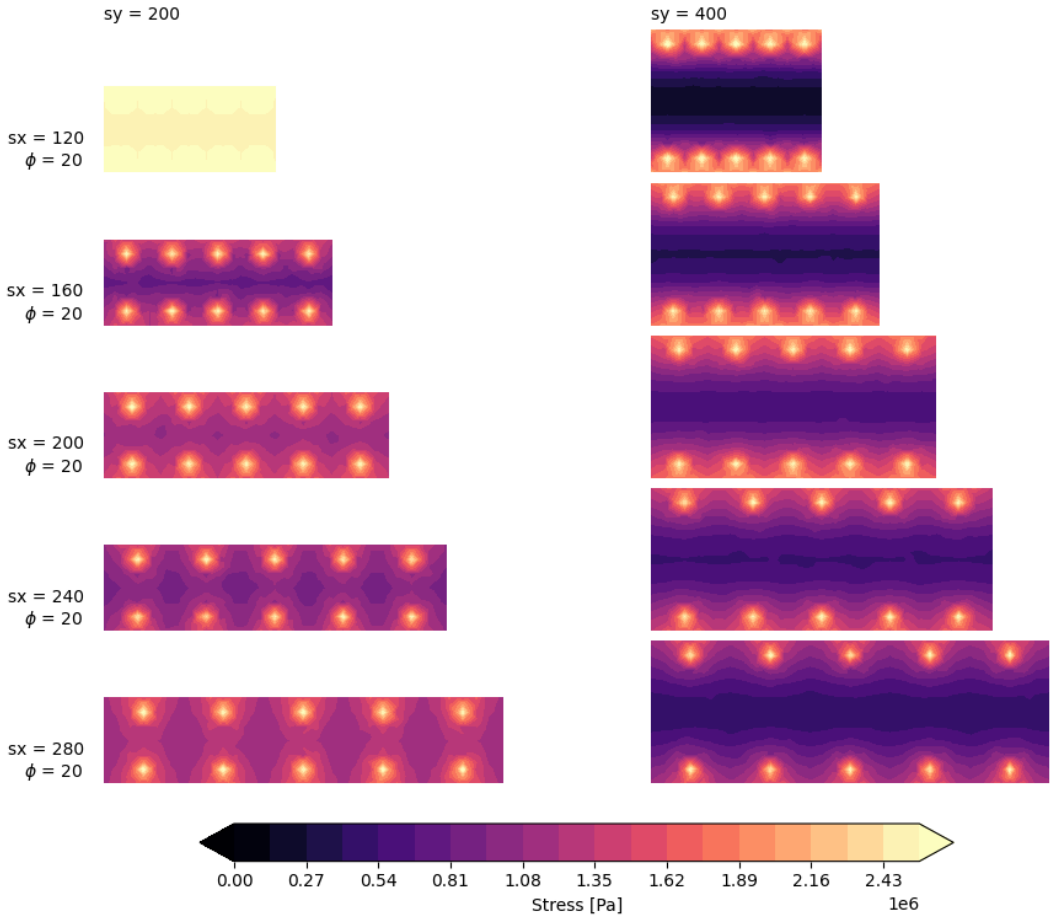

B.3.2 Concrete stress in xz-plane

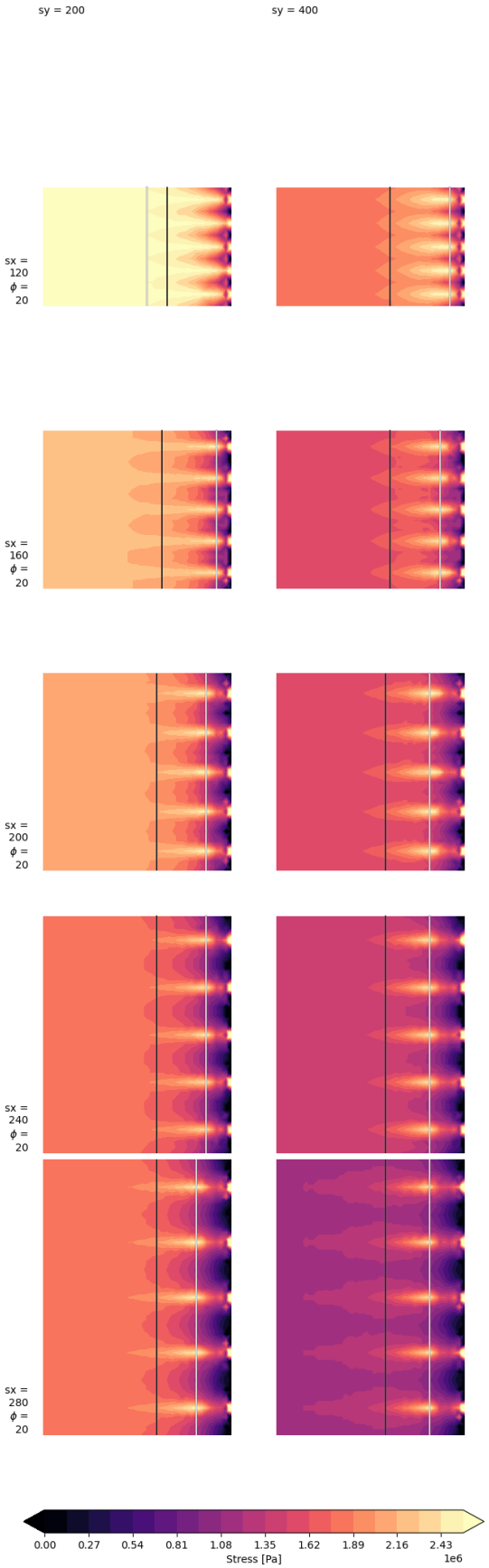

B.3.3 Concrete stress in yz-plane

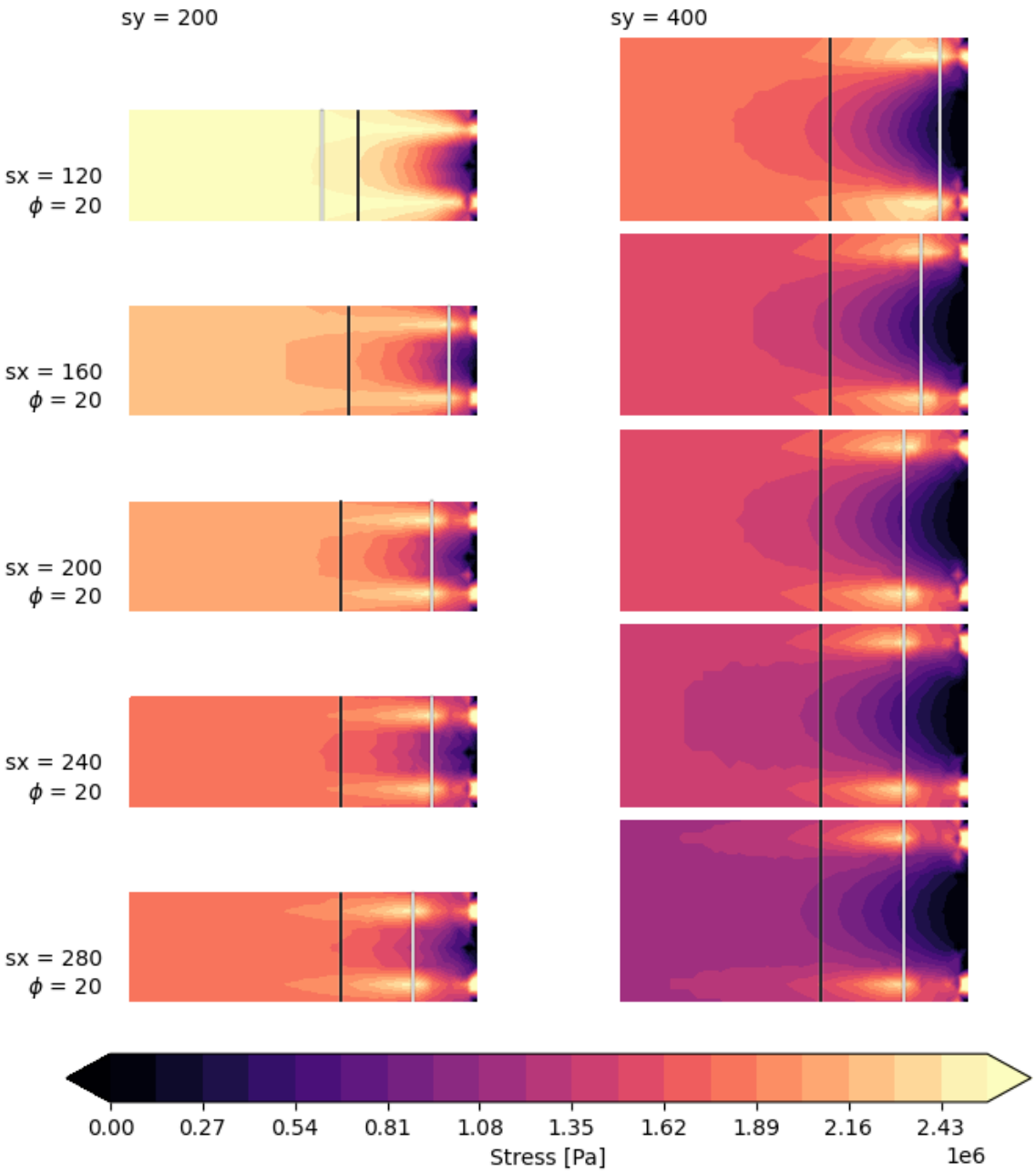

B.3.4 Concrete stress along x-direction

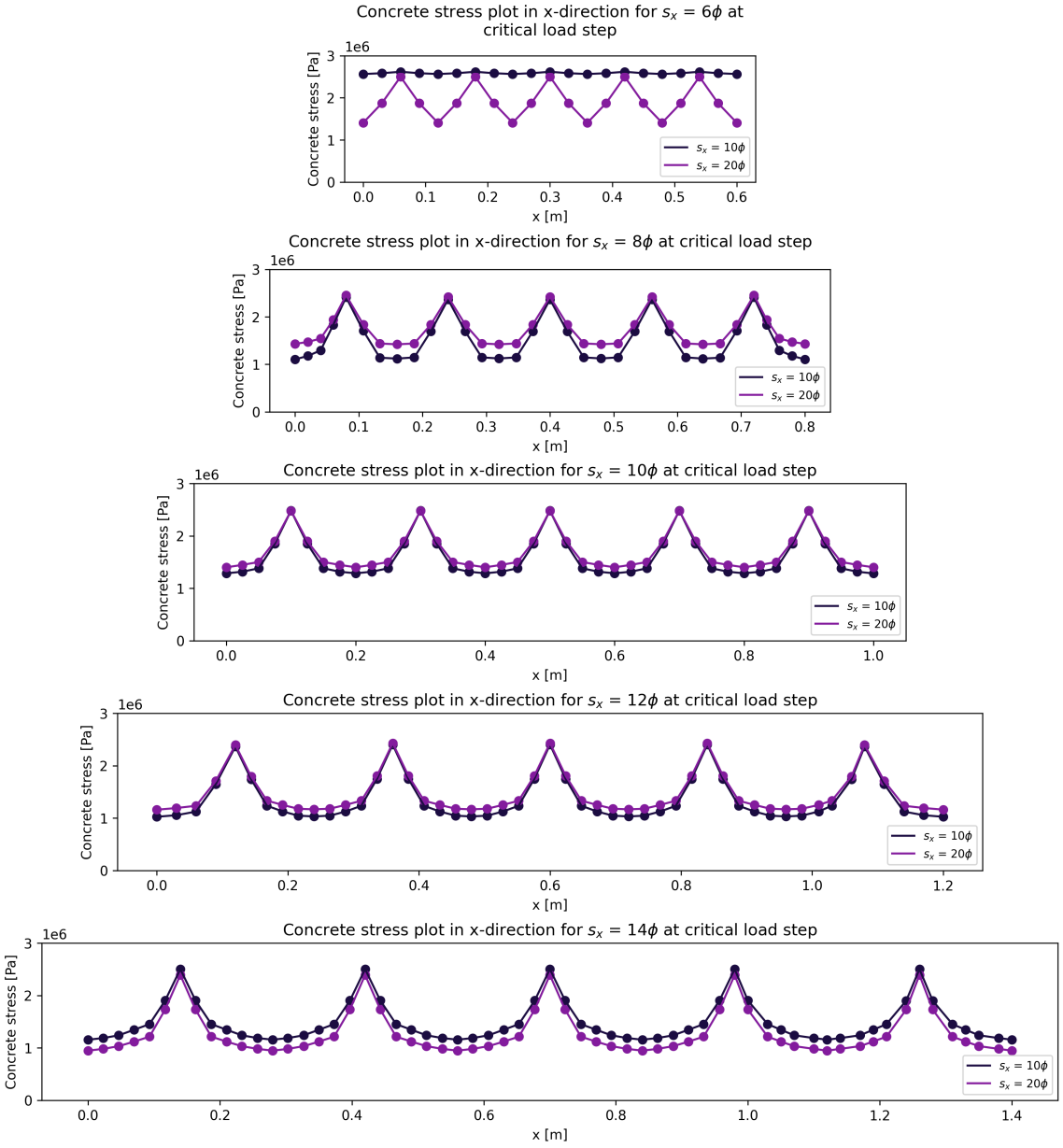

B.3.5 Concrete stress along y-direction

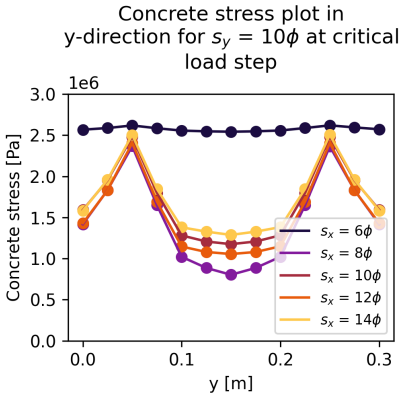

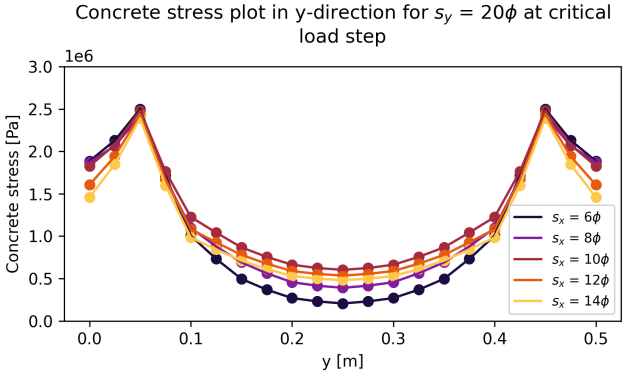

B.4 Detailed figures

In this section, the previously presented stress plots are shown in a more detailed view.

B.4.1 Cross section stress plots in xy-plane

Thinner member

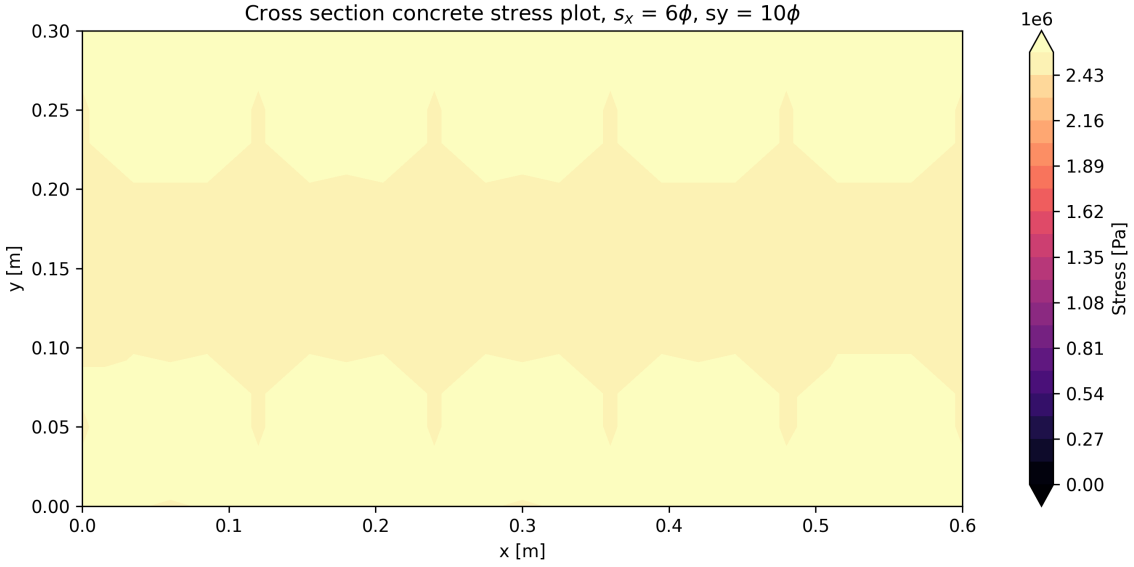

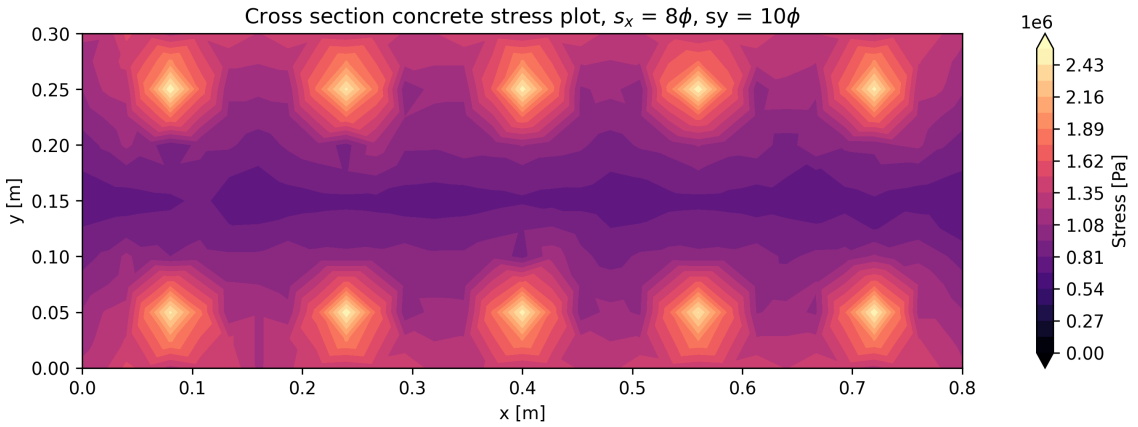
Cross section concrete stress plot, s_x = 8ϕ, sy = 10ϕ
y [m]
x [m]
1e6
Stress [Pa]

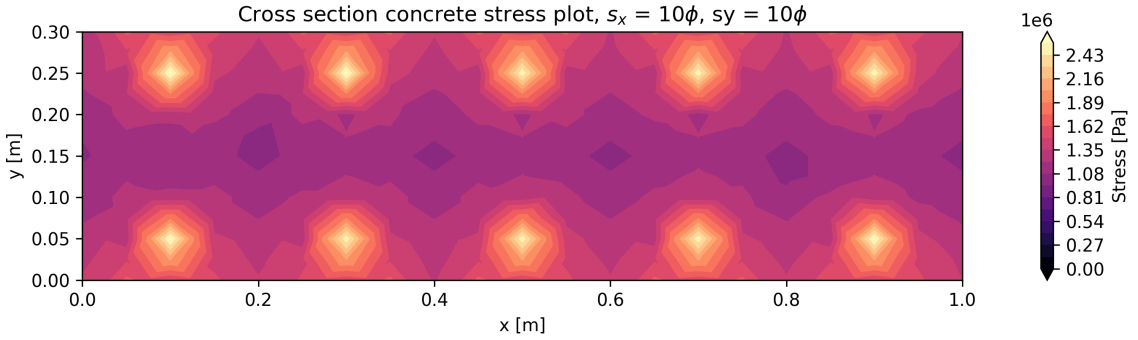
Cross section concrete stress plot, s_x = 10ϕ, sy = 10ϕ
y [m]
x [m]
1e6
Stress [Pa]

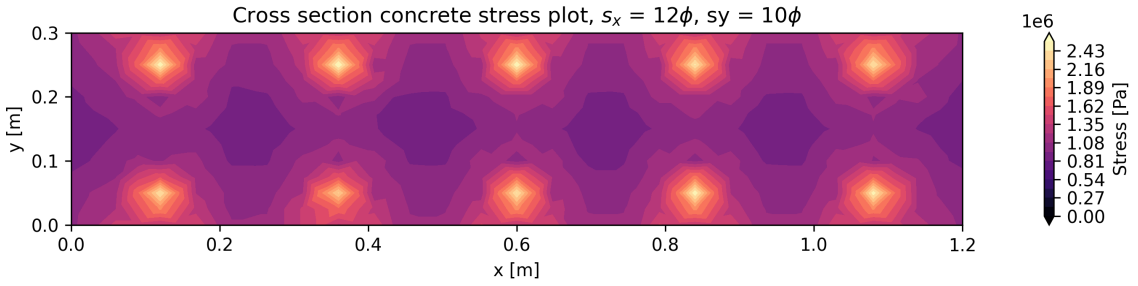
Cross section concrete stress plot, s_x = 12ϕ, sy = 10ϕ
y [m]
x [m]
1e6
Stress [Pa]

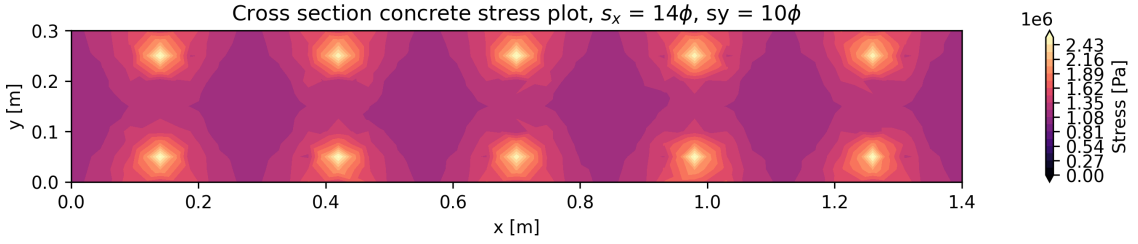
Cross section concrete stress plot, s_x = 14ϕ, sy = 10ϕ
y [m]
x [m]
1e6
Stress [Pa]

Thicker member

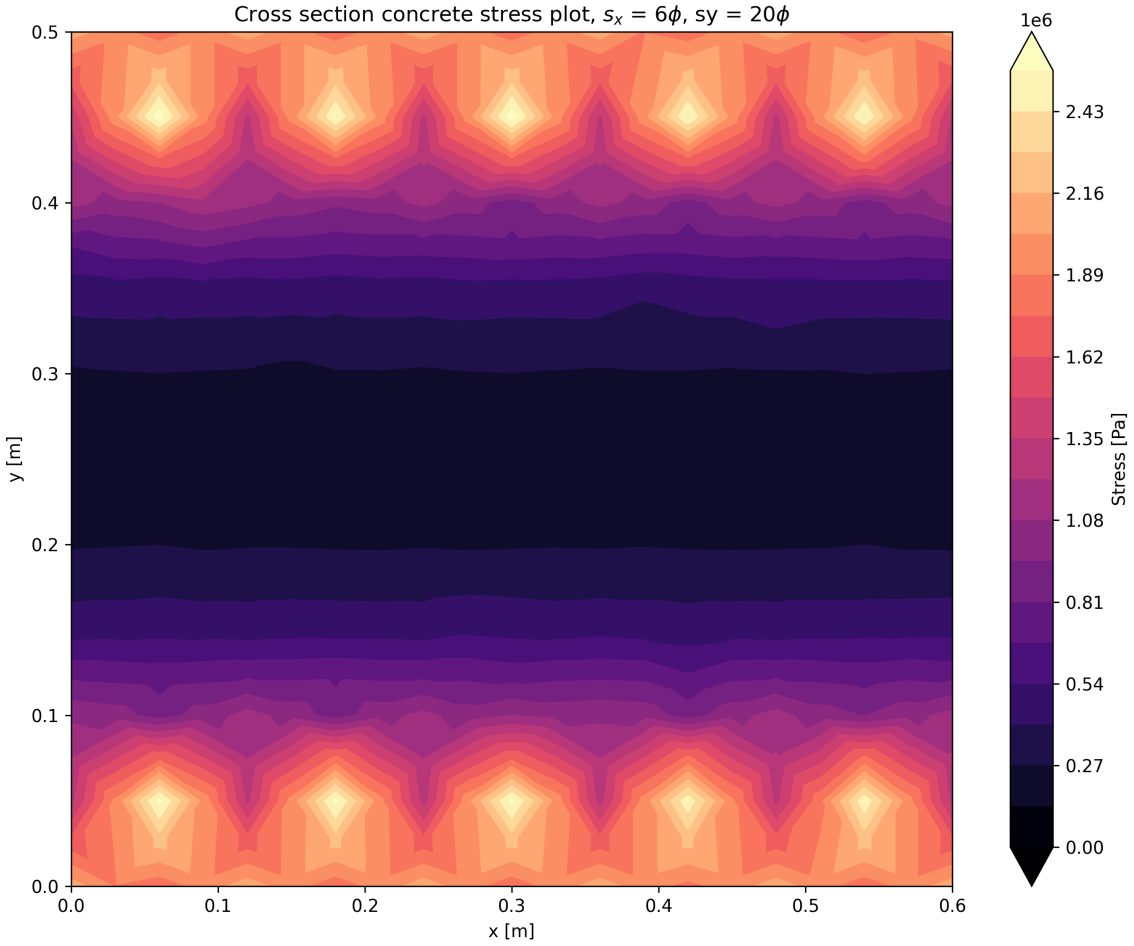

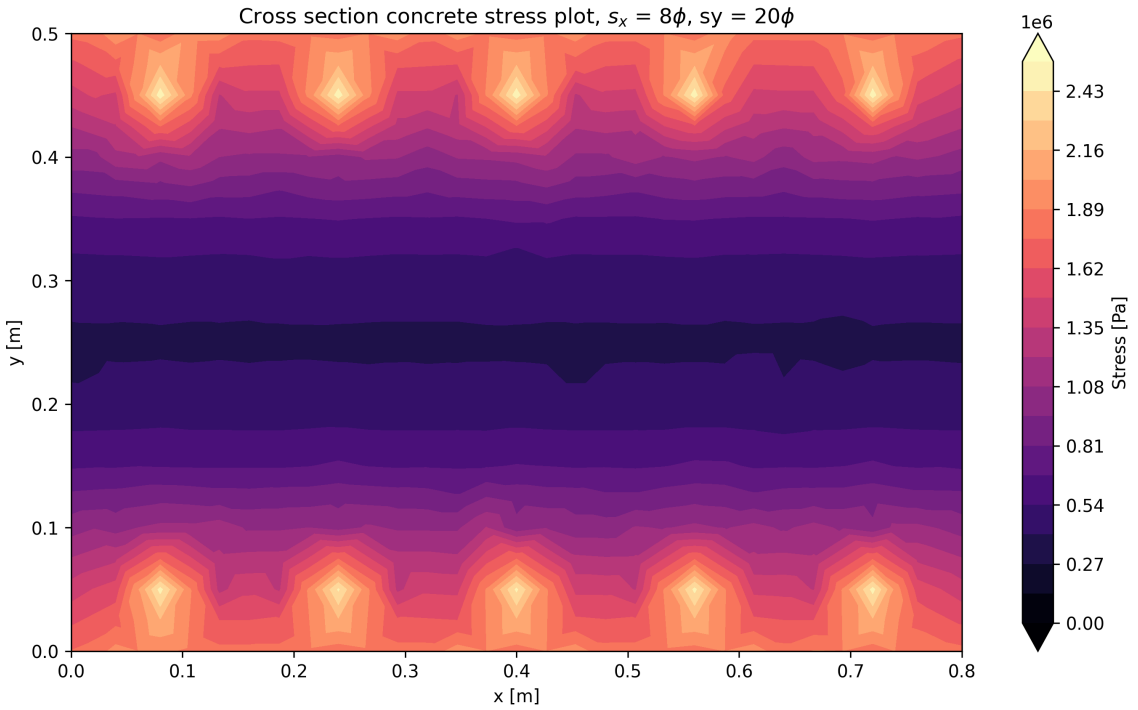
Cross section concrete stress plot, s_x = 8ϕ, sy = 20ϕ
y [m]
x [m]
1e6
Stress [Pa]
2.43
2.16
1.89
1.62
1.35
1.08
0.81
0.54
0.27
0.00

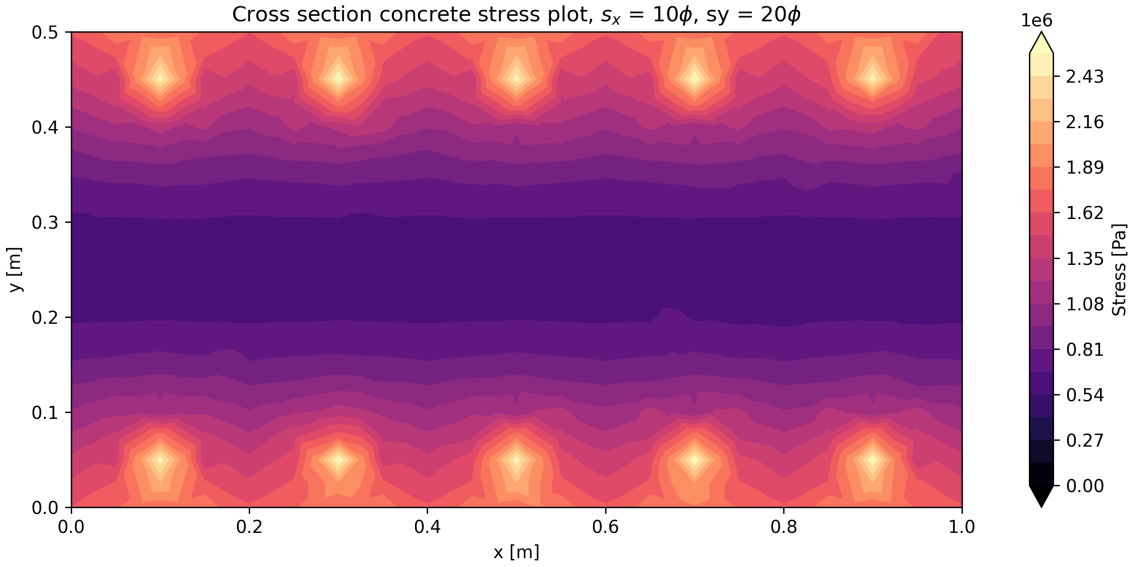
Cross section concrete stress plot, s_x = 10ϕ, sy = 20ϕ
y [m]
x [m]
1e6
Stress [Pa]
2.43
2.16
1.89
1.62
1.35
1.08
0.81
0.54
0.27
0.00

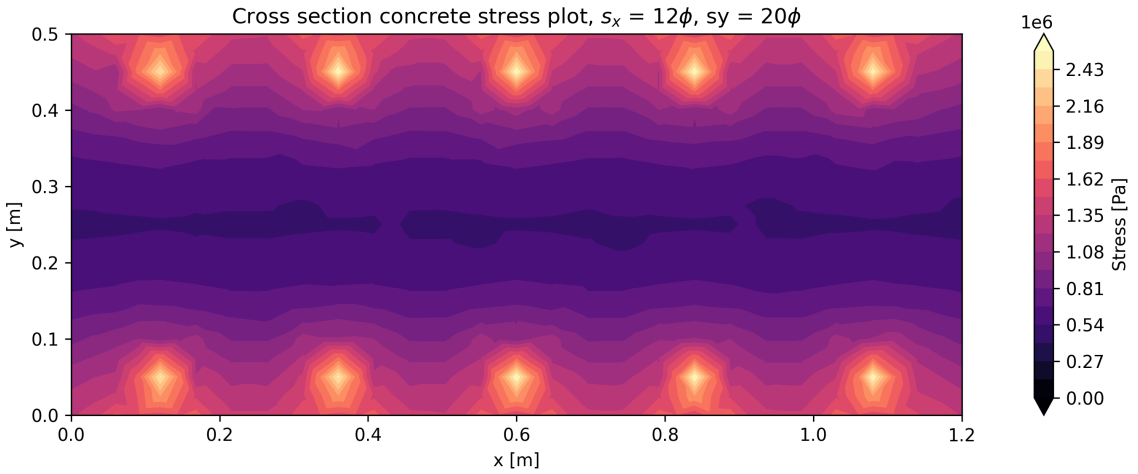
Cross section concrete stress plot, s_x = 12ϕ, sy = 20ϕ
y [m]
x [m]
1e6
Stress [Pa]
2.43
2.16
1.89
1.62
1.35
1.08
0.81
0.54
0.27
0.00

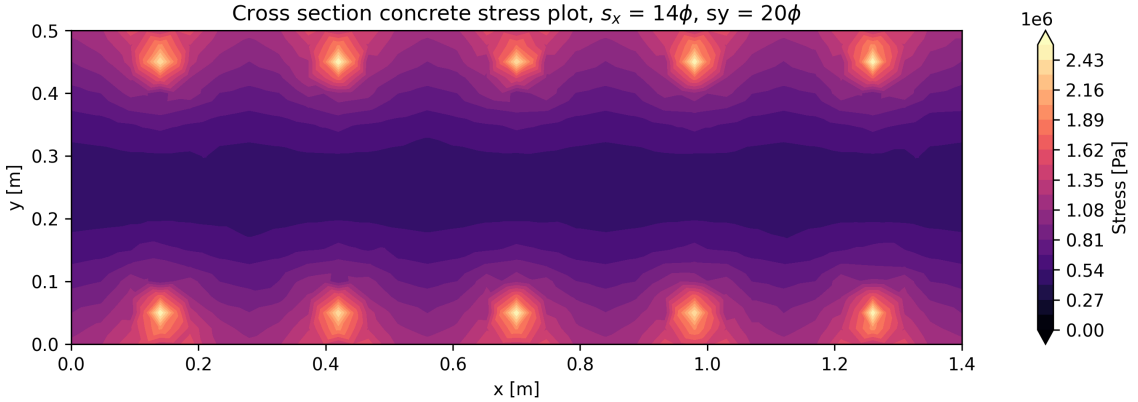
Cross section concrete stress plot, s_x = 14ϕ, sy = 20ϕ
y [m]
x [m]
1e6
Stress [Pa]
2.43
2.16
1.89
1.62
1.35
1.08
0.81
0.54
0.27
0.00

B.4.2 Longitudinal stress plots in xz-plane

Thinner member

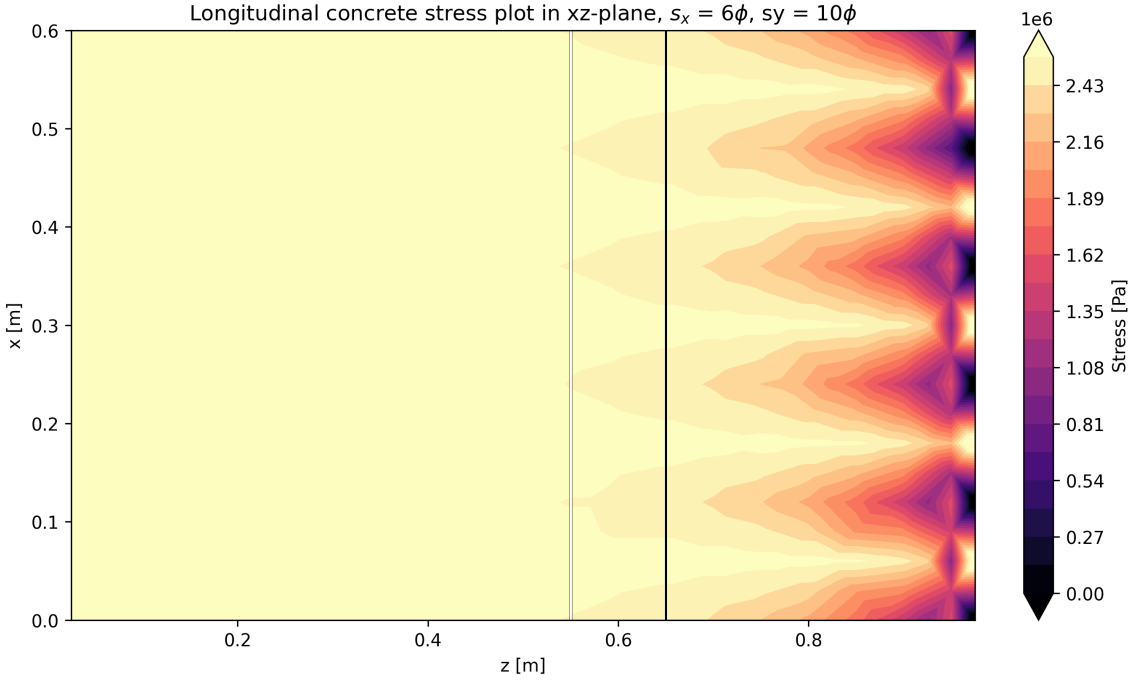

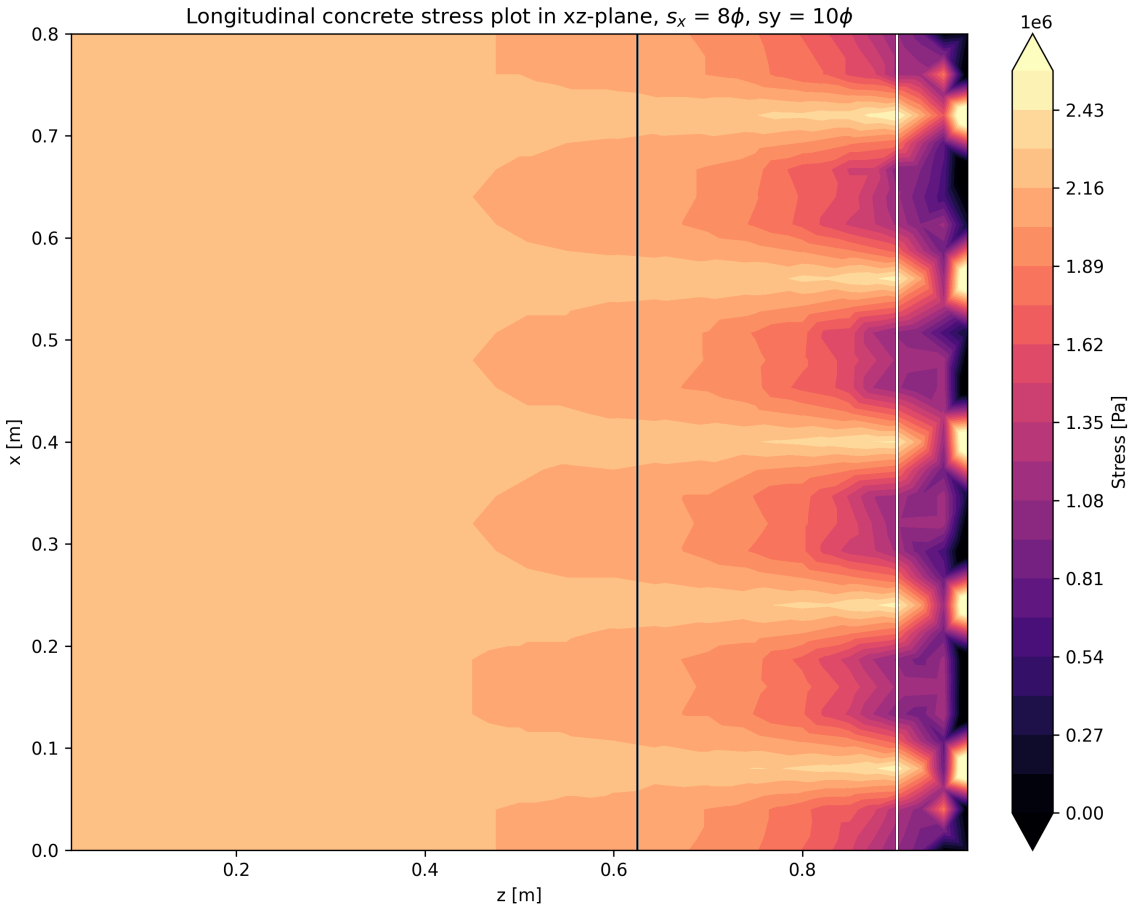
Longitudinal concrete stress plot in xz-plane, s_x = 8ϕ, sy = 10ϕ
x [m]
z [m]
0.0
0.1
0.2
0.3
0.4
0.5
0.6
0.7
0.8
0.2
0.4
0.6
0.8
1e6
2.43
2.16
1.89
1.62
1.35
1.08
0.81
0.54
0.27
0.00
Stress [Pa]

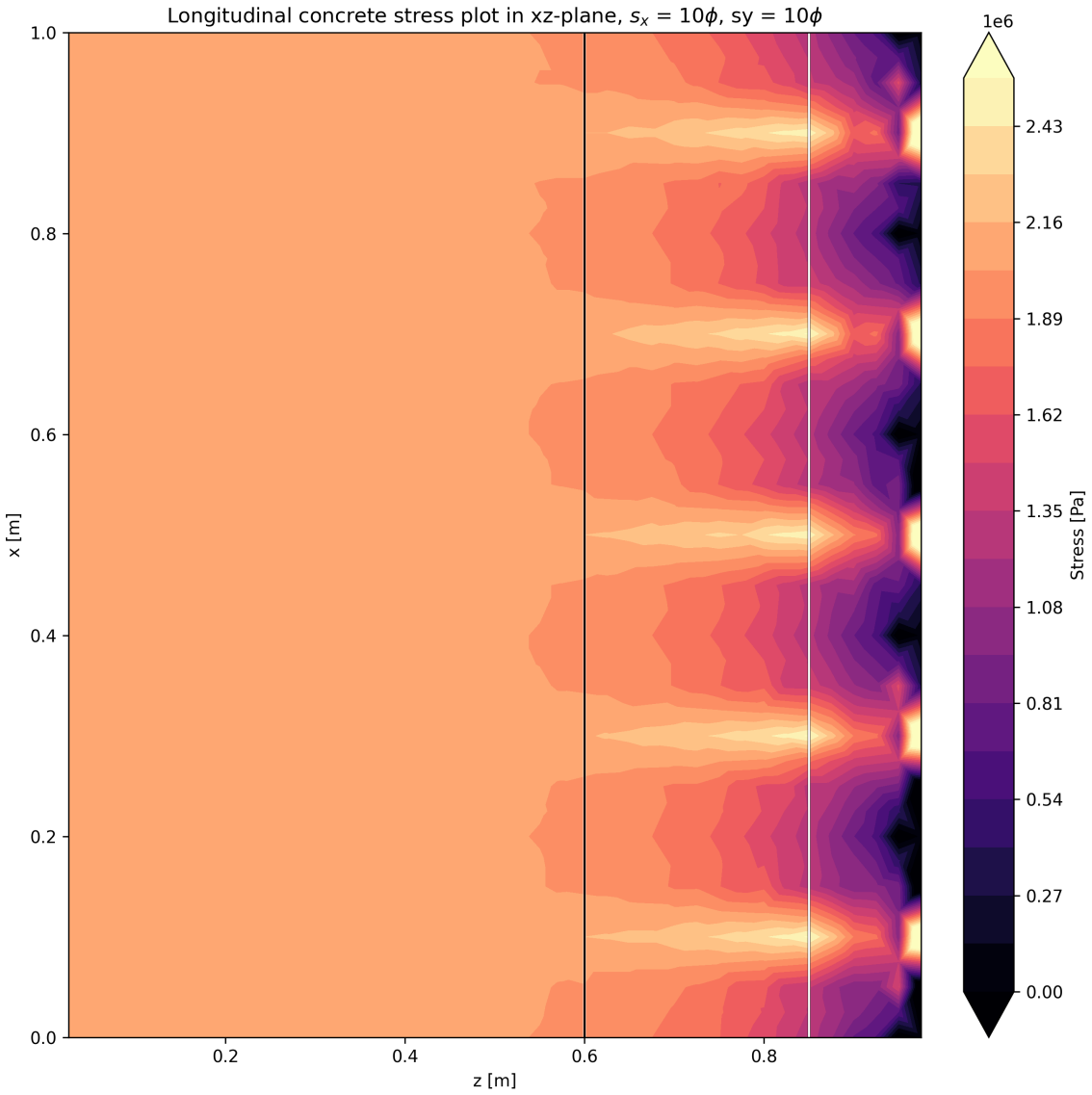
Longitudinal concrete stress plot in xz-plane, s_x = 10ϕ, sy = 10ϕ
1e6
2.43
2.16
1.89
1.62
1.35
1.08
0.81
0.54
0.27
0.00
Stress [Pa]
1.0
0.8
0.6
0.4
0.2
0.0
x [m]
0.2
0.4
0.6
0.8
z [m]

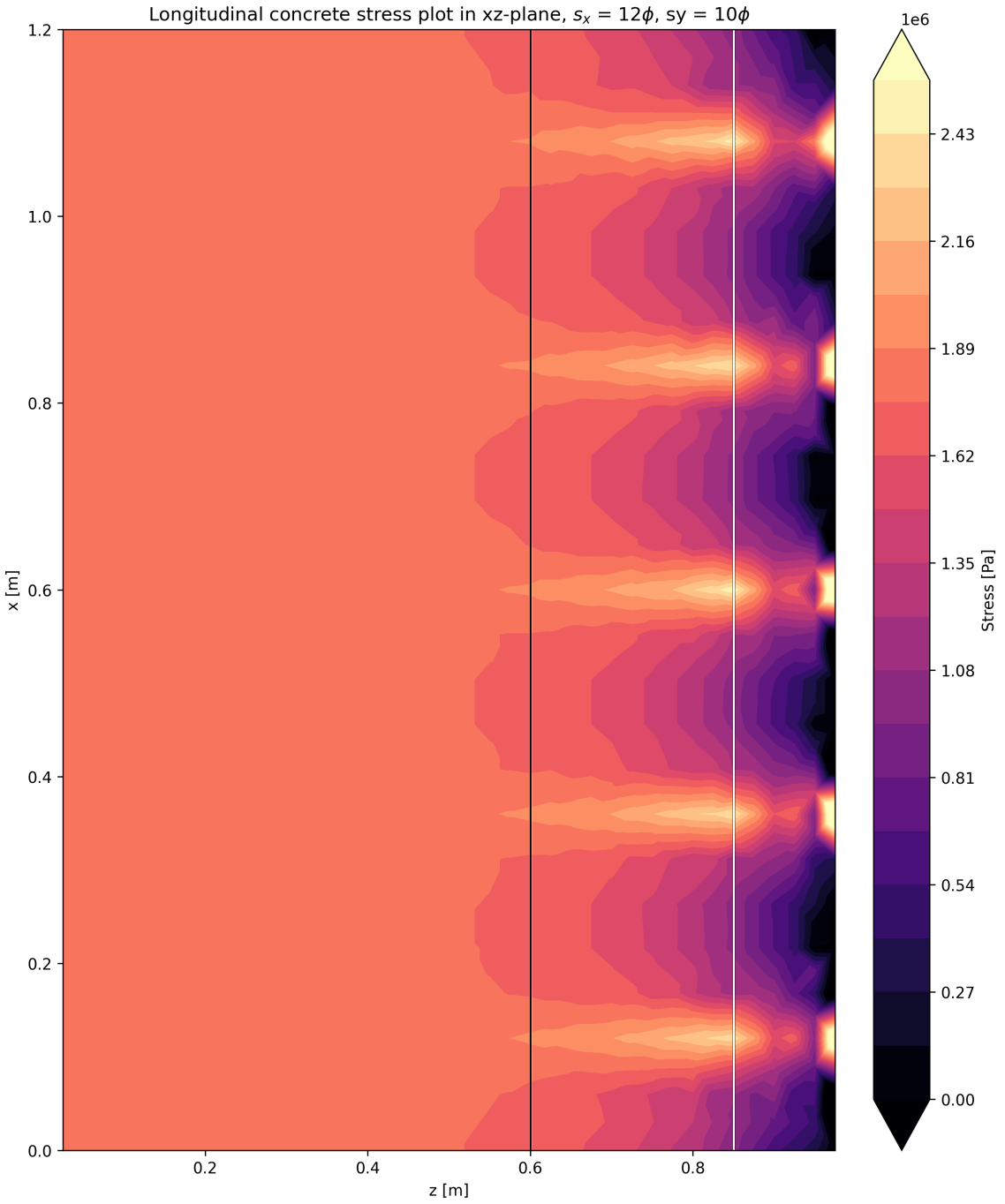
Longitudinal concrete stress plot in xz-plane, s_x = 12ϕ, sy = 10ϕ
1e6
2.43
2.16
1.89
1.62
1.35
1.08
0.81
0.54
0.27
0.00
Stress [Pa]
x [m]
z [m]
0.0
0.2
0.4
0.6
0.8
1.0
1.2
0.2
0.4
0.6
0.8

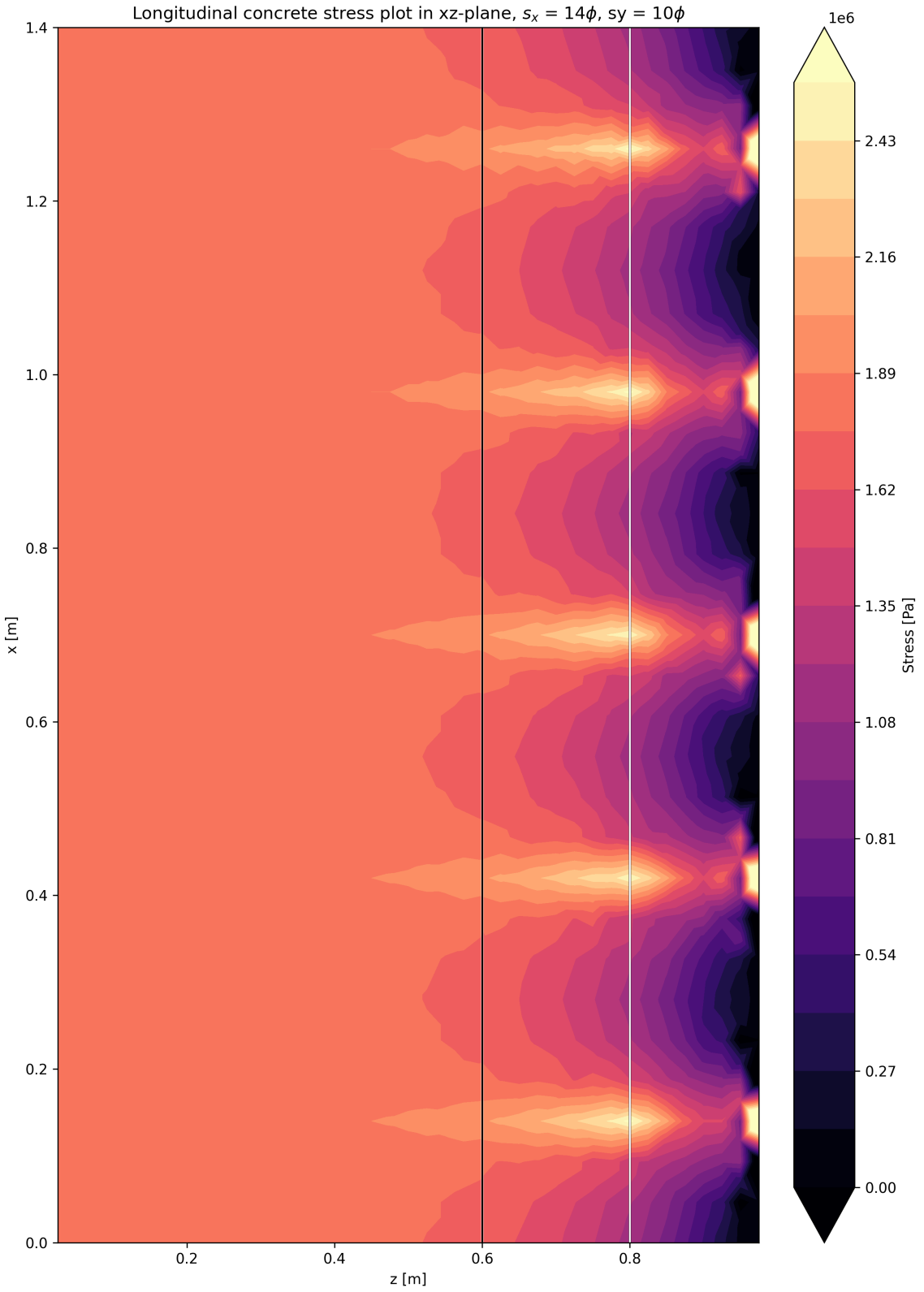
Longitudinal concrete stress plot in xz-plane, s_x = 14ϕ, sy = 10ϕ
1e6
2.43
2.16
1.89
1.62
1.35
1.08
0.81
0.54
0.27
0.00
Stress [Pa]
1.4
1.2
1.0
0.8
0.6
0.4
0.2
0.0
x [m]
0.2
0.4
0.6
0.8
z [m]

Thicker member

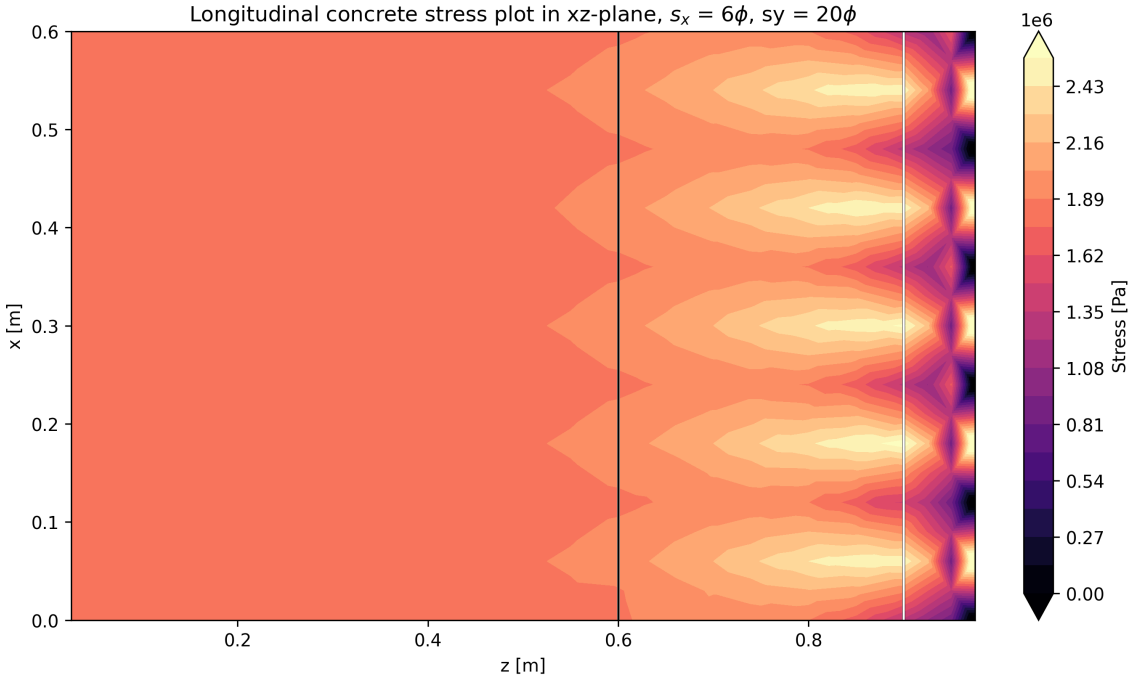

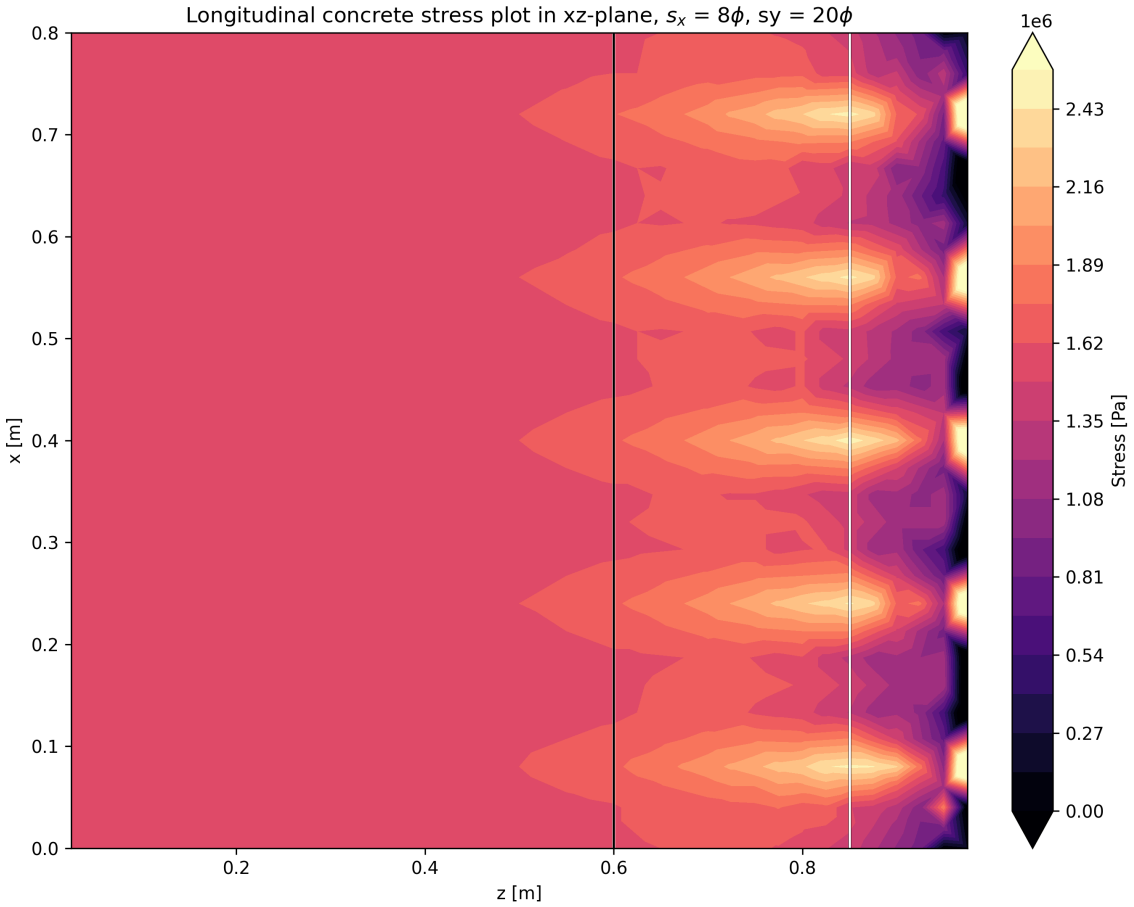

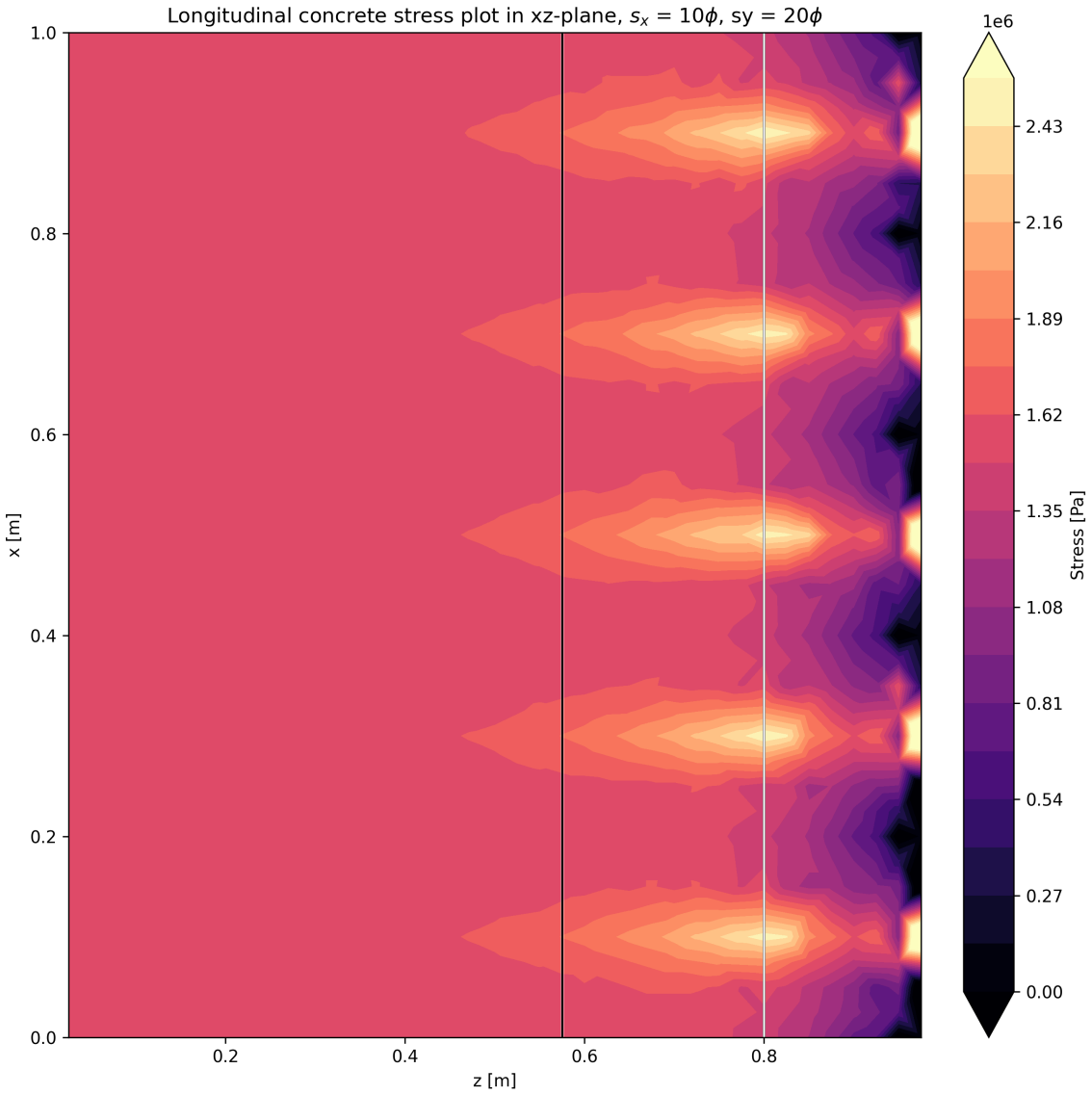
Longitudinal concrete stress plot in xz-plane, s_x = 10ϕ, sy = 20ϕ
1e6
2.43
2.16
1.89
1.62
1.35
1.08
0.81
0.54
0.27
0.00
Stress [Pa]
1.0
0.8
0.6
0.4
0.2
0.0
x [m]
0.2
0.4
0.6
0.8
z [m]

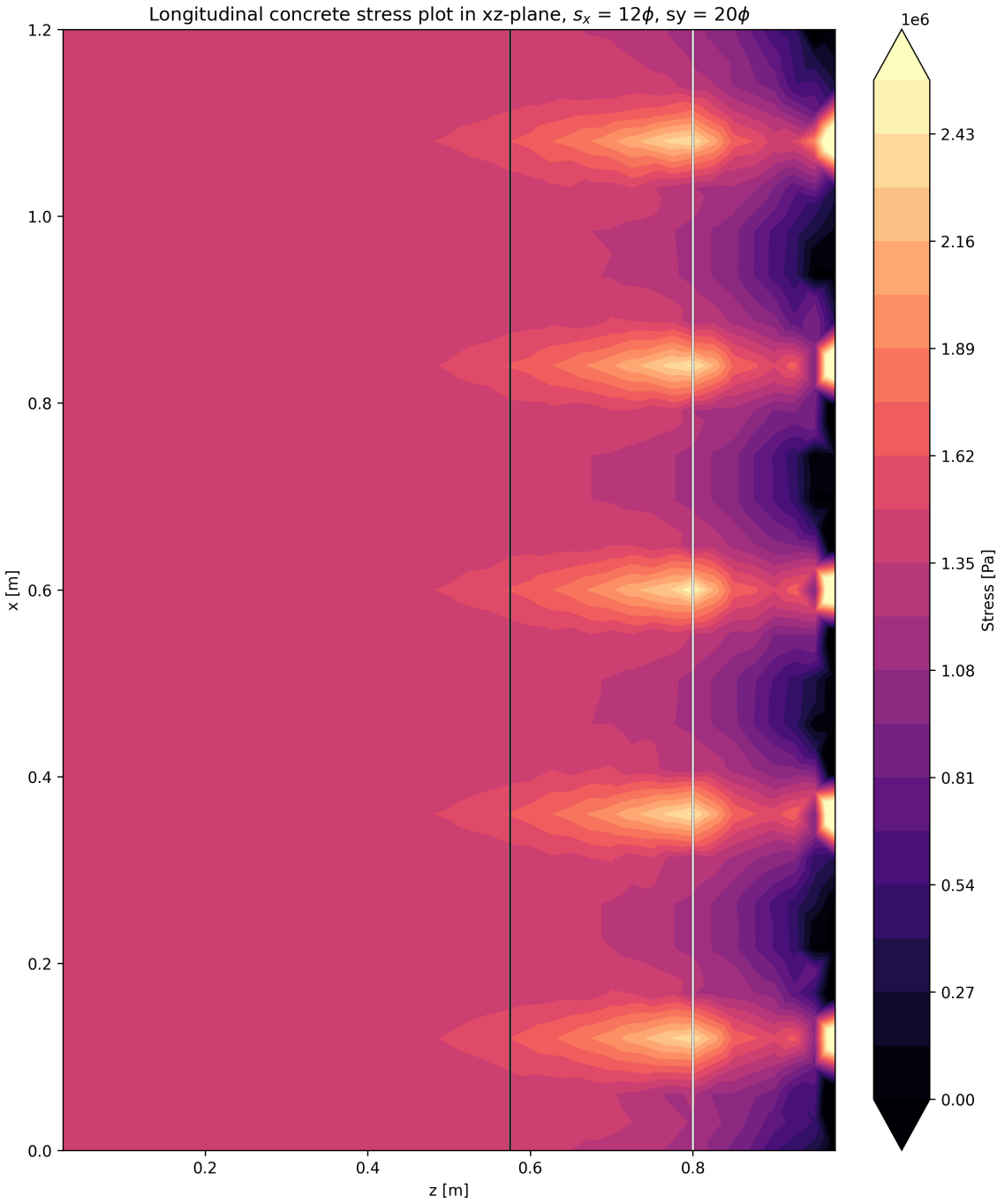
Longitudinal concrete stress plot in xz-plane, s_x = 12ϕ, sy = 20ϕ
1e6
2.43
2.16
1.89
1.62
1.35
1.08
0.81
0.54
0.27
0.00
Stress [Pa]
x [m]
z [m]
0.0
0.2
0.4
0.6
0.8
1.0
1.2
0.2
0.4
0.6
0.8

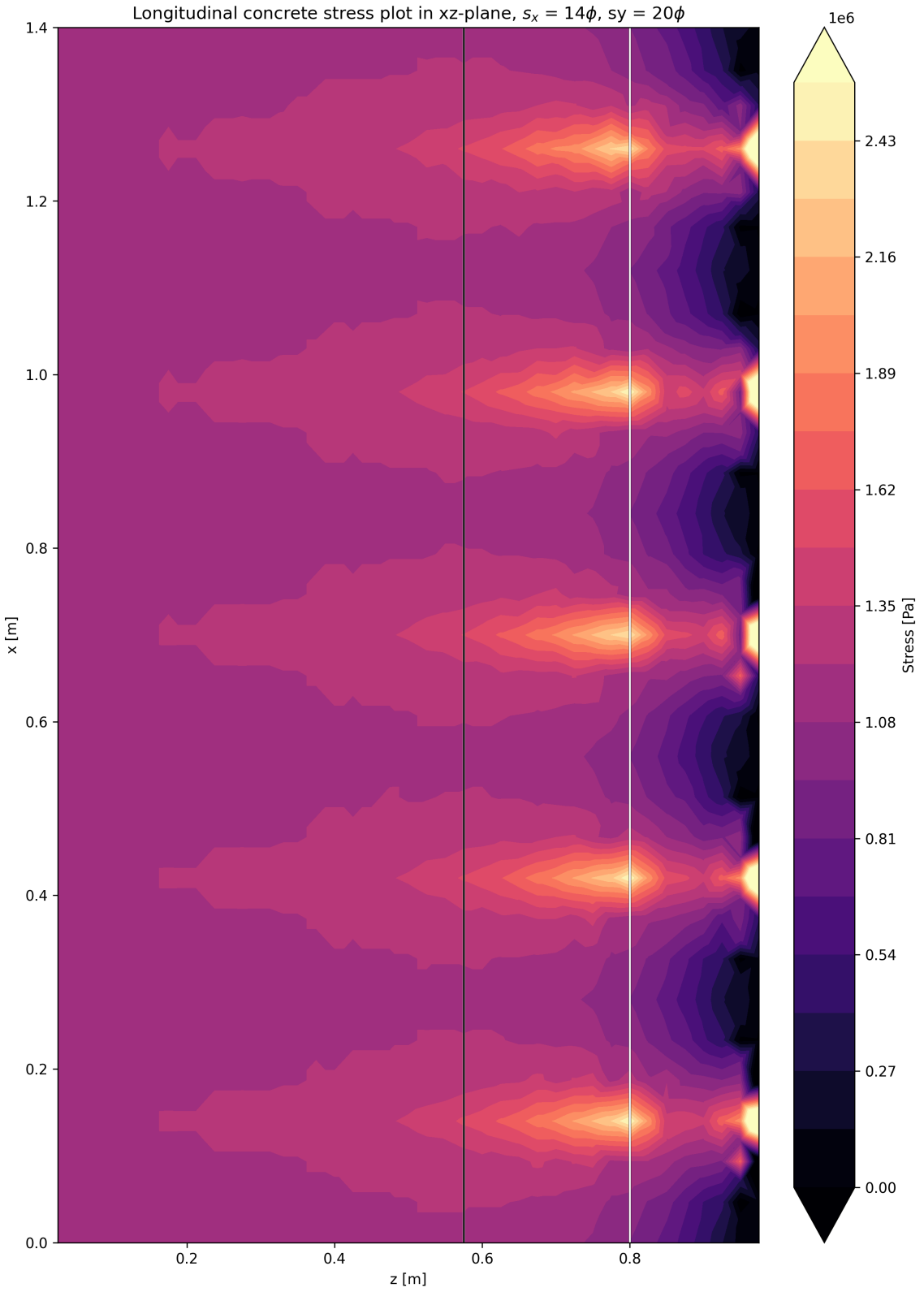
Longitudinal concrete stress plot in xz-plane, s_x = 14ϕ, sy = 20ϕ
1e6
2.43
2.16
1.89
1.62
1.35
1.08
0.81
0.54
0.27
0.00
Stress [Pa]
1.4
1.2
1.0
0.8
0.6
0.4
0.2
0.0
x [m]
0.2
0.4
0.6
0.8
z [m]

B.4.3 Longitudinal stress plots in yz-plane

Thinner member

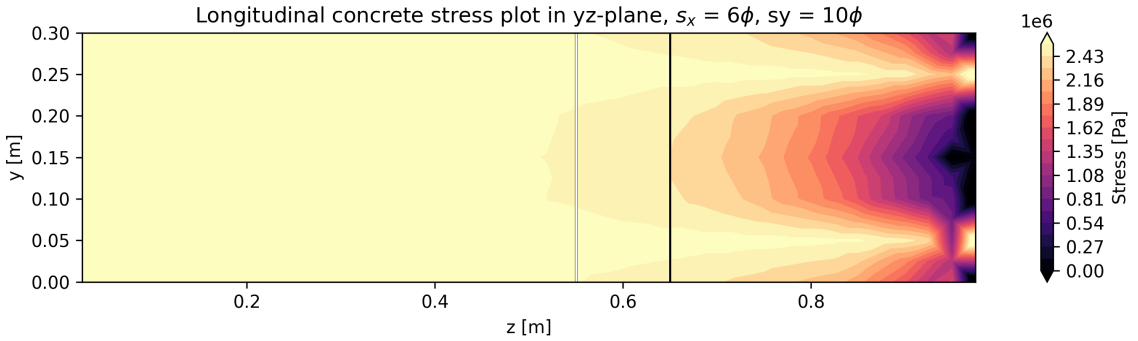

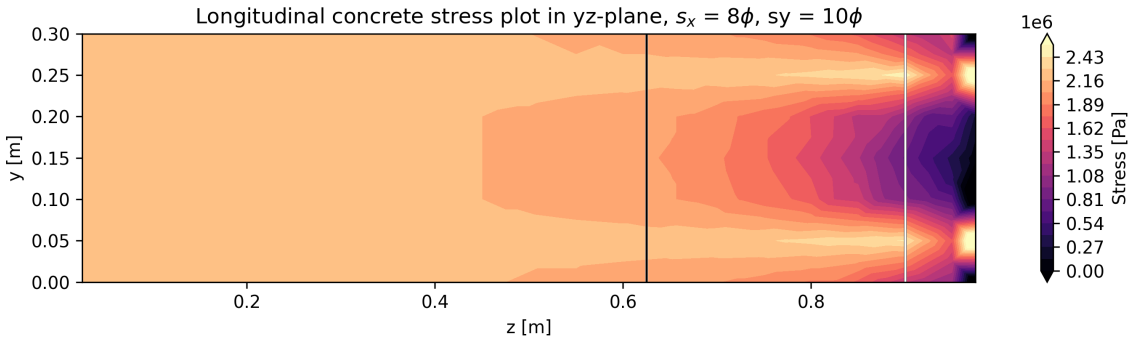

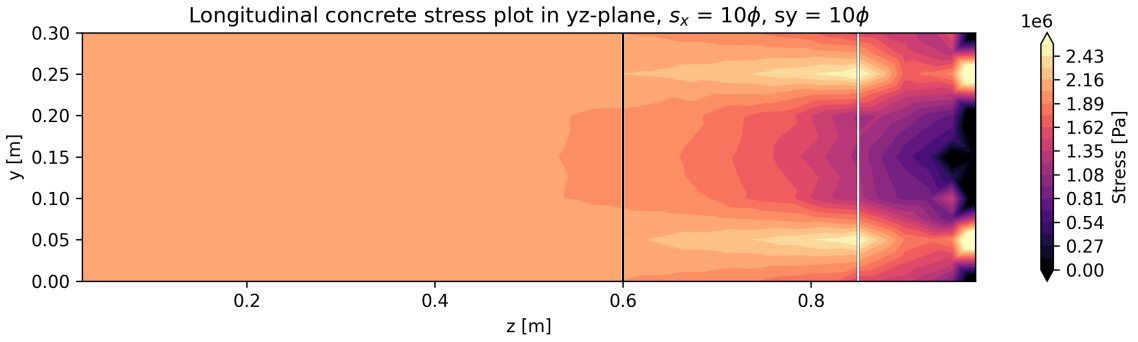

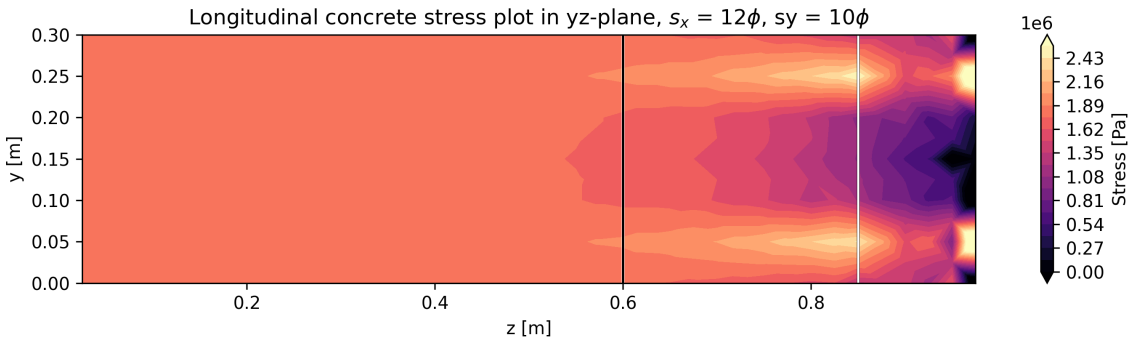

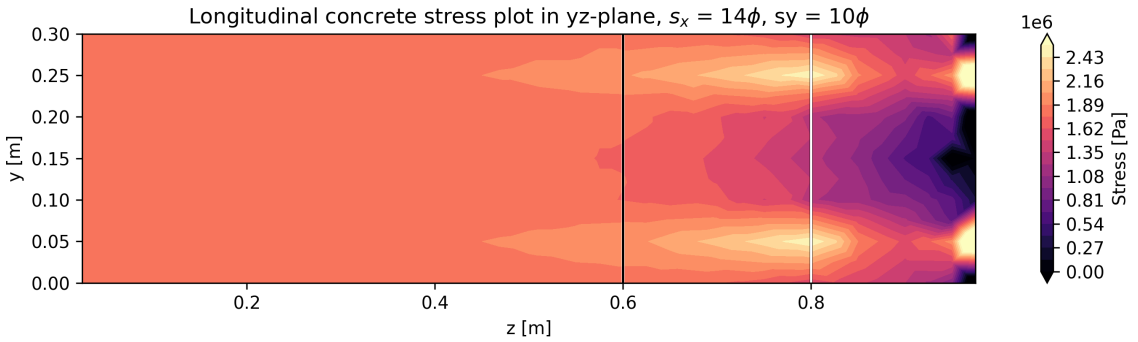

Thicker member

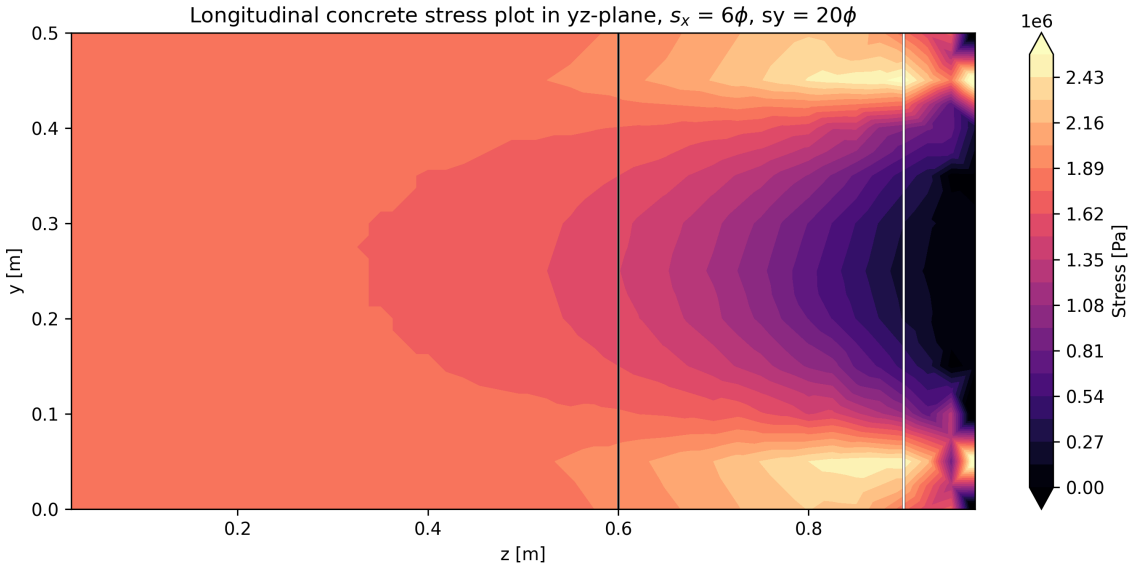

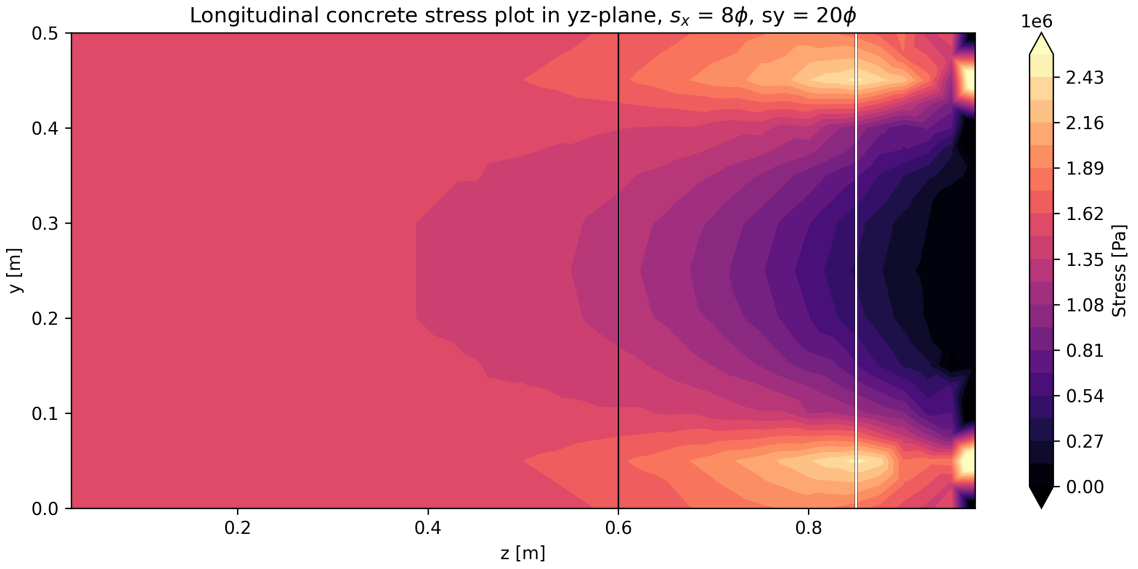

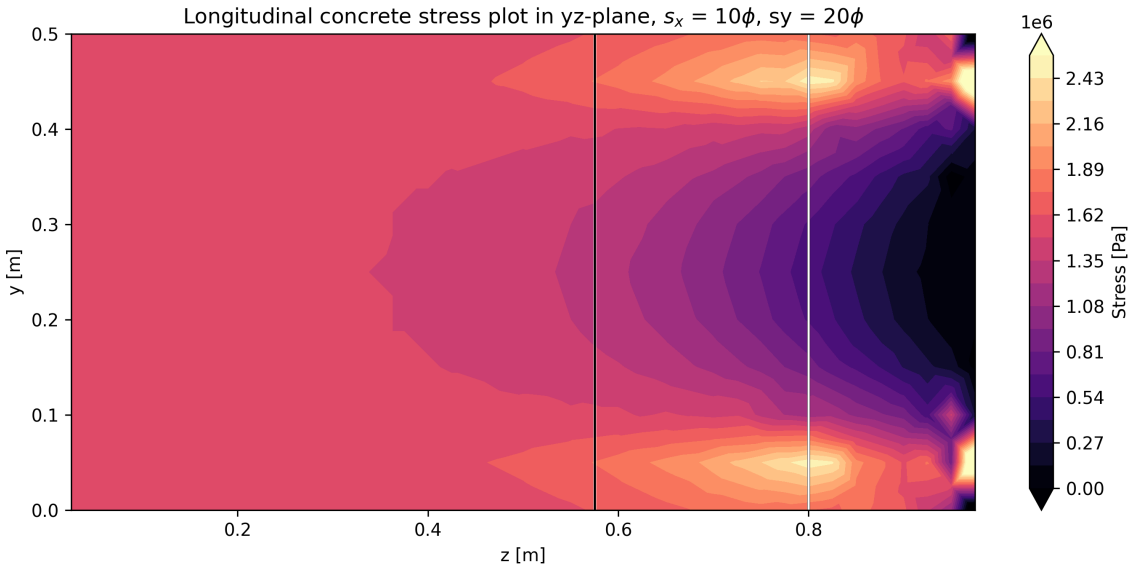
Longitudinal concrete stress plot in yz-plane, s_x = 10ϕ, sy = 20ϕ
y [m]
z [m]
0.0
0.1
0.2
0.3
0.4
0.5
0.2
0.4
0.6
0.8
1e6
2.43
2.16
1.89
1.62
1.35
1.08
0.81
0.54
0.27
0.00
Stress [Pa]

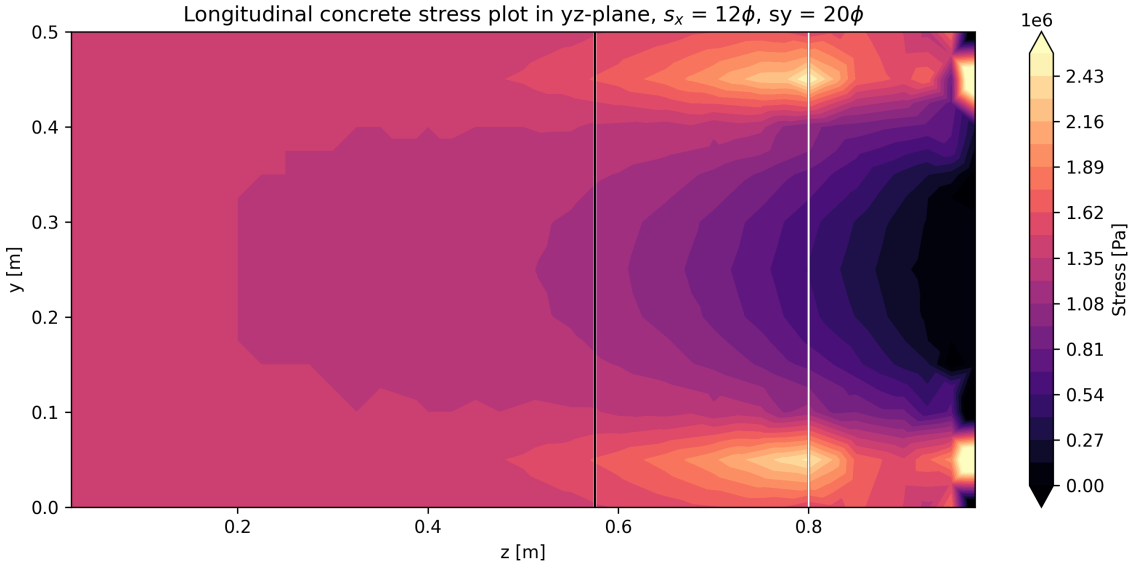
Longitudinal concrete stress plot in yz-plane, s_x = 12ϕ, sy = 20ϕ
y [m]
z [m]
0.0
0.1
0.2
0.3
0.4
0.5
0.2
0.4
0.6
0.8
1e6
2.43
2.16
1.89
1.62
1.35
1.08
0.81
0.54
0.27
0.00
Stress [Pa]

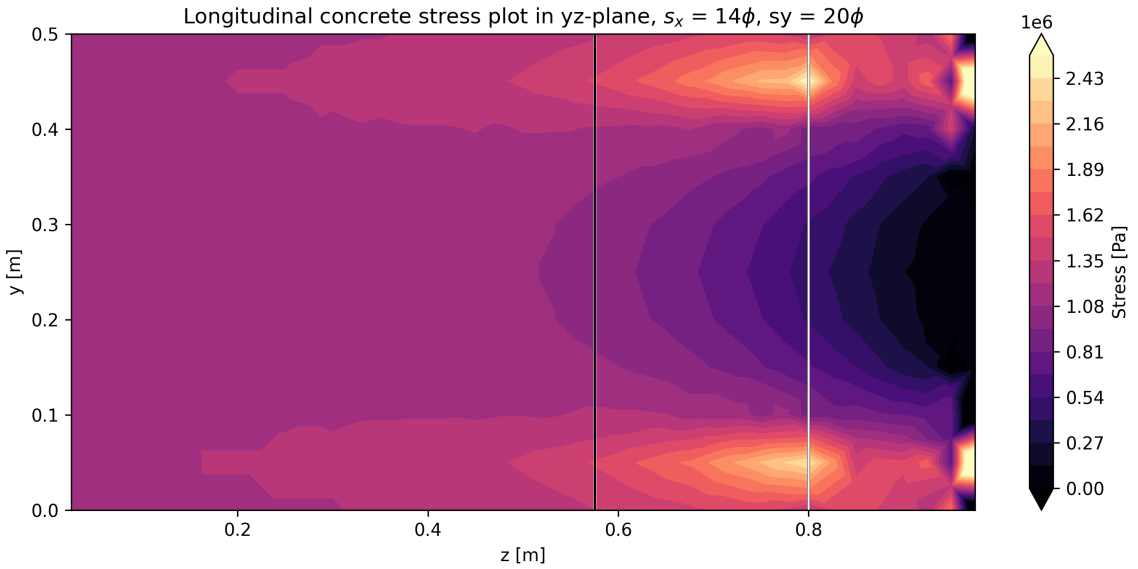
Longitudinal concrete stress plot in yz-plane, s_x = 14ϕ, sy = 20ϕ
y [m]
z [m]
0.0
0.1
0.2
0.3
0.4
0.5
0.2
0.4
0.6
0.8
1e6
2.43
2.16
1.89
1.62
1.35
1.08
0.81
0.54
0.27
0.00
Stress [Pa]

C

Analytical results

C.1 Study 1

In this section, the analytical results from study 1 are presented. Both in terms of effective area and transmission length.

C.1.1 Effective area

Ratio	$s_y = 200$ **mm**			$s_y = 400$ **mm**		
	$b_{c,eff}$ [m]	$h_{c,eff}$ [m]	$A_{c,eff}$ $[m^2]$	$b_{c,eff}$ [m]	$h_{c,eff}$ [m]	$A_{c,eff}$ $[m^2]$
$s_x = 6\phi$	1.00	0.250	0.250	1.00	0.250	0.250
$s_x = 8\phi$	1.00	0.250	0.250	1.00	0.250	0.250
$s_x = 10\phi$	1.00	0.250	0.250	1.00	0.250	0.250
$s_x = 12\phi$	1.00	0.250	0.250	1.00	0.250	0.250
$s_x = 14\phi$	1.00	0.250	0.250	1.00	0.250	0.250

Ratio	$s_y = 200$ **mm**			$s_y = 400$ **mm**		
	$b_{c,eff}$ [m]	$h_{c,eff}$ [m]	$A_{c,eff}$ $[m^2]$	$b_{c,eff}$ [m]	$h_{c,eff}$ [m]	$A_{c,eff}$ $[m^2]$
$s_x = 6\phi$	1.00	0.300	0.300	1.00	0.350	0.350
$s_x = 8\phi$	1.00	0.300	0.300	1.00	0.350	0.350
$s_x = 10\phi$	1.00	0.300	0.300	1.00	0.300	0.300
$s_x = 12\phi$	0.833	0.267	0.222	0.833	0.267	0.222
$s_x = 14\phi$	0.714	0.243	0.174	0.714	0.243	0.176

C.1.2 Transmission length

Ratio	Old EC 2		New EC 2	
	l_t [m]		l_t [m]	
	$s_y = 200$ mm	$s_y = 400$ mm	$s_y = 200$ mm	$s_y = 400$ mm
$s_x = 6\phi$	0.308	0.312	0.315	0.324
$s_x = 8\phi$	0.318	0.337	0.322	0.345
$s_x = 10\phi$	0.348	0.385	0.351	0.389
$s_x = 12\phi$	0.372	0.422	0.370	0.420
$s_x = 14\phi$	0.397	0.460	0.391	0.454

C.2 Study 2

In this section, the analytical results from study 2 are presented. Both in terms of effective area and transmission length.

C.2.1 Effective area

Ratio	$s_y = 200$ **mm**			$s_y = 400$ **mm**		
	$b_{c,eff}$ [m]	$h_{c,eff}$ [m]	$A_{c,eff}$ [m^2]	$b_{c,eff}$ [m]	$h_{c,eff}$ [m]	$A_{c,eff}$ [m^2]
$s_x = 6\phi$	0.600	0.250	0.150	0.600	0.250	0.150
$s_x = 8\phi$	0.800	0.250	0.200	0.800	0.250	0.200
$s_x = 10\phi$	1.00	0.250	0.250	1.00	0.250	0.250
$s_x = 12\phi$	1.20	0.250	0.300	1.20	0.250	0.300
$s_x = 14\phi$	1.40	0.250	0.350	1.40	0250	0.350

Ratio	$s_y = 200$ **mm**			$s_y = 400$ **mm**		
	$b_{c,eff}$ [m]	$h_{c,eff}$ [m]	$A_{c,eff}$ [m^2]	$b_{c,eff}$ [m]	$h_{c,eff}$ [m]	$A_{c,eff}$ [m^2]
$s_x = 6\phi$	0.600	0.300	0.180	0.600	0.300	0.150
$s_x = 8\phi$	0.800	0.300	0.240	0.800	0.300	0.240
$s_x = 10\phi$	1.00	0.300	0.300	1.00	0.300	0.300
$s_x = 12\phi$	1.00	0.300	0.300	1.00	0.300	0.300
$s_x = 14\phi$	1.00	0.300	0.300	1.00	0.300	0.300

C.2.2 Transmission length

Ratio	Old EC 2		New EC 2	
	l_t [m]		l_t [m]	
	$s_y = 200$ mm	$s_y = 400$ mm	$s_y = 200$ mm	$s_y = 400$ mm
$s_x = 6\phi$	0.293	0.307	0.297	0.312
$s_x = 8\phi$	0.313	0.336	0.317	0.340
$s_x = 10\phi$	0.350	0.385	0.353	0.389
$s_x = 12\phi$	0.359	0.404	0.359	0.404
$s_x = 14\phi$	0.398	0.415	0.395	0.412

D

Comparison of FEA and analytical results

D.1 Effective area comparison - study 1

The following section presents a comparison of FEA and analytical results of the effective area for study 1. Results are given in both tables and graphs.

Ratio	**FEA**		**Old EC 2**		**New EC 2**	
	$A_{c,eff}$ [m^2]		$A_{c,eff}$ [m^2]		$A_{c,eff}$ [m^2]	
	$s_y = 200$ mm	$s_y = 400$ mm	$s_y = 200$ mm	$s_y = 400$ mm	$s_y = 200$ mm	$s_y = 400$ mm
$s_x = 6\phi$	0.102	0.106	0.250	0.250	0.300	0.350
$s_x = 8\phi$	0.101	0.132	0.250	0.250	0.300	0.350
$s_x = 10\phi$	0.159	0.216	0.250	0.250	0.300	0.300
$s_x = 12\phi$	0.183	0.240	0.250	0.250	0.222	0.222
$s_x = 14\phi$	0.203	0.262	0.250	0.250	0.174	0.174

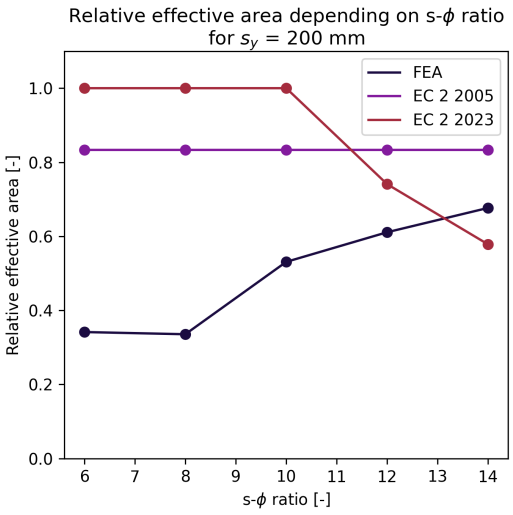

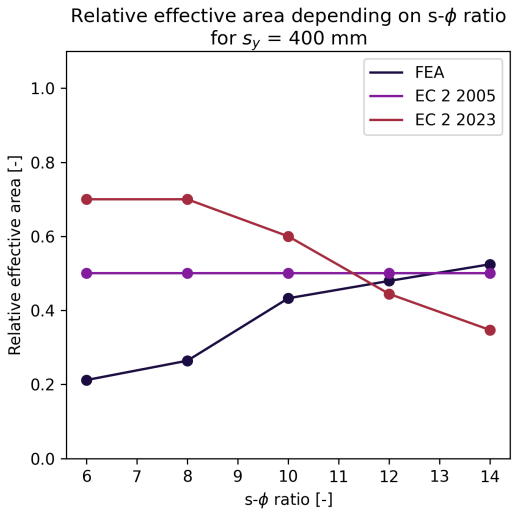

D.1.1 Effective area comparison - study 2

The following section presents a comparison of FEA and analytical results of the effective area for study 2. Results are given in both tables and graphs.

Ratio	FEA		Old EC 2		New EC 2	
	$A_{c,eff}$ [m^2]		$A_{c,eff}$ [m^2]		$A_{c,eff}$ [m^2]	
	$s_y = 200$ mm	$s_y = 400$ mm	$s_y = 200$ mm	$s_y = 400$ mm	$s_y = 200$ mm	$s_y = 400$ mm
$s_x = 6\phi$	0.177	0.108	0.150	0.150	0.180	0.180
$s_x = 8\phi$	0.110	0.158	0.200	0.200	0.240	0.240
$s_x = 10\phi$	0.158	0.216	0.250	0.250	0.300	0.300
$s_x = 12\phi$	0.165	0.225	0.300	0.300	0.300	0.300
$s_x = 14\phi$	0.216	0.230	0.350	0.350	0.300	0.300

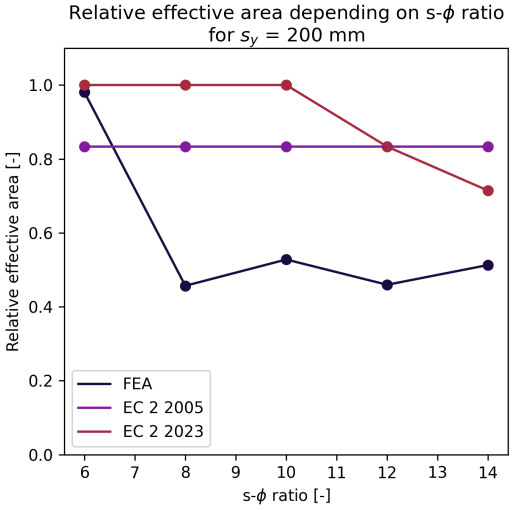

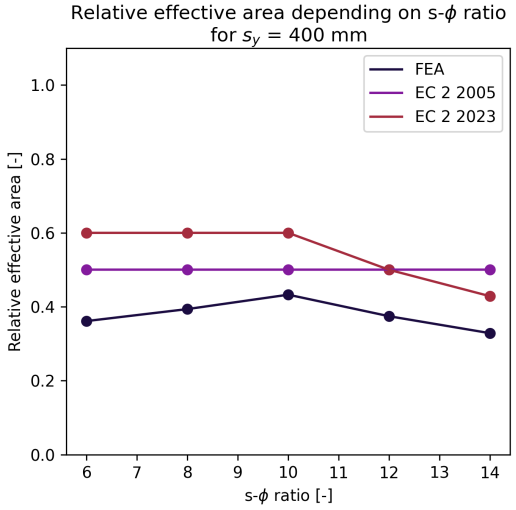

D.1.2 Transmission length comparison - study 1

The following section presents a comparison of FEA and analytical results of transmission length for study 1. Results are given in both tables and graphs.

Ratio	FEA		Analytical old EC 2		Analytical new EC 2	
	l_t [m]		l_t [m]		l_t [m]	
	$s_y = 200$ mm	$s_y = 400$ mm	$s_y = 200$ mm	$s_y = 400$ mm	$s_y = 200$ mm	$s_y = 400$ mm
$s_x = 6\phi$	0.425	0.450	0.308	0.312	0.315	0.324
$s_x = 8\phi$	0.400	0.425	0.318	0.337	0.322	0.345
$s_x = 10\phi$	0.400	0.425	0.348	0.385	0.351	0.389
$s_x = 12\phi$	0.400	0.425	0.372	0.422	0.370	0.420
$s_x = 14\phi$	0.400	0.450	0.400	0.460	0.391	0.454

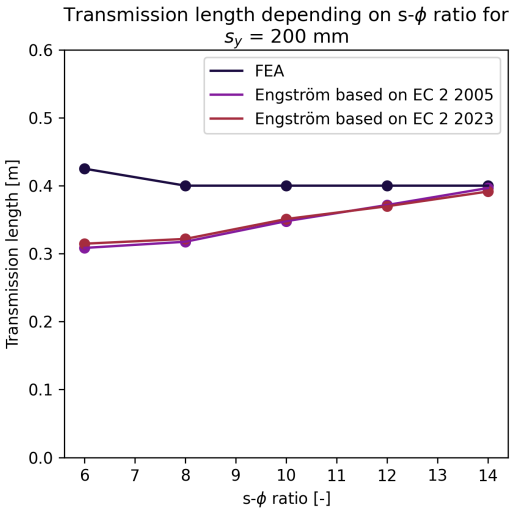

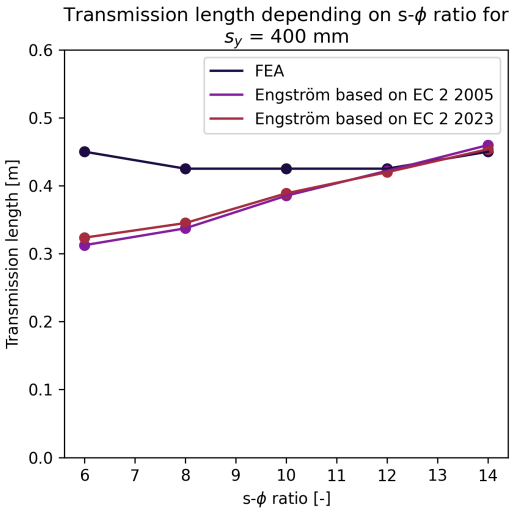

D.1.3 Transmission length comparison - study 2

The following section presents a comparison of FEA and analytical results of transmission length for study 2. Results are given in both tables and graphs.

Ratio	**FEA**		**Analytical old EC 2**		**Analytical new EC 2**	
	l_t [m]		l_t [m]		l_t [m]	
	$s_y = 200$ mm	$s_y = 400$ mm	$s_y = 200$ mm	$s_y = 400$ mm	$s_y = 200$ mm	$s_y = 400$ mm
$s_x = 6\phi$	0.350	0.400	0.293	0.307	0.297	0.312
$s_x = 8\phi$	0.375	0.400	0.313	0.336	0.317	0.340
$s_x = 10\phi$	0.400	0.425	0.350	0.385	0.353	0.389
$s_x = 12\phi$	0.400	0.425	0.359	0.404	0.359	0.404
$s_x = 14\phi$	0.400	0.425	0.398	0.415	0.395	0.412

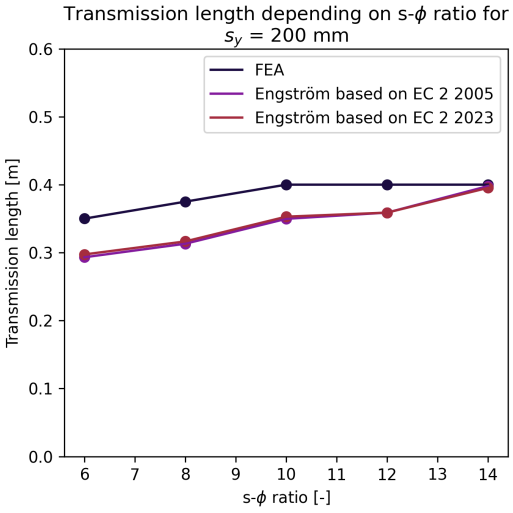

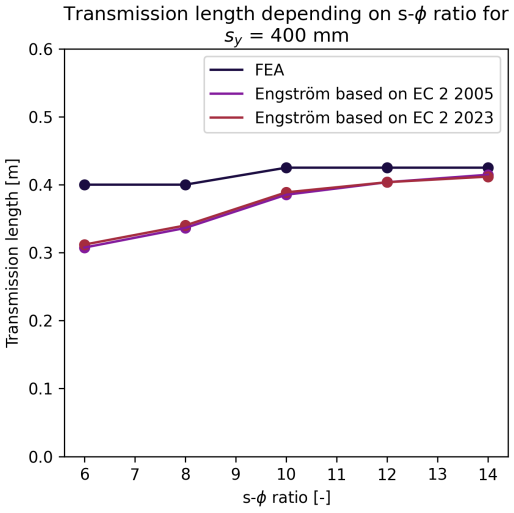

E

Material definitions

In the following appendix, the python script used to compute material definitions are attached. Each function is called with input data according to specified strength class and material definitions. The input and output from each function are described in each attached script.

E.1 Linear concrete

```
# --- LINEAR CONCRETE ----------------------------------------
def concrete_parameters(concrete_class):
    # Computes concrete parameters based on concrete class
    # according to Engstrom (2014).

    # concrete_class    Concrete strenght class [MPa]

    # fcm               Mean compressive strenght [Pa]
    # fctm              Mean tensile strenght [Pa]
    # Ecm               Young's modulus, mean value [Pa]

    # Compressive strenght
    fck = concrete_class*1e6

    # Mean compressive strength
    fcm = fck+8e6 # [Pa]

    # Mean tensile strenght according to Engstrom (2014) (3-7)
    fctm = 0.3*(fck/1e6)**(2/3)*1e6 # [Pa]

    # Young's modulus according to Engstrom (2014) (3-12)
    Ecm = 22*((fcm/10e6)**0.3)*1e9 # [Pa]

    return fcm, fctm, Ecm
# ------------------------------------------------------------
```

E.2 Non-inear concrete

```
# --- NON-LINEAR CONCRETE ------------------------------------
def concrete_parameters(concrete_class):
    # Computes concrete parameters based on concrete class
    # according to Engstrom (2014).

    # concrete_class    Concrete strenght class [MPa]

    # EPSIGT            Stress-strain relationship, softening law
    # fcm               Mean compressive strenght [Pa]
    # fctm              Mean tensile strenght [Pa]
    # Ecm               Young's modulus, mean value [Pa]
    # eps_cr            Cracking strain [-]
    # Gf                Fracture energy [N/m]

    # Compressive strenght
    fck = concrete_class*1e6

    # Mean compressive strength
    fcm = fck+8e6 # [Pa]

    # Mean tensile strenght according to Engstrom (2014) (3-7)
    fctm = 0.3*(fck/1e6)**(2/3)*1e6 # [Pa]

    # Young's modulus according to Engstrom (2014) (3-12)
    Ecm = 22*((fcm/10e6)**0.3)*1e9 # [Pa]

    # Nonlinear concrete definition - bi-linear softening law
    eps = [0]
    sig = [0]

    # Fracture energy MC2020 (14.6-9)
    Gf = 85*(fck/1e6)**0.15 # [N/m]

    # Cracking strain Hooke's Law
    eps_cr = fctm/Ecm # [-]

    # Crack openings MC2020 (14.8-7)
    w = np.array([0, 1, 5])*Gf/fctm # [m]

    # Strain law - smeared crack approach MC2020 (fig 14.8-2)
    eps.extend((w/l_elm + eps_cr).tolist()) # [-]

    # Stress law MC2020 (fig 14.8-2)
    sig.extend([fctm, 0.2*fctm, 0*fctm]) # [Pa]

    # Stress-strain relationship
    EPSIGT = [eps[0], sig[0], eps[1], sig[1], eps[2], sig[2], eps
    [3], sig[3]]

    return EPSIGT, fcm, fctm, Ecm, eps_cr, Gf
# ------------------------------------------------------------
```

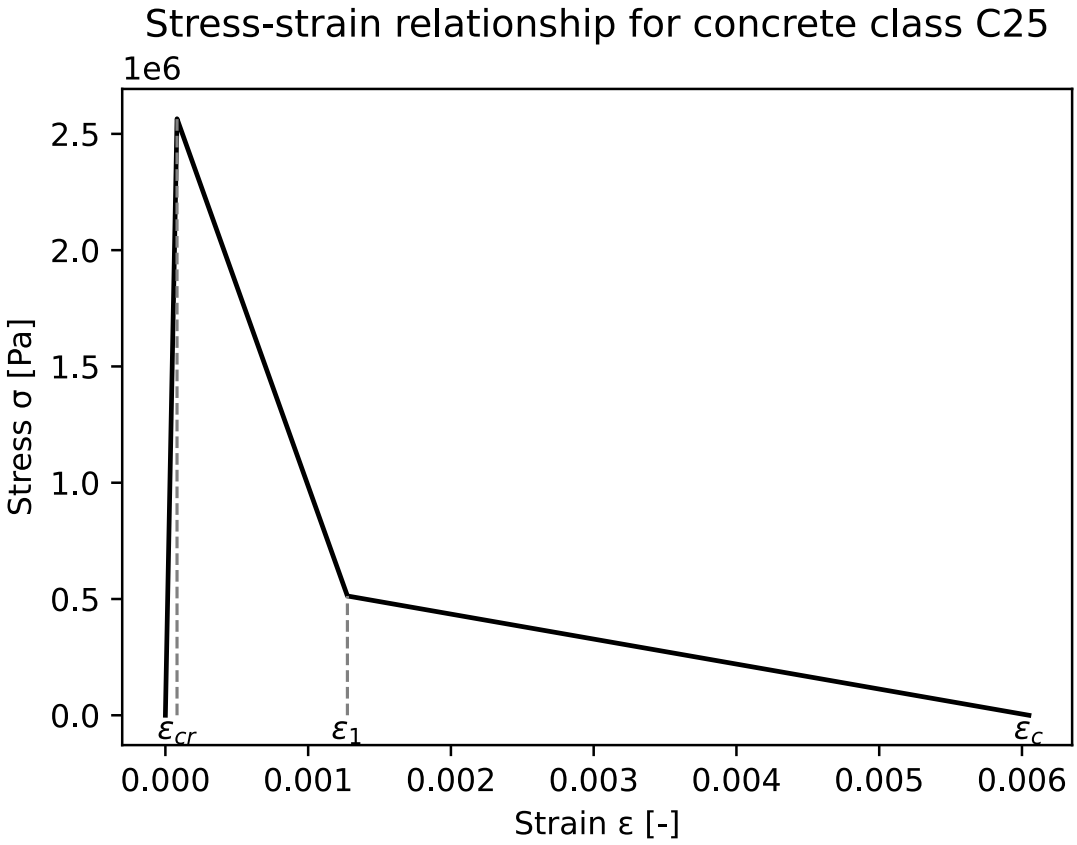

Figure E.1: Softening law for non-linear concrete material, initially used in FEA (Created by authors).

E.3 Bond-slip Reinforcement

```
# ---  BOND-SLIP REINFORCEMENT ------------------------------
Es = 200e9 # [Pa] Young's modulus of Steel

# Bond-slip relationship
# Slip in bond-slip relationship MC1990/2020
s_b = np.array([0, 1, 2, 8.5, 30])*1e-3 # [m]

# Division of first slip interval
s_b1 = np.linspace(0, s_b[1], 21) # [m]

# Shear stress in first slip interval Engstrom 2014 (5-7)
tau_b1 = (0.22*(fcm)*(s_b1/s_b[1])**0.21)# [Pa]

# Stress in bond-slip relationship MC2020/Engstrom 2014 (5-7)
tau_b = [0, tau_b1[-1], tau_b1[-1], tau_b1[-1]/3, tau_b1[-1]/3] # [
    Pa]

# Customise array for input in DIANA
BONDSLIP = []
for i in range(0, 2*(len(s_b1)+3)):
    if i < 2*(len(s_b1)): # first curve
        if is_even(i) == True:
            BONDSLIP.append(s_b1[int(i/2)])
        else:
            BONDSLIP.append(tau_b1[int((i-1)/2)])
    else:
        if is_even(i) == True:
            BONDSLIP.append(s_b[int((i-2*len(s_b1))/2+2)])
        else:
            BONDSLIP.append(tau_b[int((i-1-2*len(s_b1))/2+2)])

BONDSLIPN = []
for i in range(0, 2*(len(s_b1)+3)):
    if i < 6: # first path
        if is_even(i) == True:
            BONDSLIPN.append(-s_b[int((2*(len(s_b)-1)-i)/2)])
        else:
            BONDSLIPN.append(-tau_b[int((2*(len(s_b)-1)-(i-1))/2)])
    else:
        if is_even(i) == True:
            BONDSLIPN.append(-s_b1[int((2*(len(s_b1)-1)-(i-6))/2)])
        else:
            BONDSLIPN.append(-tau_b1[int((2*(len(tau_b1)-1)-(i-7))
    /2)])

TOTBONDSLIP = BONDSLIPN + BONDSLIP
# ------------------------------------------------------------
```

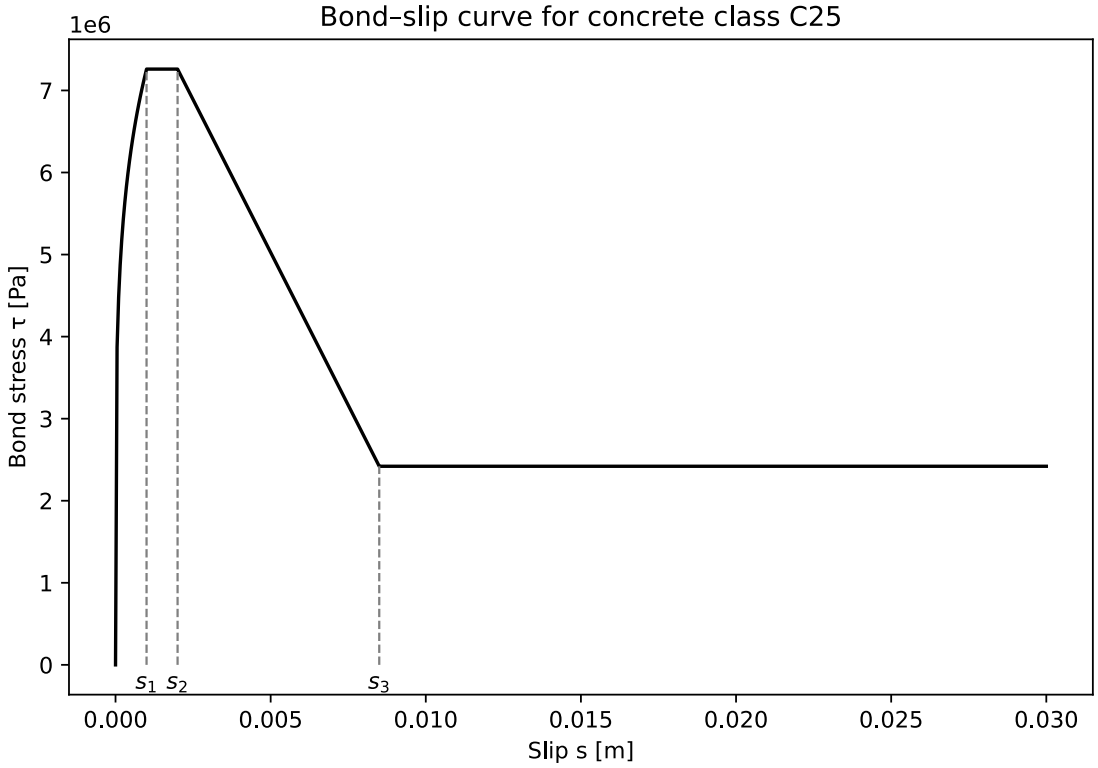

Figure E.2: Bond-slip relationship used in FEA (Created by authors).

F

Analytical method - python code

In the following appendix, the functions used to perform the analytical calculations are attached. Each function is called with input data according to each case of cross-section geometries, and the input and output variables are described in each attached script.

F.1 Effective area, width and height

```python
# --- EFFECTIVE AREA ---------------------------------------
def bhA_effective_EC(fi, sx, sy, cx, cy, nbx, nby, B, H):
    # Computes the effective area based on SS-EN 1992-1-1:2005 and
    # SS-EN 1992-1-1:2023

    # fi:               Bar diameter
    # sx, sy:           Bar spacing in x/y-direction
    # cx, cy:           Cover thickness in x/y-direction
    # nbx, nby:         Number of bars in x/y-direction
    # B:                Width
    # H:                Height

    # b_eff2023:        Effective width for entire cross section
    #                   according to EC 2 2023
    # h_eff2005/2023:   Effective height for entire cross section
    #                   according to EC 2 2005/2023
    # A_eff2005/2023:   Effective height for entire cross section
    #                   according to EC 2 2005/2023

    # --- SS-EN 1992-1-1:2005 ---
    # Definition of parameters
    d = H-cy # [m] distance from opposite edge to reinforcement
                bars
    x = -1e6 # [m] Simulate infinity large tension zone since a
                member in uniform tension is assumed

    # Effective area and height according to EC2 2005
    # Effective height
    h_eff2005 = nby*(min([2.5*(H-d),(H-x)/3, H/2]))

    # Effective area
    A_eff2005 = h_eff2005*B

```

```
    # --- SS-EN 1992-1-1:2023 ---
    # Definition of parameters
    ax = cx # Concrete cover in x-direction
    ay = cy # Concrete cover in x-direction
    b = sx # Spacing between bars (width associated with a mid bar)

    # Effective area, width and height according to EC 2 2023
    # Effective width
    b_effedge = min([ax+5*fi, 10*fi, 3.5*ax, ax+0.5*b, b]) # [m]
    b_effin = min([10*fi, b]) # [m]
    if nbx == 1:
        b_eff2023 = B # [m]
        print('Function bhA_effective_EC not defined for nbx=1')
    else:
        b_eff2023 = 2*b_effedge + (nbx-2)*b_effin # [m]

    # Effective height
    h_eff2023 = nby*(min([ay+5*fi, 10*fi, 3.5*ay, 0.5*H])) # [m]

    # Effective area
    A_eff2023 = h_eff2023*b_eff2023 # [m^2]

    return h_eff2005, A_eff2005, b_eff2023, h_eff2023, A_eff2023
# ---------------------------------------------------------------
```

F.2 Transmission length

```
# --- TRANSMISSION LENGTH -------------------------------------
def transmission_length_Engstrom(sigmas, A_eff_EC, fcm, Es, Ec, As,
    fi):
    # Calculates transmission length based on theory provided by
    # Engstrom (2014)

    # sigmas:           Steel stress at critical load step
    # A_eff_EC:         Effective area based on EC 2
    # fcm:              Concrete mean strength
    # Es, Ec:           Young's modulus for steel and concrete
    # As:               Reinforcement cross-sectional area
    # fi                Bar diameter

    # lt:               Transmission length

    # Crack width according to Engstrom (2014)
    wnet = 0.42 * ((fi*1e3*sigmas**2) / (0.22*fcm*Es*(1 + (Es/Ec)
    * (As/A_eff_EC))))**0.826 # [m]

    # Transmission length
    lt = (0.443 * (fi*1e3*sigmas) / (0.22*fcm*wnet**0.21 *
    (1 + (Es/Ec) * (As/A_eff_EC))) + 2*fi*1e3)/1e3 # [m]

    return lt
# ---------------------------------------------------------------
```

G

Post-processing - python code

In the following chapter, the functions used to perform the most essential parts of the post-processing are attached. In addition, other implemented functions that extract data from the CSV files are used but not included here. Each function is called with input data according to each case of cross-section geometries, and the input and output variables are described in each attached script.

G.1 Effective area

```
# --- EFFECTIVE AREA ---------------------------------------
def A_effective(SZZdata, FBZdata, SZZRdata, As, Ac):
    # Computes the effective area based on data in a specific
    # cross-section cut
    # SZZdata:      Stress data - reduced to load step and plane
    # FBZdata:      Reaction force data - reduced to load step
    # SZZRdata:     Reinforcement stress data - reduced to load
    #               step and plane
    # As:           Reinforcement area
    # Ac:           Concrete area

    # A_eff:        Effective area
    # sigmac:       Average concrete stress
    # sigmac_min:   Minimum concrete stress
    # sigmac_max:   Maximum concrete stress
    # eq_check:     Equilibrium check at z

    # Concrete stresses and loads in cross section
    sigmac = sum(SZZdata[0])/(len(SZZdata[0])) # [Pa] Avg stress
    sigmac_max = max(SZZdata[0]) # [Pa] Max stress
    sigmac_min = min(SZZdata[0]) # [Pa] Min stress

    # Total force in reinforcement at z
    F_s = sum(SZZRdata[0])*(As)/(len(SZZRdata[0])) # [N]
    # External force applied to reinforcement at top
    F_ext = sum(FBZdata[0]) # [N]

    # Effective area at z based on comparison with maximum stress
   in that section
    A_eff = (sigmac/sigmac_max)*(Ac) # [m^2]

```

```
    # Equilibrium check at z
    # transmitted force should be the same as the total force in
    concrete
    eq_check = (sigmac*Ac)/(F_ext-F_s) # [-]

    return A_eff, sigmac, sigmac_min, sigmac_max, eq_check
# ------------------------------------------------------------
```

G.2 transmission length

```
# --- TRANSMISSION LENGTH -----------------------------------
def transmission_length(SZZRdata, tolratio):
    # Calculates transmission length based on steel stress data a
    # the z-value where steel stress stops changing according to a
    # tolerance

    # SZZRdata:         Reinforcement stress data - reduced to
    #                   load step
    # tolratio:         Tolerance ratio for change in steel stress

    # lt:               Transmission length

    # Initiate lists
    sums = dd(float)
    counts = dd(int)

    # Sort stress value based on z-coordinate
    for SZZRi, zi in zip(SZZRdata[0], SZZRdata[3]):
        sums[zi] += SZZRi
        counts[zi] += 1

    # Compute averages and sort by X
    z_mean = [zi for zi in sorted(sums.keys())] # [m]
    SZZR_mean = [sums[zi] / counts[zi]
                 for zi in sorted(sums.keys())] # [Pa]

    # Compare stress change and return transmission length when
    tolratio is reached
    # - Data goes from bottom to top
    # - Use last value of z to ensure difference is < target
    lt = 0
    for i in range(len(SZZR_mean)):
        if i != 0:
            if abs(SZZR_mean[i]-SZZR_mean[i-1]) >
               tolratio*abs(SZZR_mean[i-1]):
                lt = L - z_mean[i-1] # [m]
                if i == 1:
                    print("Whole beam considered as transmission
    length!")
                    lt = L # [m]
                    return lt
                else:
                    return lt

```

```
43      # If the whole loop passes by
44      print("No transmission length were detected")
45      lt = 0
46  # ------------------------------------------------------------
```

DEPARTMENT OF SOME SUBJECT OR TECHNOLOGY
CHALMERS UNIVERSITY OF TECHNOLOGY
Gothenburg, Sweden
www.chalmers.se

CHALMERS
UNIVERSITY OF TECHNOLOGY